A SPECTROSCOPIC STUDY OF SQUARE PLANAR PLATINUM(II) COMPLEXES

A thesis submitted to the
UNIVERSITY OF CAPE TOWN
in fulfilment of the requirements for the degree of
DOCTOR OF PHILOSOPHY

by

GARY ANDRÉ FOULDS

Department of Inorganic Chemistry
University of Cape Town
Rondebosch
South Africa

August 1982

ACKNOWLEDGEMENTS

My sincere thanks and appreciation are due to

Professor D.A. Thornton for his excellent supervision, guidance and understanding in this study.

Drs G. Jackson and K. Koch for their invaluable assistance and interest in the nmr research.

Mrs G. Rootman for her patience and perseverance with the typing of this thesis.

Janet Yates for her help with the uv spectra.

Micky for her valued friendship and moral support.

My colleagues in the School of Chemistry.

My parents and Bebe.

The University of Cape Town and the South African Council for Scientific and Industrial Research for financial assistance.

PUBLICATIONS

1. Band assignments in the infrared spectra of pyridine and pyrazine adducts of nickel(II) glycinate by multiple isotopic labelling. G.A. Foulds, G.C. Percy and D.A. Thornton. *Spectrochimica Acta* 34A (1978) 1231.

2. Examination of the ratio ν^D/ν^H for infrared bands assigned to the C-H(D) and ring vibrations in metal complexes of quinoline, pyridine, aniline and their fully-deuterated analogues. G.A. Foulds, J.B. Hodgson, A.T. Hutton, M.L. Niven, G.C. Percy, P.E. Rutherford and D.A. Thornton. *Spectroscopy Letters* 12 (1979) 25.

3. Multiple isotopic labelling: Band assignments in the infrared spectra of 2,2'-bipyridine adducts of nickel(II) glycinate and L-α-alaninate. G.A. Foulds, G.C. Percy and D.A. Thornton. *Spectrochimica Acta* 36A (1980) 567.

4. The infrared spectra (500-140 cm^{-1}) of some diazine complexes of first transition series metal(II) ions. M.D. Child, G.A. Foulds, G.C. Percy and D.A. Thornton. *Journal of Molecular Structure* 75 (1981) 191.

5. The infrared spectra of the complexes *cis*- and *trans*-[Pt(pyrazine)$_2$-X_2] (X = Cl, Br, I, NO_2). G.A. Foulds and D.A. Thornton. *Spectrochima Acta* 37A (1981) 917.

6. The infrared spectra of aniline complexes of platinum(II) halides and nitrite. T.P.E. Auf der Heyde, G.A. Foulds, D.A. Thornton and G.M. Watkins. *Journal of Molecular Structure* 77 (1981) 19.

7. The infrared spectra of complexes of variously-substituted anilines with platinum(II) halides. T.P.E. Auf der Heyde, G.A. Foulds, D.A. Thornton and G.M. Watkins. *Spectroscopy Letters* 14 (1981) 455.

8. Phosphoric amides. Part V. An infrared spectrophotometric study of structural effects in the phosphoramidate group. G.A. Foulds, T.A. Modro and B.P. Rijkmans. *South African Journal of Chemistry* 34 (1981) 72.

9. The infrared spectra of imidazole complexes of platinum(II) halides and nitrite. S.J. Archer, T.P.E. Auf der Heyde, G.A. Foulds and D.A. Thornton. *Transition Metal Chemistry* 7 (1982) 59.

10. Isotopic labelling applied to the infrared and Raman spectra of some derivatives of Zeise's salt. T.P.E. Auf der Heyde, G.A. Foulds and D.A. Thornton. *Journal of Molecular Structure* (in press).

11. Application of spectroscopic techniques to substituted aniline derivatives of Zeise's salt. G.A. Foulds and D.A. Thornton. *Journal of Molecular Structure* (in press).

12. Spectroscopic studies of the complexes *trans*-$[PtX_2(CH_2{=}CH_2)(\text{pyrazine})]$ and *trans*-$[Pt_2X_4(CH_2{=}CH_2)_2(\text{pyrazine})]$. G.A. Foulds and D.A. Thornton. *Journal of Molecular Structure* (in press).

13. Nmr exchange studies on the complexes *trans*-$[PtX_2(CH_2{=}CH_2)(L)]$ (L = pyrazine, imidazole or *N*-methylimidazole). G.A. Foulds, G.E. Jackson and D.A. Thornton. *Journal of Molecular Structure* (in press).

SUMMARY

A number of spectroscopic techniques consisting of infrared, Raman ultraviolet and ^{1}H-nmr spectroscopy have been used in the structural analysis of square planar Pt(II) complexes.

The compounds *cis*- and *trans*-$[PtX_2L_2]$, (X = Cl, Br, I, NO_2 and L = pyrazine, imidazole and aniline) were prepared and investigated by means of infrared spectrophotometry. By means of isotopic labelling the Pt-to-ligand modes were assigned and by applying group theory the geometrical isomers of $[PtX_2L_2]$ were characterized. It was found that the *cis*-isomer was kinetically favoured whereas the *trans*-isomer was thermodynamically favoured. The ligand modes were also assigned, and distinction between the C-H stretching or bending modes and the ring stretching or bending vibrations was made *via* the ν^D/ν^H ratio. Using this technique ν^D/ν^H varies from 0.68 to 0.85 for the C-H modes and from 0.85 to 1.00 for the ring modes. The bonding in these complexes is discussed in terms of the νPt-L frequencies and in particular, the possibility of a $5d(Pt) \rightarrow \pi^*$ inverse charge transfer is suggested where L is a ligand containing empty π^* orbitals.

Zeise's salt and its bromide analogue were allowed to react with various ligands to give complexes of the type *trans*-$[PtX_2(C_2H_4)L]$, (X = Cl, Br and L = pyrazine, pyridine, imidazole, NH_3, pyridine *N*-oxide and aniline). A complete vibrational study of the complexes was made using infrared and Raman spectroscopy and the Pt-to-L modes were assigned by means of isotopic labelling. It was found that the

ligands *trans* to the ethylene exerted a marked influence on νC=C and νPt-C_2 according to their "coordinating power". As before, using the ν^D/ν^H ratio, the C-H modes and ring modes for the various ligands were distinguished. The electronic effects in these complexes were studied using ^{1}H-nmr and ultraviolet spectroscopy. It was observed that when the ligand, L, *trans* to ethylene was capable only of forming a σ bond with Pt^{2+}, variations in the electronic nature of L were faithfully transmitted through Pt^{2+} to ethylene. When L was capable of σ and π interactions with Pt^{2+}, this was not the case. It is suggested that the reason for this is the possibility of a *5d*(Pt) → π* interaction observed in the uv spectra of these complexes as a band near 300 nm.

The equivalence of the pyrazine (pz) protons in the ^{1}H-nmr spectrum of *trans*-[$PtCl_2(C_2H_4)$(pz)] indicates that the pyrazine is fluxional. Variable temperature ^{1}H-nmr runs were done, but the exchange is too fast to monitor. However, it is possible to monitor the exchange of imidazole with *trans*-[$PtX_2(C_2H_4)$(Him)] as this exchange process is slower. Band shape analysis is used and the enthalpy and entropy changes for the exchange process are calculated. All factors suggest that the exchange process is an intramolecular one at lower temperature, but may be intermolecular at higher temperature.

CONTENTS

CHAPTER FOUR

CHAPTER FIVE

CHAPTER 1

CHAPTER 1

1. INTRODUCTION

1.1 GENERAL

Platinum, the most common of the rare elements (it has an abundance of ca. 10^{-6}% of the earth's crust), occurs as a metal, as an alloy with the other rare elements, and in sulphide, arsenide, and other ores. The main sources of the metal are South Africa, the USSR, and Canada. Due to its low concentrations (it is quoted in grams per ton), extensive concentration by gravitation and flotation is required.[1]

A systematic study of the chemistry of platinum began soon after its arrival in Europe in 1741 and by as early as 1830 the first organometallic derivative, $K[Pt(C_2H_4)Cl_3].H_2O$, had been prepared. It is suggested by Hartley[2] that there were three factors which attracted interest to and sustained research on platinum.

Firstly, in the +2 state platinum forms complexes with ligands containing donor atoms from most groups in the periodic table.

Secondly, recognition of the square planar geometry of Pt^{2+} complexes opened up the possibility of *cis* and *trans* isomerism which eventually led to the discovery of the *trans*-effect in Pt^{2+} complexes in the 1920's.

Thirdly, growth in interest in platinum was triggered by the sudden developement in organometallic chemistry.

Chatt[4] showed that metal ions could be divided into two groups, class 'a' and class 'b'. Class 'a' metals are those that prefer to form complexes with elements of lower atomic number within a given group of the periodic table, whereas class 'b' metals prefer to form complexes with elements of higher atomic number in that group. Platinum was classified as a class 'b' metal and thus if allowed to react with the halides, the stability of the complexes would decrease in the order $I^- > Br^- > Cl^- >> F^-$. Pearson[5] developed a similar theory in which he states that hard acids form stronger complexes with harder bases and soft acids form stronger complexes with softer bases. The properties of 'hard' and 'soft' are related to polarizability so that platinum is a soft acid which would form a stronger complex with I^-, which is a softer base than Cl^-, for example. Thus platinum is classified as a Chatt class 'b' metal or a Pearson 'soft acid'.

The +2 oxidation state is by far the commonest oxidation state for platinum. No compounds of divalent platinum with a coordination number of less than four are known, and indeed most of the divalent compounds are four-coordinate, with square planar geometry. A number of five-coordinate complexes of divalent platinum have been made all involving ligands that are considered to be π-acceptors. Very few six-coordinate complexes have been made, and those that have are octahedral in geometry. Most octahedral platinum complexes have the metal in the +4 oxidation state.

The approximate relative energies of the d-orbitals in crystal fields of different symmetries are shown in Fig. 1. Bearing in mind that the Pt^{2+} ion has eight d-electrons it is apparent why square planar

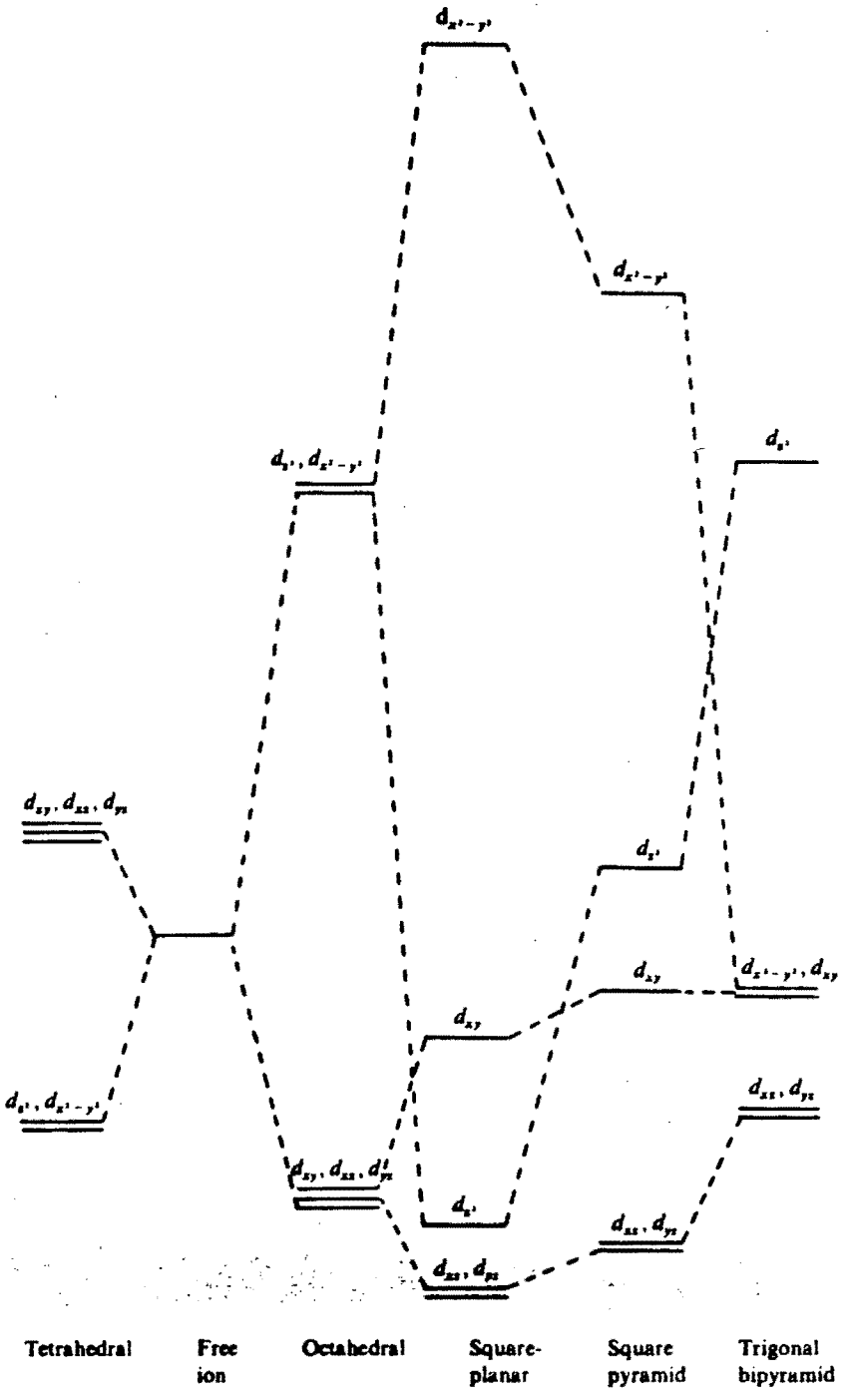

Fig. 1. Relative energies of the *d*-orbitals in different environments. (See reference 3).

geometry is favoured, since it is possible to leave the $d_{x^2-y^2}$ orbital empty.

Thus the chemistry of Pt^{2+} is essentially that of a soft acid that readily forms four coordinate complexes with square planar geometry, and to a lesser degree, five coordinate complexes with trigonal bipyramidal, square pyramidal and distorted square pyramidal geometries.[3]

1.2 METHODS OF ASSIGNING METAL TO LIGAND VIBRATIONS IN THE INFRARED SPECTRA OF TRANSITION METAL COMPLEXES

Bands in the far-infrared spectra (i.e. below about 600 cm^{-1}) arise from vibrations originating in weak bonds or involving heavy atoms or a combination of both. The fundamental vibrations in this region are metal-to-ligand stretches and bends, lattice modes and low-frequency torsional modes. It is principally the metal-to-ligand stretches and bends that yield important structural information. However, it is important to note that vibrational coupling and the occurrence of ligand modes activated by complexation may complicate the interpretation of the spectra.

The following methods have been used in the assignment of metal-ligand vibrations:

1.2.1 Comparison of the spectrum of the free ligands with that of its complex. Bands in the spectrum of the complex that are absent from the spectrum of the free ligand may be assigned as M-L modes. However, it should be noted that such assignments are very tentative since ligand vibrations activated by complexation may also appear.[6]

1.2.2 Metal-ligand vibrations of complexes having the same metal ion and a series of similar substituted ligands will appear in the same regions of the infrared spectra. νPt-N in the complexes *trans*-$[PtCl_2(CH_2CH_2)L]$ (where L = substituted aniline) were assigned in this manner.[7]

1.2.3 Normal coordinate analysis.[8] Metal-ligand and in fact all other frequencies may be predicted by calculations based on a model of the complex. However, as has been shown on numerous occasions, inaccuracies occur due to difficulty in the determination of force constants.

1.2.4 The isotopic labelling method involves labelling the ligand or metal ion with a preferably stable isotope.[9] If one then assumes that the force constants are unaltered by isotopic substitution, then shifts caused by isotopic labelling must be due to the mass effect.

The isotopic shifts may be calculated,[9] to a reasonable approximation, be assuming the labelled atom to be part of a simple diatomic oscillator. Thus the vibrational frequency

of a harmonic diatomic molecule is given by

$$\nu = \frac{1}{2\pi c} \left(\frac{f}{\mu}\right)^{\frac{1}{2}}$$

while the vibrational frequency of the corresponding isotopically-labelled species is given by

$$\nu^{i} = \frac{1}{2\pi c} \left(\frac{f}{\mu^{i}}\right)^{\frac{1}{2}}$$

where ν = vibrational frequency (wavenumber),

f = harmonic force constant,

μ = reduced mass of molecule,

c = velocity of light,

and the superscript refers to the labelled system.

The frequency shift caused by labelling is then given by

$$\frac{\nu_{i}}{\nu} = \left(\frac{\mu}{\mu_{i}}\right)^{\frac{1}{2}}$$

Thus the greatest isotope effect can be expected for deuterated and tritiated molecules where the m^{i}/m ratio is largest (m^{i} = higher mass of labelled atom and m = mass of atom with natural isotopic abundance), and shifts of up to 1000 and 1300 cm^{-1} are observed. However, the observed frequency shifts which result from labelling depend directly upon a number of factors *viz.* the extent to which the labelled atoms participate in the particular vibration, vibrational coupling, the number and nature of the atoms in the molecule that have been labelled and the extent of hydrogen bonding. Thus the observed shift will be greatest if the molecule is simple with less chance of vibrational coupling and more chance of purer vibrations.

The isotopic labelling carried out in this research to a large extent involves labelling of the ligand molecules as this method gives the most satisfactory results, *i.e.* the largest unambiguous shifts. Another method which is often costly and definitely limited by the availability of stable isotopes is isotopic labelling of the metal ion.[10] This method is ideal for specifically assigning metal-to-ligand vibrations, but the shifts are generally small due to the relatively unfavourable m^i/m ratio, and may fall within the range of experimental error.

It has been extensively shown that the isotopic labelling method of assigning bands in infrared spectra is by far the most unambiguous and simple method.[11,12] The major limitation appears to be the availability and cost of the isotopes.

1.3 GROUP THEORY AND ITS APPLICATIONS TO MOLECULAR VIBRATIONS

It is possible to predict the number of vibrational modes (and their Raman and infrared activites) if the symmetry elements of the molecule are known.[13-15] Thus if one knows the point group to which the molecule belongs then by means of the character table for that point group, the normal modes of vibration may be determined. These vibrations may then be seperated into stretches and bends and their infrared and Raman activity may be deduced.

Consider a molecule composed of N atoms. All the movements of the atoms in the molecule may be resolved into components along the x-, y- and z-axes. Thus there are $3N$ possible movements in the molecule of which six are translation and rotation, while the remaining $3N$-6 ($3N$-5 for a linear molecule) are internal molecular vibrations. These vibrations are catagorized by labelling each atom with three orthogonal position vectors and expressing the atomic displacements, for the point group of relevance, as transformation matrices whose characters, X, form a reducible representation, Γ_{total}. For example, consider a molecule of square planar *cis*-$[PtCl_2(NH_3)_2]$ whose point group is C_{2v} and for which Γ_{total} is:

C_{2v}	E	C_2	δ_v	δ_v'
Γ_{total}	15	-1	1	5

To determine the symmetry species of all the possible molecular motions, the following reduction formula is used:

$$n_i = \frac{1}{h} \Sigma \chi_R \chi_I N$$

where n_i = the number of times each irreducible representation appears in the reducible representation,

h = the order of the group,

χ_R = character of the reducible representation,

χ_I = character of the irreducible representation,

N = number of symmetry operations in each class.

Thus the 15 possible molecular motions in *cis*-$[PtCl_2(NH_3)_2]$ are:

$$\Gamma_{3N} = 5A_1 + 2A_2 + 3B_1 + 5B_2$$

The molecular translations are obtained from the character table containing columns listing the transformation properties of x, y and z, x^2, y^2, z^2, xz, yz and xy. Rotational properties associated with the point group are listed as R_x, R_y and R_z. The representations responsible for vibration are obtained by removing the translational and rotational irreducible representations. Thus for *cis*-$[PtCl_2(NH_3)_2]$ we have:

Symmetries for all molecular motions	$5A_1$	+	$2A_2$	+	$3B_1$	+	$5B_2$
Symmetries for translations	A_1			+	B_1	+	B_2
Symmetries for rotations			A_2	+	B_1	+	B_2
Symmetries for vibrations = Γ_{vib}	$4A_1$	+	A_2	+	B_1	+	$3B_2$

To determine the number of stretches and bends constituting Γ_{vib}, internal displacement vectors are chosen as a new basis for the point group representation. To determine the reducible representations for the stretches, vectors are drawn along the bonds. Any vector affected by a symmetry operations contributes nothing to the character of the matrix, while unaffected vectors contribute +1 or -1 depending on whether they are unchanged or inverted. For *cis*-$[PtCl_2(NH_3)_2]$ the operations E and δ_v' do not affect the vectors whereas C_2 and δ_v interchange them. Thus we have:

C_{2v}	E	C_2	δ_v	δ_v'
$\Gamma_{stretch}$	4	0	0	4

which reduces to

$$\Gamma_{stretch} = 2A_1 + 2B_2$$

the bends are obtained by subtracting $\Gamma_{stretch}$ from Γ_{vib} yielding

$$\Gamma_{bend} = 2A_1 + A_2 + B_1 + B_2$$

Symmetry does not allow for the seperation of two or more vibrations of the same irreducible representation. However there is usually a large frequency difference between stretching and bending modes due to significant energy difference, and thus in the example shown above one would not expect a symmetric A_1 stretch to interact with a symmetric A_1 bend although it is symmetry-allowed. It is symmetry-forbidden for an A_1 vibration, however to interact with a B_2 vibration as these are orthogonal representatives.

Another aspect that can be determined from the symmetry elements, is whether a vibration is infrared or Raman active. A vibration will be infrared active if during vibration there is a resultant change in dipole. The dipole moment changes in a similar manner as the x,y and z-coordinates and a vibration will be infrared active if it belongs to the same representation as any of the internal displacement vectors. This can be read directly from the character table. Likewise a vibration will be Raman active, depending on the polarizability of the bond, if the mode involved belongs to the same representation as any of the operations in the last column of the character table. Thus for *cis*-$[PtCl_2(NH_3)_2]$ with C_{2v} symmetry there are four metal-to-ligand stretches all of which are infrared and Raman active. They are the asymmetric and symmetric Pt-to-Cl stretches and the

asymmetric and symmetric Pt-to-NH_3 stretches. The full set of stretches and bends are shown in Fig. 2.

The same procedure may be performed for *trans*-$[PtCl_2(NH_3)_2]$ with D_{2h} symmetry and we obtain

$$\Gamma_{3N} = 2A_{1g} + 2B_{1g} + 3B_{1u} + B_{2g} + 3B_{2u} + B_{3g} + 3B_{3u}$$

$$\Gamma_{translation} = B_{1u} + B_{2u} + B_{3u}$$

$$\Gamma_{rotation} = B_{1g} + B_{2g} + B_{3g}$$

$$\Gamma_{vibration} = 2A_{1g} + B_{1g} + 2B_{1u} + 2B_{2u} + 2B_{3u}$$

$\Gamma_{vibration}$ reduces to

$$\Gamma_{stretch} = 2A_{1g} + B_{2u} + B_{3u}$$

$$\Gamma_{bend} = B_{1g} + 2B_{1u} + B_{2u} + B_{3u}$$

Of the stretches only B_{2u} and B_{3u} are infrared-active while the two A_{1g} modes are Raman-active. The B_{1g} bend is Raman-active while the two B_{1u}, the B_{2u} and B_{3u} modes are infrared-active. Thus for *trans*-$[PtCl_2(NH_3)_2]$ with D_{2h} symmetry, there are four metal-to-ligand stretches of which the asymmetric Pt-to-Cl and assymmetric Pt-to-NH_3 stretches are infrared-active while the symmetric Pt-to-Cl and symmetric Pt-to-NH_3 stretches are Raman-active. Thus, if we can identify the number of metal-to-ligand stretches in the infrared spectrum, by means of isotopic labelling for example, then we can ascertain which isomer we are dealing with.

STRETCHES

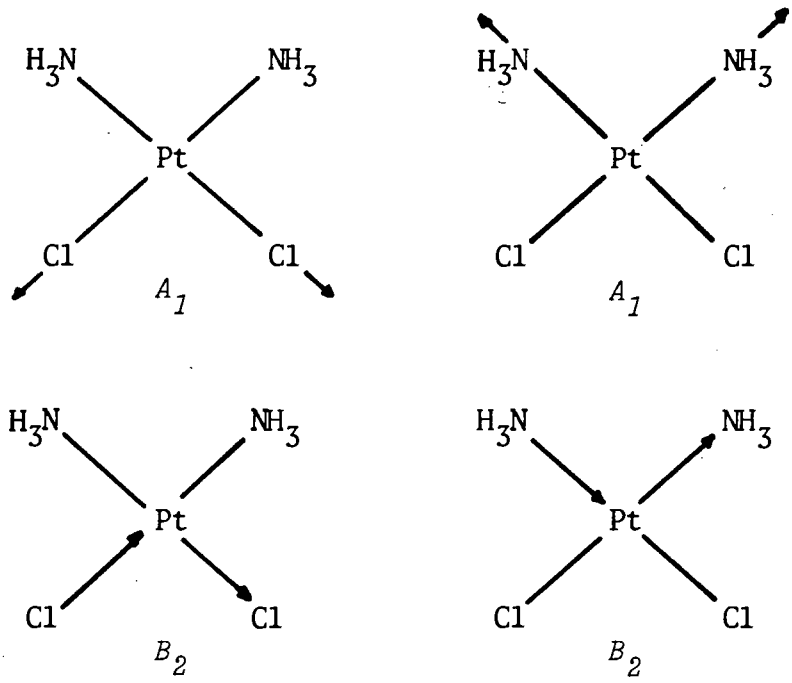

BENDS

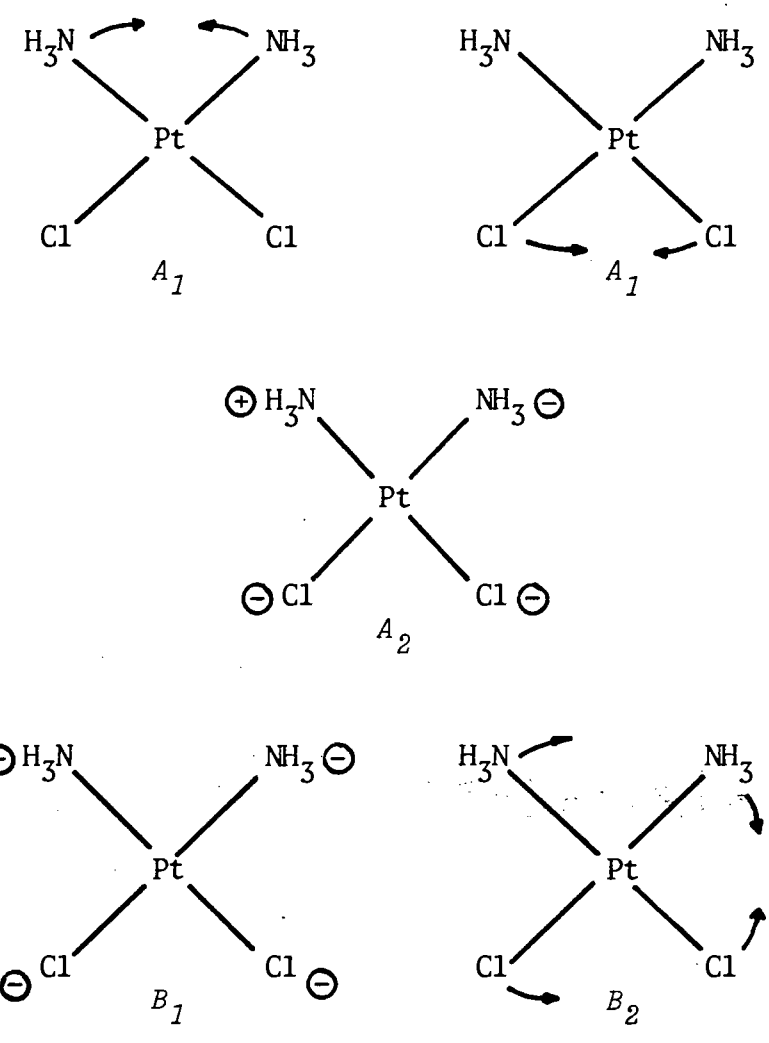

Fig. 2. Stretches and bends of *cis*-$[PtCl_2(NH_3)_2]$

The discussion so far applies when one considers the molecule to be an isolated unit[14] *e.g.* in the gaseous phase where the vibrations of the molecule are restricted only by its own point symmetry. In the solid state the molecule can no longer be regarded as a separate entity and is subject to the symmetry restrictions of its solid environment.

To perform a rigorous vibrational analysis one needs to consider the entire array of molecules which of course is an impossible task. However Site Group and Factor Group analysis are two useful approximations that can be used.

In Site Group analysis two assumptions are made. Firstly, interactions between one molecule and its surroundings are ignored, and secondly, the symmetry of the surroundings is assumed by the molecule occupying a site within it. Determination of the site symmetry is subject to the following conditions.

Firstly, the site group must be a subgroup of the space group of the crystal and the point group of the isolated molecule. Secondly, the number of equivalent sites must be equal to the number of molecules in the unit cell. Thus the site symmetry may be found if the space group, the point group of the isolated molecule and the number of molecules per unit cell are known Tables listing possible site symmetries have been devised by Halford.[16]

Factor group analysis[17] is the more rigorous of the two approximations in that it accounts for lattice modes and solid state splittings of

non-degenerate vibrations of the free molecule. However to use this approximation a full X-ray crystal structure with atomic coordinates is necessary. Reduced representations which facilitate the vibrational analysis of solids have been published by Adams and Newton.[18]

1.4 THE RATIO ν^D/ν^H USED IN THE ASSIGNMENT OF THE C-H(D) AND RING VIBRATIONS IN METAL COMPLEXES OF HETEROCYCLIC BASES

The ratio (ν^D/ν^H) between the frequencies of corresponding bands in the infrared spectra of deuterated and normal molecules can be used as an effective distinction between C-H stretching or bending modes and the ring stretching or bending vibrations in aromatic and heterocyclic compounds.[9] It has been found that the majority of the infrared bands which originate in the internal vibrations of heterocyclic bases recur on an approximately band-for-band basis in the spectra of their metal complexes.[19] Thus it is feasible to use the (ν^D/ν^H) ratio for distinction between C-H stretching or bending modes and the ring stretching or bending vibrations in the metal complexes as well.

Thornton[20] and co-workers have studied the (ν^D/ν^H) ratio for a number of complexes of heterocyclic bases and the results of their findings may be summarized as follows:

1. The ratio ν^D/ν^H varies from 0.68 to 0.85 for the C-H modes.
2. The ratio ν^D/ν^H varies from 0.85 to 1.00 for the ring modes.

Distinction between the above modes and metal-ligand modes, or bands originating in the vibrations of other functional groups or other coordinated ligands is also possible since the latter generally yield ν^D/ν^H ratios very close to unity. Where apparently anomalous ratios are observed, the possibility of incorrect assignments or vibrational coupling must be taken into account.[9]

1.5 BAND SHAPE ANALYSIS IN THE DETERMINATION OF NUCLEAR SPIN DYNAMICS

1.5.1 *Introduction*

The objective of NMR, or for that matter, any spectroscopic technique is to interpret a given spectrum in terms of macroscopic and microscopic properties of the sample being investigated. In many cases of high-resolution NMR spectroscopy one obtains a well resolved line spectrum in which the shapes of the lines are of secondary interest. For extracting information about detailed nuclear spin dynamics, it is generally necessary to analyze the total band shape.

In his treatise on band-shape analysis, Gerhard Binsch[21] covers the classical and quantum-mechanical theory in great detail and in doing so makes the following assumptions. Firstly, the only variable is the angular frequency, ω, of the observing channel, with all other instrumental parameters being regarded as constant in time or varying periodically with constant frequency and amplitude.

Secondly, we are confined to steady state conditions and transient phenomena are neglected. Thirdly, we concern ourselves primarily with exchange, although nuclear spin dynamic effects are usually attributed to exchange and relaxation. Thus the plot of $S(\omega)$ versus ω (where S is the signal intensity) will be called the band shape.

1.5.2 *Practical Band Shape Analysis*

Although it is sometimes possible to extract dynamic information from band shapes using simple formulae, the band-shape formulae are generally too complicated for algebraic analysis and one must resort to numerical methods.

The computational core common to all dynamic NMR computer programs, is the simulation of a theoretical band shape from static and dynamic input parameters. The program that we have used was developed by D.S. Stephenson and G. Binsch and is briefly described in the next paragraph.

DNMR 5[22] is an iterative simulation program that may optimize up to sixteen parameters (chemical shifts, coupling constants, populations, effective transverse relation times, exchange rate constants, two baseline parameters and the spectral origin) by a least-squares fitting of a theoretical band shape to experimental digitized NMR signal intensities. The optimization is constrained by the total experimental bandshape integral corrected for baseline increment and baseline tilt. The program outputs information about the progress

of the iteration, an error analysis of the final parameters and an agreement factor based on a calculated spectrum. It also produces plots of the original spectrum, and of the computed spectrum for comparison.

1.5.3 *Calculation of Activation Parameters*

Once the relaxation time and exchange rate constants have been measured as function of temperature, we are now in a position to calculate the activation parameters for the underlying chemical processes.

Nuclear exchange processes usually lend themselves to clearcut chemical interpretation and it is therefore standard practice to convert the corresponding rates to activation parameters. We can calculate the free energy of activation from a single rate constant at a single temperature by means of the Eyring equation

$$k = \kappa(k_B T/h)\exp(-\Delta G^{\ddagger}/RT)$$

Rate constants measured over a range of temperatures may be converted to Arrhenius activation energies and frequency factors or to enthalpies and entropies of activation by using the following formulae

$$k = A_{exp}(-E_a/RT)$$

$$k = \kappa(k_B T/h)\exp(-\Delta H^{\ddagger}/RT)\exp(\Delta S^{\ddagger}/R)$$

Thus by fitting a straight line to the logarithmic variants of the above equations we may extract the parameters of interest from the

slopes and intercepts. However it is essential that error analysis be performed as explained in the next section.

1.5.4 *Error Analysis*

Dynamic parameters extracted from NMR band shapes are subject to systematic as well as statistical errors.[23,24] Consider the error analysis equations derived for the Eyring and Arrhenius equations.

$$(\sigma_{\Delta G^{\ddagger}}/\Delta G^{\ddagger})^2 \simeq [\ln(k_B T/hk)]^{-2} \, (\sigma_k/k)^2 + (\sigma_T/T)^2$$

$$(\sigma_{E_a}/E_a)^2 \simeq [2T^2/(\Delta T)^2] \, (\sigma_T/T)^2 + 2[\Delta(\ln k)]^{-2} \, (\sigma_k/k)^2$$

In the former error analysis equation, derived for the Eyring equation, it is shown that for a typical case with T = 300°K and k = 100 sec^{-1}, a relative statistical error of 100% in the rate constant introduces a relative error of 4% in the $\Delta G^{\ddagger}$, and a temperature incorrect by 6°K an error of 2% in $\Delta G^{\ddagger}$. Thus for this case there is a total standard deviation of 4.5%. Contrast this with the error analysis equation derived for the Arrhenius equation, where for a temperature range of ΔT = 20°K an error of 25% in k causes an error of 26% in the activation energy, and an error of 3°K in T an error of 21% in E_a, this gives rise to a combined error of 34%.

Thus $\Delta G^{\ddagger}$ is insensitive to errors in k and T while E_a is very sensitive to errors in k and T. This is due to the fact that although $\Delta H^{\ddagger}$ and $\Delta S^{\ddagger}$ are error sensitive, the errors tend to cancel each other with the result that $\Delta G^{\ddagger}$ is insensitive to error ($\Delta G^{\ddagger} = \Delta H^{\ddagger} - T\Delta S^{\ddagger}$).

Considering the above it is shown that the best region to determine k is near coalescence where the line shape is most sensitive to k. As we diverge from coalescence the magnitude of the error tends to increase, and it is for this reason that a least squares fit with error propagation is preferable to the normal graphical method.

CHAPTER 2

CHAPTER 2

2. PHYSICAL METHODS

2.1 Infrared Spectra

The mid region of the infrared spectra (4000 - 300 cm^{-1}) was determined on Beckman IR-12 and Perkin-Elmer 180 spectrophotometers using CsBr plates and Nujol mulls for the regions 2000 - 1500 cm^{-1} and 1300 - 300 cm^{-1}, and CsBr plates and hexachlorobutadiene mulls for the regions 4000 - 2000 cm^{-1} and 1500 - 1300 cm^{-1}. The far infrared spectra were determined as Nujol mulls between polyethylene plates on a Perkin-Elmer 180 spectrophotometer (500 - 150 cm^{-1}) and on a Digilab FTS 16 B/D interferometer.

The wavenumber precision of the Beckman IR-12 is better than 0.5 cm^{-1} for the region 2000 - 300 cm^{-1}, and better than 0.75 cm^{-1} for the region 4000 - 2000 cm^{-1}. For maximum precision the frequencies were read directly from the wavenumber drum and not from the chart paper. Both the Perkin-Elmer 180 spectrophotometer and Digilab FTS 16 B/D interferometer have a reproducibility of better than 1 cm^{-1} in the far infrared region, the advantage of the latter being that it extends to a much lower wavenumber limit.

2.2 Electronic Spectra

The electronic spectra were run on a Varian Superscan 3 ultra-violet and visible spectrophotometer in the absorbance mode using $CHCl_3$ as solvent.

2.3 ^{1}H-Nuclear Magnetic Resonance Spectra

The ^{1}H - NMR spectra were obtained at 90 MHz on a Bruker WH 90 Fourier transform spectrophotometer and at 100 MHz on a Varian XL 100 continuous wave spectrophotometer. $CDCl_3$, acetone-d_6 and DMF-d_7 were used as solvents and locks depending on solubility of the complexes while TMS was used as a reference.

2.4 Raman Spectra

The Raman spectra were recorded on a Coderg PHO instrument using a Spectra Physics Model 164 Ar^+-laser for excitation. The compounds were contained in a spinning cell to prevent burning. Laser powers were kept around 350 mW at the sample. The spectra were recorded using the 488.0 and 514.5 nm lines with interference filters to remove plasma lines.

Different slit widths were used to optimise signal-to-noise ratio and resolution. The spectrometer has slits which can be set at several fixed distances, with widths approximately calibrated in cm^{-1} for the 632.8 nm line of a He-Ne laser. To obtain the slit width

in cm^{-1} at the excitation frequency, the calibrated numbers must be multiplied by 1.51 for the 514.5 nm line and by 1.68 for the 488.0 nm line (thus the resolution should be worse for the 488 than the 514.5 nm spectra). Taking the above into account an S1 slit is 1 cm^{-1} at 632.8 nm, 1.51 cm^{-1} at 514.5 nm and 1.68 cm^{-1} at 488 nm.

Compounds which have absorption bands overlapping with the laser excitation lines often give rise to the resonance Raman effect. This is not critical as resonance Raman does not shift the frequencies of the vibrational bands and only the relative intensities of certain bands will be noticably altered.

Finally it should be noted that in Raman spectroscopy the relative intensities of combination and overtone bands are much weaker than in the infrared. Consequently all the vibrational bands observed in the Raman spectra are due to fundamental modes, unless they are part of a Fermi-resonance system.

2.5 Microanalyses

Microanalyses were performed by Mr W.R.T. Hemsted on a Heraeus Univeral Combustion Analyser Model CHN-micro.

CHAPTER 3

CHAPTER 3

3. THE STRUCTURAL ANALYSIS OF *CIS*- AND *TRANS*-$[PtX_2L_2]$, WHERE X = Cl, Br, I, NO_2 AND L = PYRAZINE, IMIDAZOLE AND ANILINE

3.1 Introduction

Square planar geometry is common among complexes of transition elements near the end of the transition series, with platinum being no exception. In fact the detection of geometric isomers and isomerisation studies of square planar complexes so far, is limited almost exclusively to derivatives of palladium and platinum. This is almost certainly due to the ease of preparation and identification of the electroneutral complexes $[PtX_2L_2]$ where X is an anionic ligand and L is a neutral ligand. These complexes may exist as *cis*- or *trans*-isomers.

The general rule for complexes of the type $[PtX_2L_2]$ is that the *cis*-isomers are enthalpy-favoured, but that entropy changes in solution favour the *trans*-form. These factors are often finely balanced,

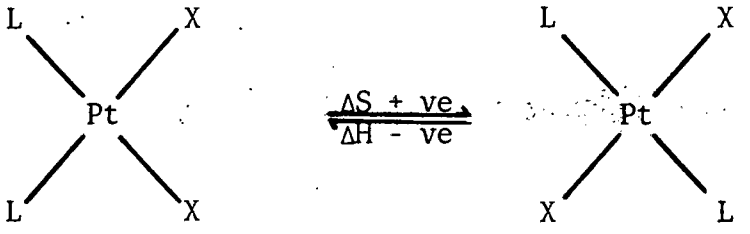

cis-isomer *trans*-isomer

allowing the observation of both geometries in solution. Factors which influence the equilibrium position are the type of ligand, the solvent or the temperature. However it is apparent that many interrelated factors contribute to the stability of each isomer. Some generalizations nevertheless can be made.

There is a tendency towards the more stable *trans*-isomer along the series $Cl^- < Br^- < I^-$, which is most probably related to the internal bond energies since this is also the order of increasing "softness" for the halide ions.[25,26]

The influence of solvent and internal bond energies is important as both ΔH and ΔS will contain contributions from them. The solvent probably effects the entropy term considerably whereas the enthalpy term is probably affected most by change in the internal bond energies. Thus the *cis*-isomers will be favoured if the bonding between Pt-X and Pt-L is dissimilar or if the solvent is polar, whereas the *trans*-isomer will be favoured if the bonding between Pt-X and Pt-L is similar or if the solvent is non-polar.[27,28]

It has long been recognized that there is a link between geometric isomerization and nucleophilic ligand substitution in these square planar complexes. However, there is still a lot of doubt as to which mechanism is taking place, and in fact different authors have used the same evidence to support radically different opinions.

Cis- and *trans*-platinum(II) complexes can be isomerized in solution in the presence of a nucleophile, thermally, photochemically and

spontaneously. The more general isomerization mechanisms to date are:

The Consecutive or Double Displacement Mechanism.

Scheme 1 depicts the double displacement isomerization mechanism.[29] L can be any neutral ligand and X is a halogen.

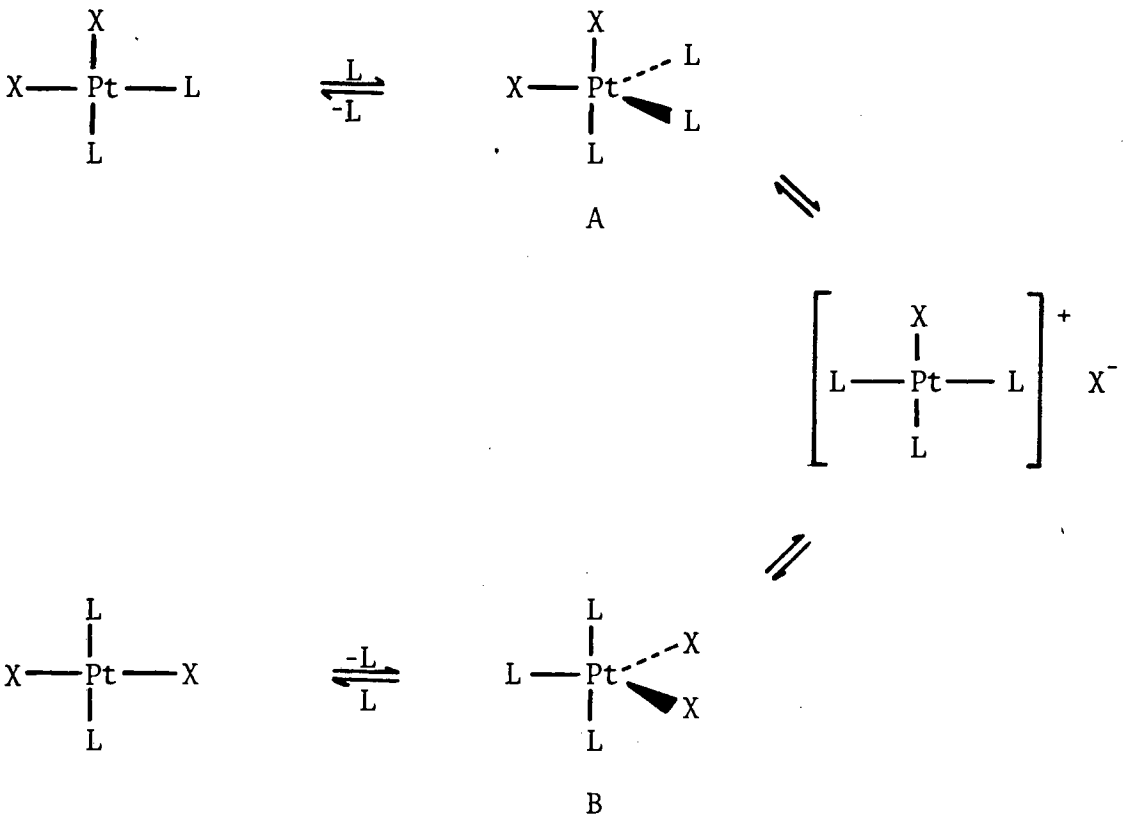

SCHEME 1

Two steps are needed to achieve isomerization, as the substitutions at platinum are stereospecific. In the first, L replaces halide to form $[PtXL_3]^+X^-$. The second involves the attack of X^- on $[PtXL_3]^+$. If this goes through intermediate A the original isomer is reformed, but if it goes through B the *trans*-isomer is generated.

The Pseudorotation Mechanism

This mechanism is a shortened version of the double displacement mechanism shown in Scheme 1. A pseudorotation mechanism could convert A into B directly and if this process were faster than either or both of the steps linking A and B with the ionic intermediate $[PtXL_3]^+$, then the isomerization process would proceed via pseudorotation. Scheme 2 shows both the double displacement and pseudorotation mechanisms competing in the isomerization of *cis*-$[PtI_2L_2]$ to *trans*-$[PtI_2L_2]$.[30]

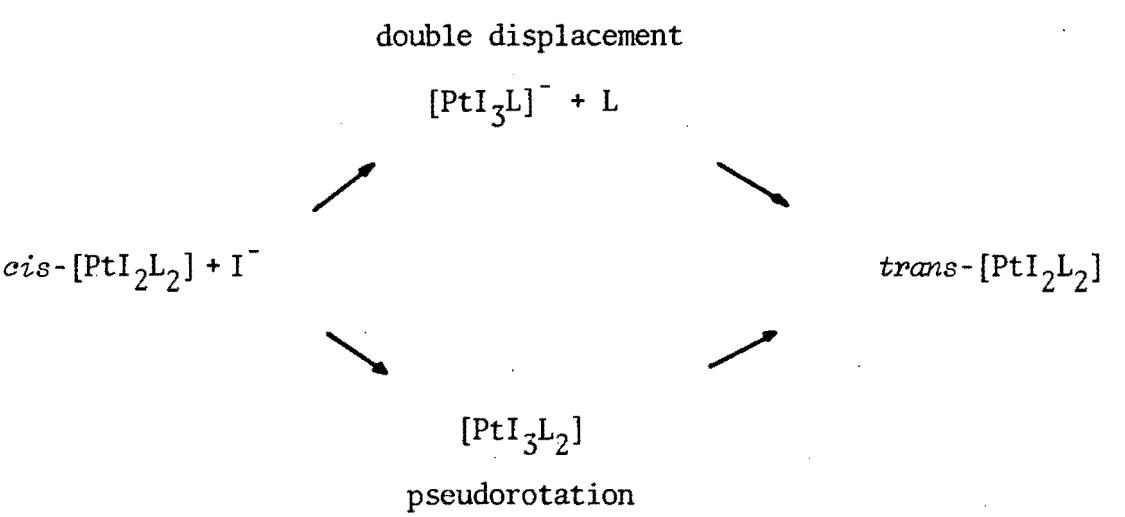

SCHEME 2

The Ionic-Intermediate Mechanism[31]

This is a refinement of the double displacement mechanism and is shown in Scheme 3. It allows all the L ligands to become equivalent and involves an ionic intermediate which implies that the rate of isomerization should increase with increasing solvent polarity. However

the reverse is found experimentally indicating that perhaps this is an unsatisfactory mechanism. It should be noted that some of these ionic intermediates have been isolated.[32,33]

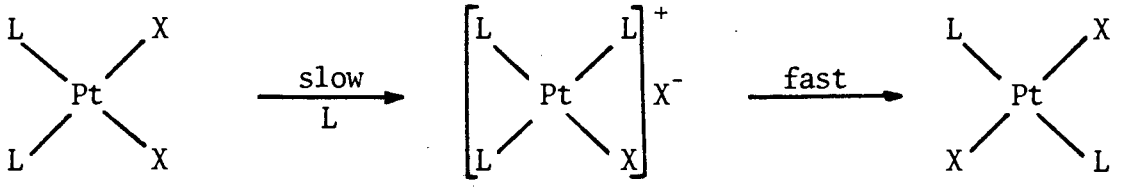

or

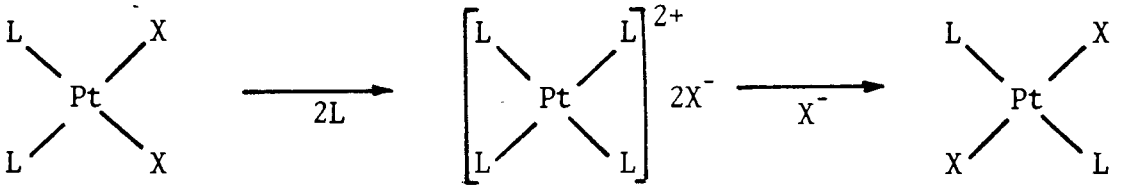

SCHEME 3

Considering the above discussion which briefly touches on some of the mechanistic routes possible in square planar geometrical isomerism, it appears that the field is essentially diverse and that many areas such as the effect of solvation, light *etc.* still need to be considered.

Another feature that has illicited much interest in square planar complexes of the type $[PtX_2L_2]$ is their medicinal use. It was the discovery of the anti-tumour activity of *cis*-$[Pt(NH_3)_2Cl_2]$ that led to an extensive investigation of the potential anti-cancer properties

of metal complexes. To date the most promising complexes are those containing Pt^{2+} with two *cis*- leaving groups of intermediate lability (*e.g.* chloride, but not iodide, as the "harder" chloride facilitates easier leaving) and two amines.[34,35]

The biological mode of action of these platinum complexes is not fully understood and various modes of action have been proposed. Apparently the interchange between a displaced ligand and a DNA nitrogen occurs via the hydrated divalent platinum ion and proceeds by means of a S_N2 mechanism.[36] The square planar nature of the Pt(II) complex lends itself to apical attack by the incoming H_2O to form the five-coordinate intermediate. This process is shown in Scheme 4.

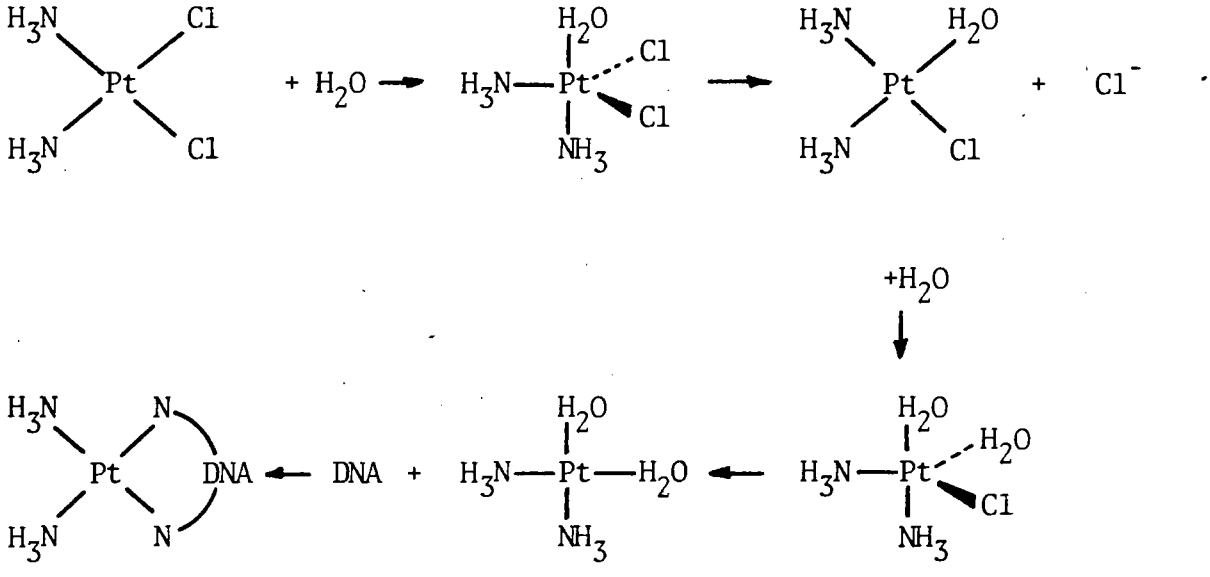

SCHEME 4

The aquation of *trans*-$[Pt(NH_3)_2Cl_2]$ results in only one chloride being removed, which explains the biological inactivity of the *trans*-complex. Inhibition of the DNA requires blocking of two sites (as is the case with the *cis*-complex) rather than one (as is the case with the *trans*-complex).[36]

Inhibition is the result of *inter*- and *intra*-strand lesions which confuse the cancer cells' repair mechanism. These lesions are effected by means of a cross-linkage between nitrogens of two neighbouring purines to form a purine-Pt-purine bridge.[34,35,37] Platinum complexes differ from other anti-cancer theraputicals in that they give rise only to *intra*-strand lesions as shown in the final complex in Scheme 4. This is evident from X-ray studies of *cis*-$[Pt(NH_3)_2Cl_2]$ in which the two chlorides are 3.3 A° apart,[38] whereas the *inter*-strand distance is 8.0 A°.[34,37]

Apart from the leaving groups, another method of modifying the reactivity of the platinum complex is by varying the carrier ligand. This would result in different steric, electronic and basic properties. It is the carrier ligand that determines the drug's ability to penetrate the cell's membrane and hence size, lipid solubility and non-toxicity are important. The strength of Pt-carrier ligand bond must be such that it is strong enough to prevent ligand exchange with other potential ligands found in the body. In terms of HSAB the ligand must not be too hard so as to strengthen the Pt-leaving ligand bond, by means of HSAB symbiosis, and thereby preventing the latter's reaction at the DNA.[34] Likewise it must not be too soft so as to allow the capture of the complex by a soft RS group in preference to the DNA. It has

been generally found that ligands containing nitrogen as the donor atom fall into this desirable category of ligand. The ligands used in this study are pyrazine, aniline and imidazole.

3.2 PREPARATION OF COMPOUNDS

3.2.1 Cis- *and* trans-[*Pt(pyrazine)*$_2$*X*$_2$], *(X = Cl, Br, I, NO*$_2$*)*

The *cis*-chloride, bromide and nitrite were prepared by adding an aqueous solution of K_2PtX_4 (1 mmol, 0.415 g for X = Cl; 0.593 g for X = Br and 0.457 g for X = NO_2) dropwise to a three-fold excess of aqueous pyrazine (3 mmol, 0.24 g) with stirring. The precipitation product was collected by filtration, washed successively with water, ethanol and ether and dried under reduced pressure over silica gel. *Cis*-[$Pt(pz)_2I_2$] was similarly prepared from an aqueous solution of K_2PtCl_4 (1 mmol, 0.415 g) to which KI (12 mmol, 2 g) had been added. The resultant solution was then added dropwise to the aqueous pyrazine solution (3 mmol, 0.24 g). It is essential that the Pt(II) salt solution is added to the excess pyrazine solution, as the reverse could lead to the formation of polymeric pyrazine complexes where the pyrazine forms a bridging structure via the two N atoms available for coordination.

The *trans*-complexes were obtained by dissolving the corresponding *cis*-complex (1 mmol, 0.426 g for X = Cl, 0.515 g for X = Br and 0.609 g for X = I) in a minimum volume of *N*,*N*-dimethylformamide (≈5 ml) at 70°C.

Pyrazine (4 mmol, 0.32 g) was added, the solution was refluxed for 15 minutes and allowed to cool. Concentrated HX (X = Cl, Br, I : ≈ 1 ml) was added to take up free pyrazine and to supply X^- ions. The resulting solution was warmed (10 minutes) and allowed to cool. Precipitation was induced by the addition of a molar solution of NaX (≈20 ml). The bright yellow crystals were collected, washed and dried as described for the *cis*-isomers. Due to the tendency of *cis*-$[Pt(pz)_2(NO_2)_2]$ to decompose with heat, the *trans*-$[Pt(pz)_2(NO_2)_2]$ was prepared by adding a large excess of $NaNO_2$ (12 mmol, 0.828 g) to a solution of K_2PtCl_4 (1 mmol, 0.415 g) in water. An excess of aqueous pyrazine (3 mmol, 0.08 g) was added. After 24 hours, the white crystals were collected and recrystallized from a warm (60°C) solution of *N*,*N*-dimethylformamide in water. The product was washed and dried as described for the *cis*-isomer.

The deuterated complexes were similarly prepared from pyrazine-d_4 of 98% isotopic purity supplied by Merck, Sharp and Dohme (Canada) Ltd.

3.2.2 Cis- *and* trans-$[Pt(aniline)_2X_2]$, $(X = Cl, Br, I, NO_2)$

The *cis*-complexes were prepared by adding a concentrated solution of freshly distilled aniline (2.5 mmol, 0.233 g) in ethanol (3 ml) to an aqueous solution of K_2PtX_4 (1 mmol, 0.415 g for X = Cl, 0.593 g for X = Br, 0.781 g for X = I and 0.457 g for X = NO_2). After a few minutes, precipitation occurred, and the pale grey products were collected by filtration, washed successively with water, ethanol and ether and dried under reduced pressure over silica gel.

The *trans*-complexes were prepared by dissolving the *cis*-isomers (1 mmol, 0.452 g for X = Cl, 0.541 g for X = Br, 0.635 g for X = I and 0.473 g for X = NO_2) in a minimum volume of *N*,*N*-dimethylformamide (5 ml) to which an excess of aniline (4 mmol, 0.372 g) was subsequently added. To the solution sufficient HX (X = Cl, Br, I : 1 ml) was added to take up free aniline and to supply X^- ions (for X = NO_2 aqueous $NaNO_2$ was used). The solution was warmed for a few minutes (60°C) and allowed to cool. Precipitation of the *trans*-complex was induced by adding a molar solution of NaX in water (≃ 20 ml). The products were collected, washed and dried as described for the *cis*-isomer.

The labelled complexes were similarly prepared from aniline-d_5 of 99% isotopic purity supplied by Merck, Sharp and Dohme (Canada) Ltd. and aniline-^{15}N of 97% isotopic purity supplied by BOC Prochem Ltd.

3.2.3 Cis- *and* trans-$[Pt(imidazole)_2X_2]$, *(X = Cl, Br, I,* NO_2*) and* $[Pt(imidazole)_4]X_2$, *(X = Cl, Br, I)*

Cis-$[Pt(Him)_2I_2]$ was prepared by dissolving K_2PtCl_4 (1 mmol, 0.415 g) in water (25 ml). KI (4 g) was added to yield a solution of approximately 0.05 *M* PtI_4^{2-} and 1 *M* I^-. Imidazole (2 mmol, 0.136 g) was added to this solution with stirring upon which the *cis*-compound precipitated immediately and was collected by filtration, washed with water, ethanol and ether and dried under reduced pressure over silica gel.

Cis-$[Pt(Him)_2X_2]$, (X = Cl, Br) was prepared by suspending the *cis*-diiodo compound (1 mmol, 0.585 g) in 50 ml of a 1 *M* aqueous solution of $NaNO_3$. To this was added an aqueous solution of $AgNO_3$ (2 mmol, 0.34 g). The suspension was stirred for one hour before the AgI precipitate was filtered, leaving the *cis*-diaquo complex in the filtrate. After the addition of a twentyfold excess of NaX (1.17 g for X = Cl, 2.06 g for X = Br) the *cis*-dichloro and *cis*-dibromo compounds precipitated. The products were collected, washed and dried as described for the *cis*-iodo complex.

Cis-$[Pt(Him)_2(NO_2)_2]$ was prepared by adding an aqueous solution of imidazole (2 mmol, o.136 g) to an aqueous solution of $K_2Pt(NO_2)_4$ (1 mmol, 0.457 g). The dinitrito complex precipitated after 15 minutes and was collected, washed and dried as described for the *cis*-iodo complex.

$[Pt(Him)_4]I_2$ was prepared by adding a large excess of imidazole (12 mmol, 0.816 g) to a concentrated solution of *cis*-$[Pt(Him)_2I_2]$ (1 mmol, 0.585 g) in acetone (≈50 ml). After approximately two days the desired compound crystallized. It was collected by filtration, washed with acetone and ether and dried under reduced pressure over silica gel.

$[Pt(Him)_4]X_2$, (X = Cl, Br) were prepared from *cis*-$[Pt(DMSO)_2X_2]$ (X = Cl, Br) (1 mmol, 0.422 g for X = Cl, 0.511 g for X = Br) dissolved in *N*,*N*-dimethylformamide (≈3 ml). A threefold excess of imidazole (0.816 g) was added to the respective solutions which were heated at 70°C for thirty minutes. The solutions were cooled and diluted with

with acetone upon which white precipitates formed. The products were collected, washed and dried as described for $[Pt(Him)_4]I_2$.

The *trans*-$[Pt(Him)_2X_2]$, (X = Cl, Br, I) were prepared by dissolving the *cis*-isomer (1 mmol, 0.402 g for X = Cl, 0.491 g for X = Br, 0.585 g for X = I) in *N*,*N*-dimethylformamide (≈5 ml) containing 1 g of $(CH_3CH_2)_4N^+X^-$ (X^- = Cl^-, Br^-, I^-). The solutions were refluxed for fifteen minutes upon which they turned from colourless to yellow. HX (X = Cl, Br, I) was added (≈1 ml) to bind free imidazole molecules and the solution was allowed to cool. Precipitation of the products was induced by adding about 25 ml of 1 *M* aqueous solution of NaX (X = Cl, Br, I). The yellow crystalline products were collected by filtration, washed with water, ethanol and ether and dried under reduced pressure over silica gel. *Trans*-$[Pt(Him)_2(NO_2)_2]$ was prepared in a similar fashion as the *trans*-halogen complexes with the exception that an excess of $NaNO_2$ (6 mmol, 0.414 g) was used to take up free imidazole.

The Him-d_3 labelled complexes were similarly prepared from 1,2,4,5-tetradeuteroimidazole (Him-d_4) of 98% isotopic purity supplied by Merck, Sharp and Dohme (Canada) Ltd. The deuteroimine (ND) groups of Him-d_4 undergo rapid exchange in aqueous or ethanolic solution to yield complexes comprising 2,4,5-trideuteroimidazole (Him-d_3).

3.3 ANALYSES OF COMPOUNDS

Table 1. Analytical data on the complexes *cis*- and *trans*-[Pt(pyrazine)$_2$X$_2$], (X = Cl, Br, I, NO_2)

Calculated	Calculated			Found		
	%C	%H	%N	%C	%H	%N
cis-[Pt(pz)$_2$Cl$_2$]	22.5	1.9	13.2	21.6	1.9	12.3
cis-[Pt(pz)$_2$Br$_2$]	18.6	1.6	10.9	18.1	1.6	10.6
cis-[Pt(pz)$_2$I$_2$]	15.8	1.3	9.2	15.8	1.3	9.0
cis-[Pt(pz)$_2$(NO_2)$_2$]	21.5	1.8	18.8	19.9	1.7	17.6
trans-[Pt(pz)$_2$Cl$_2$]	22.5	1.9	13.2	22.8	1.9	13.4
trans-[Pt(pz)$_2$Br$_2$]	18.6	1.6	10.9	18.7	1.6	10.0
trans-[Pt(pz)$_2$I$_2$]	15.8	1.3	9.2	15.7	1.3	8.9
trans-[Pt(pz)$_2$(NO_2)$_2$]	21.5	1.8	18.8	21.1	1.8	18.4

Table 2. Analytical data on the complexes *cis*- and *trans*-[Pt(aniline)$_2$X$_2$], (X = Cl, Br, I, NO_2)

Complex	Calculated			Found		
	%C	%H	%N	%C	%H	%N
cis-[Pt(an)$_2$Cl$_2$]	31.9	3.1	6.2	32.5	3.2	6.5
cis-[Pt(an)$_2$Br$_2$]	26.6	2.6	5.2	26.5	2.6	5.2
cis-[Pt(an)$_2$I$_2$]	22.7	2.2	4.4	23.0	2.4	4.5
cis-[Pt(an)$_2$(NO_2)$_2$]	30.4	3.0	11.8	30.4	3.0	11.8
trans-[Pt(an)$_2$Cl$_2$]	31.9	3.1	6.2	32.3	3.2	6.2
trans-[Pt(an)$_2$Br$_2$]	26.6	2.6	5.2	26.0	2.5	5.1
trans-[Pt(an)$_2$I$_2$]	22.7	2.2	4.4	22.7	2.3	4.6
trans-[Pt(an)$_2$(NO_2)$_2$]	30.4	3.0	11.8	31.6	3.1	11.7

Table 3. Analytical data on the complexes *cis*- and *trans*-$[Pt(Him)_2X_2]$, (X = Cl, Br, I, NO_2) and $[Pt(Him)_4]X_2$, (X = Cl, Br, I).

Complex	Calculated			Found		
	%C	%H	%N	%C	%H	%N
cis-$[Pt(Him)_2Cl_2]$	17.9	2.0	13.9	17.7	2.1	13.9
cis-$[Pt(Him)_2Br_2]$	14.7	1.6	11.4	14.6	1.7	11.2
cis-$[Pt(Him)_2I_2]$	12.3	1.4	9.6	12.1	1.4	9.4
cis-$[Pt(Him)_2(NO_2)_2]$	17.0	1.9	19.9	16.8	2.1	19.3
$[Pt(Him)_4]Cl_2$	26.7	3.0	20.8	26.3	3.05	20.0
$[Pt(Him)_4]Br_2$	23.0	2.6	17.9	23.4	2.7	18.0
$[Pt(Him)_4]I_2$	20.0	2.2	15.5	20.6	2.4	15.6
trans-$[Pt(Him)_2Cl_2]$	17.9	2.0	13.9	18.3	2.1	14.1
trans-$[Pt(Him)_2Br_2]$	14.7	1.6	11.4	15.0	1.7	11.3
trans-$[Pt(Him)_2I_2]$	12.3	1.4	9.6	12.9	1.4	9.3
trans-$[Pt(Him)_2(NO_2)_2]$	17.0	1.9	19.9	17.6	1.9	19.0

TABLE 4

Mid-i.r. frequencies of complexes cis-$[Pt(pz)_2X_2]$ (cm^{-1})

Cl	Cl d_4	Br	Br d_4	I	I d_4	NO_2	NO_2 d_4	Ratio d_4/h_4	Assignment	
3104						3094				13
3086	2336	3088	2332	3080	2332	3076	2322	0.76±0.01		20b
	2312	3066	2306	3070	2305	3058	2310	0.75±0.01	νC-H	2
3056	2292	3044	2288	3044	2282	3035	2292	0.75±0.01		7b
3030	2277	3022	2268	3022	2270	3010		0.75		
2984	2246	2980[a]		2976		2988		0.75		
1590	1554	1586[a]	1547	1585	1548	1596	1566	0.98		8a
1514	1497	1515	1498	1518	1499	1523		0.99		8b
1482	1314	1481	1310	1484	1319	1486	1342	0.89±0.01	ν ring	19a
1467	1295	1477	1293	1478	1290			0.88±0.01		19a
	1274		1272		1270		1279			19a
1413	1168	1407	1172	1411	1171	1417	1170	0.83		19b
						1408	1407	1.00	νNO_2 asym.	
		1384	1154	1384	1151	1396		0.83	ν ring	19b
1375		1371[a]		1362		1356				
1341		1331[a]		1335		1337[a]				
						1329	1333	1.00	νNO_2 sym.	
1153	1133	1153	1133	1155	1128	1158	1135	0.98	ν ring	12
1118	833[a]	1115	832[a]	1114	831[a]	1121	834[a]	0.75±0.01	δC-H	18a
1077	1055[a]	1080	1049	1071	1049[a]	1076	1063	0.98±0.01		14
1072	1028	1066	1021	1063	1022		1056	0.96	ν ring	14
1013	869	1012	863	1013	862	1014	873	0.86±0.01		1
969[a]		973[a]		969[a]		983[a]			γC-H	5
						913	908	0.99	δNO_2	
802	631[a]	807	629[a]	801	644[a]	816[a]	648[a]	0.79±0.02	γC-H	10b
739	603	739	600	736	604	744[a]	611[a]	0.83±0.01	γ ring	11
721	711	722	721	721	721	721	721	1.00±0.01		11
697	687	694	690	693	697	697	697	1.00±0.01		4
	665		661		668		675		δ ring	4
653	603	656	618	652	633	657[a]	615	0.94±0.03		6a
		648	600	647	604	612	606	0.95±0.04		6a
						581			NO_2 wag	
486	466	488	455	486	445	486	469	0.95±0.03	γ ring	16b
478	446	475	444	468	428	469	440	0.93±0.02		16b

[a] Mean of doublet.

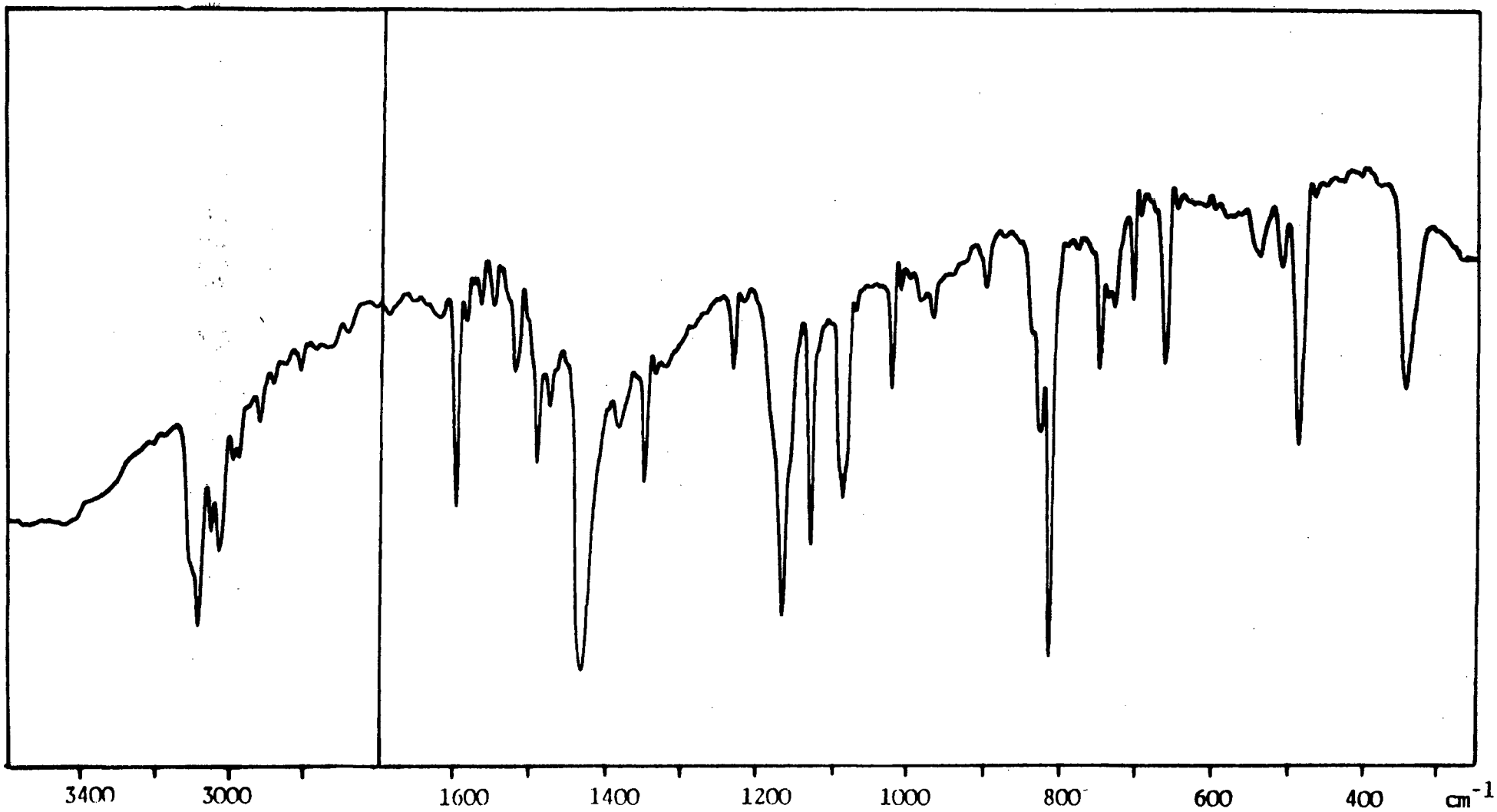

Figure 3. The infrared spectrum of *cis*-$[Pt(pz)_2Cl_2]$

TABLE 5

Mid-i.r. frequencies of complexes trans-$[Pt(pz)_2X_2]$ (cm^{-1})

Cl	Cl d_4	Br	Br d_4	I	I d_4	NO_2	NO_2 d_4	Ratio d_4/h_4	Assignment	
3100		3096		3092		3092	2340	0.76		13
3088	2334	3084	2334	3080	2334			0.76±0.01		20b
3074	2317	3068	2314	3067	2308	3074	2316	0.75	νC-H	2
3056	2295		2290		2282		2292	0.75		7b
3023	2278	3021	2276	3023	2272	3032	2270	0.75		
2980	2250		2248	2974		2984		0.75		
1591	1551	1590	1552	1589	1550	1596	1557	0.98±0.01		8a
1522	1503	1519	1502	1518	1503	1523	1500	0.99±0.01		8b
1485	1316	1485	1316	1481	1315		1334	0.89		19a
	1277		1277				1277		ν ring	19a
1417	1179	1421	1177	1418	1174	1428	1179	0.83		19b
1406	1162	1408	1162	1399	1159	(1398)	1164	0.83		19b
						1398	1404	1.00	νNO_2 asym.	
						1332	1334	1.00	νNO_2 sym.	
1343		1340		1336		(1332)				
1158	1134	1158	1134	1156	1133	1153	1137	0.98±0.01	ν ring	12
1118	836	1117	833[a]	1115	833[a]	1117	830[a]	0.75±0.01	δC-H	18a
1082	1057	1081	1054	1082	1052	1081	1058	0.98±0.01		14
1073	1029	1073	1027	1074	1026		1031	0.96	ν ring	14
1012	864	1012	865	1014	862	1011	871	0.85±0.01		1
						981[a]	993	1.01	δNO_2	
969[a]		973[a]								5
815	632	819[a]	631	819[a]	630	820[a]	641	0.78±0.01	γC-H	10b
742	613	741	613	741	611	744	617	0.83±0.01		11
721	721	722	722	721	721	721	720	1.00	γ ring	11
701	678	699	676	697	676	695	672	0.97		4
693	665	693	666	693	664		666	0.96		4
653	613	653	613	652	611	662	617	0.94±0.01	δ ring	6a
						620	617	1.00	NO_2 wag	
504	467	506	469	505	469	502	467	0.93	γ ring	16b

[a]Mean of doublet

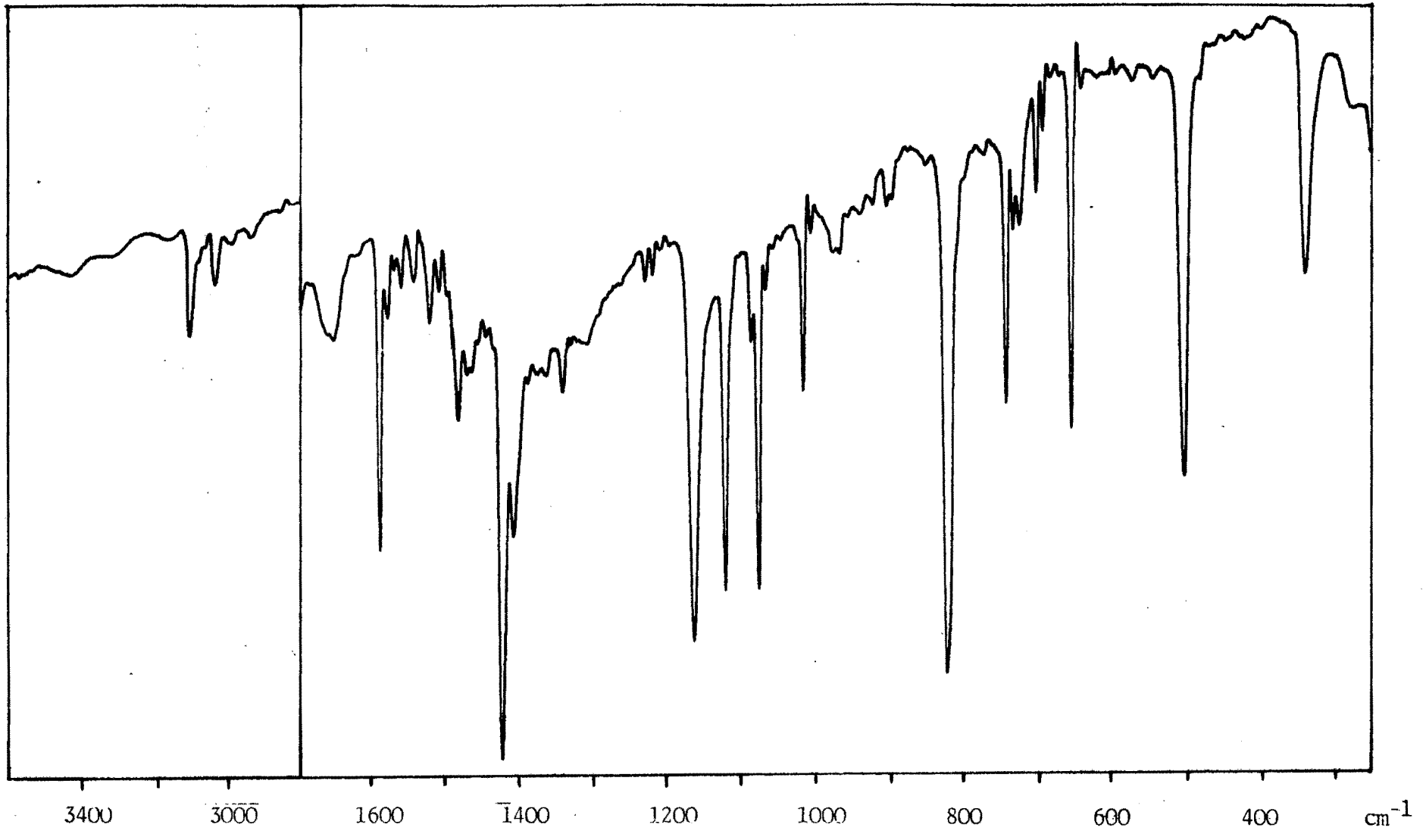

Figure 4. The infrared spectrum of *trans*-$[Pt(pz)_2Cl_2]$

TABLE 6

Far-i.r. frequencies (cm^{-1}) of complexes cis- and trans-$[Pt(pz)_2X_2]$ with d_4-sensitivities in parentheses.

X = Cl	X = Br	X = I	$X = NO_2$	Assignment
trans-$[Pt(pz)_2X_2]$				
504(37)	506(37)	505(36)	502(35)	ligand γ ring
344(2)	208 (6)	180(2)	303(0)	νPt-X
286(13)	300(10)	289(12)	275(12)	νPt-pz
222(9)	244(6)	233(6)	226(7)	δpz-Pt-pz
166(0)	169(0)	121(0)	245(2)	δpz-Pt-X and
27(0)	122(0)	88(0)	162(0)	δX-Pt-X
122(0)	87(0)		135(0)	
			100(0)	
cis-$[Pt(pz)_2X_2]$				
486(20)	488(33)	486(41)	486(17)	ligand γ ring
478(32)	475(31)	468(40)	469(29)	
342(0)	217(3)	173(2)	321(0)	νPt-X
338(0)	189(5)	167(4)	303(0)	
255(10)	255(2)	230(13)	229(10)	νPt-pz
226(4)	233(10)	222(10)	224(5)	
203(4)			209(17)	δpz-Pt-pz
169(0)	189(1)	122(3)	133(0)	δpz-Pt-X and
126(0)	170(0)	88(0)		δX-Pt-X
122(0)	126(0)			
	121(0)			

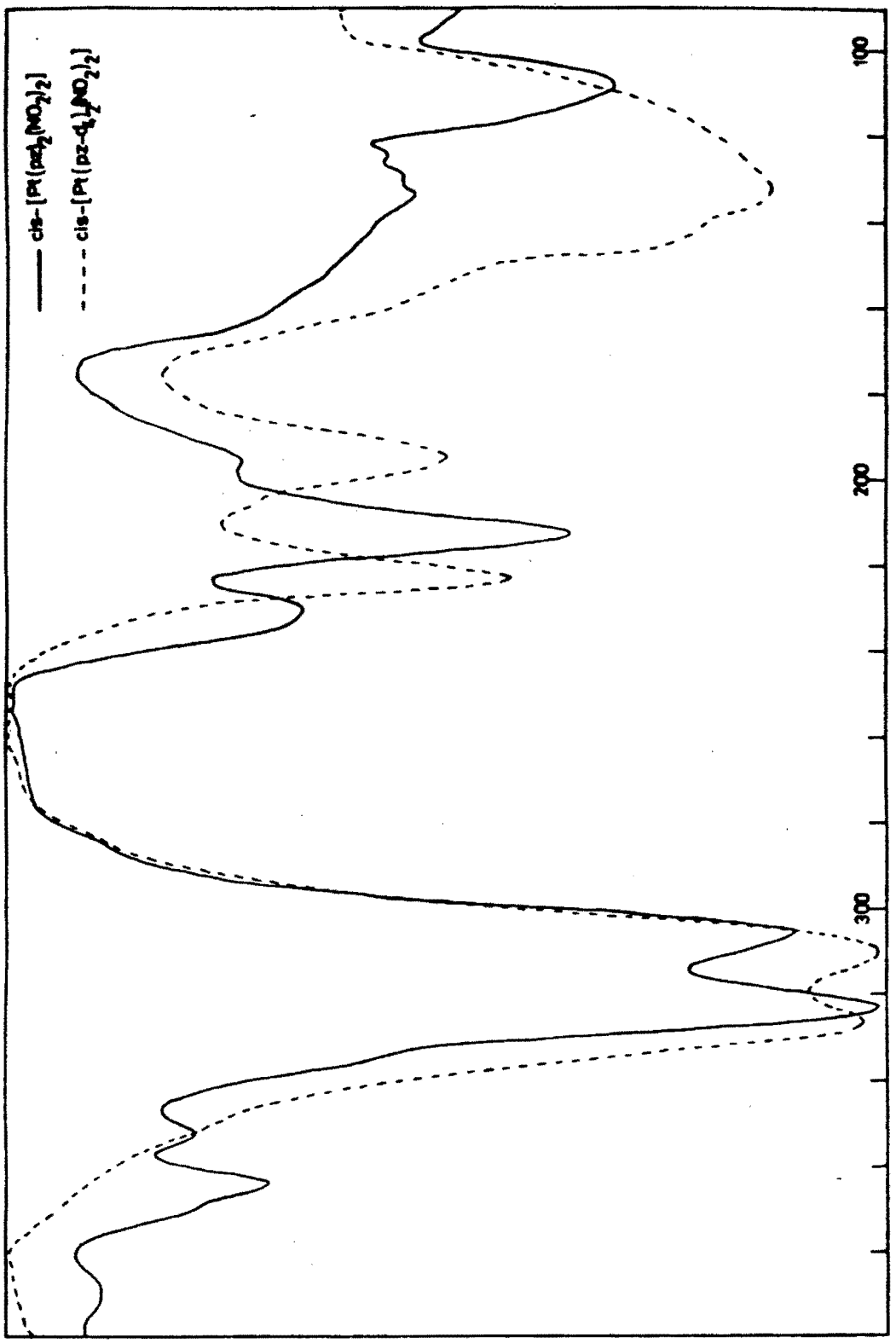

Fig. 5. Far-infrared spectra of *cis*-$[Pt(pz)_2(NO_2)_2]$ and its pz-d_4 labelled analogue.

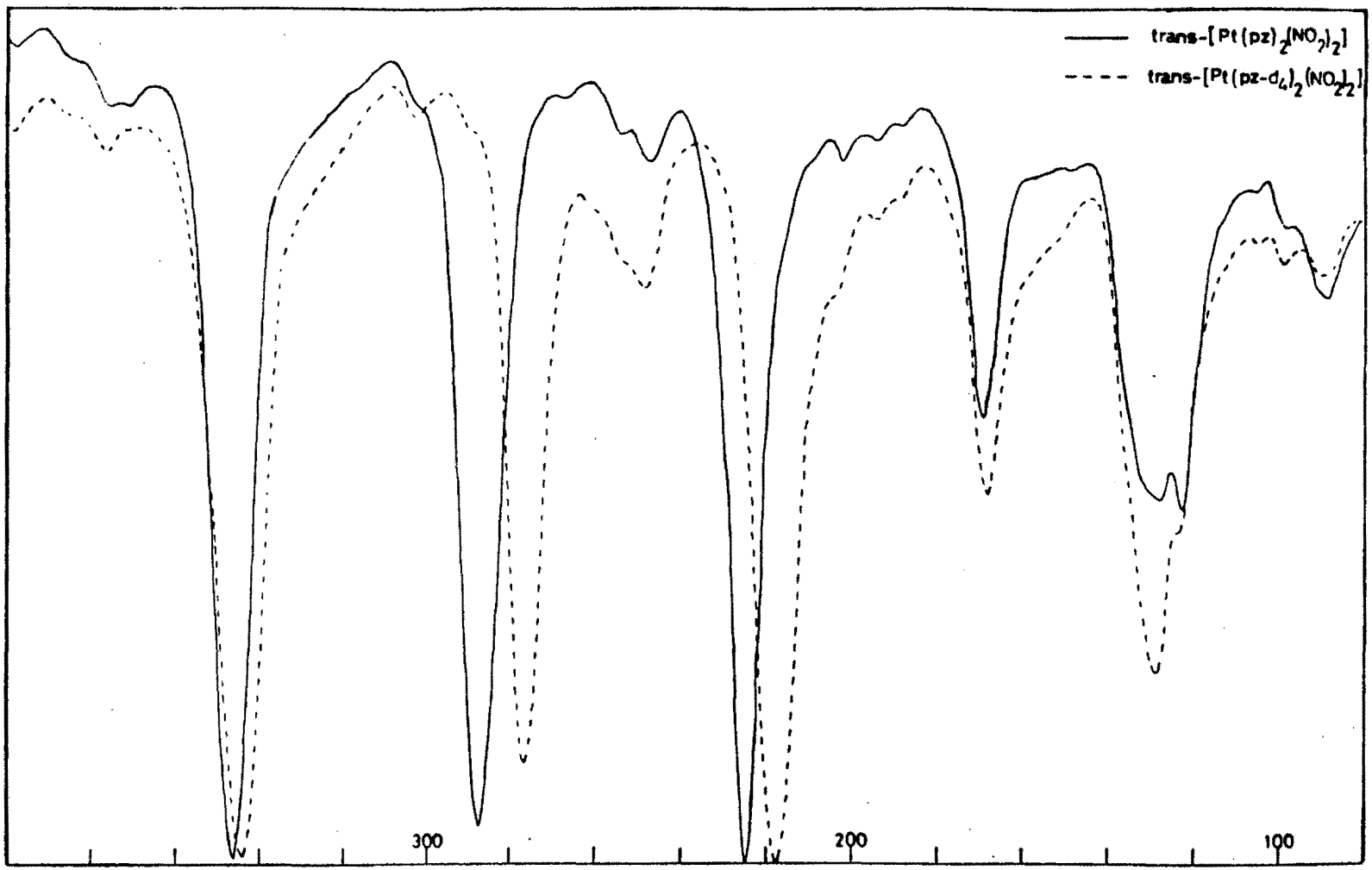

Fig. 6. Far-infrared spectra of *trans*-$[Pt(pz)_2(NO_2)_2]$ and its pz-d_4 labelled analogue.

TABLE 7.

Internal frequencies (cm^{-1}) in cis-$[Pt(an)_2X_2]$.

Cl[a]	Cl d_5	Br	Br d_5	I	I d_5	NO_2	NO_2 d_5	Ratio d_5/h_5	Assignment
3252(6)	3252	3236	3220	3226	3227	3286	3289	1.00±0.01	νN-H
3210(6)	3210	3191	3186	3195	3196	3206	3210	1.00	
3130(2)	3129	3124	3125	3109		3125	3127[b]	1.00	νN-H...X
3050(0)	2372		2346	3046	2354[b]	3054	2357[b]	0.77±0.01	νC-H
	2280		2280		2275		2280	0.75	
1589(5)	1563	1569[b]	1564	1570	1565	1584	1565	0.99±0.01	NH_2 scissor
1598(0)	1592	1596[b]	1595	1601	1587	1598	1575	0.99±0.01	ν ring
1493(0)	1420	1494	1419	1493	1420	1493	1419	0.95	
1467(0)	1382	1468	1382	1463	1380	1468	1396	0.94±0.01	
1275(-)		1330		1339		1324	1318	0.99	
1191(tb)	1194[b]	1204	1172	1210	1202	1222	1212	0.99±0.02	
1175(5)	1140	1177	1136	1187	1173	1193	1195	0.98±0.02	νC-N
1164(0)	841	1160	838	1160	837	1166	837	0.72	δC-H
1069(0)	817	1069	815	1069	813	1071	818	0.76	
1028(0)	776	1028	772	1031	765	1027	789	0.75±0.02	
1004(0)	749	1005	752	1004	752	1004	752	0.75	
1120(sh)	1122					1149	1147	1.00	NH_2 twist
979(0)		971		976[b]		971			
899(0)	640	898	628	920	630	915	651	0.70±0.02	γC-H
854(0)	835	849	838			837	831	0.99±0.01	
806(7)	594	802	599	801	594	798	595	0.75±0.01	γC-H
758(1)	547	758	542	757	541	769	550	0.72±0.01	
689(1)	443	690		693		693	430	0.63±0.01	
720(11)		706	708	723	724	725	728	1.00	NH_2 wag
668(0)	659[b]	684	660			669	651	0.97±0.02	δ ring
617(0)	594	617	599	619	594	617[b]	609	0.97±0.02	
544(0)	519	542	507	540	504	540	515	0.94±0.01	
577(8)	567	570	565	578	562	586	563	0.98±0.02	NH_2 rock
507(-)						504[b]			
452(6)	410	449[b]	407	438	404	450[b]	417[b]	0.92±0.01	
222(0)	210	222	212	226	213	213	203	0.95±0.01	γ ring
						1418[b]	1419	1.00	νNO_2 asym.
						1355	1354	1.00	νNO_2 sym.
						831	831	1.00	δNO_2
						610	609	1.00	NO_2 wag

[a] Figures in parentheses are the ^{15}N-induced shifts (cm^{-1}). tb = too broad for shift to be determined, sh = shoulder.

[b] Mean of doublet.

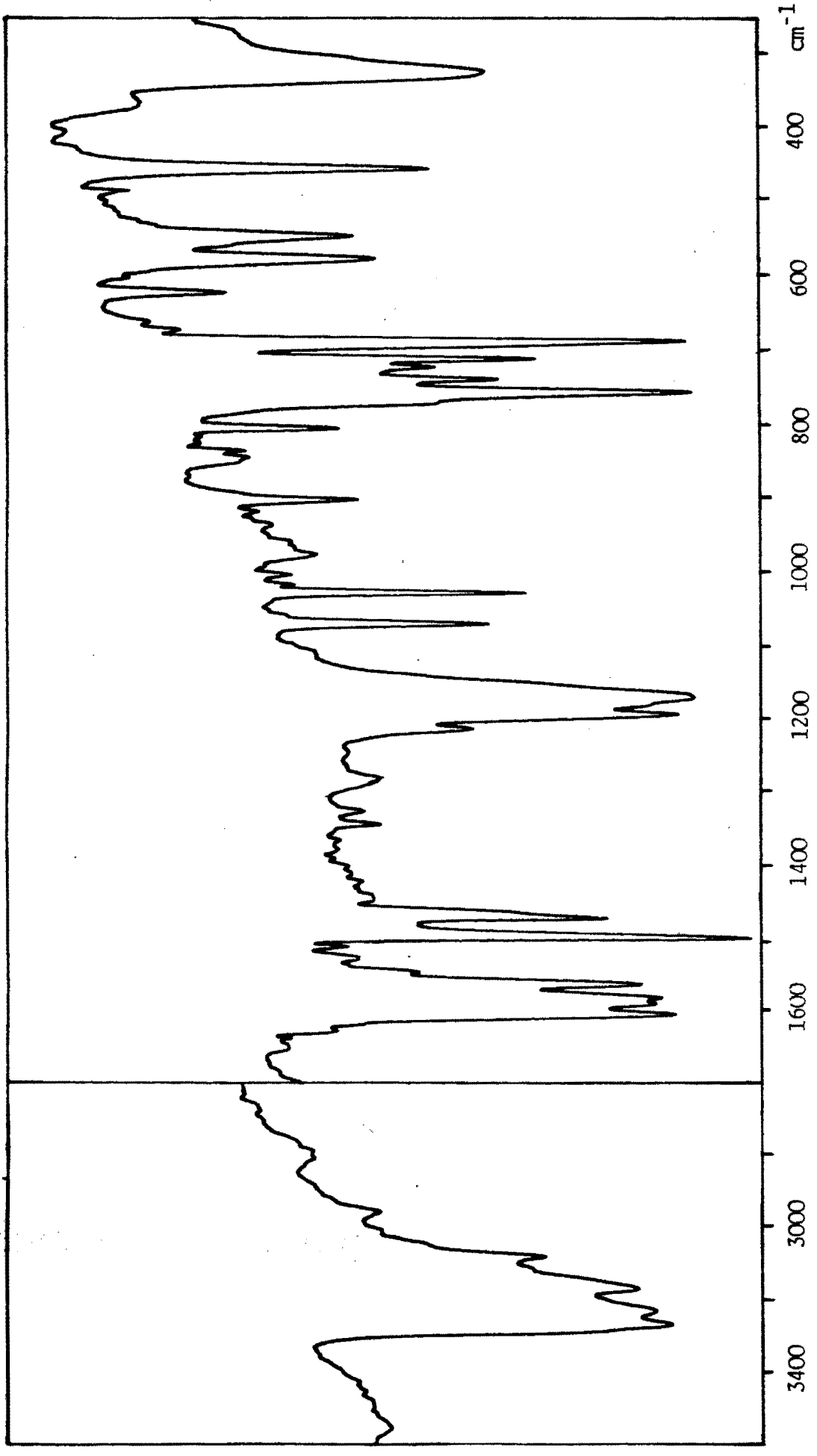

Figure 7. The infrared spectrum of *cis*-$[Pt(an)_2Cl_2]$

TABLE 8.

Internal ligand frequencies (cm^{-1}) in *trans*-$[Pt(an)_2X_2]$.

Cl[a]	Cl d_5	Br	Br d_5	I	I d_5	NO_2	NO_2 d_5	Ratio d_5/h_5	Assignment
3253(8)	3253	3233	3233	3219	3219	3243	3242	1.00	νN-H
3190[b](7)	3190[b]	3204	3205	3193	3198	3150	3146	1.00	νN-H
3127(1)	3128[b]	3130	3134	3126	3124			1.00	νN-H....X
3083(tb)	2392[b]	3042	2380	3073	2378		2350	0.78 0.01	νC-H
3046(tb)			2273[b]	3035	2268[b]			0.75	νC-H
1588(3)	1561	1579[b]	1571[b]	1578	1567[b]	1600	1571[b]	0.99 0.01	NH_2 scissor
1597(0)	1592	1598	1591	1597	1582	1608	1603	1.00 0.01	ν ring
1491(0)	1426	1494	1436	1495	1424[b]	1495	1407	0.95 0.01	ν ring
1467(0)	1382	1466	1382	1466	1380	1471	1381	0.94	ν ring
1343(0)	1300	1343	1299	1342	1300	1337		0.97	ν ring
1190(3)	1191[b]	1201[b]	1200	1201[b]	1200	1208[b]	1205[b]	1.00	ν ring
1173(th)	1140	1174	1140	1173	1134	1184	1137	0.97 0.01	νC-N
1163(sh)	841	1148	841	1150	841	1150	837	0.73 0.01	δC-H
1069(0)	817	1069	818	1070	814	1072	823	0.76 0.01	δC-H
1028(0)	766	1029	764	1027	762	1025	750	0.74 0.01	δC-H
1147(sh)	1126	1148	1113	1150	1134	1150	1137	0.98 0.01	NH_2 twist
898(0)	641	903[b]	643		641	907	650	0.71 0.01	γC-H
856(1)	835	850	833	841	835	823	823	0.99 0.01	
806(7)	593	807	594	807	593	803	597	0.74	γC-H + NH_2 wag
785(9)	749	782	744	777	747		728	0.96 0.01	NH_2 wag
757(0)	547	756	548	754	545	754	543	0.72	γC-H
688(0)		691[b]		687		691			γC-H
617(1)	593	617	594	618	593	625	597	0.96 0.01	δ ring
577(8)		575	570	580	570	587	576	0.98 0.01	δ ring
561(6)	520	560	519	558	520	554	525	0.94 0.01	NH_2 rock
		526							NH_2 rock
449(4)	441	461[b]	414	445	409	458	417	0.91 0.01	NH_2 rock
220	208	227	215	221	211	221	210	0.95 0.01	γ ring
						1406	1407	1.00	$νNO_2$ asym.
						1337	1337	1.00	$νNO_2$ sym.
						823	823	1.00	$δNO_2$
						625	625	1.00	NO_2 wag

[a] Figures in parentheses are the ^{15}N-induced shifts (cm^{-1}), tb = too broad for shift to be determined, sh = shoulder.

[b] Mean of doublet.

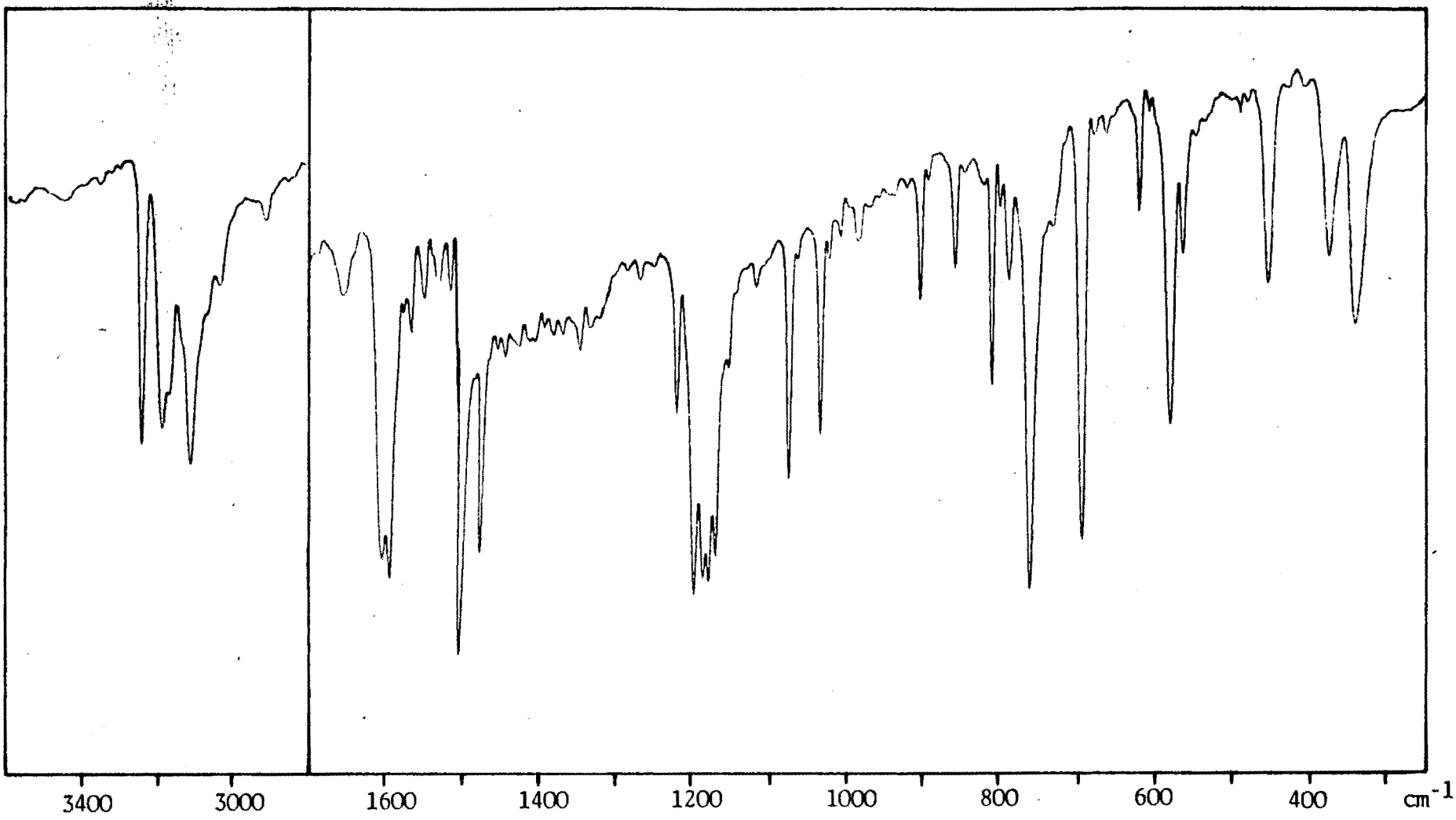

Figure 8. The infrared spectrum of *trans*-$[Pt(an)_2Cl_2]$

TABLE 9.

Far-infrared frequencies (cm^{-1}) for the complexes $[Pt(an)_2X_2]$.

X = Cl (^{15}N-, d_5-shift)	X = Br (d_5-shift)	X = I (d_5-shift)	X = NO_2 (d_5-shift)	Assignment
cis-$[Pt(an)_2X_2]$				
451(5,41)	446(39)	439(36)	450(29)[a]	NH_2 rock
374(4,11)	367(12)	350(10)[a]	370(7)[a]	νPt-an
330[a](0,0)	223(0)	167(7)[b]	332(0)[a]	νPt-X
293(2,10)	290(10)[a]	300(10)	298(10)	νPt-an
220[a](0,12)	236(7)[a]	217(10)[a]	215(10)	γ ring
177(2,5)	171(5)	167(7)[c]	178(8)	δan-Pt-an
147(0,3)	141(1)	134(3)	144(2)[a]	δan-Pt-X
109(tb)[d]	107(0)	98(-)	105(0)	δX-Pt-X
trans-$[Pt(an)_2X_2]$				
449(5,38)	461(47)[a]	445(36)	458(40)	NH_2 rock
374(4,12)	383(12)[a]	366(10)	387(14)	νPt-an
340(0,0)	234(0)	168(5)[b]	312(0)	νPt-X
222(0,13)	240(12)	213(8)[a]	223(12)	γ ring
177(0,5)	177(6)	168(5)[c]	179(7)	δan-Pt-an
142(0,2)	140(0)	146(5)	148(4)[a]	δan-Pt-X
121(0,0)	114(0)	97(0)	117(0)	δX-Pt-X

[a] Mean of split peak.

[b] Coincident with δan-Pt-an.

[c] Coincident with νPt-X.

[d] Too broad for shift to be determined.

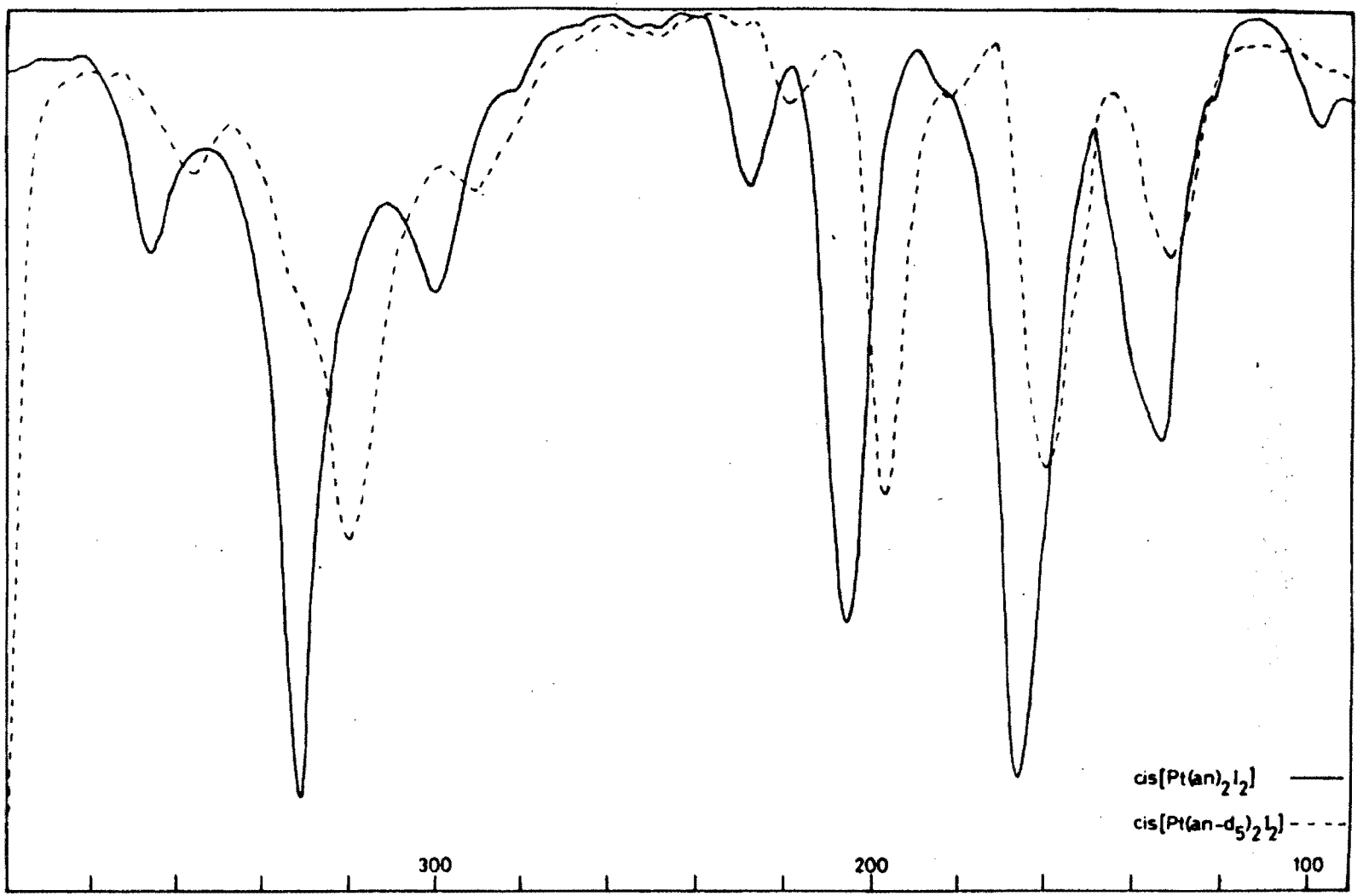

Fig. 9. Far-infrared spectra of *cis*-$[Pt(an)_2I_2]$ and its an-d_5 labelled analogue.

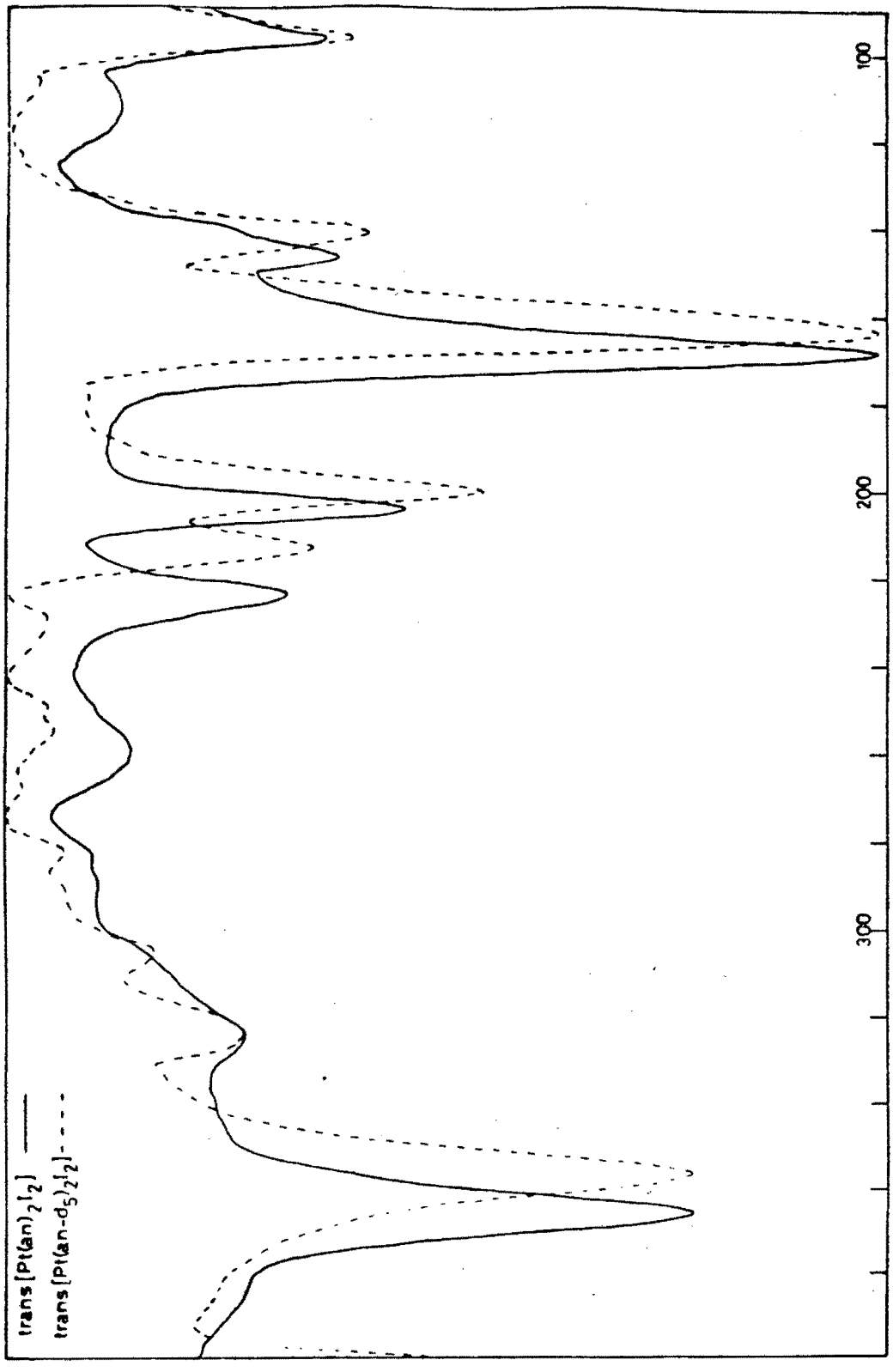

Fig. 10. Far-infrared spectra of *trans*-[Pt(an)$_2$I$_2$] and its an-d_5 labelled analogue.

TABLE 10.

Vibrational frequencies for the complexes *cis*-[Pt-(Him)$_2$X$_2$] and *cis*-[Pt(Him-d_3)$_2$X$_2$] (cm^{-1})

Cl	Cl d_3	Br	Br d_3	I	I d_3	NO_2	NO_2 d_3	Ratio d_3/h_3	Assignment
3240[a]	3240[a]	3215[a]	3215[a]	3281	3279	3290	3286	1.00	νN-H
3132	2362	3130	2350	3128	2350	3164	2380	0.75	νC-H
	2348					3142	2342	0.75	
1544	1490	1540	1493	1539	1490	1555	1472[a]	0.96±0.01	ν ring
1502	1460	1505	1463	1500	1459	1521		0.97	
1432	1407	1430	1404	1430		1412	1406	0.98±0.01	
						1359	1356	1.00	νNO_2
1266	945	1271[a]	948	1262	940	1270	941	0.75±0.01	δC-H
1241	1201[a]	1230	1190	1225	1203	1222	1195	0.97±0.01	δN-H
1185	1154	1180	1150	1177	1150	1139	1129	0.98±0.01	ν ring
1140		1135		1137		1144			
1090[a]	882[a]	1089[a]	882[a]	1093[a]	880[a]	1099[a]	897	0.81±0.01	δC-H
1070	822	1069	821	1068	821	1073	833[a]	0.77±0.01	
962	978	964	977	960	973	965	978	1.01±0.01	δ ring
918	723	919	742	918	736	914	737	0.81±0.01	γC-H
848	754	845	767	840	769	837	781	0.91±0.02	δ ring
795	661	785		772	648	828	656	0.82±0.03	γC-H
						828	827	1.00	δNO_2
738	608	764	605	759	596	764	617	0.80±0.01	γC-H
	680	722	719	701	701	725	718	0.98±0.05	γN-H
665	587	662		658	578		593	0.87±0.03	γ ring
656	559	652	558	649	560[a]	657	582	0.86±0.02	
						657	656	1.00	NO_2 wag
621	533	615	530	609	524	619	521	0.85±0.01	γ ring
323	323	213	213	171	171	315	315	1.00	νPt-X
		203	203	166	166	307	307	1.00	
291	284	291	282	280	272	227	221	0.97	νPt-Him
278	271	278	273	265	258	208	202	0.97±0.01	
236	223	247	246	226	226	247	247	0.98±0.04	δL-Pt-L
167	166	170	170					1.00±0.01	
		151	150	150	150	151	151	1.00±0.01	
126	123	121	121	120	120	121	121	1.00±0.02	

[a] Mean of doublet.

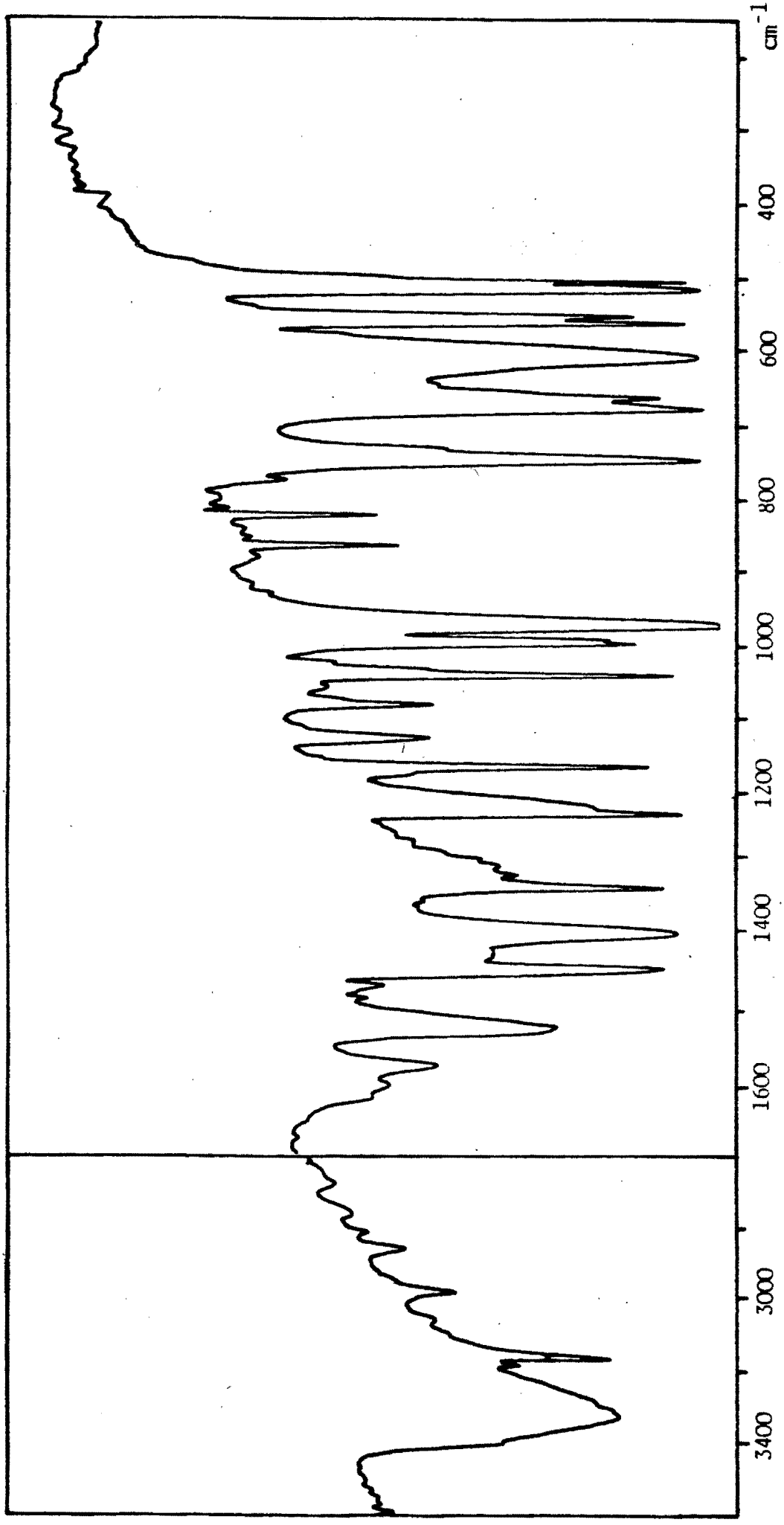

Figure 11. Infrared spectrum of *cis*-$[Pt(Him)_2I_2]$

TABLE 11.

Vibrational frequencies for the complexes *trans*-[Pt(Him)$_2$X$_2$] and *trans*-[Pt(Him-d_3)$_2$X$_2$ (cm^{-1})

Cl	Cl d_3	Br	Br d_3	I	I d_3	NO_2	NO_2 d_3	Ratio d_3/h_3	Assignment
3318	3318	3315	3317	3265	3265			1.00	νN-H
3146	2346	3143	2344	3147	2370	3152	2378	0.75	νC-H
3137	2333	3124	2326	3130	2356	3144	2342	0.74±0.01	
1542	1490	1542	1474	1547	1470	1554	1474	0.96±0.01	ν ring
1502[a]	1474	1503	1462	1504	1458	1513	1463	0.97±0.01	
1434	1407	1430	1400	1433		1440	1407	0.98	
						1403	1401	1.00	νNO_2
1333	1285	1332	1288	1334		1333		0.97±0.01	ν ring
1265	940	1266	941	1270	942	1272	947	0.74	δC-H
1230	1190[a]	1225	1195[a]	1264	1196[a]	1242	1206	0.97±0.02	δN-H
1178	1151	1175	1178	1137	1148	1192	1159	0.99±0.02	ν ring
1131		1128				1149			
1104	889[a]	1102[a]	884[a]	1098	884[a]	1103	886[a]	0.81±0.01	δC-H
1070	822	1069	816	1069	819	1075	828	0.77±0.01	
963	940	962	941	963	979	968	981	1.00±0.02	δ ring
919	733	916	737	917	735	916	727	0.80±0.01	γC-H
862	769	858	778		777	875	775	0.90±0.01	δ ring
842	657	834	647	825	645	827	637	0.78±0.01	γC-H
						827	828	1.00	δNO_2
752	572	749	586	748	587	772	581	0.77±0.02	γC-H
708	707	706	699	707	717	752		1.00±0.01	γN-H
657	557	659[a]	554	656	559	659	566	0.85±0.01	γ ring
						648	648	1.00	NO_2 wag
613	523	609	511	605	518	619	527	0.85±0.01	γ ring
						364	363	1.00	NO_2 rock
350	350	224	224	179	179	326	322	1.00±0.01	γPt-X
287	280	313	301	301	292	280	272	0.97±0.01	γPt-Him
244	244	246	246	255	255			1.00	
226	226			228	228	228	228	1.00	
186	185	187	178	204	204	210	210	0.98±0.03	δL-Pt-L
156	151	158	158	158	158	180	179	0.99±0.02	
132	132			141	141	155	155	1.00	
121	121	120	120	124	124	132	132	1.00	

[a] Mean of doublet.

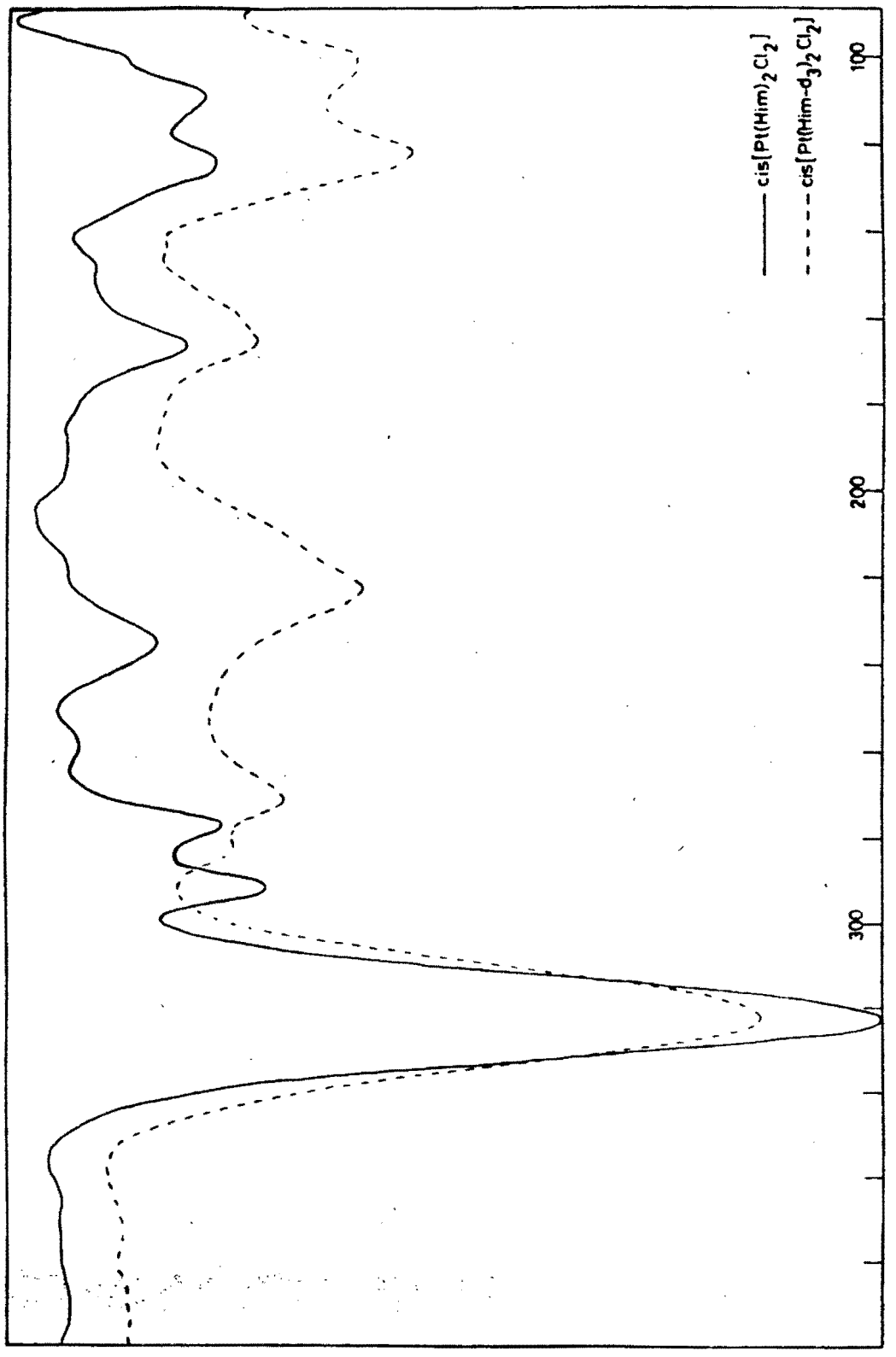

Fig. 12. Far-infrared spectra of *cis*-$[Pt(Him)_2Cl_2]$ and its Him-d_3 labelled analogue.

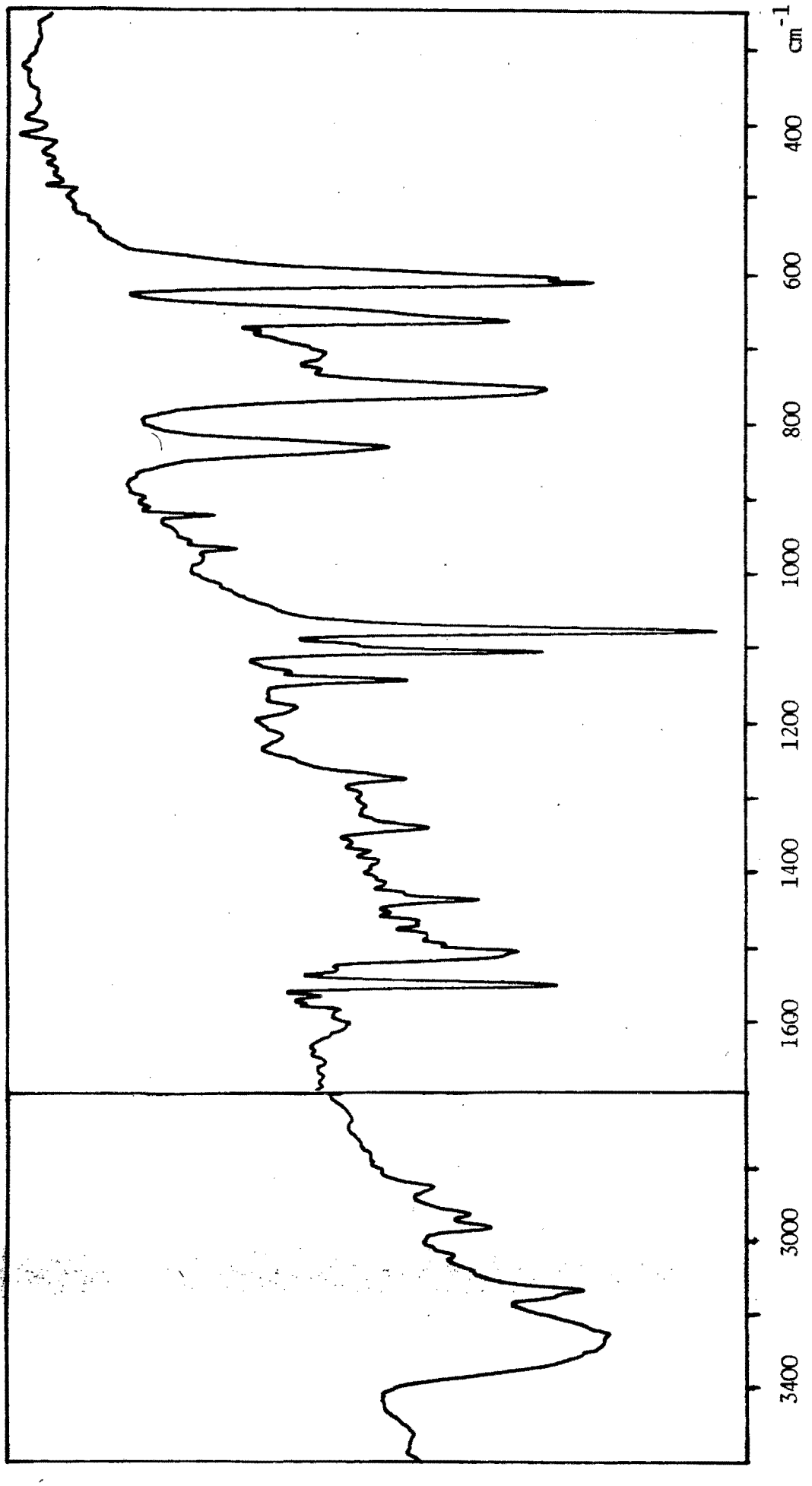

Figure 13. Infrared spectrum of *trans*-$[Pt(Him)_2I_2]$

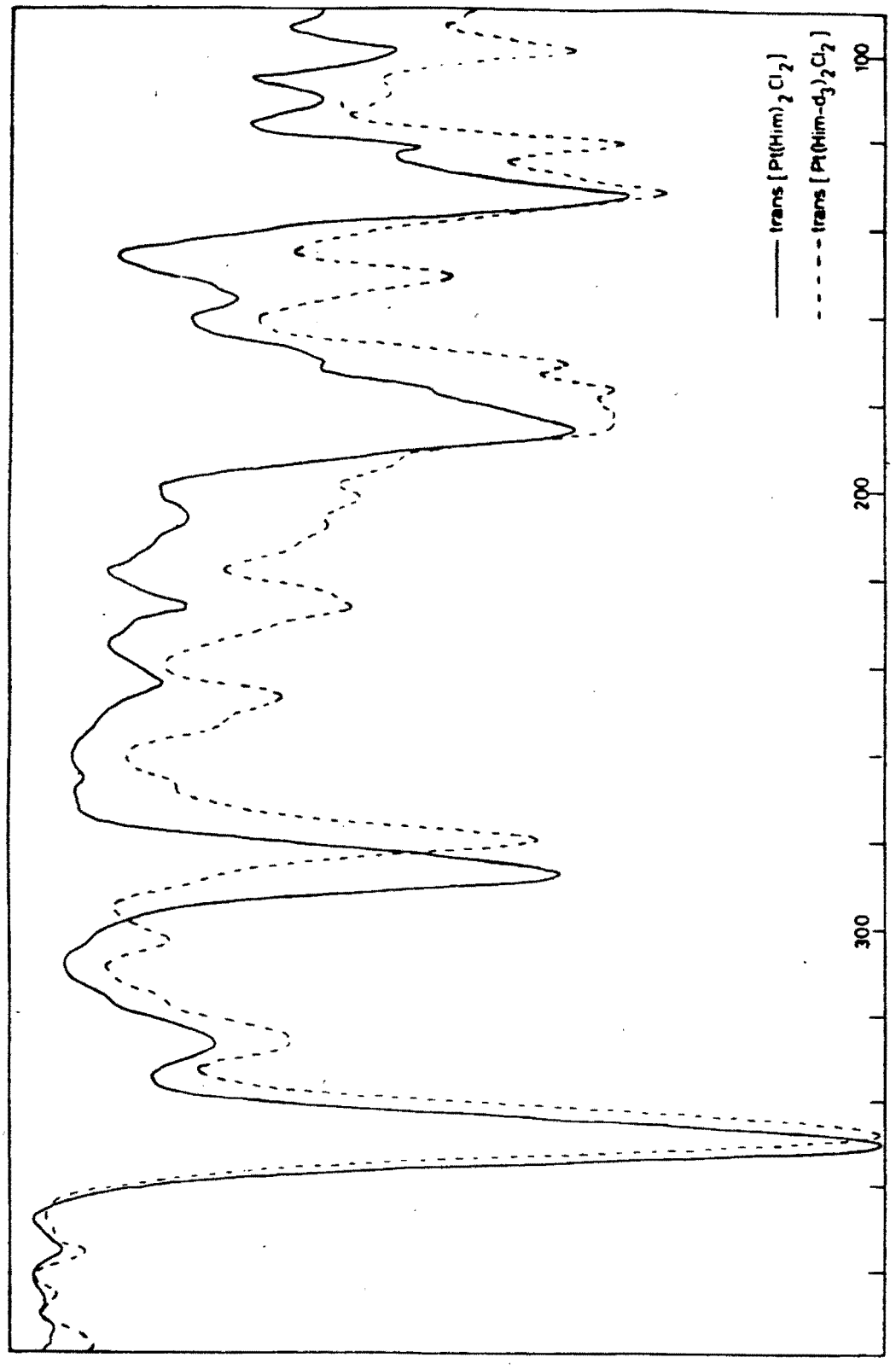

Fig. 14. Far-infrared spectra of *trans*-[Pt(Him)$_2$Cl$_2$] and its Him-d_3 labelled analogue.

TABLE 12.

Vibrational frequencies for the complexes $[Pt(Him)_4]X_2$ and $[Pt(Him\text{-}d_3)_4]X_2$ (cm^{-1})

Cl	Cl d_3	Br	Br d_3	I	I d_3	Ratio d_3/h_3	Assignment
3110	2326	3102	2322	3100	2320	0.75	ν C-H
1541	1491	1541	1488	1541	1479	0.97±0.01	ν ring
1505	1455	1501	1455	1497	1454	0.97	ν ring
1429	1406	1428	1402	1429	1406[a]	0.98	ν ring
1327	1292	1336	1289	1334	1302	0.97±0.01	ν ring
1270	939[a]	1269	936[a]	1266	938[a]	0.74	δ C-H
1255	1199[a]	1250	1196[a]	1244	1201[a]	0.96±0.01	δ N-H
1187	1126	1184	1125	1181	1131[a]	0.95±0.01	ν ring
1141		1137		1133			
1092	884[a]	1095	883[a]	1097	883[a]	0.81±0.01	δ C-H
1069	817	1068	816	1068	820	0.76±0.01	δ C-H
965	983	963	981	960	987	1.02±0.01	δ ring
911	742	915	743	915	733	0.81±0.01	γ C-H
870	783	870	779	861	775	0.90	δ ring
850	660	854	660	854	657	0.77±0.01	γ C-H
765[a]	581	767[a]	578	767[a]	573	0.75±0.01	γ C-H
722	721	721		726	723	1.00	γ N-H
671[a]	547	670[a]	543	665	537	0.81±0.01	γ ring
617	527	615	526	611	526	0.86±0.01	γ ring
237	255	270	255	266	256	0.94±0.02	ν Pt-N
150	148	150	141	149	148	0.97±0.03	δ N-Pt-N
120	120	120	122	118	116	1.00±0.02	lattice

[a] Mean of doublet.

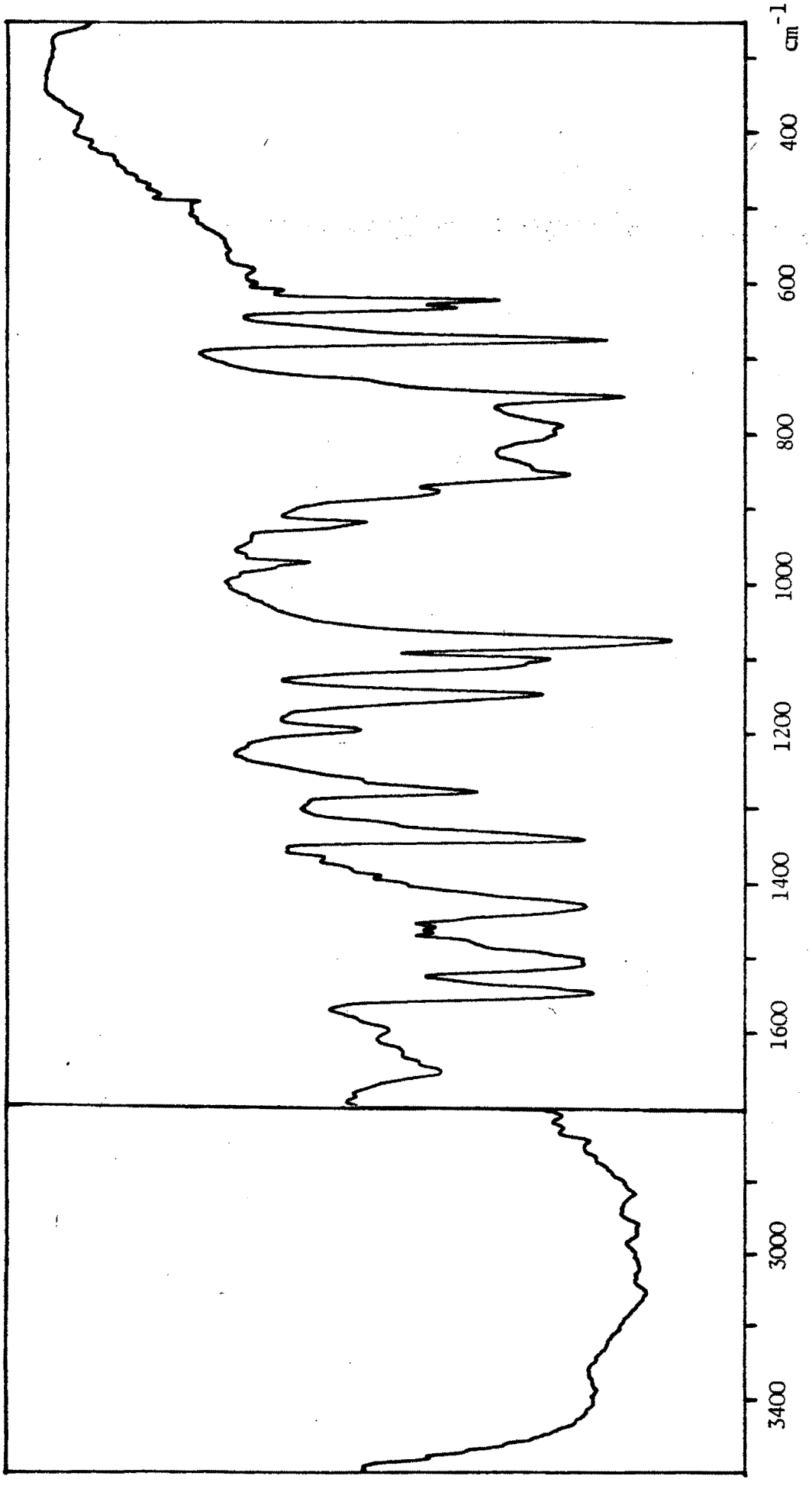

Figure 15. Infrared spectrum of $[Pt(Him)_4Cl_2]$

3.5 DISCUSSION

3.5.1 *Band Assignments in the Infrared Spectra of* cis- *and* trans- $[Pt(pz)_2X_2]$, *(X = Cl, Br, I, NO_2)*

These newly-described platinum complexes have the stoichiometry $[Pt(pz)_2X_2]$ and are therefore almost certainly square planar complexes of C_{2v} *(cis)* and D_{2h} *(trans)* site symmetries, with pyrazine acting as a monodentate nitrogen donor. For simplicity the mid- and far-infrared regions will be discussed seperately.

The region 4000 - 400 cm^{-1}

Since the band of lower frequency in the spectrum of pyrazine is at 416 cm^{-1} and since the frequency of this band is significantly raised by complexation, this region incorporates all the internal ligand modes of pyrazine (Tables 4 and 5). Pyrazine resembles pyridine in that, apart from minor shifts and splittings, each ligand band is faithfully reproduced in the spectra of its complexes.[39-51] Hence, given the reliable assignments of Simmons *et al.*[52] which are based on a study of the spectra of pz and pz-d_4, it is possible to provide firm assignments for each ligand band in the spectra of the complexes. Where this procedure gives rise to any doubts as to the respective assignments of neighbouring bands, use may be made of the ν^D/ν^H ratio[20] to resolve the issue.

The assignments given in Tables 4 and 5 are based on those reported

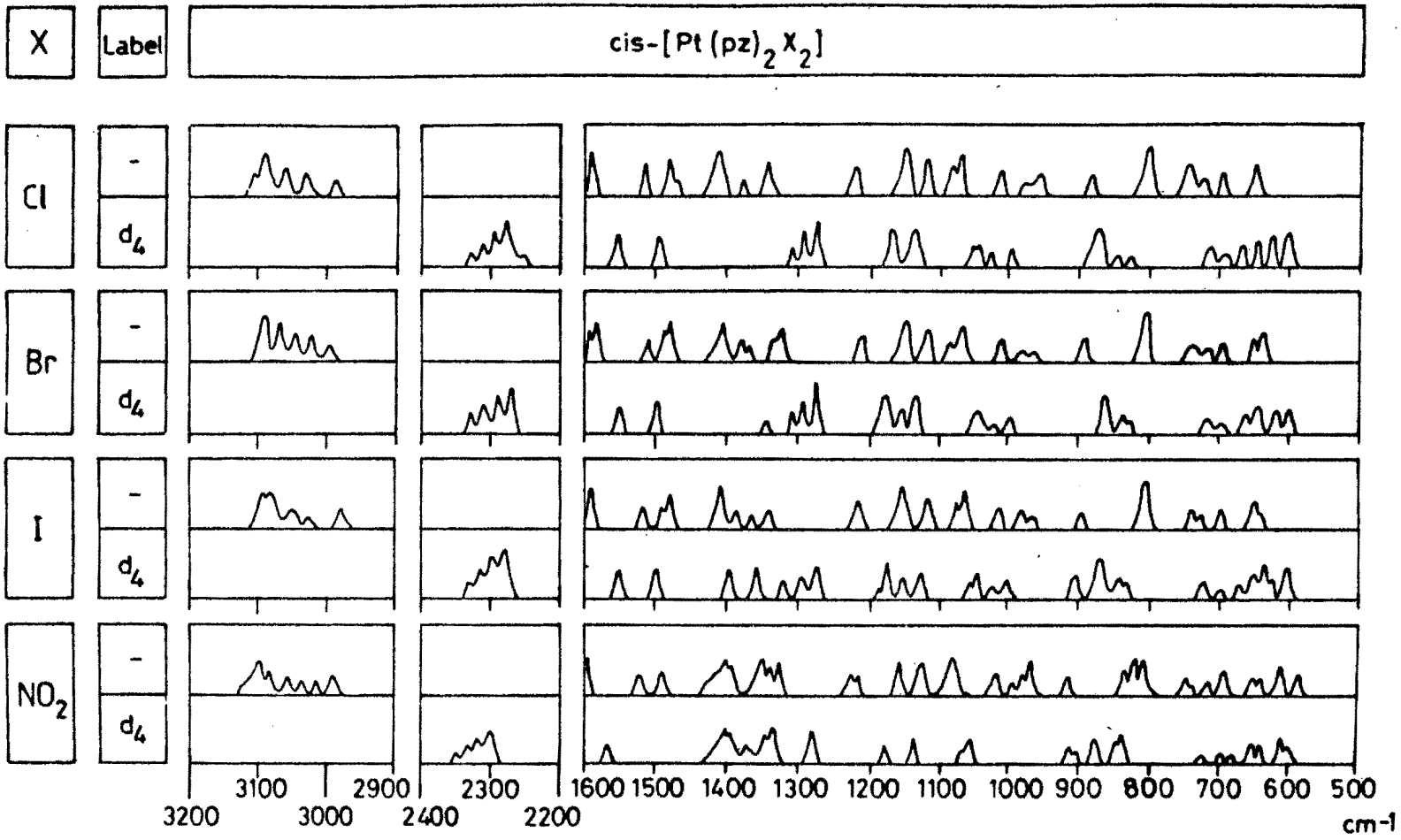

Fig. 16. Infrared spectra (3200-500 cm^{-1}) of *cis*-$[Pt(pz)_2X_2]$ and *cis*-$[Pt(pz\text{-}d_4)_2X_2]$.

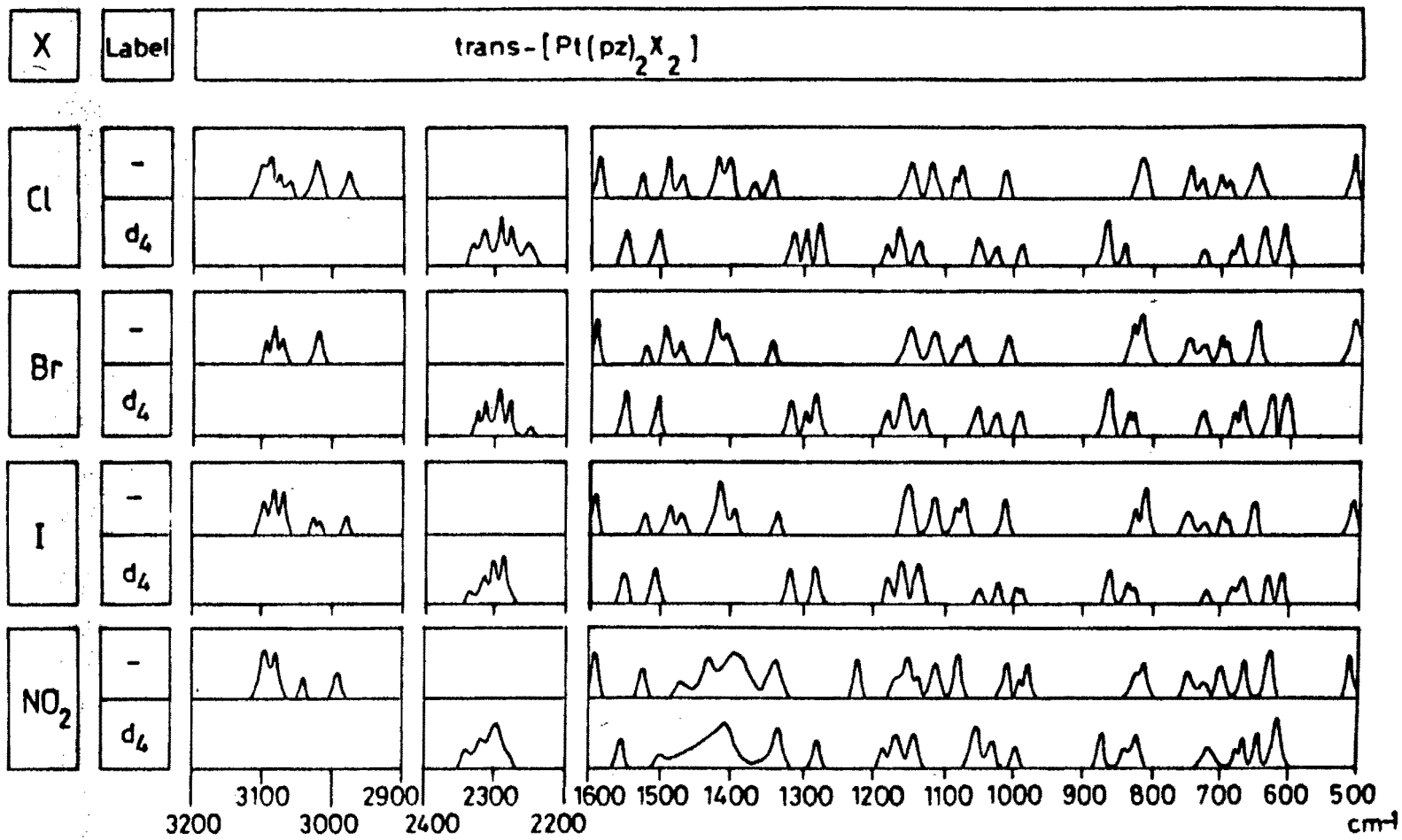

Fig. 17. Infrared spectra (3200-500 cm^{-1}) of *trans*-$[Pt(pz)_2X_2]$ and *trans*-$[Pt(pz\text{-}d_4)_2X_2]$.

for pz and pz-d_4[53] and in relation to those given for pyridine and its complexes[54-56] as well as the requirements of the ν^D/ν^H ratio. All C-H absorptions originating in the mulling agent have been avoided using hexachlorobutadiene mulls in the appropriate regions.

A noteworthy feature of the spectra of the *cis*-complexes is the additional splitting observed in several bands, but notably in the γ ring mode (16b) which clearly provides a diagnostic distinction between the *cis*- and *trans*-complexes. The complexes with X = NO_2 exhibit additional absorptions in the NO_2 stretching and bending regions, but these are easily distinguished by their ν^D/ν^H ratio being close to or equal to unity.

The region 400 - 50 cm^{-1}

Deuteration of pyrazine provides a clear distinction between νPt-pz and νPt-X bands in the spectra of both the *cis*- and *trans*-complexes (Table 6). These distinctions are confirmed by the sensitivities of the respective bands to halide substitution (Fig. 18). The assignments are more precisely made in the chloro, iodo and nitrito complexes since in the bromides, the proximity of νPt-pz and νPt-Br enhances the prospects for coupling between these modes. This is evident from the sensitivity of νPt-Br to pyrazine deuteration in the bromo complexes.

As expected from their C_{2v} symmetry, both νPt-pz and νPt-X are doubled in the *cis*-complexes. The doublet character of νPt-X is clearer than that of νPt-pz because one component of the latter coincides with, or is close to, δpz-Pt-pz. In such cases of coincidence, δpz-Pt-pz

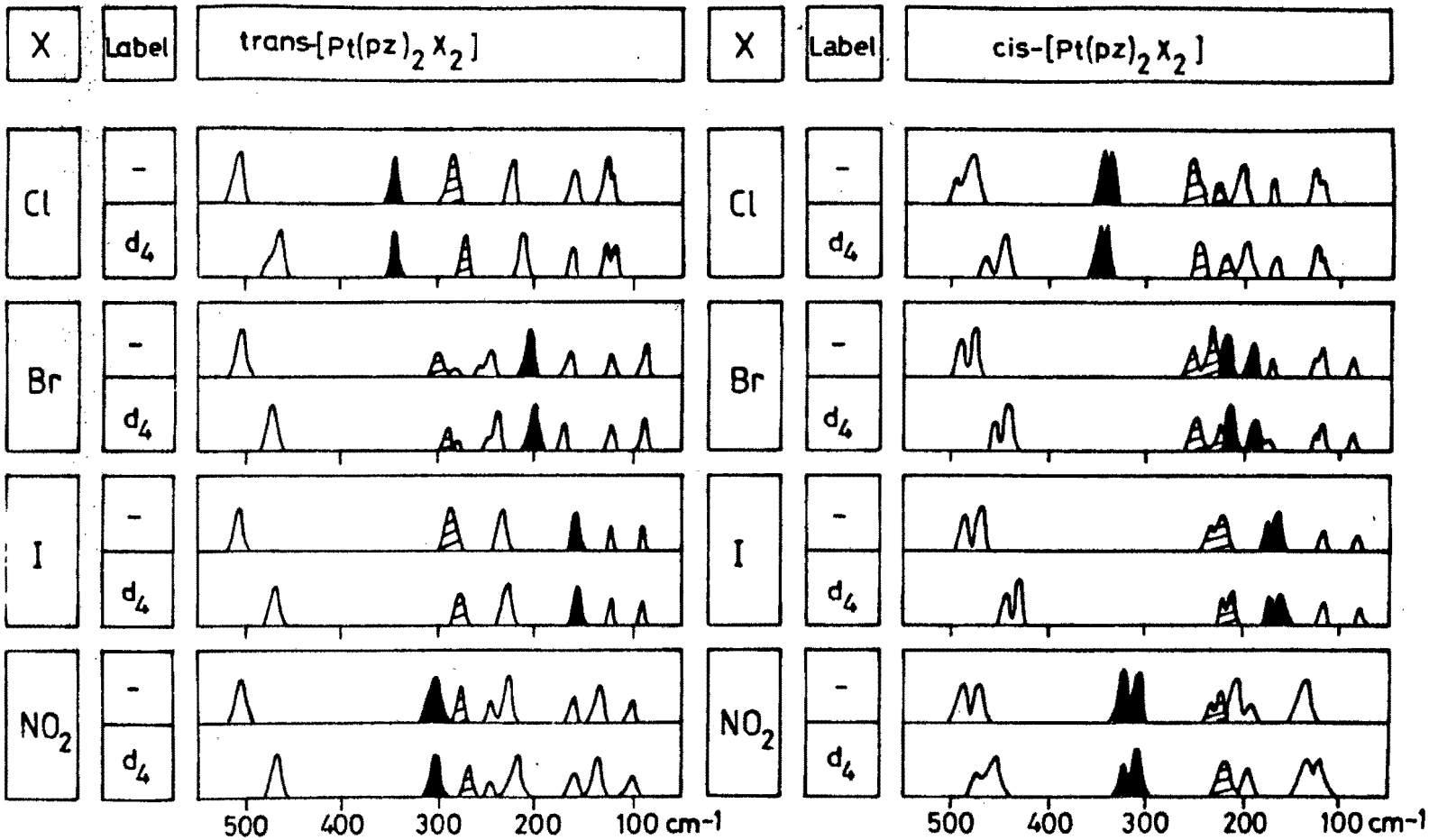

Fig. 18. Far-infrared spectra of the complexes $[Pt(pz)_2X_2]$ and $[Pt(pz\text{-}d_4)_2X_2]$. Shaded peaks: νPt-pz, solid peaks: νPt-X.

acquires a relatively high sensitivity to pyrazine deuteration.

An interesting feature of the spectra is the significantly lower νPt-pz values in the *cis*-complexes. It is clear that in these compounds the steric effect of neighbouring coordinated pyrazines serves to weaken the Pt-pz bonds. A clearcut distinction between the δpx-Pt-X and δX-Pt-X bands is not possible on the basis of the deuteration study.

3.5.2 *Band Assignments in the Infrared Spectra of* cis- *and* trans-$[Pt(an)_2X_2]$, *(X = Cl, Br, I, NO_2)*

Relative to pyridine complexes, the assignment problem for coordinated aniline is more complex because of the additional bands originating in the internal vibrations of the amino group. It is convenient to discuss the mid- and far-i.r. spectra seperately.

Aniline ligand vibrations

Except for the out-of-plane ring deformation at 230 cm^{-1}, all the internal modes of coordinated aniline have frequencies greater than 400 cm^{-1} and are therefore well seperated from the metal-ligand bands. ^{15}N-labelling is the best technique for assigning the vibrations involving the nitrogen atom because the small size of the shifts which occur (relative to those resulting from d_5-labelling) facilitates identification of corresponding bands between the labelled and unlabelled spectra. Thus the νN-H bands, the NH_2 scissoring, wagging and rocking

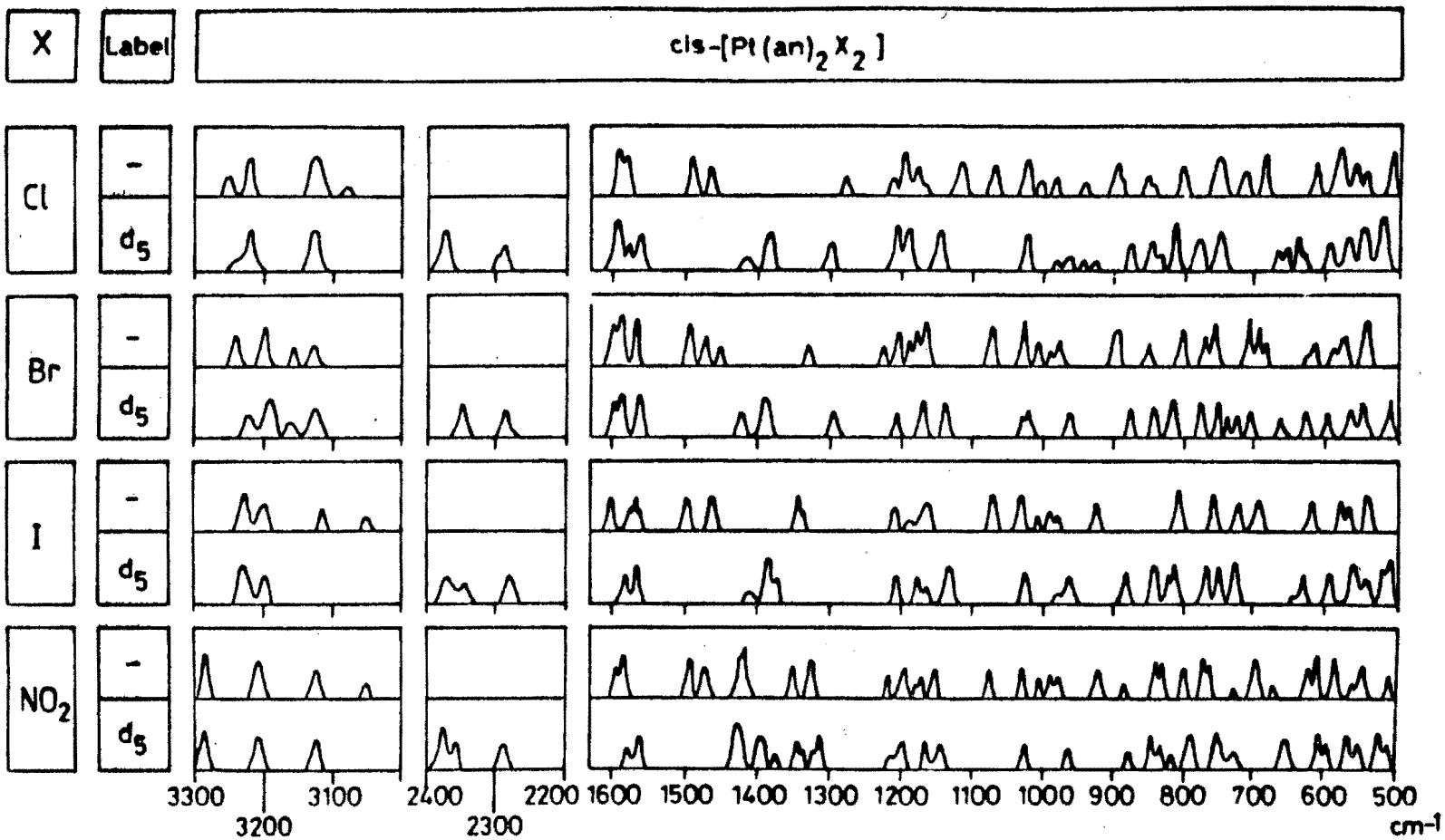

Fig. 19. Infrared spectra (3300-500 cm^{-1}) of the complexes *cis*-$[Pt(an)_2X_2]$ and *cis*-$[Pt(an\text{-}d_5)_2X_2]$.

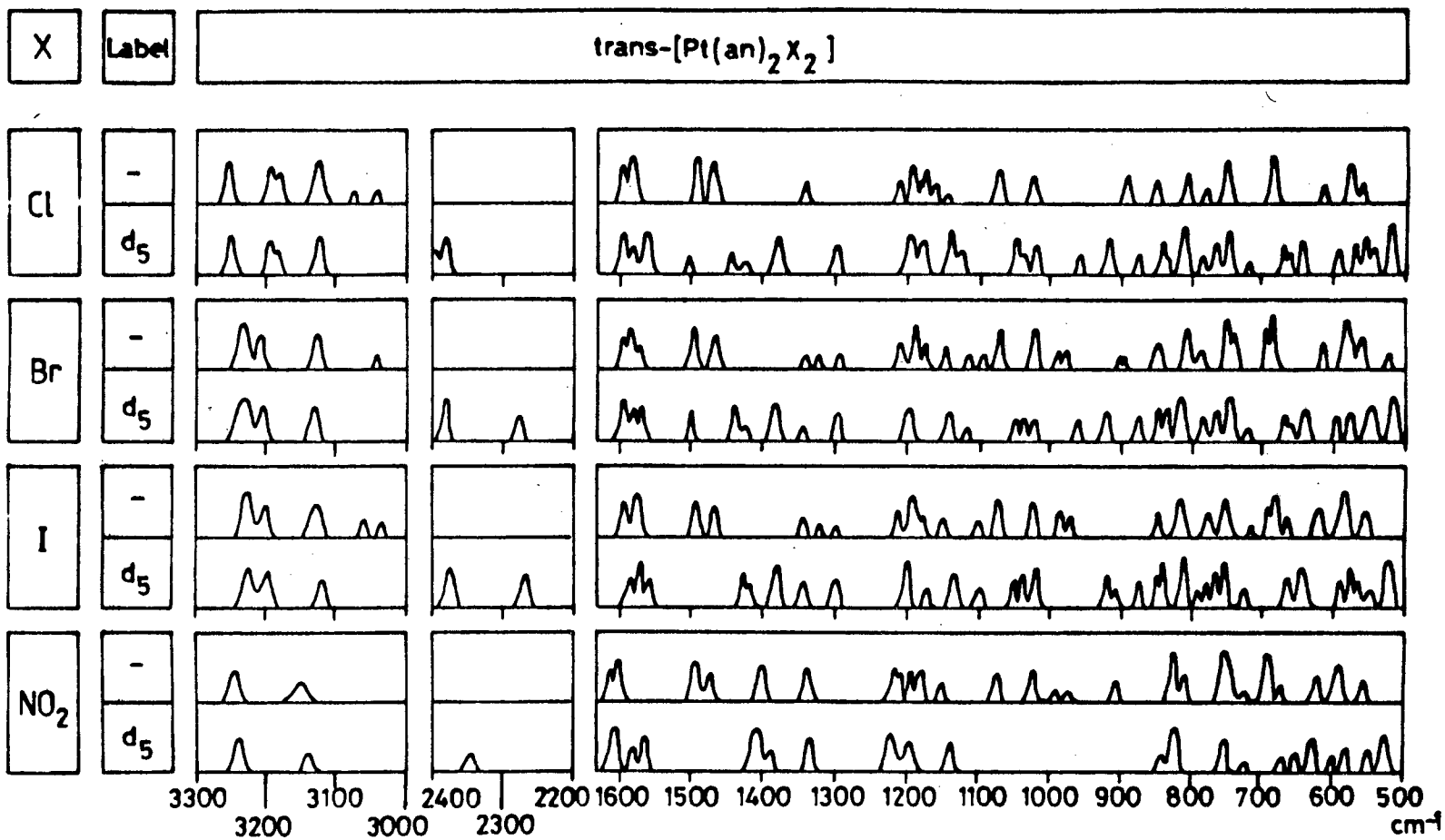

Fig. 20. Infrared spectra (3300-500 cm^{-1}) of the complexes *trans*-$[Pt(an)_2X_2]$ and *trans*-$[Pt(an\text{-}d_5)_2X_2]$.

modes and νC-N are readily identified by their ^{15}N-shifts which are between 3 and 11 cm^{-1} towards lower frequencies.

Ring (d_5) deuteration complements the ^{15}N-labelling technique by providing firm distinction between the ring and C-H modes of the aniline ring. Here, use is made of the ν^D/ν^H ratio.[20] The assignments given in Tables 7 and 8 are based on those resulting from the deuteration study of aniline made by Evans.[57] All C-H absorptions originating in the mulling agent have been avoided by using hexachlorobutadiene mulls in the appropriate regions. It is worth noting here that the band reported by Evans at 390 cm^{-1} in aniline is not observed in the spectrum of freshly-distilled aniline. It is only present in the spectra of darkened (aged) samples of the base.

Metal-ligand vibrations

The spectra in the range 400 - 90 cm^{-1} are depicted in Figure 21 and the frequencies and shifts which occur on labelling are reported in Table 9. All complexes were deuterated but only the *cis*- and *trans*-chlorides were ^{15}N-labelled.

The NH_2 rocking mode is observed as a strong band within the narrow range 461 - 439 cm^{-1}. It shifts 5 cm^{-1} on ^{15}N-labelling and approximately 40 cm^{-1} on aniline deuteration. It is followed by the νPt-an mode within the range 390 - 350 cm^{-1}. This band shifts 4 cm^{-1} on ^{15}N-labelling and approximately 10 cm^{-1} on d_5-labelling. As expected from their C_{2v} symmetry, the *cis*-complexes yield a second νPt-an band within the range 300 - 290 cm^{-1}. This latter band, which also shifts

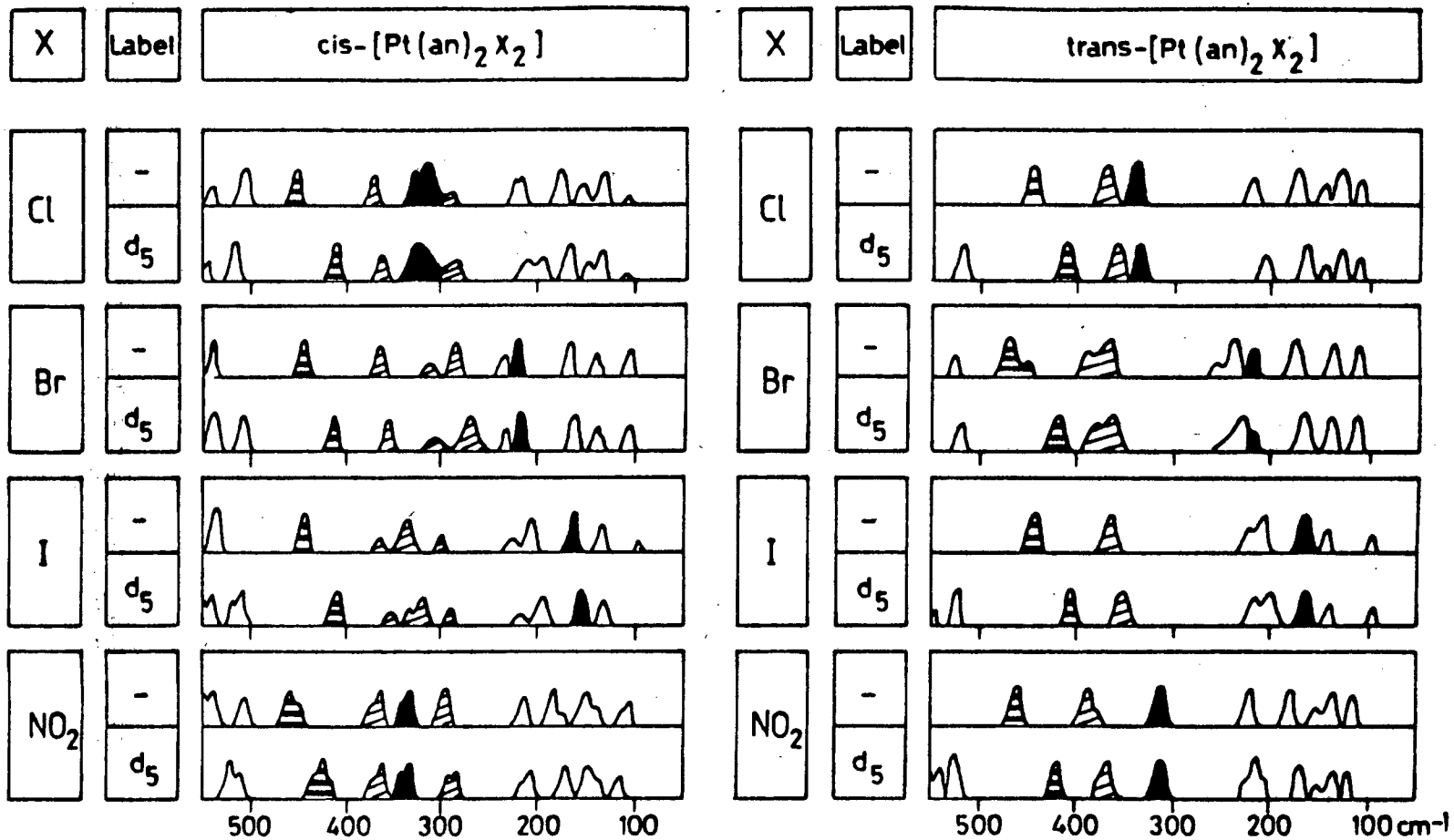

Fig. 21. Far-infrared spectra of the complexes $[Pt(an)_2X_2]$ and $[Pt(an\text{-}d_5)_2X_2]$.
Solid bands: νPt-X, shaded bands: νPt-an, bands with horizontal bars: NH_2 rock.

10 cm^{-1} on d_5-labelling, is observed as a weak shoulder on the νPt-Cl band in the *cis*-chloro complex and exhibits further splitting in the other *cis*-complexes.

The νPt-X bands are readily recognized from the fact that they are completely unaffected by ^{15}N- and d_5-labelling. An exception is Pt-I in both the *cis*- and *trans*-iodo complexes where it exhibits a shift of 7 and 5 cm^{-1}, respectively, on d_5-labelling. This shift is clearly a result of coincidence with the δan-Pt-an mode which is, of course, *d*-sensitive. Broadening of νPt-X is observed in the *cis*-complexes with clearcut splitting in two cases (X = Cl, NO_2). The C_{2v} symmetry of these complexes requires two νPt-X bands. νPt-X shifts in the sequence ∿330, ∿230, ∿170 cm^{-1} for X = Cl, Br, I, respectively. These frequencies yield the reasonable ratios: 0.68 for νPt-Br / νPt-Cl and 0.51 for νPt-I / νPt-Cl.

The band of lowest frequency in the spectrum of aniline (the γ ring mode) is observed at 230 cm^{-1}. It recurs in the spectra of the complexes within the range 240 - 210 cm^{-1} where it is recognized by its *d*-sensitivity of between 7 and 12 cm^{-1}.

The three remaining bands in the spectrum are assigned, in order of decreasing frequency, to the three bending modes, δan-Pt-an, δan-Pt-X and δX-Pt-X since they are progessively less sensitive to d_5-labelling. Furthermore, with one exception, these frequencies are inversely related to the halide masses, following the sequence Cl > Br > I.

3.5.3 *Band Assignments in the Infrared Spectra of* $[Pt(Him)_4]X_2$, *(X = Cl, Br, I)*

Only one rather broad and weak band is observed within the range 4000 - 3000 cm^{-1} (Table 12). Its frequency is too low for νN-H which is not observed in these spectra. Rather, it is assigned to νC-H as it undergoes a low frequency shift of approximately 800 cm^{-1} on d_3-labelling.

The bands within the range 1600 - 600 cm^{-1} comprise the C-H, N-H and ring vibrations of coordinated imidazole. Apart from minor shifts and splittings, almost every infrared band of free imidazole recurs in the spectra of the complexes. Therefore, it was unnecessary to label the protons in the 1-position for the purposes of distinguishing between the C-H and N-H modes. Rather, this distinction is based on the earlier labelling study of imidazole and its complexes.[53,58] Distinction between the C-H and ring modes is based on the ν^D/ν^H ratio.[20]

The far-infrared spectra of these complexes are very simple, comprising only three bands which are assigned, in order of decreasing frequency, to νPt-Him, δHim-Pt-Him and a lattice mode. νPt-Him undergoes a d_3-induced shift of between 10 and 20 cm^{-1}. The simplicity of the spectra is accounted for by the absence of metal-halide modes since the halides lie outside the coordination sphere. The νPt-Him frequencies are slightly halogen-dependent in the sequence Cl > Br > I.

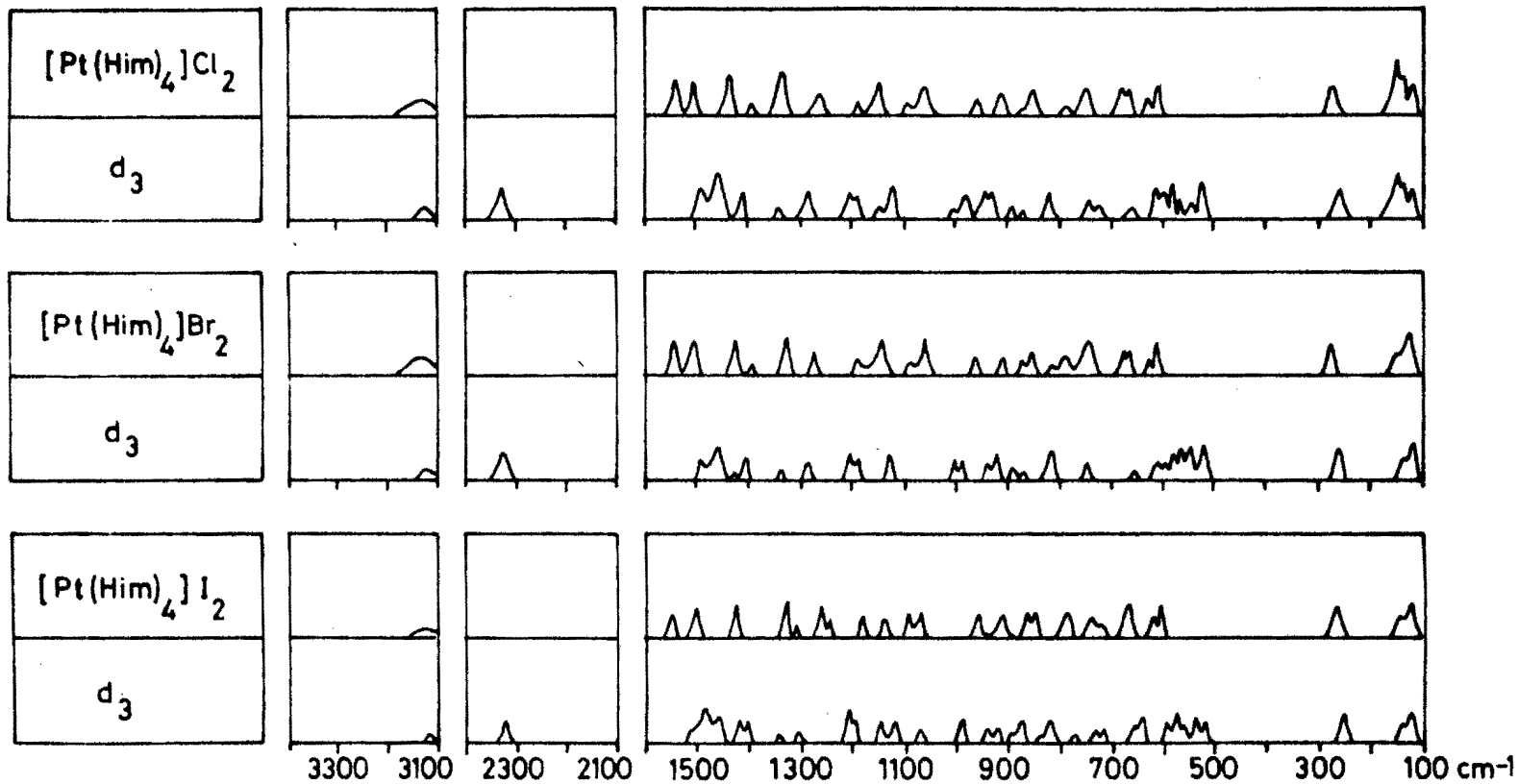

Fig. 22. Infrared spectra 3300-100 cm^{-1}) of the complexes $[Pt(Him)_4X_2]$ (X = Cl, Br, I) and their Him-d_3 labelled analogues.

3.5.4 *Band Assignments in the Infrared Spectra of* cis- *and* trans- $[Pt(Him)_2X_2]$, *(X = Cl, Br, I, NO_2)*

The spectra of these complexes (Tables 10 and 11) differ from those discussed above in the 4000 - 3000 cm^{-1} region, where the νN-H and νC-H bands are of much greater intensity. Distinction between the νN-H and νC-H bands is readily made from the fact that the former are unaffected by d_3-labelling while the latter shift some 800 cm^{-1} to lower frequency.

Assignment of the bands within the range 1600 - 600 cm^{-1} follows the procedure discussed for the $[Pt(Him)_4]X_2$ complexes. In the nitrite complexes, the NO_2 stretching and bending modes may be distinguished by their lack of sensitivity to d_3-labelling and their uniqueness to the spectra of these complexes.

Only one imidazole band occurs below 600 cm^{-1} (at 174 cm^{-1}) so that the majority of bands in the far-infrared region (Figure 25) are metal-ligand bands. The νPt-X bands have been assigned by Reedijk *et al.*[32] to the most intense bands in the spectra and their assignments are confirmed here by complete absence of any shift on d_3-labelling in the halide complexes. A small shift in νPt-NO_2 in *trans*-$[Pt(Him)_2(NO_2)_2]$ is indicative of slightly coupling with νPt-Him in this complex. The νPt-X bands in the *cis*-complexes are characterized by their breadth. In three cases (X = Br, I, NO_2) the two components of νPt-X expected in C_{2v} symmetry may be independently observed. In the *trans*-complexes (D_{2h} symmetry) only a single, sharp νPt-X band is observed.

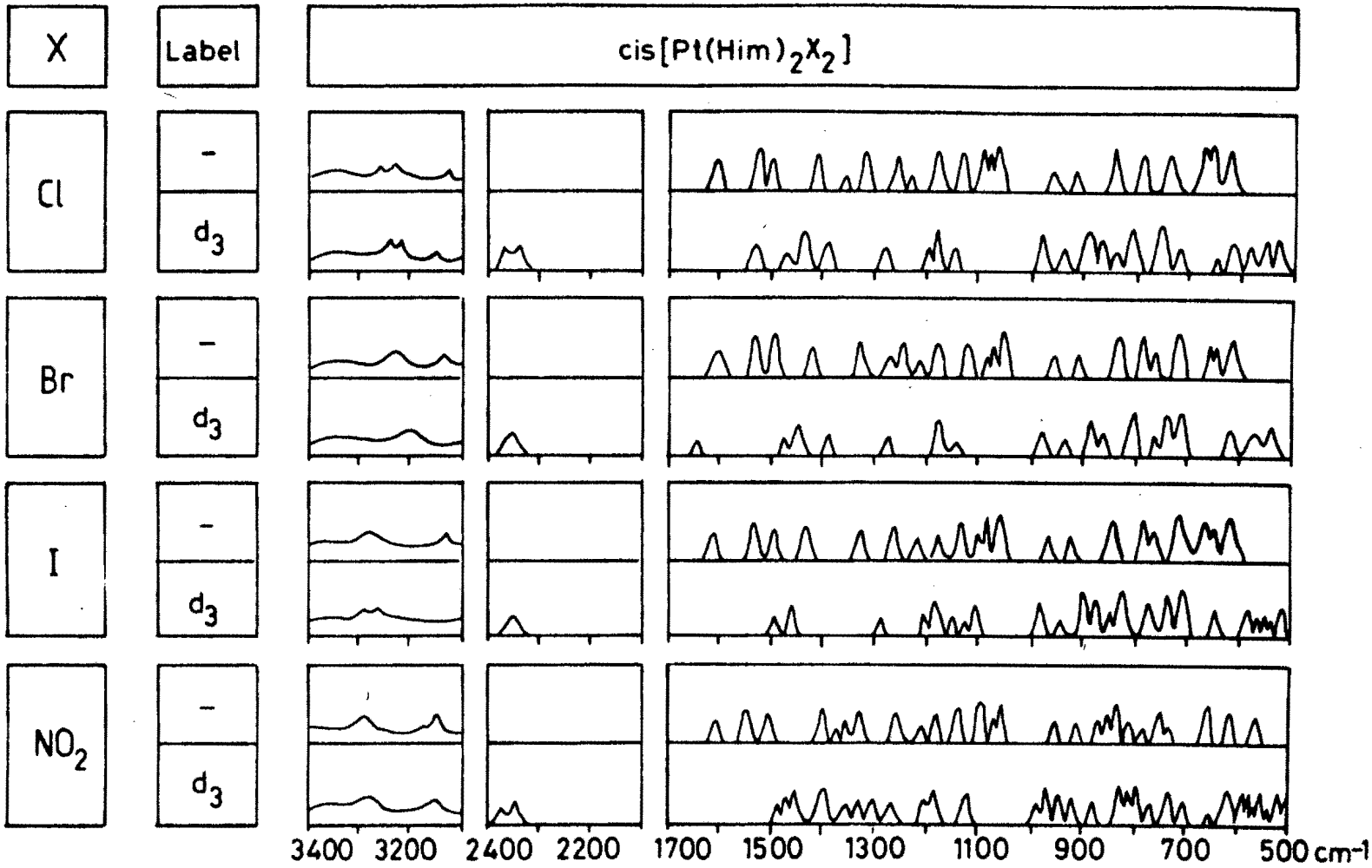

Fig. 23. Infrared spectra (3400-500 cm^{-1}) of the complexes *cis*-$[Pt(Him)_2X_2]$ and their Him-d_3 labelled analogues.

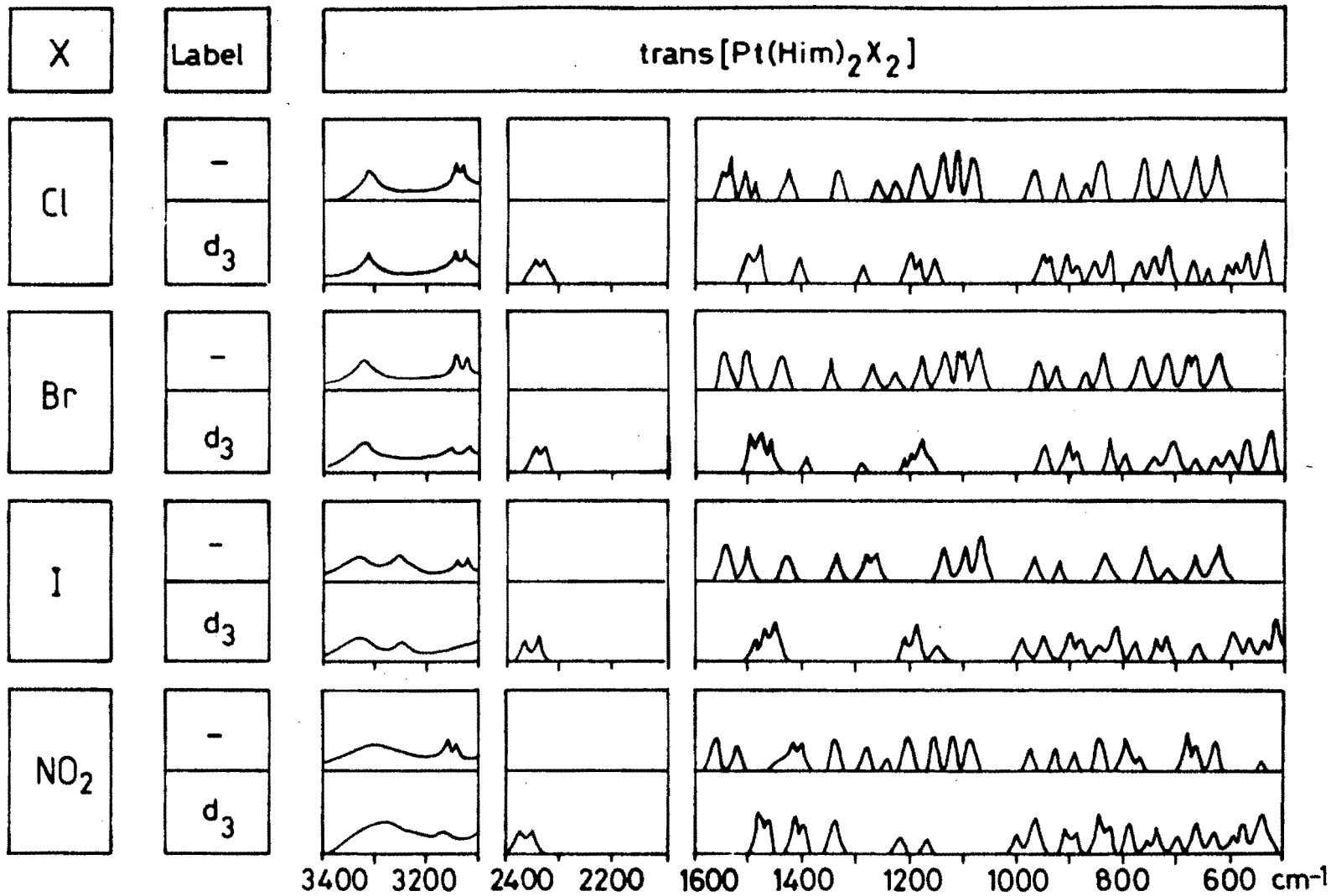

Fig. 24. Infrared spectra (3400-500 cm^{-1}) of the complexes *trans*-$[Pt(Him)_2X_2]$ and their Him-d_3 labelled analogues.

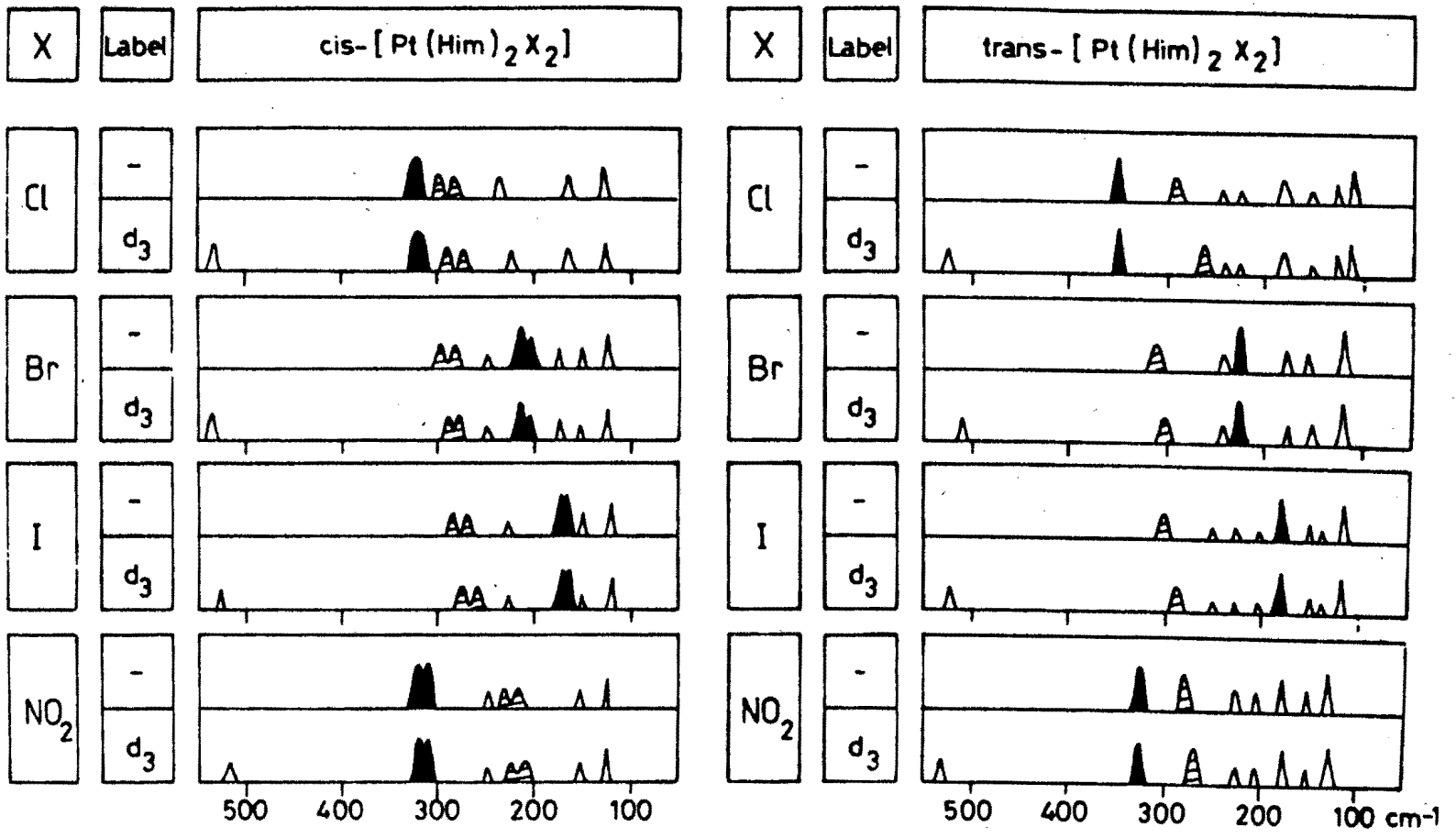

Fig. 25. Far-infrared spectra of the complexes *cis*- and *trans*-$[Pt(Him)_2X_2]$.
Solid bands: νPt-X, shaded bands: νPt-Him.

The labelling study of the complexes $\nu Pt(Him)_4 X_2$ revealed νPt-Him as a moderately strong band near 270 cm^{-1}. Bands which are significantly sensitive to d_3-labelling (shifts between 5 and 12 cm^{-1}) were observed near this frequency in the *cis*- and *trans*-complexes. As befits their respective symmetries, two such bands are observed in the *cis*- and one in the *trans*-complexes. In the *cis*-NO_2 complex, their frequencies are somewhat lower (208 and 227 cm^{-1}) suggesting that, in this complex, the Pt-Him bonds are weaker.

Between three and six additional bands are observed in the far-infrared spectra. Few of these exhibit any d_3-sensitivity. Furthermore, the presence of an imidazole band (at 174 cm^{-1} in the free base) complicates the assignment question. It was therefore not possible to distinguish between the three bending modes expected to occur in this region.

3.5.5 *Comparison of the platinum-to-ligand stretch and its implications for the structure of the complexes* cis- *and* trans-$[PtX_2L_2]$, *(X = Cl, Br, I) and (L =* NH_3, *an, pz, py, Him).*

The data for these complexes are listed in Table 13. The common factor in all the complexes is that they all obey their respective point group symmetry rules, *i.e.* for the *cis*-complexes, with C_{2v} point group symmetry, there are two Pt-L stretches, while for the *trans*-complexes, with D_{2h} symmetry, there is only one Pt-L stretch.

Table 13. νPt-L (cm^{-1}) for the complexes *cis*- and *trans*-$[PtX_2L_2]$, (X = Cl, Br, I) and (L = NH_3, an, pz, py, Him)

	Cis			*Trans*		
L	X = Cl	Br	I	X = Cl	Br	I
NH_3[a]	517	513	491	509	502	498
	508	499	477			
an	374	367	350	374	383[b]	366
	293	290	300			
pz	255	255	230	286	300	289
	226	233	222			
py[c]	256	259	244	285	296	290
	232	230	220			
Him	291	291	280	287	313	292
	278	278	265			

a - data from reference 2, page 115.
b - split band
c - data from reference 59

are when this plane is parallel to the plane passing through Pt, X and N (i) and when it is at 90° to the plane passing through Pt, X and N (ii) as shown in Figure 26.

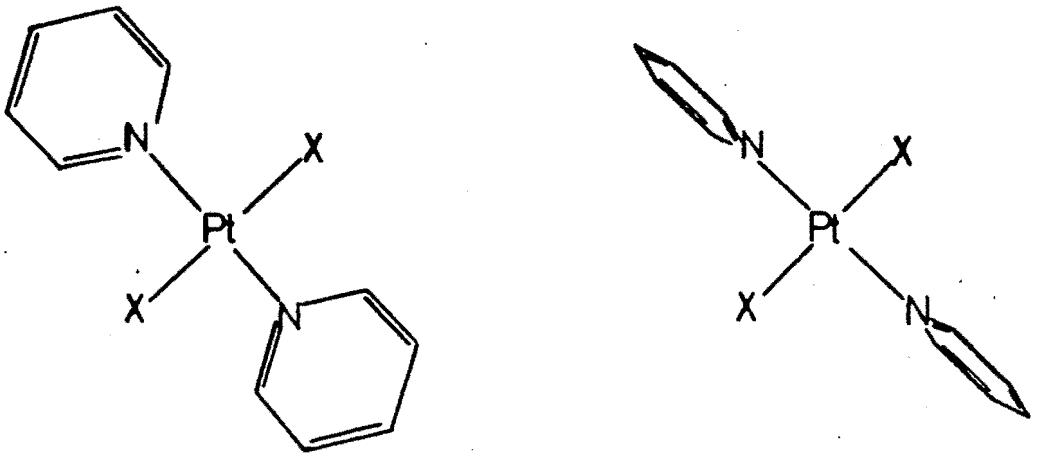

Figure 26. Two possible orientations of the pyridine ring in *trans*-$[Pt(py)_2X_2]$

If the molecule has axes assigned as shown in Figure 27, then the π^* orbitals of the pyridine ring, which are situated above and below the plane of the ring (see Figure 28) can overlap with the d_{yz} orbital of Pt in case (i) to effect the charge transfer and with the d_{xy} orbital of Pt in case (ii) to effect the charge transfer. The latter seems more likely due to steric considerations. Crystal structures have been determined for the complexes *trans*-$[PtX_2(py)_2]$ where X = Cl,[60] I[61] and SCN.[62] In the case where X = Cl, the angle between the plane passing through the pyridine ring and the plane passing through

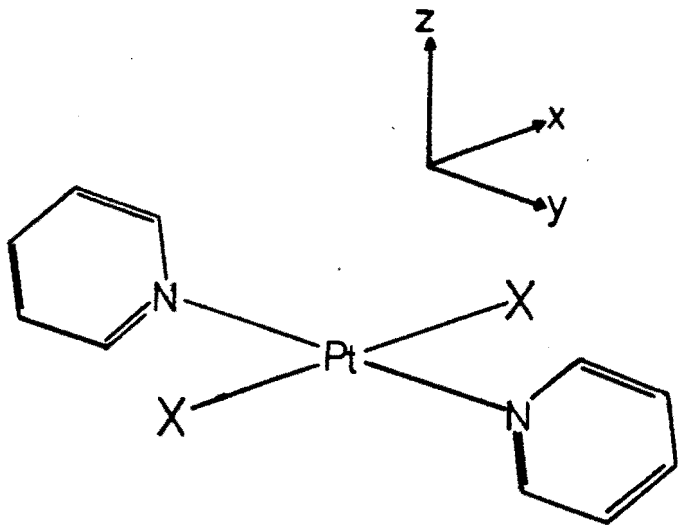

Figure 27. *x*, *y* and *z* axes assigned to *trans*-$[Pt(py)_2X_2]$

Pt, Cl and N is 56.2°. The analagous angle for the complex where X = I is 75° while it is 89° for the case where X = SCN. However it could also be argued that this angle is largely dependent on the crystal packing and thus no definite conclusion can be made.

Another noticeable feature is the large difference between νPt-L for L = NH_3 and aniline and νPt-L for L = pyrazine, pyridine and imidazole, with the former appearing at much higher frequency. This appears to be inconsistent with what has been discussed above for surely, if there is backbonding in the case where L = pz, py and Him, then νPt-L for these complexes should be higher. This can be explained if one considers the mode of action of νPt-L. In the case where L = NH_3 and aniline, the Pt^{2+} is vibrating "against" a light group *viz.* NH_3 and effectively NH_2. However in the case where L = pz, py and Him, the Pt^{2+} is effectively vibrating "against" the whole ring, even more so if there is back-bonding and thus the frequency of νPt-L is lower due

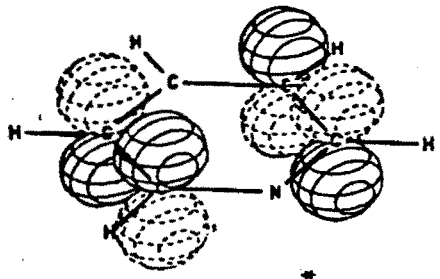

$^2A_2$ E= 0.1099 π^*_4

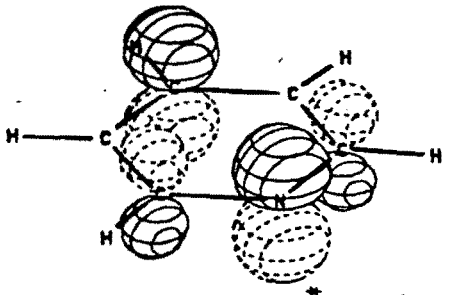

$^3B_1$ E= 0.1107 π^*_5

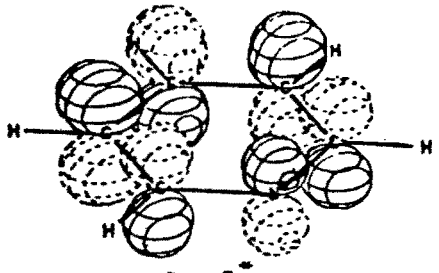

$^4B_1$ π^*_6

Figure 28. The π^* orbitals of pyridine (See reference 109)

to the mass effect. One can only suggest that νPt-L in the latter case would have appeared at even lower frequency if there was no $5d(\mathrm{Pt}) \rightarrow \pi^*$ charge transfer.

CHAPTER 4

CHAPTER 4

4. THE STRUCTURAL ANALYSIS OF VARIOUS DERIVATIVES OF ZEISE'S SALT, $K[PtCl_3(CH_2CH_2)].H_2O$

4.1 INTRODUCTION

In 1830, Zeise prepared the first organometallic complex, $K[PtCl_3(CH_2CH_2)].H_2O$, but it was only in about 1950 that its true structure, as shown in Figure 29, was determined.

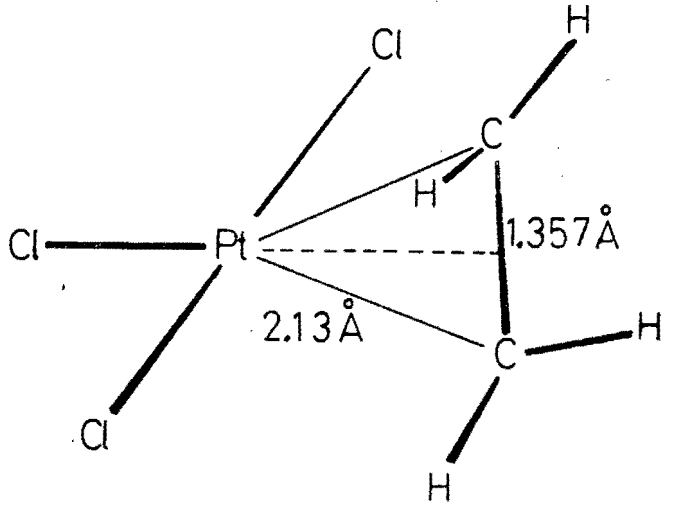

Figure 29. The structure of $[PtCl_3(C_2H_4)]^-$. (See reference 1, p.96)

Zeise's salt can be prepared by interacting an aqueous solution of $K_2[PtCl_4]$ with gaseous ethylene over a period of approximately ten days. Likewise the bromide analogue of Zeise's salt, $K[PtBr_3(CH_2CH_2)].H_2O$, may be prepared by interacting an aqueous solution of $K_2[PtBr_4]$

with gaseous ethylene with the interaction period being less in this case *viz.* approximately three days.

It has been found[63] that the reaction of $[PtX_4]^{2-}$ with a ligand, L, as shown below:

$$[PtX_4]^{2-} + L \rightarrow [PtX_3L]^- + X^-$$

normally follows a two-term rate law given by:

$$\text{rate} = (k_1 + k_2[L])\ [PtX_4^{2-}]$$

Thus if k_1 is large, the rate is first-order corresponding to the solvent dependent path, whereas if k_2 is large the rate is second-order corresponding to the solvent independent path.

When L = C_2H_4, k_1 is zero,[64,65] indicating that the aquo species $[PtX_3(H_2O)]^-$ is not involved in the rate determining step of the reaction. Hence the reaction pathway can be depicted as in Scheme 5.

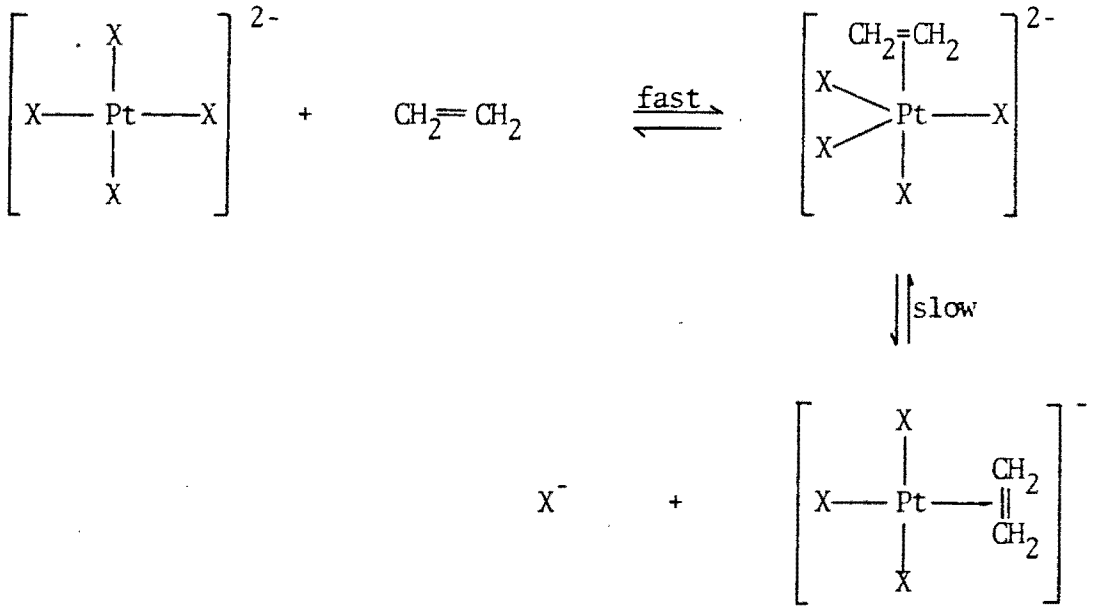

SCHEME 5

The main feature of $K[PtCl_3(C_2H_4)]$ is that the C=C axis of the coordinated ethylene is perpendicular to one of the expected bond directions from the platinum ion (see Figure 29). This feature is accounted for by the suggestion that there are two components to the bonding.

Firstly there is overlap of the π-electron density of the ethylene with a σ-type acceptor orbital on the platinum, and secondly there is "back-bonding" of electron density from a filled platinum *d*-orbital to the π^* antibonding orbitals of the ethylene.[67] The bonding is shown diagramatically in Figure 30.

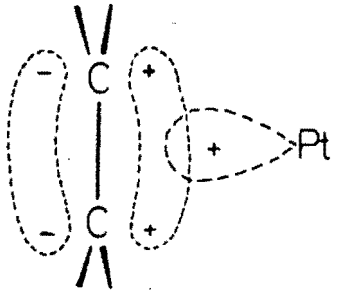

Donation from filled π orbitals to vacant metal orbital

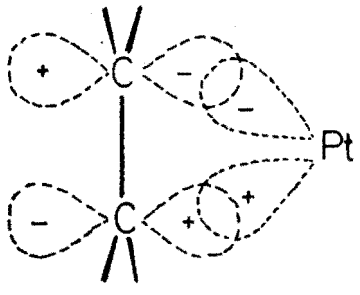

Back-bonding from filled metal orbital to acceptor π^* orbitals

Figure 30. The molecular orbital views of ethylene-platinum bonding

The "backbonding" theory is substantiated by the fact that in every case, except the anion of Zeise's salt, there is a lengthening of the C=C bond,[68] and that in the ultraviolet spectra there is a band at approximately 300 nm corresponding to the $5d(Pt) \rightarrow \pi^*$(ethylene) transition.[69]

When Zeise's salt is reacted with a monodentate ligand, L, this ligand will generally go *trans* to the ethylene, because of the latter's strong *trans*-effect.[70] The strong *trans*-effect of ethylene is manifested very clearly by some of the physical properties of Zeise's salt and its derivatives.

Numerous crystal structure determinations of $K[PtX_3(CH_2CH_2)]$ have been performed,[71-75] and it is interesting to look at the Pt-Cl bond lengths in $K[PtCl_3(C_2H_4)]$ and the Pt-Br bond lengths in $K[PtBr_3(CH_2CH_2)]$. Table 14 lists some of the crystallographic data.

Table 14. Pt-X (X = Cl, Br) bond lengths (Å) of $K[PtX_3(C_2H_4)]$

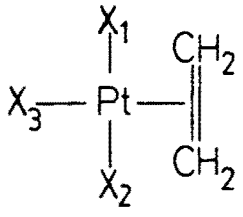

X	$Pt-X_1$	$Pt-X_2$	$Pt-X_3$
Cl	2.29	2.27	2.39
	2.30	2.30	2.34
	2.31	2.30	2.33
Br	2.43	2.42	2.52

As can be seen the Pt-X bond length for the halide *trans* to the ethylene is considerably longer than the other two Pt-X bond lengths where the halides are *trans* to each other. This indicates that, even in the crystalline state, the *trans*-effect of ethylene is a pronounced one.

A second interesting feature of the *trans*-effect of ethylene is the increased reactivity of normally unreactive ligands with the Pt^{2+} ion. A good example of this is the fact that pyridine *N*-oxide does not react with K_2PtCl_4 in aqueous solution, but reacts almost immediately with an aqueous solution of $K[PtCl_3(C_2H_4)]$ to form *trans*-$[PtCl_2(C_2H_4)(pyO)]$.[76] The reason for this is that C_2H_4 is a better *trans*-directing group than Cl^- and hence the relative ease of displacement.

Related to the crystal structure data, the infrared spectra also show the difference in the Pt-to-X stretches. The $[PtX_3(C_2H_4)]^-$ ion has C_{2v} symmetry for which group theory predicts:

$$\Gamma_{vib} = 5A_1 + A_2 + 3B_1 + 3B_2$$
$$\Gamma_{stretch} = 3A_1 + B_1 + B_2$$
$$\Gamma_{bend} = 2A_1 + A_2 + 2B_1 + 2B_2$$

The stretches are assigned as follows:

A_1 { $Pt\text{-}C_2$ symmetric stretching; $Pt\text{-}X_2$ symmetric stretching; $Pt\text{-}X_{trans}$ stretching

B_1 $Pt\text{-}C_2$ antisymmetric stretching

B_2 $Pt\text{-}X_2$ antisymmetric stretching

Thus, although there is the possibility of vibrational coupling,[77] it is expected that the two Pt-X_2 stretching modes should occur at higher frequency that νPt-X_{trans}. In the case where X = Cl, ν_{asym} Pt-Cl_2 occurs at 334 cm^{-1}, ν_{sym} Pt-Cl_2 at 324 cm^{-1}, while νPt-Cl_{trans} occurs at 307 cm^{-1}. The trend is repeated in the case where X = Br with the exception that ν_{sym} Pt-Br is not resolved. Thus ν_{asym} Pt-Br occurs at 241 cm^{-1} whereas νPt-Br_{trans} occurs at 215 cm^{-1}. Hence the infrared results effectively substantiate the crystal structure data.

Considering the above we may conclude that unless a monodentate ligand, L, has a stronger *trans*-effect than ethylene, it is likely to form *trans*-$[PtX_2(C_2H_4)L]$ when it reacts with $K[PtX_3(C_2H_4)]$ as shown in Scheme 6.

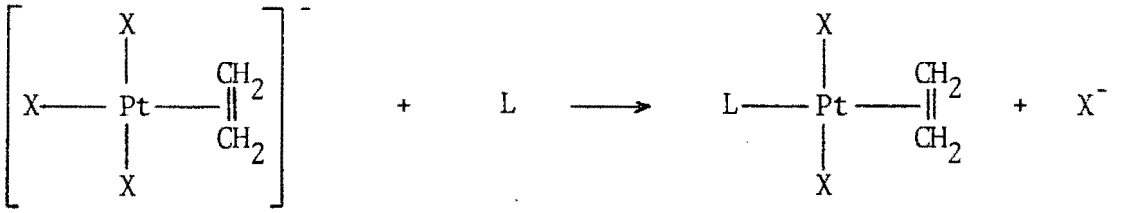

SCHEME 6

Clearly there is no change in the C_{2v} symmetry of the molecule when X^- is displaced by L, and group theory predicts the following platinum-to-ligand stretching vibrations:

A_1 { Pt-C_2 symmetric stretching; Pt-X_2 symmetric stretching; Pt-L stretching

B_1	Pt-C_2 antisymmetric stretching
B_2	Pt-X_2 antisymmetric stretching

As will be shown later, these vibrations may be seperated by means of isotopic labelling techniques.

The electronic transitions that can occur in *trans*-$[PtX_2(C_2H_4)(L)]$ are interesting, particularly if L is capable of effecting electronic transitions itself. Consider the molecule of *trans*-$[PtX_2(C_2H_4)(L)]$ with axes as shown in Figure 31.

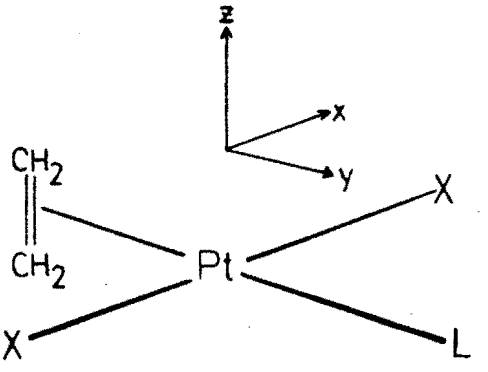

Figure 31. Orientation of the x, y and z axes in the molecule *trans*-$[PtX_2(C_2H_4)(L)]$

Apart from the normal Laporte-forbidden $d \rightarrow d$ transitions that occur for Pt^{2+}, there are various ligand-metal interactions which may occur.[78-82] These transitions are listed below:

$\pi \rightarrow \pi^*$ (coordinated ethylene)

$X^- \rightarrow Pt^{2+}$ charge transfer

$5d(Pt) \rightarrow \pi^*$(ethylene) inverse charge transfer

It has been suggested that it is the $5d(Pt) \rightarrow \pi^*$(ethylene) inverse charge transfer which is responsible for the orientation of the coordinated ethylene perpendicular to the plane of the square. Clearly, in this orientation, it is the d_{xz} orbital of the platinum that overlaps with the empty π^* orbitals of ethylene.

In the above discussion we have assumed that L does not interact with Pt^{2+} except in the form of a σ-bond. Suppose that L has empty π^* orbitals that may accept electron density from Pt^{2+} *e.g.* if L = pyridine.

There are two orientations of the pyridine ring that facilitate overlap of its π^* orbitals with occupied *d*-orbitals of Pt^{2+}. Firstly, the pyridine ring may be perpendicular to the plane passing through X, X, Pt and N and in this case overlap would occur between the π^* orbitals of pyridine and the d_{xy} orbital of Pt^{2+}. It should be noted that this is sterically favourable, since the interaction between the α-H of pyridine and the X atoms is minimized. Alternatively the pyridine ring may lie parallel to the X, X, Pt, N plane, and in this case overlap of the π^* orbitals of pyridine will occur with the d_{xz} orbital of Pt^{2+}. However, apart from being sterically unfavourable this also requires sharing of the d_{xz} orbital with the π^* orbitals of the ethylene.

Crystal structures have been determined for *trans*-[$PtCl_2(C_2H_4)$ (R-pyridine)] (where R = *p*-CH_3, *p*-CN and 2,4,6-tri-CH_3)[83-84] and it was

observed that in the cases where R = *p*-CH_3, *p*-CN, the pyridine ring lies at an angle of 50° to the Cl, Cl, Pt, N plane, whereas the corresponding angle in the complex with R = 2,4,6-tri-CH_3 was 90°. However it should be noted that the ideality of the angle in the latter case is most probably influenced by the steric effects of the bulky α-CH_3 groups.

In solution the situation may be different. Meester and Stufkens[69] have assigned a band at 320 nm in the ultraviolet spectrum of *trans*-$[PtCl_2(CH_2CH_2)(py)]$ as a $5d(Pt) \rightarrow \pi^*$(pyridine) inverse charge transfer but as is shown later this may overlap with the $5d(Pt) \rightarrow \pi^*$(ethylene) inverse charge transfer.

In this chapter, a series of complexes *trans*-$[PtX_2(C_2H_4)L]$, (X = Cl, Br; L = NH_3, pyridine *N*-oxide, pyridine, imidazole, pyrazine, aniline and a series of substituted anilines, (R-an), have been prepared, with a view to obtaining information about the bonding and electronic effects taking place. The techniques used are infrared, Raman, ^1H nuclear magnetic resonance and ultraviolet spectrophotometry.

4.2 PREPARATION OF COMPOUNDS

Preparation of $K[PtX_3(C_2H_4)].H_2O$, *(X = Cl, Br)*

These compounds were prepared in a similar manner to that reported by Chatt and Searle. A solution containing 0.024 mol of $K_2[PtX_4]$,

(10 gram for X = Cl and 14 gram for X = Br) dissolved in water (45 ml) and HX (5 ml) (sp. gr. 1.18 for HCl and 1.50 for HBr) was placed in a 250 ml round-bottomed flask. The inlet to the flask was connected to a cylinder of ethylene gas. The flask was then flushed with ethylene and at all times a positive pressure of ethylene was applied. It was then clamped in an automatic shaker and allowed to shake at ambient temperature (20°C). In the case where X = Cl, the solution changed from dark red to golden yellow in seven days, while the similar change for X = Br was effected in three days. The resultant golden yellow solutions were placed in evaporating dishes and the water was allowed to evaporate, leaving a crystalline residue of $K[PtX_3(C_2H_4)]$ with small traces of KX and unreacted $K_2[PtX_4]$. This residue was then crushed and the $K[PtX_3(C_2H_4)]$ was extracted with ethanol (100 ml). The suspensions were filtered to remove KX and unreacted $K_2[PtX_4]$, and the yellow filtrates were evaporated to dryness to yield the desired products.

The deuterated analogues were similarly prepared using ethylene-d_4 of 99% isotopic purity supplied by Merck, Sharp and Dohme (Canada) Ltd.

4.2.2 *Preparation of the complexes* trans-$[PtX_2(C_2H_4)L]$, *(X = Cl, Br; L = NH_3, aniline (an), pyridine* N-*oxide (pyO), pyridine (py) and imidazole (Him))*

The complexes *trans*-$[PtX_2(C_2H_4)L]$, (X = Cl, Br; L = NH_3, py and Him) were prepared by adding a concentrated aqueous solution of L (1.2 mmol)

(0.021 g for L = NH_3, 0.0948 g for L = py and 0.082 g for L = Him) to an aqueous solution of $K[PtX_3(C_2H_4)].H_2O$ (1 mmol) (0.369 g for X = Cl and 0.502g for X = Br). The complexes precipitated immediately. They were collected by filtration, washed with H_2O and dried over silica gel under reduced pressure.

The complexes *trans*-$[PtX_2(C_2H_4)L]$, (X = Cl, Br; L = pyO and an) were prepared by adding a concentrated ethanolic solution of L (1 mmol) (0.095 g for L = pyO and 0.093 g for L = an) to an ethanolic solution of $K[PtX_3(C_2H_4)].H_2O$ (1.2 mmol) (0.440 g for X = Cl and 0.602 g for X = Br). The mixture was stirred overnight. The ethanol was allowed to evaporate until crystallization was essentially complete. The crystals were collected, washed and dried as described above.

The deuterated complexes were similarly prepared using the following labelled compounds supplied by Merck, Sharp and Dohme (Canada) Ltd. (isotopic purity in parentheses): ethylene-d_4 (99%), ammonia-d_3 (99%), aniline-d_5 (98%), imidazole-d_4 (98%) and the following labelled compounds supplied by BOC Prochem Ltd.: pyridine-d_5 (99%) and pyridine-d_5 *N*-oxide (98%). The deuteroimine (ND) groups of 1,2,4,5-tetradeuteroimidazole (Him-d_4) undergo rapid exchange in aqueous or ethanolic solution to yield complexes containing 2,4,5-trideuteroimidazole (Him-d_3).

4.2.3 *Preparation of the complexes* trans-$[PtX_2(C_2H_4)pz]$ *and* $[Pt_2X_4(C_2H_4)_2pz]$, *(X = Cl, Br, I; pz = pyrazine)*

The complexes *trans*-$[PtX_2(C_2H_4)pz]$, (X = Cl, Br) were prepared by adding a dilute aqueous solution of $K[PtX_3(C_2H_4)].H_2O$ (1 mmol in 50 ml) dropwise to a concentrated aqueous solution of pyrazine (10 mmol in 20 ml) with stirring). The solution was allowed to stir for five minutes, after which the bright yellow complex was collected by filtration, washed with H_2O and dried under vacuum over silica gel.

The complex *trans*-$[PtI_2(C_2H_4)(pz)]$ was prepared by metathetic replacement of Cl^- by I^- in $K[PtCl_3(C_2H_4)].H_2O$ before addition to the aqueous solution of pyrazine. 1 mmole of $K[PtCl_3(C_2H_4)].H_2O$ was dissolved in 50 ml H_2O. To this solution was added 12 mmol (2 g) of KI in 10 ml H_2O, with constant stirring. After approximately five minutes the solution turned dark brown and was stirred until small bubbles started to appear on the sides of the beaker indicating that all the Cl^- ions had been replaced by I^- ions and that ethylene was starting to be evolved. The dark brown solution of $K[PtI_3(C_2H_4)]$ was now added dropwise to a concentrated aqueous solution of pyrazine (10 mmol in 20 ml) with stirring. The solution was allowed to stir for five minutes after which the bright orange complex was filtered, washed successively with a 1 *M* aqueous solution of KI (25 ml) and water and dried under vacuum over silica gel.

The complexes *trans*-$[Pt_2X_4(C_2H_4)_2(pz)]$, (X = Cl, Br) were made by adding a dilute aqueous solution of pyrazine (1 mmol in 25 ml) dropwise to a concentrated aqueous solution of $K[PtX_3(C_2H_4)]$ (3 mmol in 15 ml) with stirring. The bright yellow complexes, which precipitated immediately, were filtered, washed with H_2O and dried under vacuum over silica gel.

The complex *trans*-$[Pt_2I_4(C_2H_4)_2(pz)]$ was prepared by metathetic replacement of Cl^- by I^- in $K[PtCl_3(C_2H_4)].H_2O$ before aqueous pyrazine was added. 3 mmol of $K[PtCl_3(C_2H_4)].H_2O$ was dissolved in 15 ml of H_2O. To this solution was added 36 mmol (6 g) of KI in 15 ml H_2O with constant stirring. The solution turned brown and was stirred until small bubbles appeared on the sides of the beaker indicating that all Cl^- ions had been replaced by I^- ions and that ethylene was starting to be evolved. A dilute aqueous solution of pyrazine (1 mmol in 20 ml) was added dropwise to the brown solution of $K[PtI_3(C_2H_4)].H_2O$. The dark orange complex, which precipitated immediately, was collected by filtration, washed successively with a 1 *M* aqueous solution of KI and H_2O and dried under vacuum over silica gel.

The deuterated complexes were prepared in a similar fashion using pyrazine-d_4 of 98% isotopic purity and ethylene-d_4 of 99% isotopic purity supplied by Merck, Sharpe and Dohme (Canada) Ltd.

4.2.4 *Preparation of the complexes* trans-$[PtCl_2(C_2H_4)(R\text{-}an)]$ *(R-an = substituted aniline)*

The substituted aniline complexes of $K[PtCl_3(C_2H_4)].H_2O$ were made by adding a concentrated ethanolic solution of freshly distilled (or crystallized) substituted aniline (1 mmol) to an excess of $K[PtCl_3(C_2H_4)].H_2O$ (1.2 mmol) in ethanol. The mixture was allowed to stir overnight. The ethanol was allowed to evaporate until

crystallization was essentially complete. The products were collected by filtration, washed with H_2O and dried under vacuum over silica gel.

4.3 ANALYSES OF COMPOUNDS

Table 15. Analytical data on the complexes *trans*-$[PtX_2(C_2H_4)(L)]$, (X = Cl, Br; L = NH_3, aniline, pyridine *N*-oxide, pyridine and imidazole)

Complex	Calculated			Found		
	%C	%H	%N	%C	%H	%N
trans-$[PtCl_2(C_2H_4)(NH_3)]$	7.7	2.3	4.5	7.8	2.3	4.6
trans-$[PtCl_2(C_2H_4)(an)]$	24.8	2.8	3.6	24.9	3.0	3.8
trans-$[PtCl_2(C_2H_4)(pyO)]$	21.6	2.3	3.6	21.6	2.2	3.7
trans-$[PtCl_2(C_2H_4)(py)]$	22.5	2.4	3.8	22.5	2.6	3.8
trans-$[PtCl_2(C_2H_4)(Him)]$	16.6	2.2	7.7	17.7	2.4	7.9
trans-$[PtBr_2(C_2H_4)(NH_3)]$	6.0	1.8	3.5	6.1	1.8	3.7
trans-$[PtBr_2(C_2H_4)(an)]$	20.2	2.3	2.9	20.3	2.3	3.0
trans-$[PtBr_2(C_2H_4)(pyO)]$	17.6	1.9	2.9	17.9	1.9	3.1
trans-$[PtBr_2(C_2H_4)(py)]$	18.2	2.0	3.0	18.3	2.0	3.1
trans-$[PtBr_2(C_2H_4)(Him)]$	13.3	1.8	6.2	13.5	1.7	6.3

Table 16. Analytical data on the complexes *trans*-$[PtX_2(C_2H_4)(pz)]$, (X = Cl, Br, I) and *trans*-$[Pt_2X_4(C_2H_4)_2(pz)]$, (X = Cl, Br, I)

Complex	Calculated			Found		
	%C	%H	%N	%C	%H	%N
trans-$[PtCl_2(C_2H_4)(pz)]$	19.3	2.1	7.5	19.0	2.2	7.5
trans-$[PtBr_2(C_2H_4)(pz)]$	15.6	1.7	6.0	15.0	1.6	6.3
trans-$[PtI_2(C_2H_4)(pz)]$	12.9	1.4	5.0	13.5	1.3	6.2
trans-$[Pt_2Cl_4(C_2H_4)_2(pz)]$	14.4	1.8	4.2	14.5	1.8	4.3
trans-$[Pt_2Br_4(C_2H_4)_2(pz)]$	11.4	1.4	3.3	11.4	1.4	3.2
trans-$[Pt_2I_4(C_2H_4)_2(pz)]$	9.3	1.2	2.7	8.5	1.1	3.2

Table 17. Analytical data on the complexes *trans*-$[PtCl_2(C_2H_4)(R\text{-an})]$, (R-an = substituted anilines)

Complex *trans*-$[PtCl_2(C_2H_4)(R\text{-an})$ R	Calculated			Found		
	%C	%H	%N	%C	%H	%N
H	24.8	2.8	3.6	24.9	3.0	3.8
p-NO_2	22.2	2.3	6.5	22.1	2.4	6.5
p-OCH_3	26.0	3.1	3.4	26.0	3.1	3.5
p-I	18.7	2.0	2.7	19.0	2.0	2.9
p-OPh	35.1	3.1	2.9	36.0	3.2	3.2
p-CH_3	26.9	3.2	3.5	26.9	3.3	3.6
p-CH_2CH_3	29.0	3.6	3.4	31.6	3.8	4.0
p-*t*-Butyl	32.5	4.3	3.2	32.8	4.5	3.5
p-Br	20.6	2.1	3.0	21.2	2.3	3.0
m-NO_2	22.2	2.3	6.5	22.2	2.2	6.6
m-Cl	22.7	2.4	3.3	23.0	2.4	3.5
m-F	24.0	2.5	3.5	24.6	2.5	3.6
m-I	18.7	2.0	2.7	18.8	1.9	2.7
m-Br	20.6	2.1	3.0	21.2	2.2	3.2
m-CH_3	26.9	3.2	3.5	28.7	3.4	3.8
3,4-di-CH_3	29.0	3.9	3.4	29.9	3.8	3.7

4.4 INFRARED AND RAMAN RESULTS

Table 18. Internal ligand frequencies (cm^{-1}) and assignments for the complexes *trans*-$[PtCl_2(C_2H_4)L]$

L	Unlabelled	C_2D_4-labelled	L-deuterated	Assignment[a]
NH_3	3296	3302	2470	νN-H
	3228	3234	2346	
			2324	
			3078	νC-H
			3012	
			2981[b]	
	1610	1607	1017[b]	NH_2 scissor
	1431	1064	1430	CH_2 scissor
	1421	1057	1419	
	1265br	1260br	974	NH_2 twist
	1265br	958	1255br	νC-C
	1023	759br	1026	CH_2 wag
	1010		1007	
	818[b]	807[b]	817	
	745[b]	740[b]	557	NH_2 wag
	694	508	704	CH_2 rock
py	3098 (3098)[c]	2368 (2368)[c]	3092	νC-H (ethylene)
	3078 (3076)	2334 (2331)	3078 (3083)[c]	
	3066 (3064)	2287 (2294)	3062 (3067)	
	2980 (2977)	2214 (2224)	2980 (2973)	
		(3081)	2370	νC-H (py)
		(3067)	2342	
	3030 (3046)	3040 (3046)	2310 (2316)	
			2294 (2297)	
			2268 (2289)	
	1610 (1606)	1602 (1608)	1569 (1569)	(8a)
	(1570)	(1571)	1534 (1528)	(8b)
	1473 (1528)	1472	1324	ν ring (19a)
	1438	1434	1239	(19b)
	1418	962 (964)	1429 (1426)	CH_2 scissor
	1395	1393 (1374)	1381	ν ring (14)
	1343	1342	1324	
	1257 (1258)	962 (964)	1260 (1260)	νC-C (ethylene)
	1245	1243	980 (985)	(3)
	1214 (1211)	1210 (1215)	889 (896)	δC-H (py) (9a)
	1153 (1156)	1151 (1159)	845 (842)	(15)
	1075 (1070)	1065 (1074)	831	δC-H (py) (18b)
	1068 (1050)	1065 (1054)	835	
	1038 (1032)	716	1040	CH_2 wag
	1026	1019	1025	ε ring (12)
	1017 (1018)	1006 (1020)	1025	(1)
	979	978	980 (985)	
	944	943		
	873	872 (822)	703 (705)	γC-H (py) (10b)
	764	760 (772)	571	(11)
	705 (702)	512 (514)	703 (680)	CH_2 rock
	692 (655)	688	528	γC-H (py) (4)
	652 (646)	650 (650)	635 (623)	ε ring (6a)
	445	443 (432)	406	γ ring (16b)

Table 18 continued/

L	Unlabelled	C_2D_4-labelled	L-deuterated	Assignment[a]
pyO	3106			
	3082			
	3062	2332		νC-H (ethylene)
	3048	2224	3085	
	3036	2194	3012	
	3014	3100	2390	
		3078	2303	νC-H(pyO)
		3052	2294	
		3038	2166	
		3024		
	1613	1612	1568	ν ring + νN-O (ν_4)
	1433	1464	1333	ν ring (ν_5)
	1411	950	1412	CH_2 scissor
	1364	1339	1333	ν ring (ν_{16})
	1254	1254	1135	νN-O (ν_6)
	1232	950	1231	νC-C (ethylene)
	1192	1190	985	(ν_7)
	1167	1165	853	(ν_{18})
	1096	1095	816	δC-H(pyO) (ν_{19})
	1072	1071	781	(ν_8)
	1049	1052	760	
	1027	1025	1008	δ ring (ν_9)
	1010	1008	725	γC-H(pyO) (ν_{22})
	1010	802	1008	CH_2 wag
	944	943	651	γC-H(pyO) (ν_{26})
	826	823	559	(ν_{23})
	781	778	546	(ν_{27})
	726	518	725	CH_2 rock
	679	676	651	γ ring (ν_{28})
	574	571	559	(ν_{11})
	511	511[b]	509	γN-O (ν_{21})
an	3240	3236	3238	νN-H
	3208	3202	3206	
	3128	3124	3126	νN-H----Cl
		2362		
		2306		νC-H (ethylene)
		2222		
			2342	
			2292	νC-H (an)
			2284	
			2270	
	1600	1597	1587	ν ring
	1578	1577	1565[b]	NH_2 scissor
	1494	1491	1425	ν ring
	1470[b]	1469[b]	1381	
	1425	808	1425	CH_2 scissor
	1255	959	1255	νC-C (ethylene)
			1160[b]	
	1161	1158	1132	ν ring + NH_2 twist

Table 18 continued/

L	Unlabelled	C_2D_4-labelled	L-deuterated	Assignment[a]
an	1068	1064[b]	841	δC-H
	1027	1025	820	
	1014[b]	684	1014[b]	CH_2 wag
	902	899	638	γC-H (an)
	798	795	747	NH_2 wag
	755[b]	753[b]	559	γC-H (an)
	686	684	559	γ ring
	554	552	559	NH_2 rock
	543	541	499	δ ring
	538	536	499	
Him	3248	3240	3246	νN-H
	3166	3164	2382	νC-H(Him)
	3152	3150	2366	
	3144	3144	2338	
	3082	3078		νC-H (ethylene)
		2396		
		2358		
		2326		
		2278		
		2218		
	2972	2970	2978	νN-H----Cl(Him)
	2868	2867	2894	
	1546	1544	1468	ν ring
	1505	1504	1456	
	1442	1439	1429	
	1429		1429	CH_2 scissor
	1326	1325		
	1262	1261	946	δC-H(Him)
	1257	958	1257	νC-C (ethylene)
	1234	1234	1197	δN-H
	1187	1186	1127	ν ring
	1141	1140	889	δC-H(Him)
	1095[b]	1095[b]	817	
	1069	1066	772	
	1031	742	1032	CH_2 wag
	1014		1014	
	838	838	722	δ ring
	758	515	752	CH_2 rock
	744	742	591	γC-H(Him)
	648	647	552	γ ring
	620	619	527	
	616	615	521	

a Numbers in parentheses refer to the band numbers given in references [94] (L = pyO) and [95] (L = py)

b Mean of doublet.

c Numbers in parentheses refer to Raman frequencies.

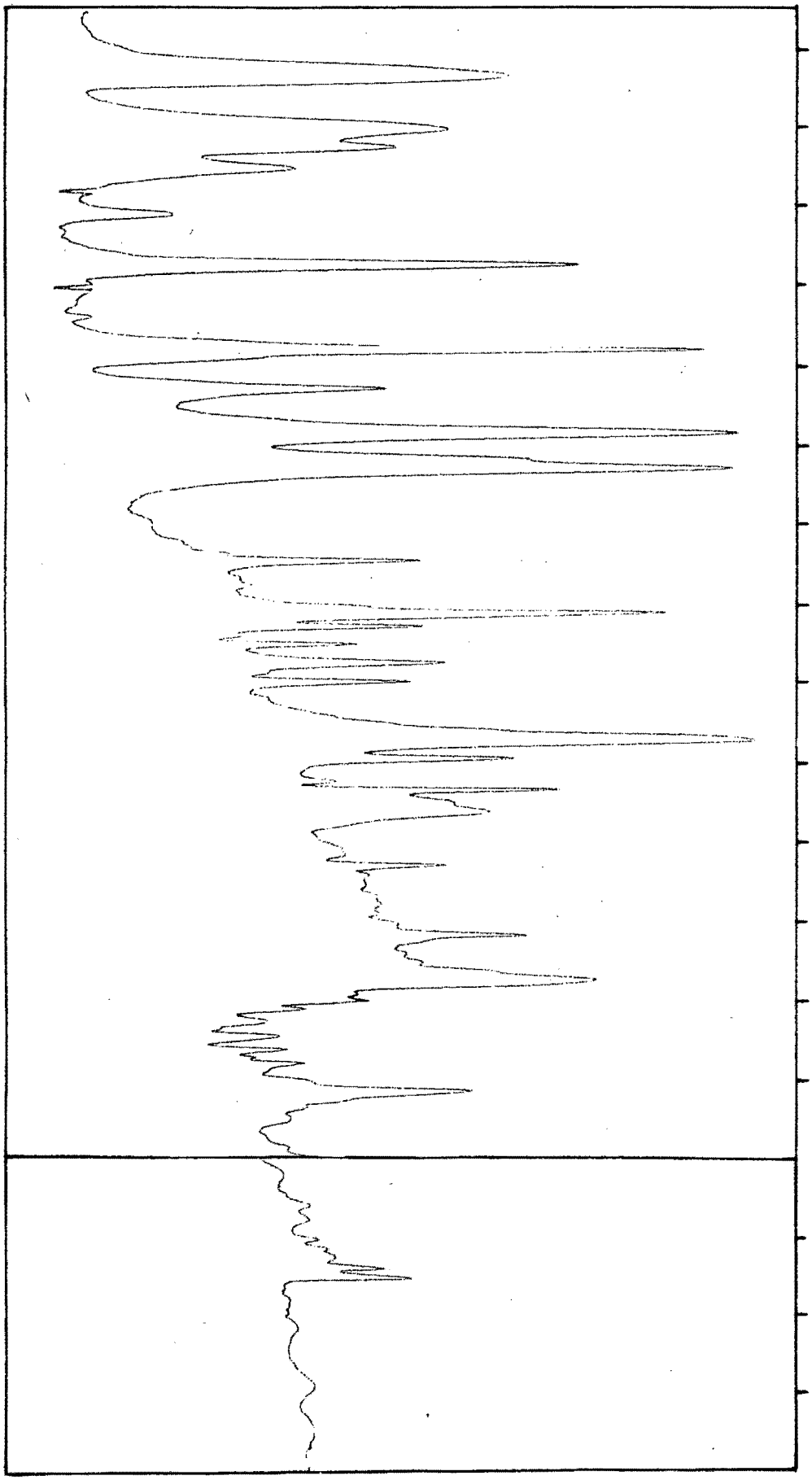

Figure 32. Infrared spectrum of *trans*-$[PtCl_2(C_2H_4)(pyO)]$

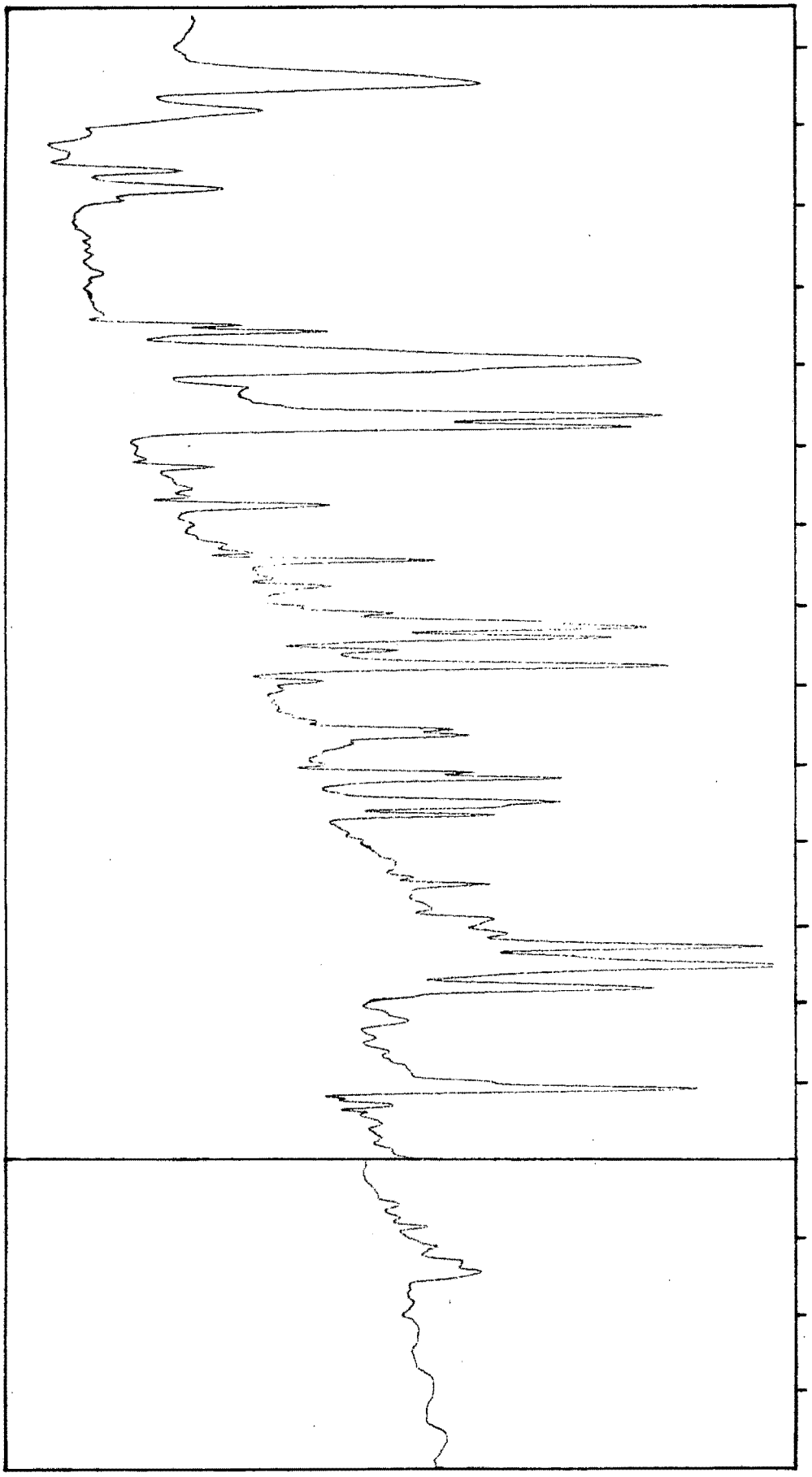

Figure 33. Infrared spectrum of *trans*-$[PtCl_2(C_2H_4)(py)]$

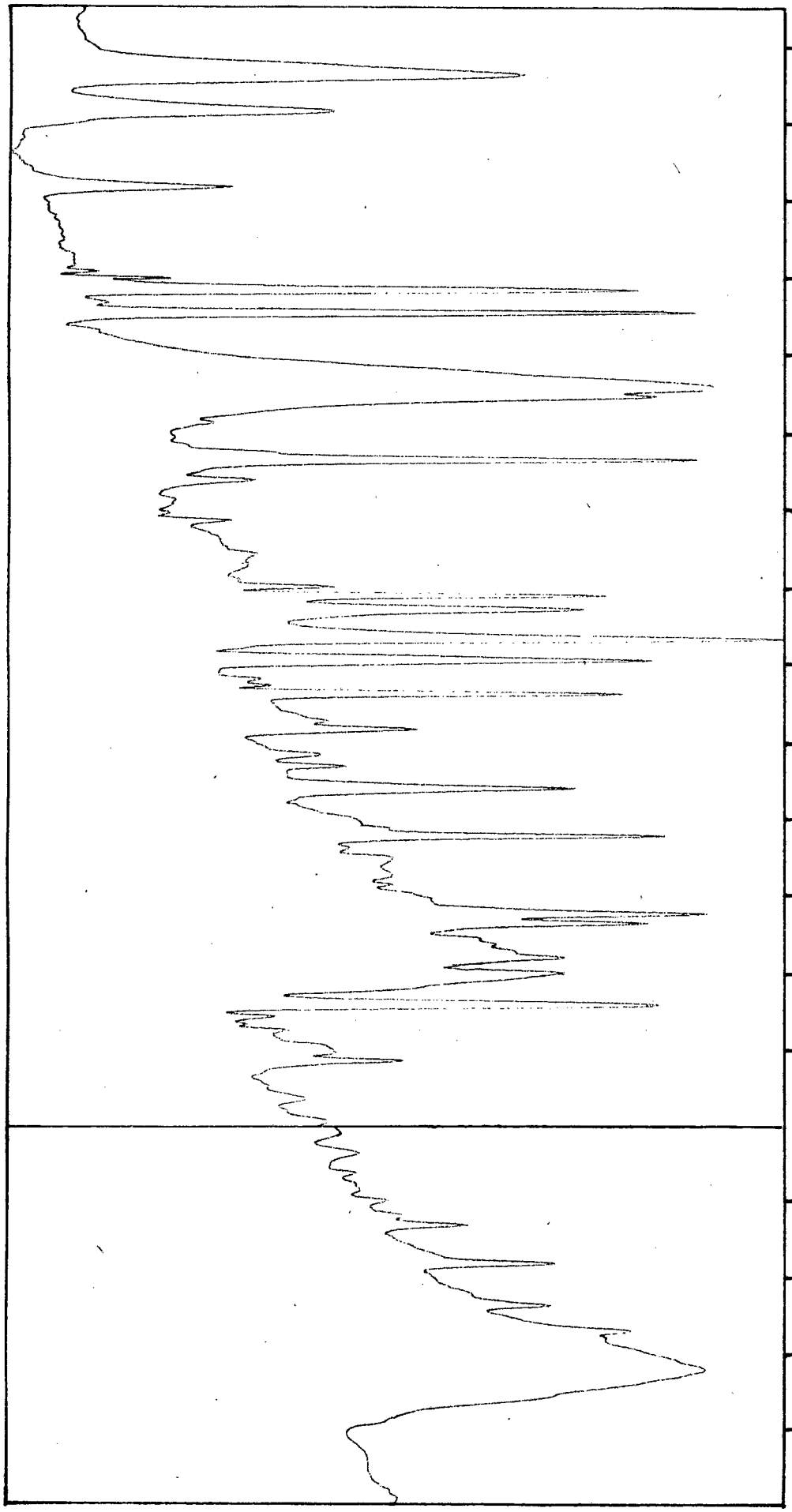

Figure 34. Infrared spectrum of *trans*-$[PtCl_2(C_2H_4)(Him)]$

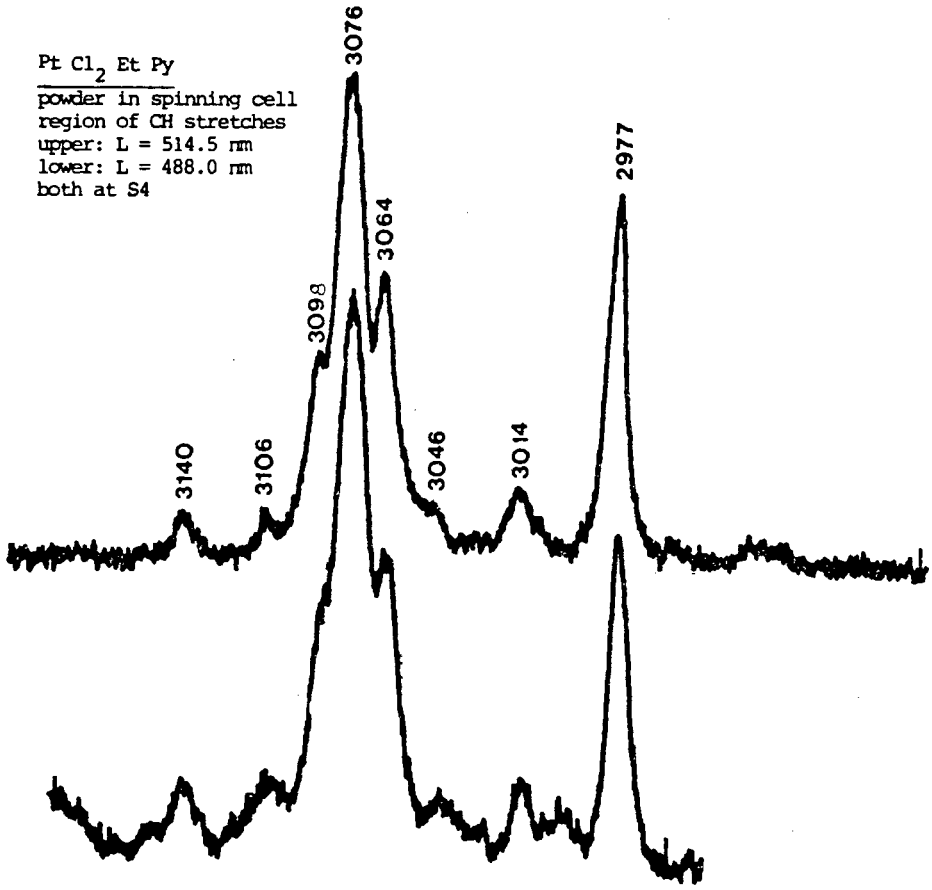

Figure 35. Raman spectrum of *trans*-$[PtCl_2(C_2H_4)(py)]$

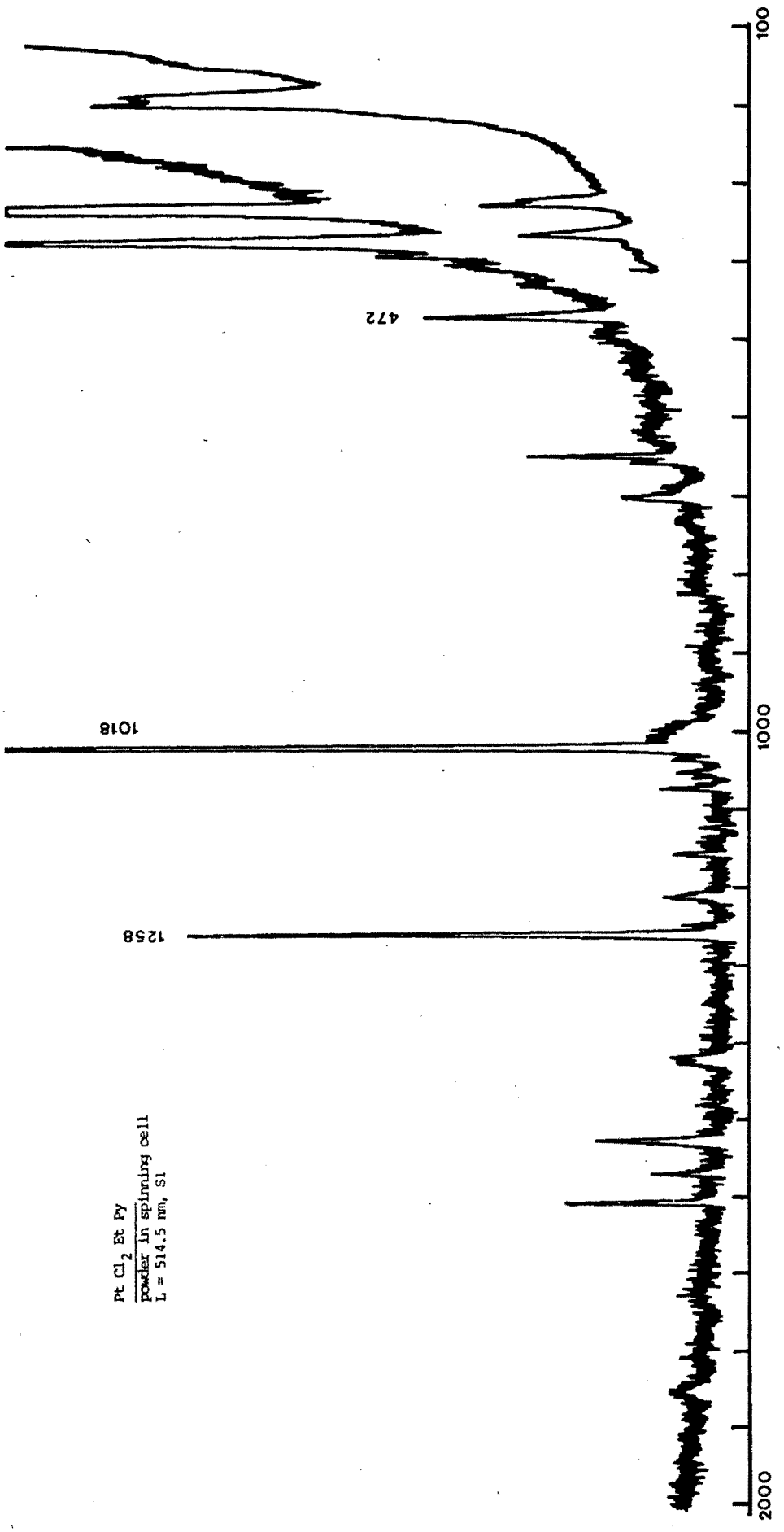

Figure 35 continued/

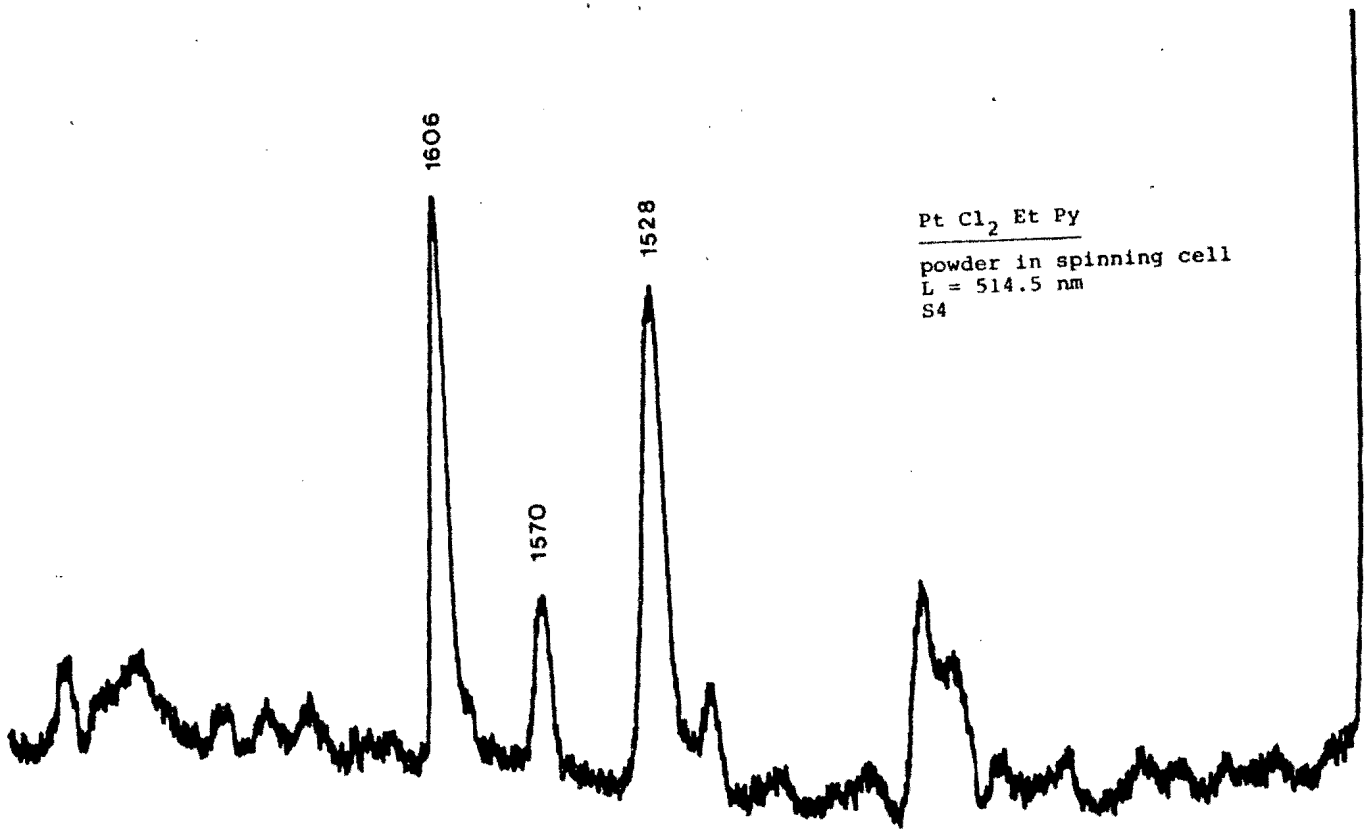

Figure 35 continued/

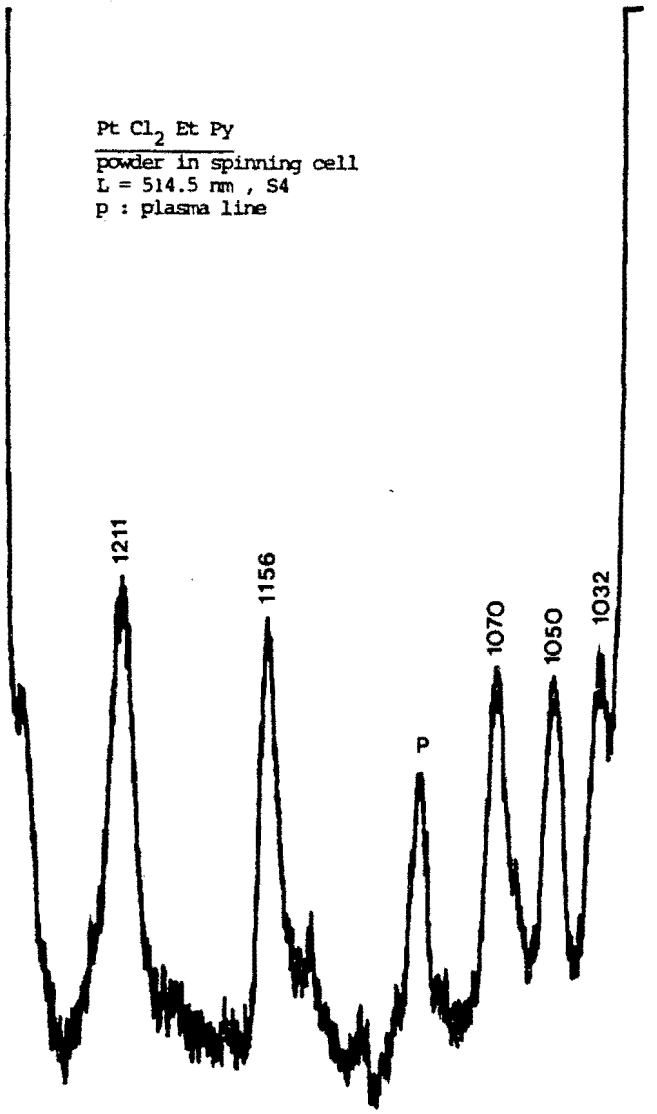

Figure 35 continued/

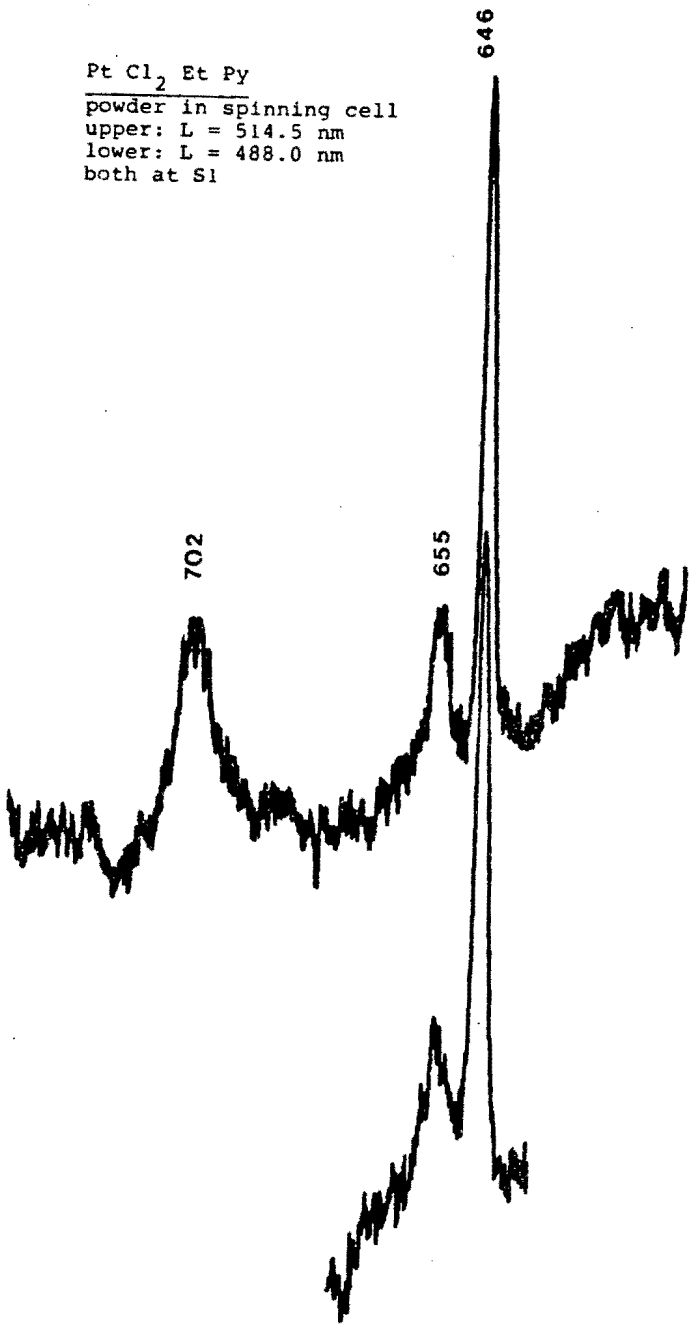

Figure 35 continued/

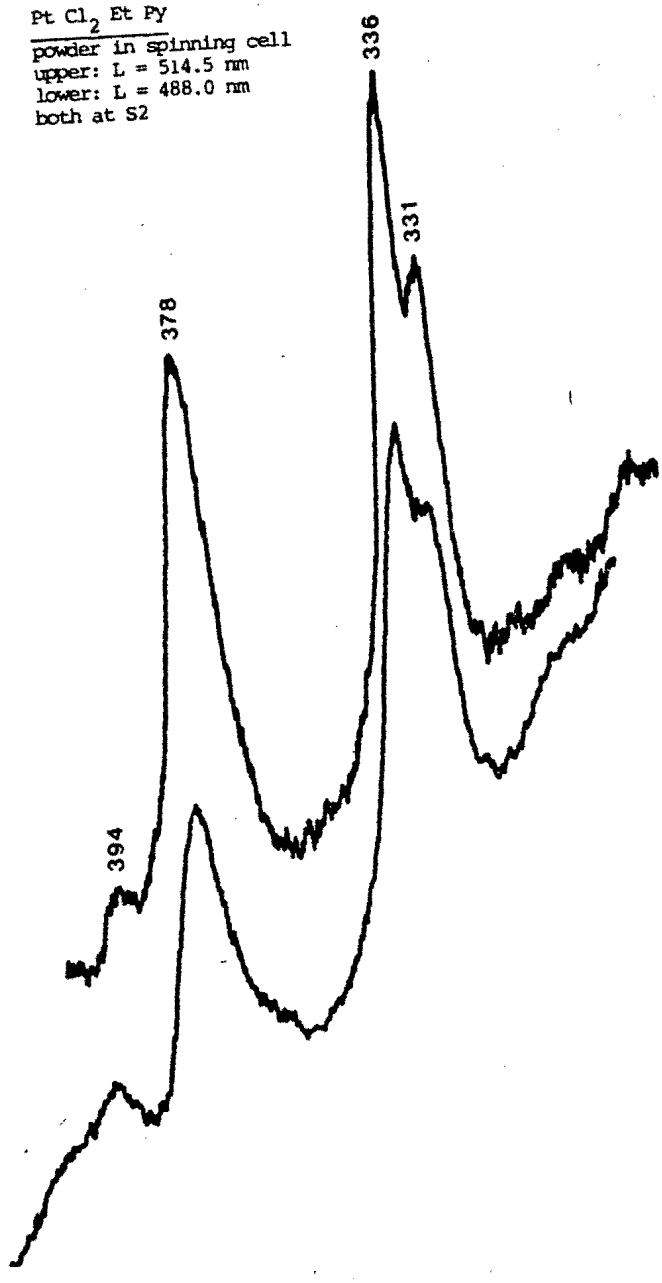

Figure 35 continued/

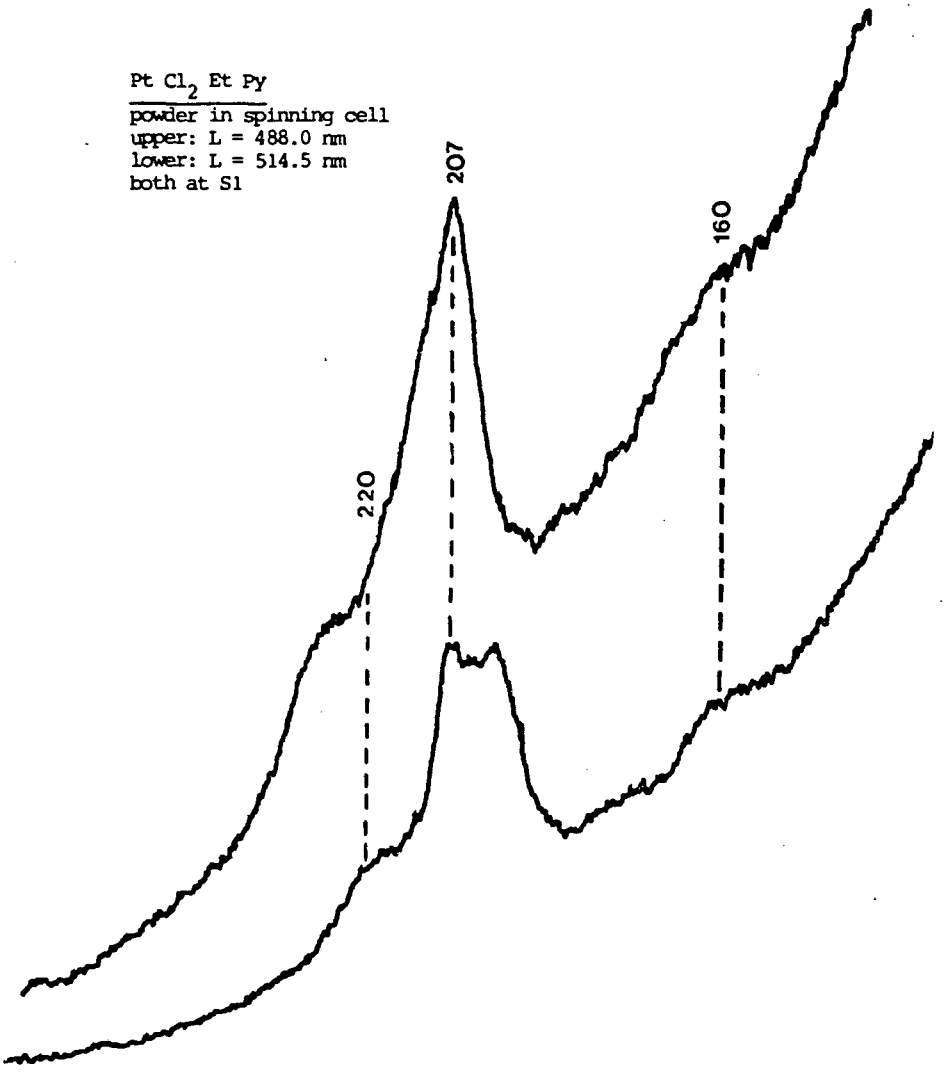

Figure 35 continued/

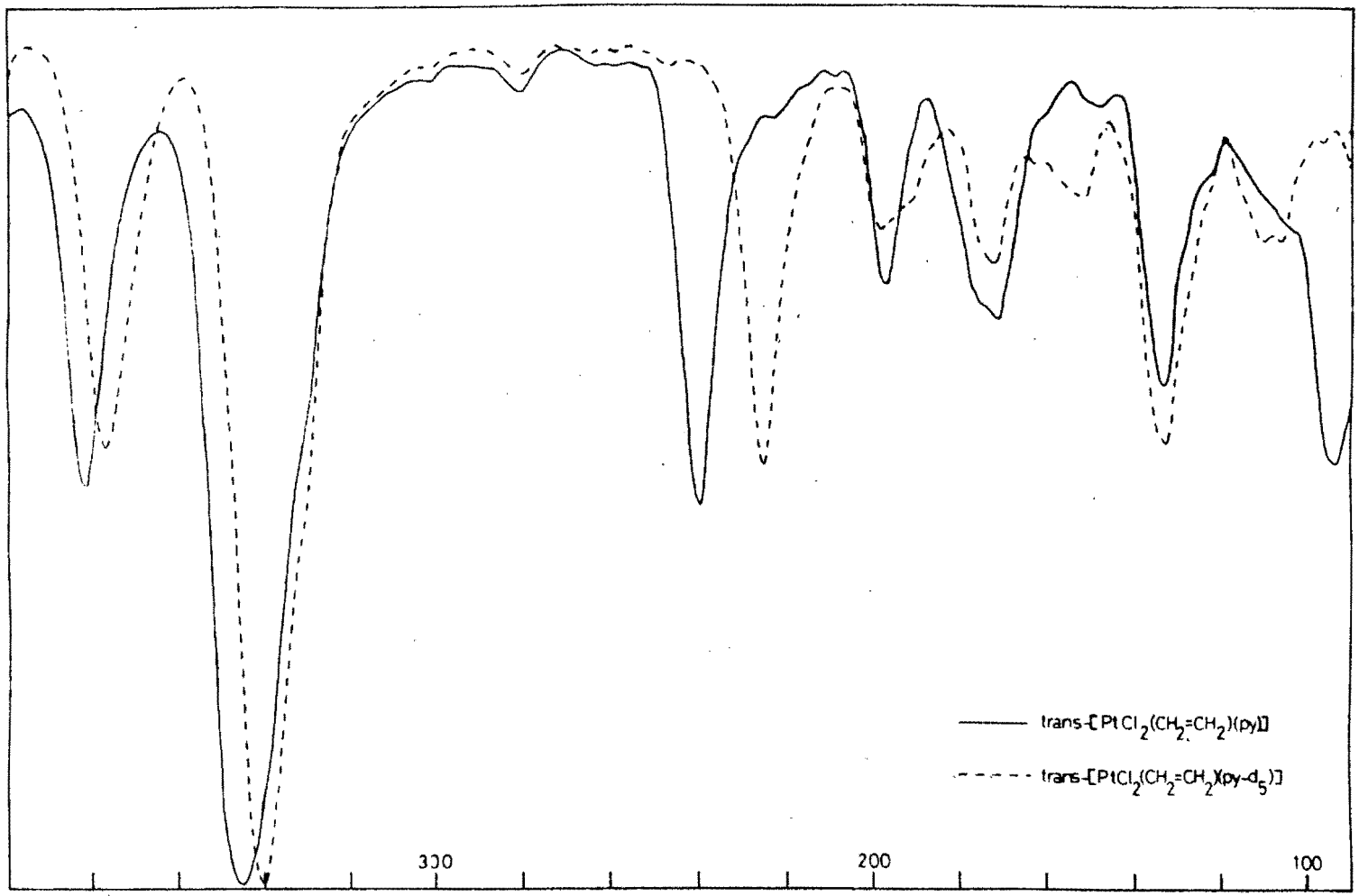

Figure 36. The infrared spectrum of *trans*-$[PtCl_2(CH_2CH_2)(py)]$ and its deuterated analogue *trans*-$[PtCl_2(CH_2CH_2)(py\text{-}d_5)]$

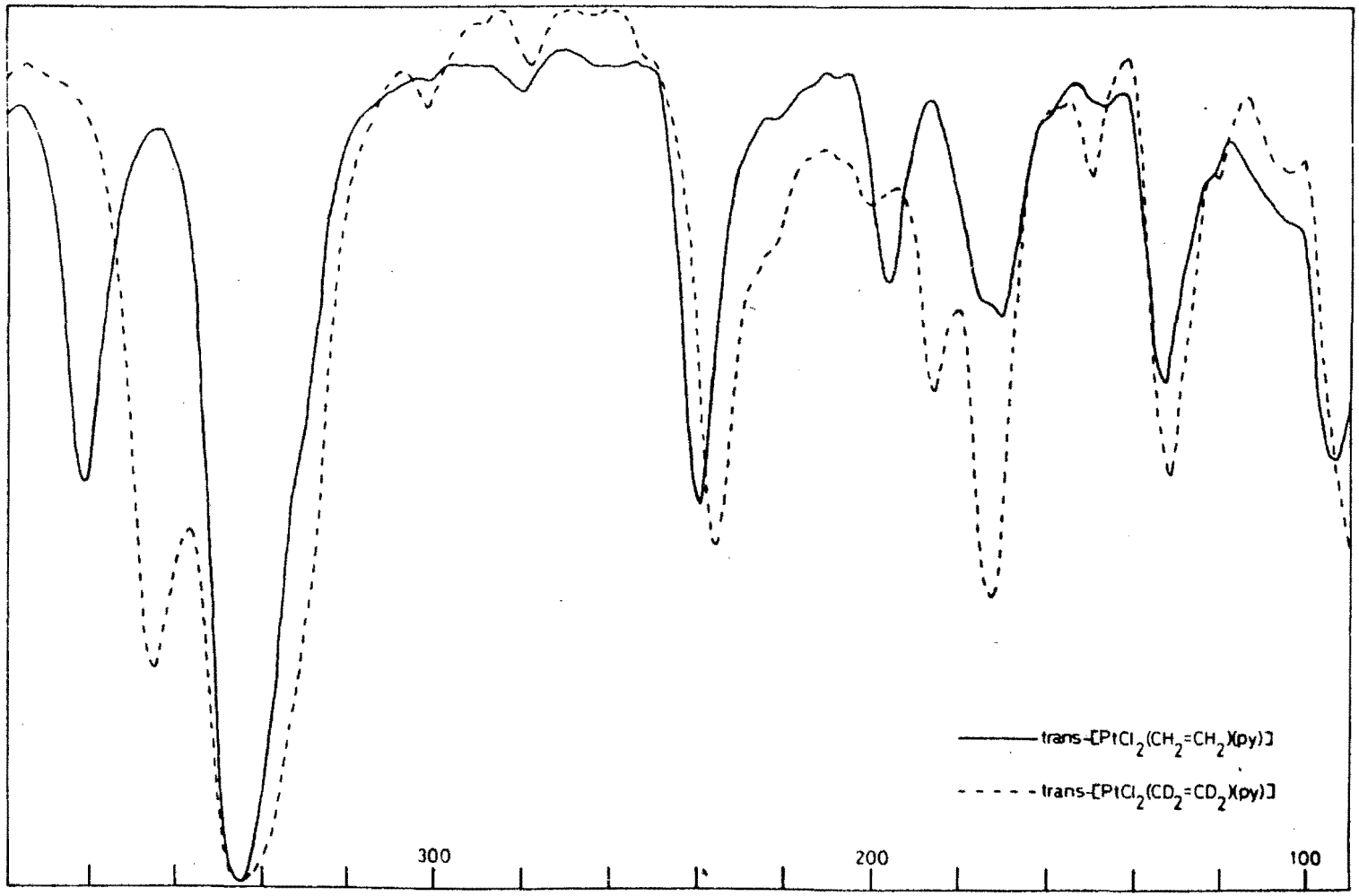

Figure 37. The infrared spectrum of *trans*-$[PtCl_2(CH_2CH_2)(py)]$ and its deuterated analogue *trans*-$[PtCl_2(CD_2CD_2)(py)]$

Table 19. Internal ligand frequencies (cm^{-1}) and assignments for the complexes *trans*-$[PtBr_2(C_2H_4)L]$

L	Unlabelled	C_2D_4-labelled	L-deuterated	Assignment[a]	
NH_3	3294	3300	2455		
	3222	3230	2344	νN-H	
			2320		
	3010	2198	3009	νC-H	
	2976		2976		
	1607	1613		NH_2 scissor	
	1417	1057	1417	CH_2 scissor	
	1271	1271[b]	974	NH_2 twist	
	1263	959	1263	νC-C	
	1015	759 br	1015	CH_2 wag	
	1004		1004		
	747	750	561	NH_2 wag	
	693	509	701	CH_2 rock	
py	3090	2220		νC-H (ethylene)	
	3071				
			2370	νC-H (py)	
			2289		
	1605	1606	1566	ν ring	(8a)
	1595				(8b)
	1480	1480	1322		(19a)
	1449	1451	1236		(19b)
	1425	963	1425	CH_2 scissor	
	1394	1394	1334	ν ring	(14)
	1350	1351	1314		
	1257	963	1257	νC-C (ethylene)	
	1240	1240	979	δC-H (py)	(3)
	1210	1212	888		(9a)
	1156	1156	844		(15)
	1090	1090	835		(18b)
	1069	1068	829		
	1050	741	1040	CH_2 wag	
	1030		1025		
	1021	1019	1020	δ ring	(12)
	1016	1006	1010		(1)
	973	974	980		
	939	940			
	870	870	716	γC-H (py)	(10b)
	760	758	572		(11)
	700	510	701	CH_2 rock	
	689	690	529	γC-H (py)	(4)
	654	653	636	δ ring	
	648	648	626		(6a)
	447	447	405	γ ring	(16b)

Table 19 continued/

L	Unlabelled	C_2D_4-labelled	L-deuterated	Assignment[a]
an	760	761	558	γC-H (an)
	749	754		
	686	686	558	γ ring
	554	554		NH_2 rock
	541	541	497	δ ring
Him	3250	∿3240	∿3235	νN-H
	3141	3144	2370	νC-H (Him)
	3130	3134	2345	
		2346		νC-H (ethylene)
	1541	1538	1485	ν ring
	1506	1505	1470	
	1430	1432	1425	
	1424	812	1425	CH_2 scissor
	1329	1329	974	δC-H (Him)
	1261	1261	939	
	1251	959	1251	νC-C (ethylene)
	1229	1229	1185	δN-H
	1175	1176	1118	ν ring
	1129	1130	1110	
	1105	1106	892	δC-H (Him)
	1072	1070[b]	818	
	1018	756	1018	CH_2 wag
	1013		1013	
	955	953	818	δ ring
	917	917	782	
	867	867	732	
	844	845	729	
	754	756	586	δC-H (Him)
	702 (sm)			CH_2 rock
	650	651	558	γ ring
	614	614	520	

a Numbers in parentheses refer to the band numbers given in references [94] (L = pyO) and [95] (L = py)

b Mean of a doublet

Table 20. Metal-ligand frequencies and isotopically-induced shifts (cm^{-1}) in the infrared spectra of the complexes *trans*-$[PtX_2(C_2H_4)L]$[a]

L,X	νPt-C_2	νPt-L	νPt-X	Other
NH_3,Cl	478(5,1) 384(22,8)	471(0,30)	335(3,5)	221(7,12) 167(5,17)
NH_3,Br	381(8,2)	473(0,31)	248(2,1)	223(5,18) 169(0,5) 118(3,0) 100(0,0)
py,Cl	474(40,5) {472}(40,0)[b] 381(12,5) {378}(17,0)	239(3,14) {227}(-,17)[b]	345(0,4) {336}(0,0)[b] {331}(0,0)	{207}(11,5) 196(10,0) 171(0,0) {160}(0,10) 151(1,18) 133(1,0)
py,Br	468(38,0) 374(17,0)	260(3,30)	260(3,3)	217(1,5) 177(5,0) 149(-,0) 120(2,0) 92(2,0)
pyO,Cl	549(31,3) 427(29,2)	451(4,26) 401(3,22)	345(tb,2)	219(7,5) 207(12,6) 170(0,1) 144(0,2) 122(1,0) 100(0,-)
pyO,Br	-[c] 424(19,0)	445(0,21) 397(0,18)	251(0,0)	219(2,0) 201(15,2) 170(-,0) 133(0,2) 117(3,0) 90(8,0)
an,Cl	476(45,0) 384(15,3)	434(3,30) 384(2,11)	338(tb,0)	204(17,3) 158(0,2) 141(2,1) 120(2,2)
an,Br	477(42,0) 384(9,2)	434(0,31) 384(9,19)	248(2,0)	195(13,1) 140(0,0) 125(2,1) 116(2,0) 92(0,4)

Table 20 continued/

L,X	νPt-C_2	νPt-L	νPt-X	Other
Him,Cl	485(41,0) 389(17,0)	266(4,11)	347(2,0)	198(0,0) 178(1,0) 150(0,0) 120(0,7) 100(2,3)
Him,Br	477(36,0) 389(15,0)	278(3,7)	226(0,3)	187(11,1) 134(0,2) 115(0,0) 93(0,0)

[a] Figures in parentheses are the shifts (cm^{-1}) induced by C_2D_4-labelling and deuterations of L, respectively. Negative shifts are written as zero shifts. tb = too broad for shift to be determined.

[b] Figures in braces are the bands observed in the Raman spectra.

[c] No band observed in unlabelled spectrum. Bands are observed at 522 and 545 cm^{-1} in C_2D_4-labelled and L-deuterated spectra, respectively.

Table 21. Mid-ir data for the complexes of type (I) and type (II)

X = Cl			X = Br			X = I			Assignment	
-	C_2D_4	pz-d_4	-	C_2D_4	pz-d_4	-	C_2D_4	pz-d_4		
Type (I) complexes										
3113	3112	2324	3104	3106	2372	3103		2304		
3097	3097							2293	νC-H(pz)	
			3094	3093						
3050	3054	2290								
3072	2314			2310						
2990	2204	2990		2206					νC-H(ethylene)	
	2176			2130						
1484	1484	1322				1483	1484	1424	γ ring	(19a)
1462	1267	1462								
1423	1425	1166	1419	1417	1167	1422	1418	1175	γ ring	(19b)
1412	936	1401	1390	940	1413				CH_2 scissor	
1163	1166	1130	1164	1164	1140	1167	1167	1139	γ ring	(12)
1125	1125	876	1110	1109	868	1121	1120	873	δC-H(pz)	(18a)
1056	1056		1083	1064						
		1040				1070	1067	1054	γ ring	(14)
1050	1049	1076	1056							
1011		1012	1008							
	751			745	1005	1017	737	1014	CH_2 wag	
1003		1002	1003							
981	983	845			868		979	906	γ ring	(1)
828	514	818		518	840			842	CH_2 rock	
817	813	640	817	817	668			651	δC-H(pz)	(10b)
						808	807			
812	813	634	808	809	634			611	γ ring	(11)
482	482	449	506	508	471	512	487	447	γ ring	(16b)
Type (II) complexes										
3112	3106	2377	3106	3104	2368			2317		
3080		2346	3093	3095	2345			2295	νC-H(pz)	
3062	3056	2301			2287					
2983			3007						νC-H(ethylene)	
1484	1484	1325			1287			1293	ν ring	(19a)
1427	1266	1423	1423		1427	1420		1426	CH_2 scissor	
1427	1419	1175	1419	1419	1171	1420	1422	1174	ν ring	(19b)
1260	962	1260	1254	982	1253				νC-C(C_2H_4)	
1169	1160	1138	1163	1163	1138	1171	1172	1134	ν ring	(12)
						1118	1120	874		
1121	1118	846	1110	1110		1111	1110	843	δC-H(pz)	(18a)
			1090	1090						
1085	1083	1037	1083	1082					ν ring	(14)

Table 21 continued/

X = Cl			X = Br			X = I			Assignment	
-	C_2D_4	pz-d_4	-	C_2D_4	pz-d_4	-	C_2D_4	pz-d_4		
Type (II) complexes (cont.)										
1027	761	1027	1008	755	1007	1010	725	1012	CH_2 wag	
1014	750	1027	1002	725	1002	1004				
957	955	882							ν ring	(1)
828	601		694	519	698				CH_2 rock	
798	793	643	807	807	645				γ ring	(11)
725	721	725	728	725		726	725	725		
500	504[a]	460	506	495	462	509	512	447	γ ring	(16b)

[a] Mean of a doublet

Table 22. Far-ir data for complexes of type (I) and type (II)[a]

X	νPt-C_2 cm^{-1}	νPt-N cm^{-1}	νPt-X cm^{-1}	Other cm^{-1}
Type (I) complexes				
Cl	463(10,0)	211(0,31)	342(1,0)	230(15,0) 176(0,14) 140(0,6)
Br	472(33,0)	210(0,11)	254(4,2)	149(0,0)
I	480(40,16)	209(masked)	181(0,0)	223(25,0) 168(masked) 140(masked)
Type (II) complexes				
Cl	471(39,1) 386(19,0)	187(23,10)	349(1,1)	210(10,0) 166(2,0) 140(13,8)
Br	479(41,2) 396(15,0)	177(0,5)	252(2,2)	198(11,2) 160(0,6) 137(9,4)
I	487(sh,0) 396(31,15)	170(0,8)	182(2,2)	198(18,3) 162(2,0) 139(0,0)

[a] Figures in parentheses are the shifts on ethylene-d_4 and pyrazine-d_4 labelling, respectively.

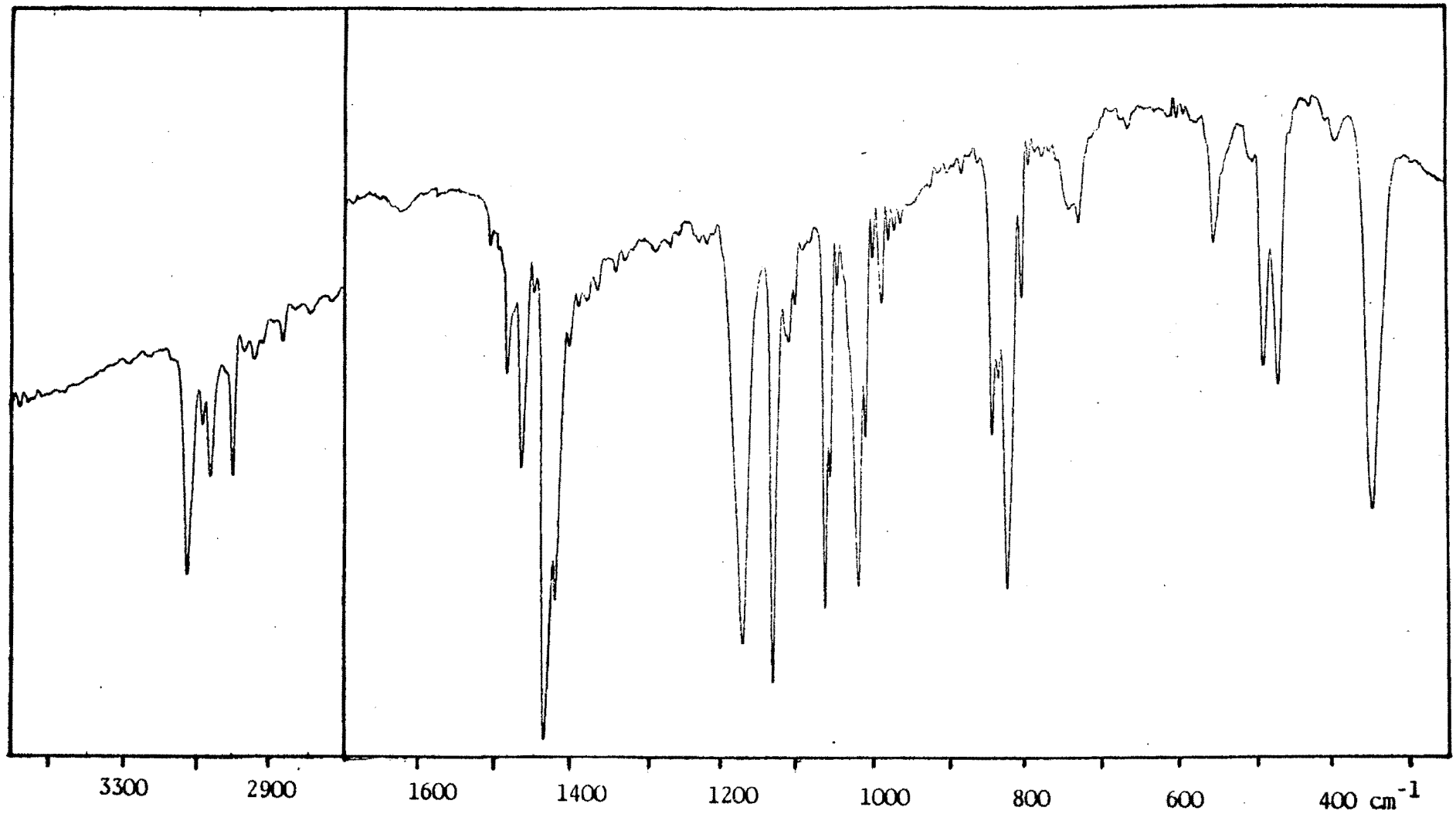

Figure 38. Infrared spectrum of *trans*-$[PtCl_2(C_2H_4)(pz)]$

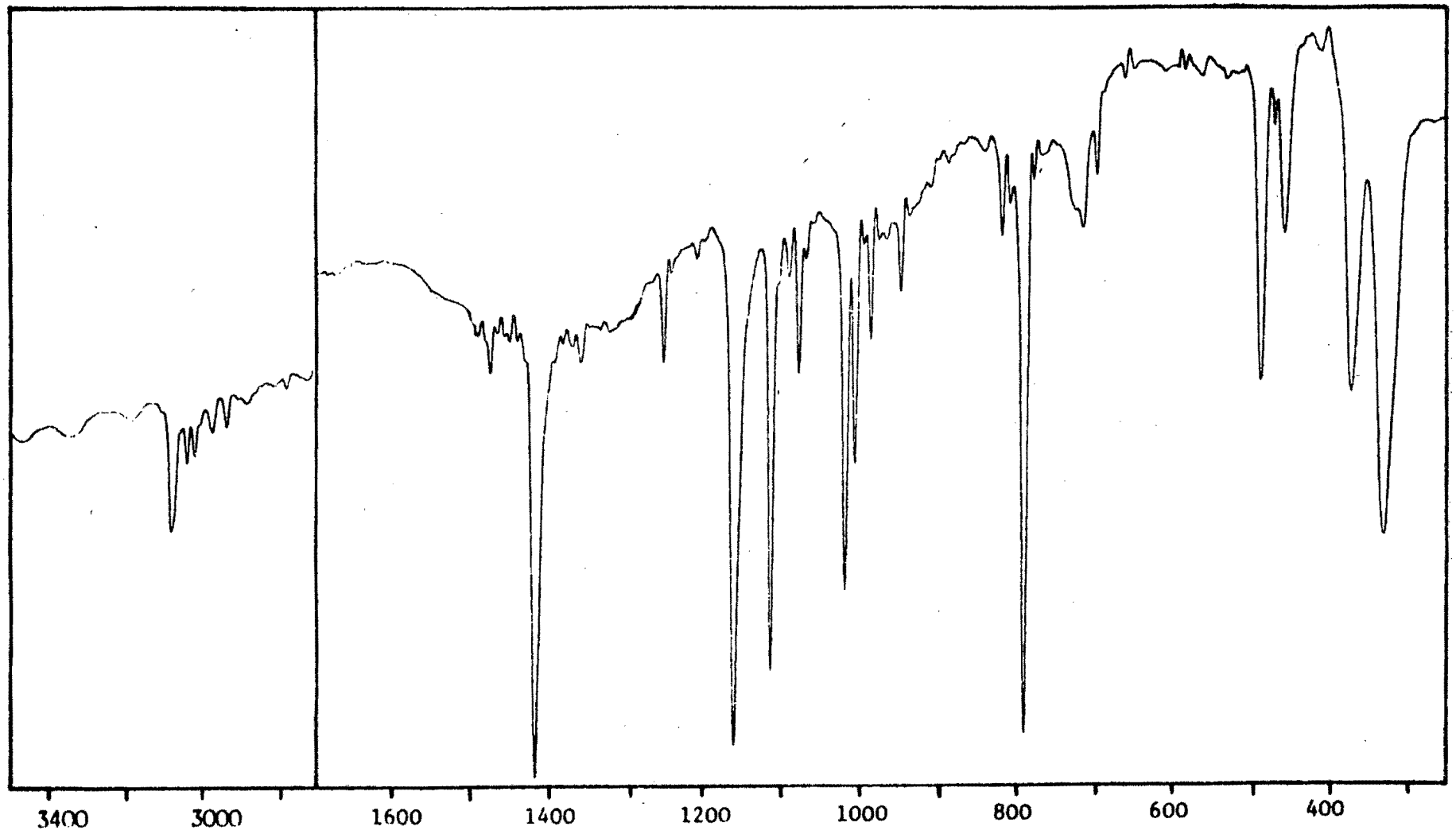

Figure 39. Infrared spectrum of *trans*-$[Pt_2Cl_4(C_2H_4)_2(pz)]$

Table 23. Infrared stretching frequencies for the complexes *trans*-$[PtCl_2(CH_2{=}CH_2)(R\text{-an})]$

Substituent	σ	ν_{as}Pt-C_2 cm^{-1}	ν_sPt-C_2 cm^{-1}	νC-C cm^{-1}	νPt-N cm^{-1}
p-NO_2	0.778	430	372	1222	394
m-NO_2	0.710	437[a]	370	1222	393
m-Br	0.391	450[a]	381	1220	395
m-Cl	0.373	449[a]	383	1230[a]	403
p-I	0.352	446[a]	379	1235[a]	392
p-F	0.337	453	383	masked	400
p-I	0.276	451	380[a]	1222	399
p-Br	0.232	456	383	1226	400
H	0	479	385	1255	410
p-OC_6H_5	-0.028	480	384	masked	419
m-CH_3	-0.069	484	383	1253	420
p-*t*-C_4H_9	-0.120	483	389	1257	412
p-CH_3	-0.170	488	389[a]	1256[a]	420
3,4-di-CH_3	-0.240	487	387	1252	433
p-OCH_3	-0.268	498	390	1263sh	426

[a] Mean of doublet

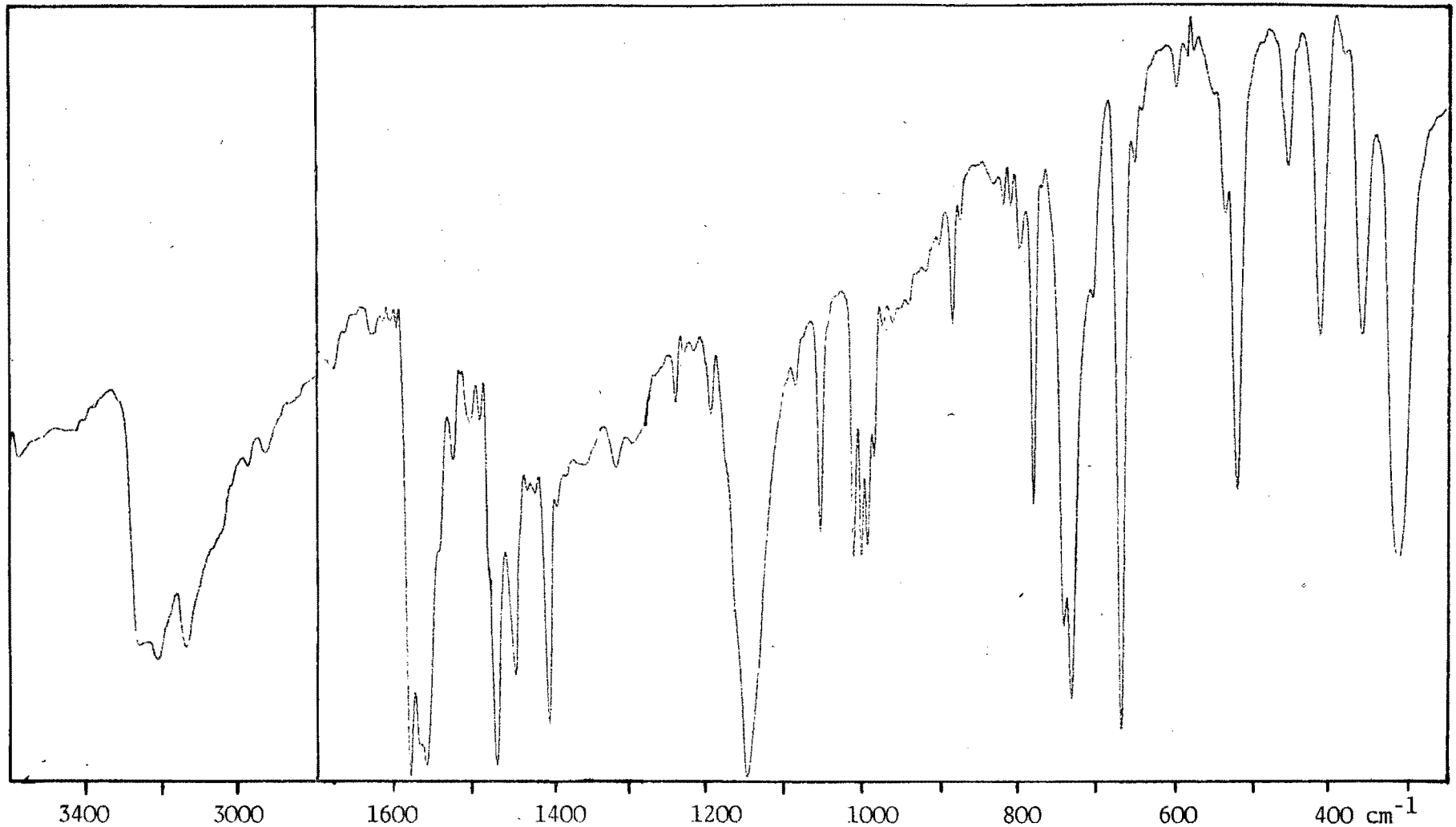

Figure 40. Infrared spectrum of *trans*-$[PtCl_2(C_2H_4)(an)]$

4.5 ^{1}H-NMR RESULTS

Table 24. ^{1}H-nmr data for *trans*-$[PtX_2(C_2H_4)(pyO)]$, (X = Cl, Br)[a]

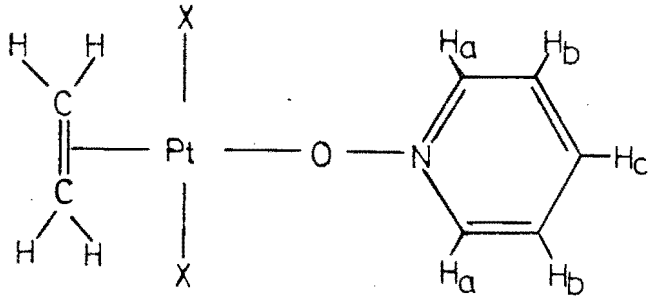

Olefin protons

X	J_{Pt-H} (Hz)	Chemical shift (ppm)
Cl	60.4	4.36
Br	61.2	4.50

N-oxide protons

X	Chemical shift (ppm)		
	H_a	H_b	H_c
Cl	8.58	7.69	7.87
Br	8.54	7.69	7.84

[a] The ^{1}H-nmr spectra were run on a Bruker WH 90 spectrophotometer, using $CDCl_3$ as solvent and lock and TMS as a reference.

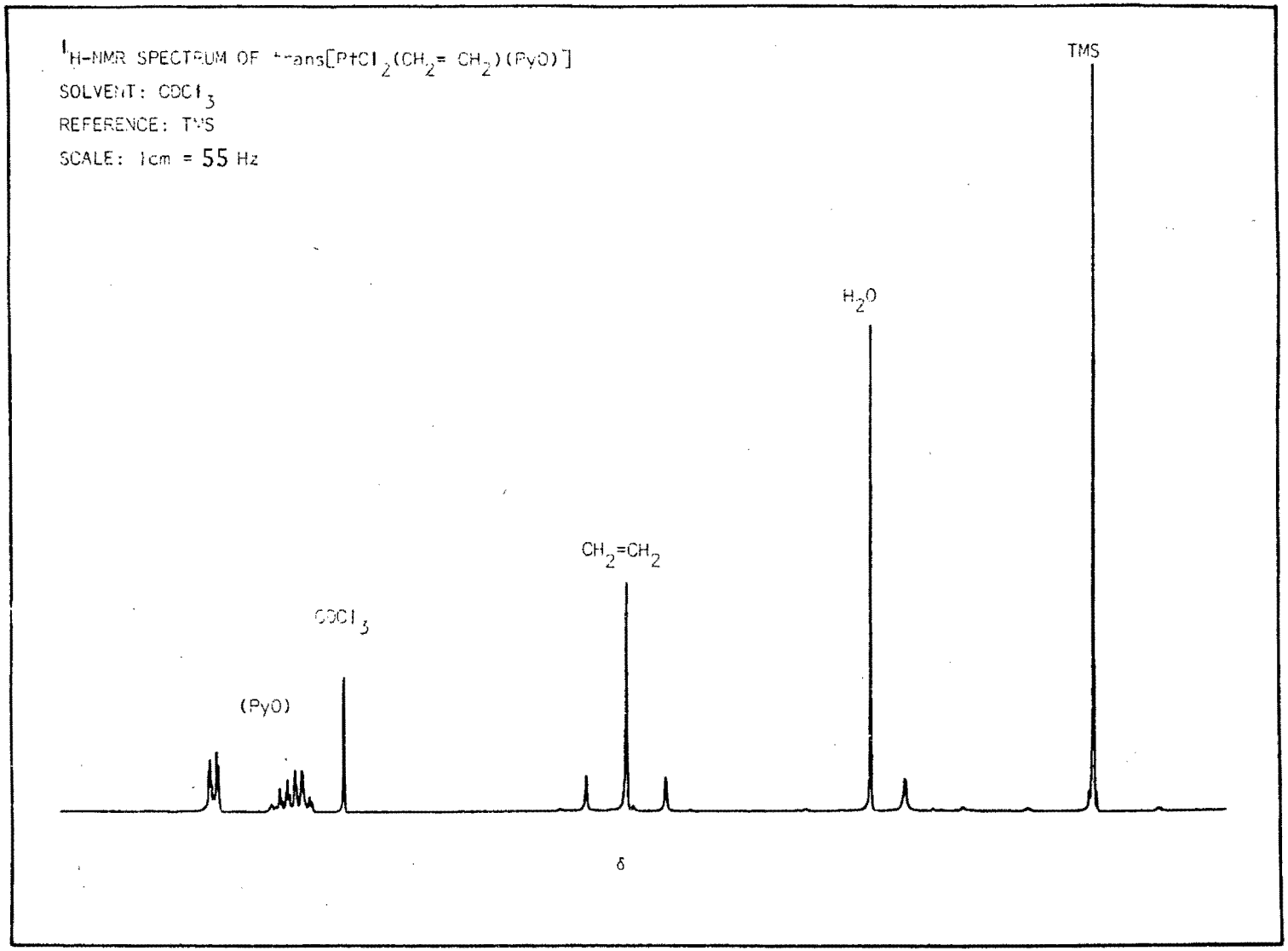

Figure 41. ^{1}H-nmr spectrum of *trans*-[$PtCl_2(CH_2{=}CH_2)(pyO)$]

Table 25. ^{1}H-nmr data for *trans*-$[PtX_2(C_2H_4)(py)]$, (X = Cl, Br)[a]

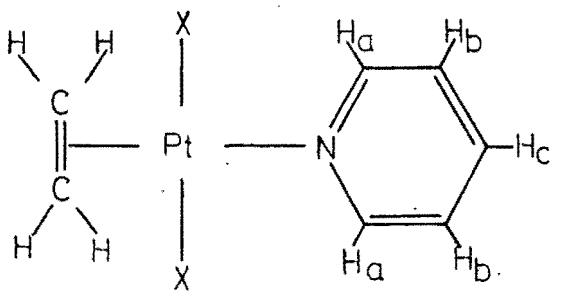

Olefin protons

X	J_{Pt-H} (Hz)	Chemical shift (ppm)
Cl	61.2	4.88
Br	61.2	5.02

Pyridine protons	Chemical shifts (ppm)		
X	H_a	H_b	H_c
Cl	8.90	7.49	7.90
Br	8.94	7.47	7.90

a The ^{1}H-nmr spectra were run on a Bruker WH 90 spectrophotometer using $CDCl_3$ as solvent and lock and TMS as a reference.

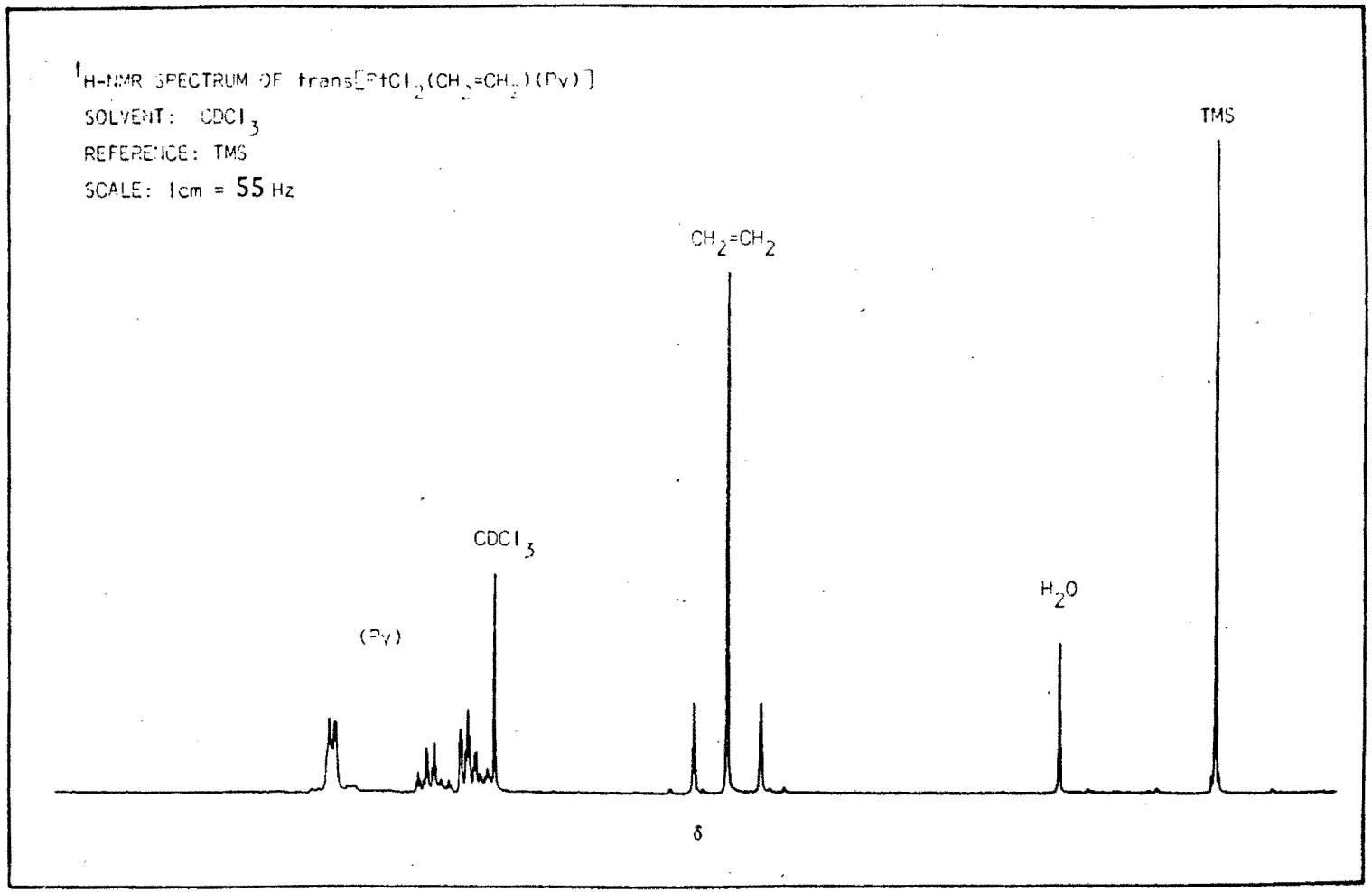

Figure 42. ^{1}H-nmr spectrum of *trans*-$[PtCl_2(CH_2{=}CH_2)(py)]$

Table 26. ^{1}H-nmr data for *trans*-$[PtX_2(C_2H_4)(an)]$, (X = Cl, Br)[a]

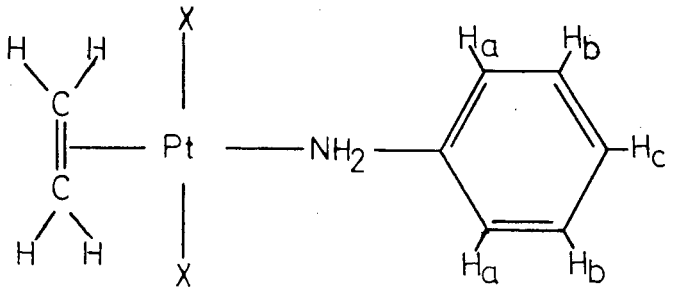

Olefin protons

X	J_{Pt-H} (Hz)	Chemical shift (ppm)
Cl	63	4.69
Br	62	4.79

Aniline protons

X	Chemical shift (ppm)		
	H_a	H_b	H_c
Cl	multiplet at 7.35		
Br	multiplet at 7.36		

[a] The ^{1}H-nmr spectra were run on a Bruker WH 90 spectrophotometer using a $CDCl_3$ as solvent and lock and TMS as reference.

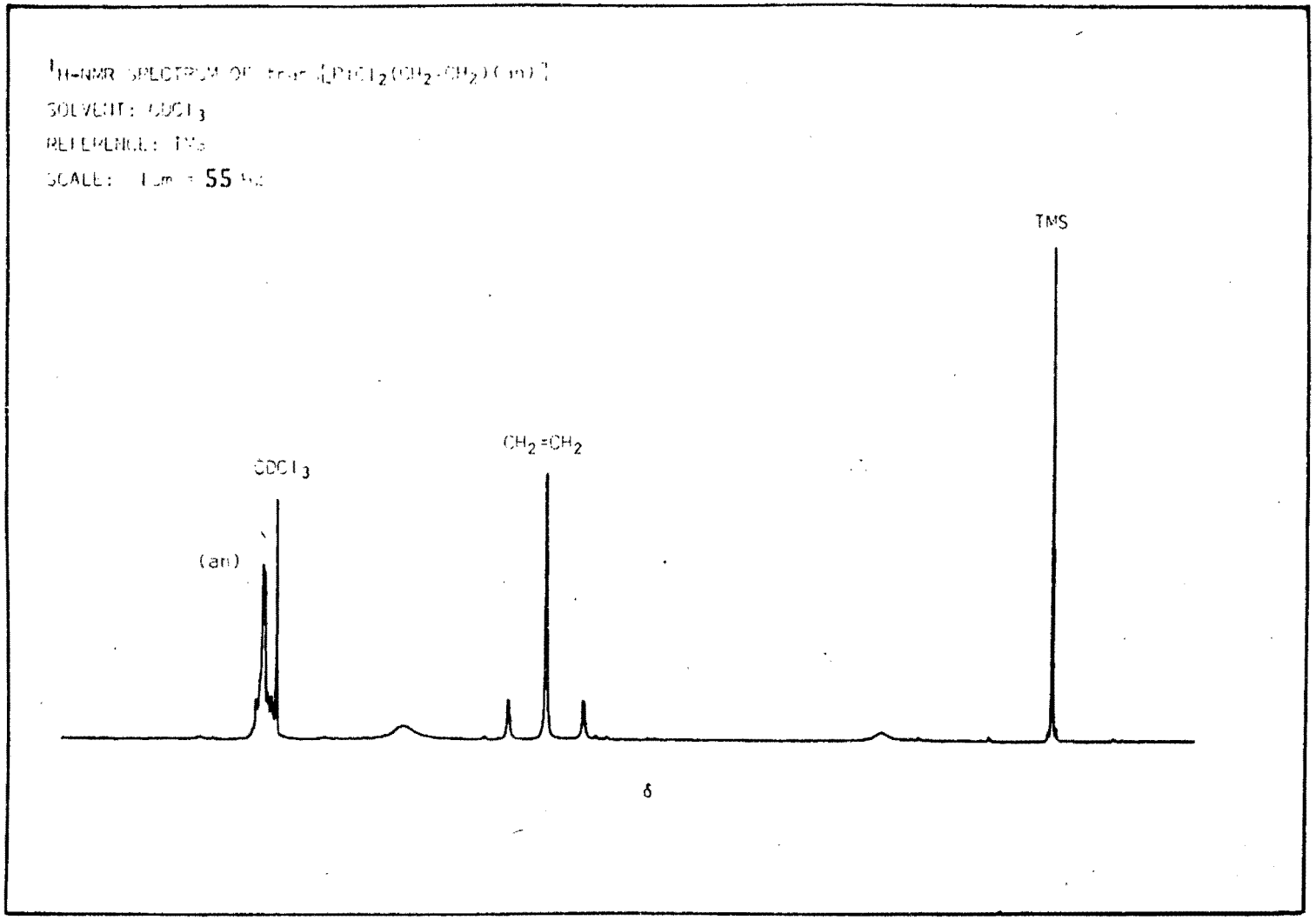

Figure 43. ^{1}H-nmr spectrum of *trans*-$[PtCl_2(CH_2{=}CH_2)(an)]$

Table 27. ^{1}H-nmr data for *trans*-[$PtX_4(C_2H_4)(Him)$], (X = Cl, Br)[a]

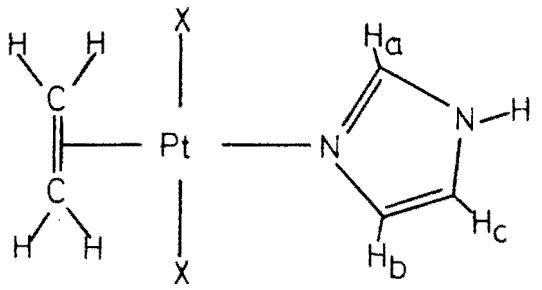

Olefin protons

X	^{J}Pt-H (Hz)	Chemical shift (ppm)
Cl	60.3	4.70
Br	60.0	4.87

Imidazole protons				Chemical shift (ppm)		
X	^{J}Pt-H_a	^{J}Pt-H_b	^{J}Pt-H_c (Hz)	H_a	H_b	H_c
Cl	19.8	19.8	b	8.49	7.72	7.05
Br	19.8	19.8	b	8.49	7.79	7.09

[a] The ^{1}H-nmr spectra were run on a Bruker WH 90 spectrophotometer using $CDCl_3$ as solvent and lock and TMS as a reference.

[b] Coupling was not observed.

Table 28. ^{1}H-nmr data for *trans*-$[PtX_2(C_2H_4)(NH_3)]$, (X = Cl, Br)[a]

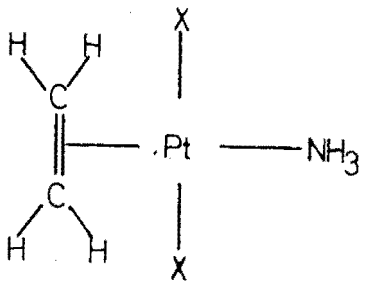

Olefin protons

X	$^{J}_{Pt-H}$ (Hz)	Chemical shift (ppm)
Cl	63	4.73
Br	62	4.81

[a] The ^{1}H-nmr spectra were run on a Bruker WH 90 spectrophotometer using $CDCl_3$ as solvent and lock and TMS as a reference

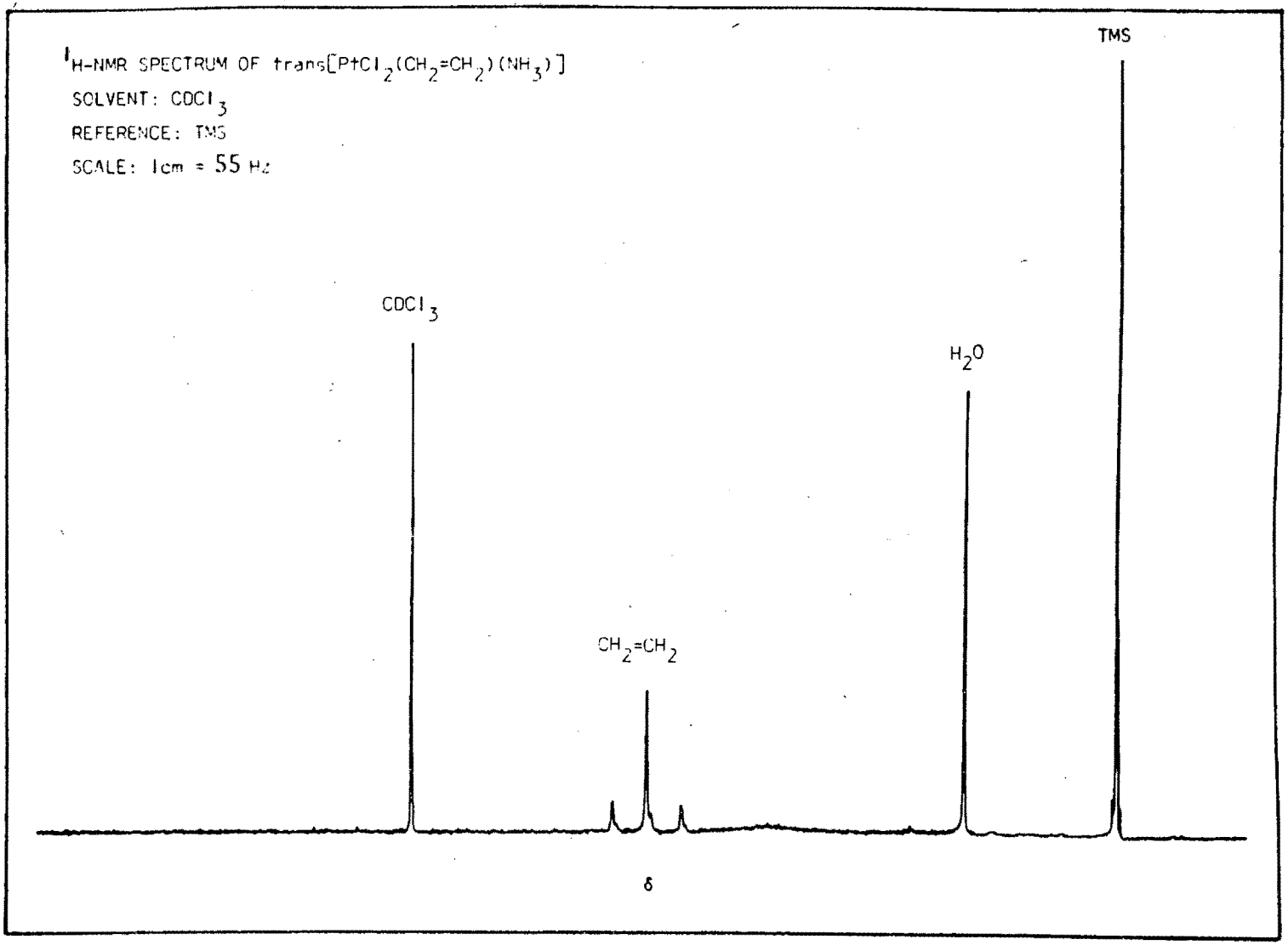

Figure 44. ^{1}H-nmr spectrum of *trans*-[PtCl$_2$(CH$_2$=CH$_2$)(NH$_3$)]

Table 29. ^{1}H-nmr data for *trans*-$[PtX_2(C_2H_4)(pz)]$, (X = Cl, Br, I)[a]

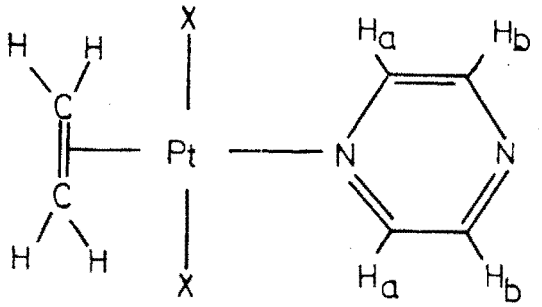

Olefin protons		
X	J_{Pt-H} (Hz)	Chemical shift (ppm)
Cl	63	5.00
Br	63	5.13
I	b	5.30

Pyrazine protons	Chemical shift (ppm)	
X	H_a	H_b
Cl	singlet at 8.95[c]	
Br	singlet at 8.91[c]	
I	singlet at 8.90[c]	

a The ^{1}H-nmr spectra were run on a Bruker WH 90 spectrophotometer using $CDCl_3$ as a solvent and lock and TMS as a reference.
b Platinum satellites could not be determined.
c Indicates fluxional character of pyrazine.

Table 30. ^{1}H-nmr data for *trans*-$[Pt_2X_4(C_2H_4)_2(pz)]$, (X = Cl, Br, I)[a]

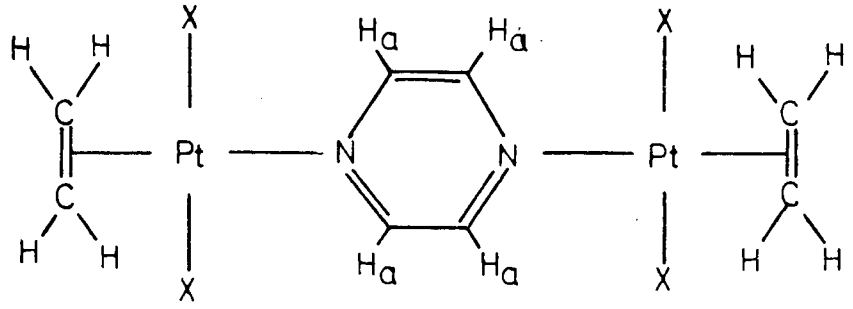

Olefin protons

X	J_{Pt-H} (Hz)	Chemical shift (ppm)
Cl	63	5.08
Br	64	5.19
I	b	5.28

Pyrazine protons	Chemical shift (ppm)
X	H_a
Cl	9.35
Br	9.25
I	8.94

a The ^{1}H-nmr spectra were run on a Bruker WH 90 spectrophotometer, using $CDCl_3$ as a solvent and lock and TMS as a reference

b Platinum satellites could not be determined

Table 31. ^{1}H-nmr data for *trans*-$[PtCl_2(C_2H_4)(p\text{-R-an})]$, (*p*-R-an = *para* substituted aniline)[a]

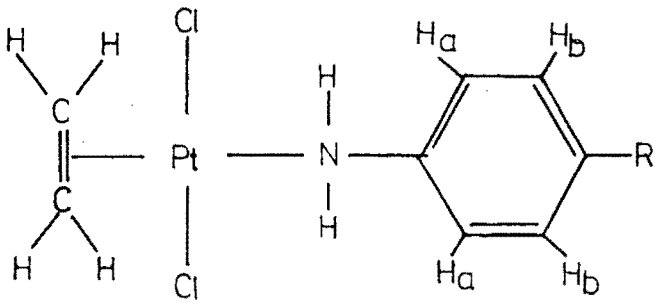

R	Olefin protons		Aniline protons		Other
	J_{Pt-H}(Hz)	δ[b]	δ_{H_a}[b]	δ_{H_b}[b]	δ[b]
p-CH_3	63.9	4.66	7.28	7.13	2.31 (CH_3)
p-*t*-Butyl	63	4.69	7.33[c]	7.33[c]	1.31 3(CH_3)
p-Br	64	4.71	7.49	7.28	
p-I	64	4.70	7.68	7.15	
p-OPh	64	4.70	7.36	6.96	7.14[d] (OPh)
p-OCH_3	63	4.67	7.35	6.85	3.78 (OCH_3)
p-NO_2	64	4.68	8.25	7.58	

a The ^{1}H-nmr spectra were run on a Bruker WH 90 spectrophotometer, using $CDCl_3$ as a solvent and lock and TMS as a reference

b Chemical shift in ppm

c H_a and H_b occur at same chemical shift

d Average of multiplet

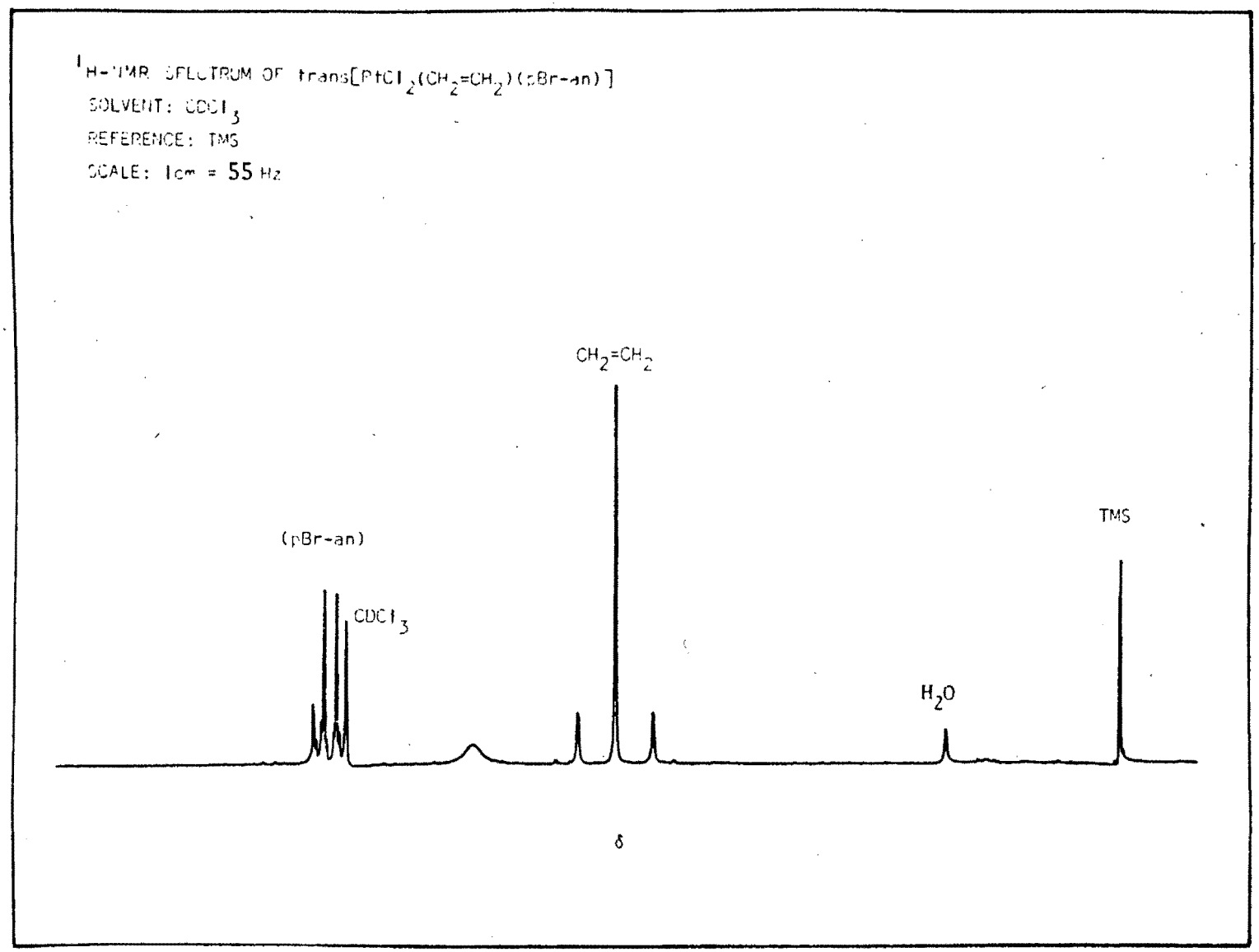

Figure 45. ^{1}H-nmr spectrum of *trans*-[$PtCl_2(CH_2{=}CH_2)$(*p*-Br-an)]

Table 32. ^{1}H-nmr data for *trans*-$[PtCl_2(C_2H_4)(m\text{-R-an})]$, (*m*-R-an = *meta* substituted aniline)[a]

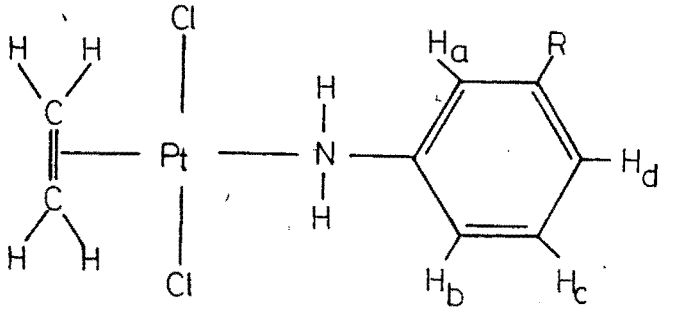

R	Olefin protons $J_{Pt\text{-}H}$(Hz)	Olefin protons δ[b]	Aniline protons δ_{H_a}[b] δ_{H_b}[b] δ_{H_c}[b] δ_{H_d}[b]	Other δ[b]
m-CH_3	64	4.67	multiplet at 7.20[c]	2.36, (CH_3)
m-NO_2	64	4.65	multiplet at 7.66[c]	
m-Cl	64	4.70	multiplet at 7.34[c]	
m-F	64	4.72	multiplet at 7.20[c]	
m-I	64	4.72	multiplet at 7.38[c]	
m-Br	64	4.72	multiplet at 7.36[c]	

a The ^{1}H-nmr spectra were run on a Bruker WH-90 spectrophotometer, using $CDCl_3$ as a solvent and lock and TMS as a reference

b Chemical shift in ppm

c Average of multiplet

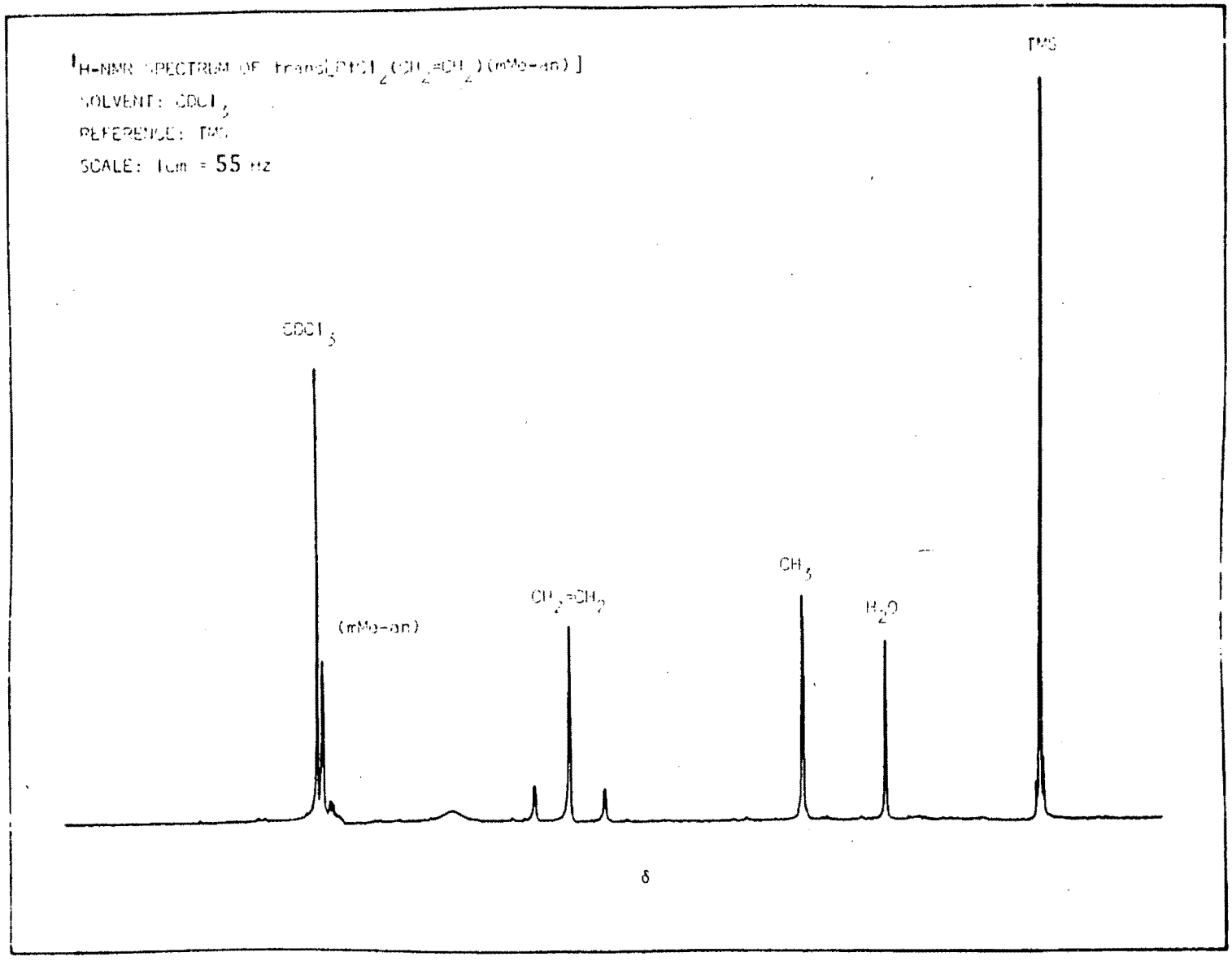

Figure 46. ^{1}H-nmr spectrum of *trans*-[$PtCl_2(CH_2{=}CH_2)$*m*-Me-an)]

Table 33. ^{1}H-nmr data for *trans*-[$PtCl_2(C_2H_4)$(3,4-di-CH_3-aniline)][a]

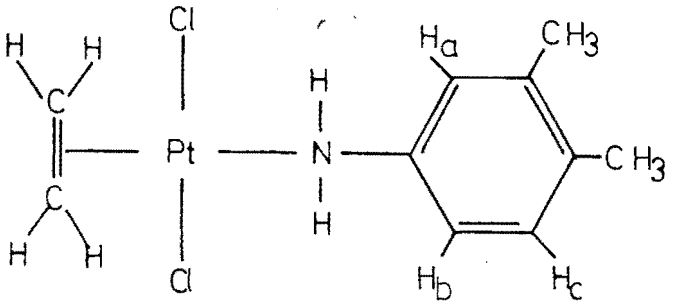

Olefin protons		Aniline protons			Other
J_{Pt-H}(Hz)	δ[b]	δH_a[b]	δH_b[b]	δH_c[b]	δ[b]
64	4.66	multiplet at 7.20[c]			2.20 (CH_3)
					2.25 (CH_3)

a The ^{1}H-nmr spectra were run on a Bruker WH 90 spectrophotometer, using $CDCl_3$ as a solvent and lock and TMS as a reference

b Chemical shift in ppm

c Average of multiplet

4.6 ULTRAVIOLET RESULTS

Table 34. Uv data for the complexes *trans*-$[PtX_2(C_2H_4)(L)]$, (X = Cl, Br; L = Cl, Br, py, an, NH_3, Him, pyO)[a]

X	L	λ_{max}(nm)	ε	Assignment
Cl	Cl	201	8650	π → π*(ethylene)
		236	1926	Cl^- → Pt^{2+}
		258	1831	Cl^- → Pt^{2+}(Cl opposite ethylene)
		320	190	5d(Pt) → π*(ethylene)
	py	242	3522	Cl^- → Pt^{2+}
		258	5240	π → π*(py) + π → π*(ethylene)
		261	5304	
		309	1304	5d(Pt) → π*(ethylene) 5d(Pt) → π*(py)
	NH_3	248[b]	4355	Cl^- → Pt^{2+}
		262	4549	π → π*(ethylene)
		300	2819	5d(Pt) → π*(ethylene)
	pyO	245	8548	Cl^- → Pt^{2+}
		271	11127	π → π*(pyO) + π → π*(ethylene)
		328	353	5d(Pt) → π*(ethylene)
	Him	239	1818	Cl^- → Pt^{2+}
		267	2409	π → π*(Him) + π → π*(ethylene)
		301	1273	5d(Pt) → π*(ethylene) 5d(Pt) → π*(Him)
	an	254[c]	6301	Cl^- → Pt^{2+} + π → π*(ethylene)
		304	1613	5d(Pt) → π*(ethylene)
Br	Br	204	20214	π → π*(ethylene)
		256[c]	2371	Br^- → Pt^{2+}
		302	943	5d(Pt) → π*(ethylene)
	py	241	4697	Br^- → Pt^{2+}
		263	5101	π → π*(py) + π → π*(ethylene)
		316	1035	5d(Pt) → π*(py) 5d(Pt) → π*(ethylene)
	NH_3	240	1368	Br^- → Pt^{2+}
		259	1701	π → π*(ethylene)
		302	517	5d(Pt) → π*(ethylene)
	pyO	245	8366	Br^- → Pt^{2+}
		267	8216	π → π*(pyO) + π → π*(ethylene)
		346	508	5d(Pt) → π*(ethylene)
	Him	240	2635	Br^- → Pt^{2+}
		261	2750	π → π*(Him) + π → π*(ethylene)
		308	769	5d(Pt) → π*(Him) 5d(Pt) → π*(ethylene)
	an	243	7191	Br^- → Pt^{2+}
		253[b]	6228	π → π*(an) + π → π*(ethylene)
		308	1284	5d(Pt) → π*(ethylene)

a $CHCl_3$ used as solvent in all cases except for X = Cl; L = Cl and X = Br; L = Br where H_2O was used as solvent

b Shoulder

c Broad band

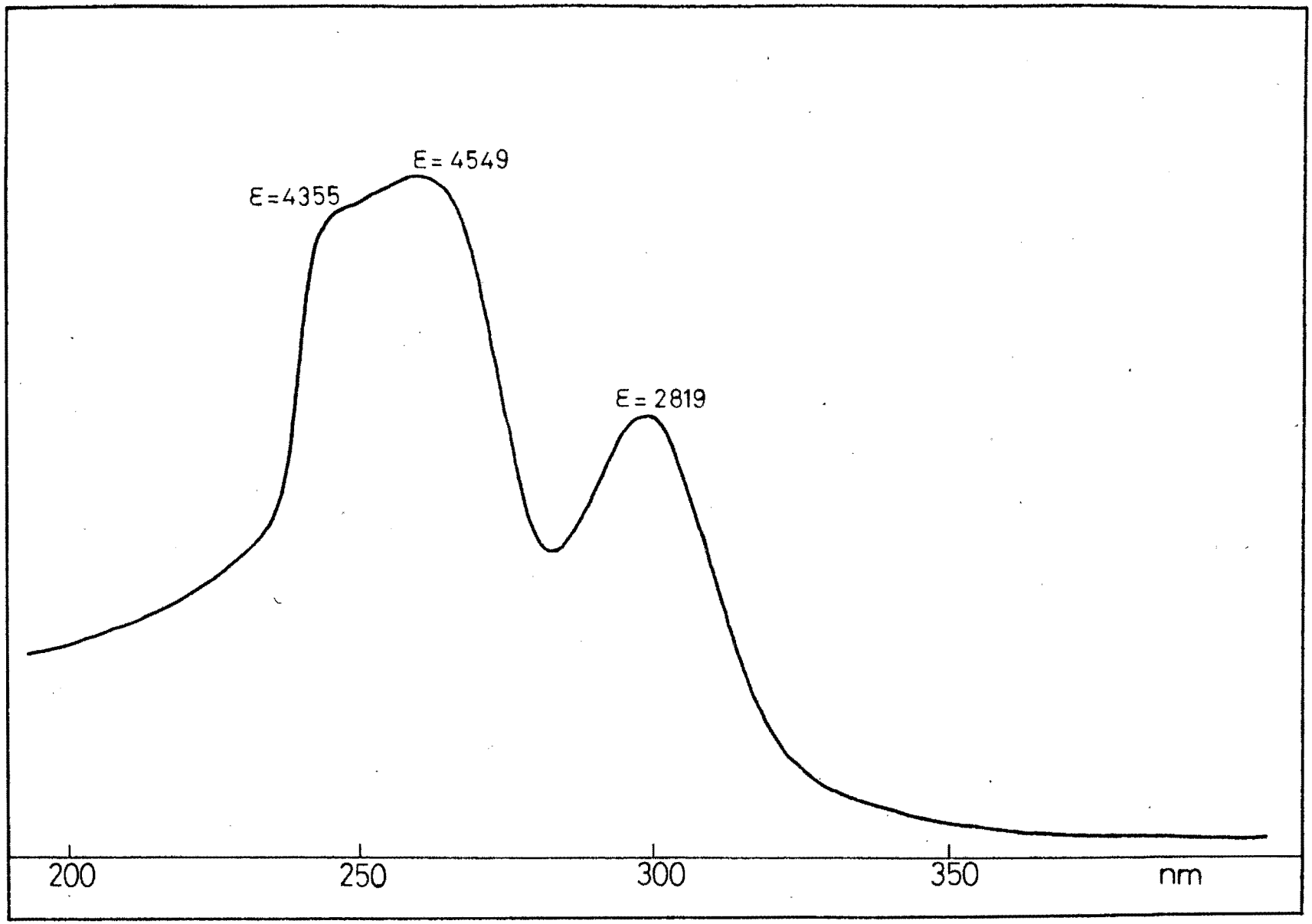

Figure 47. The uv spectrum of *trans*-$[PtCl_2(C_2H_4)(NH_3)]$

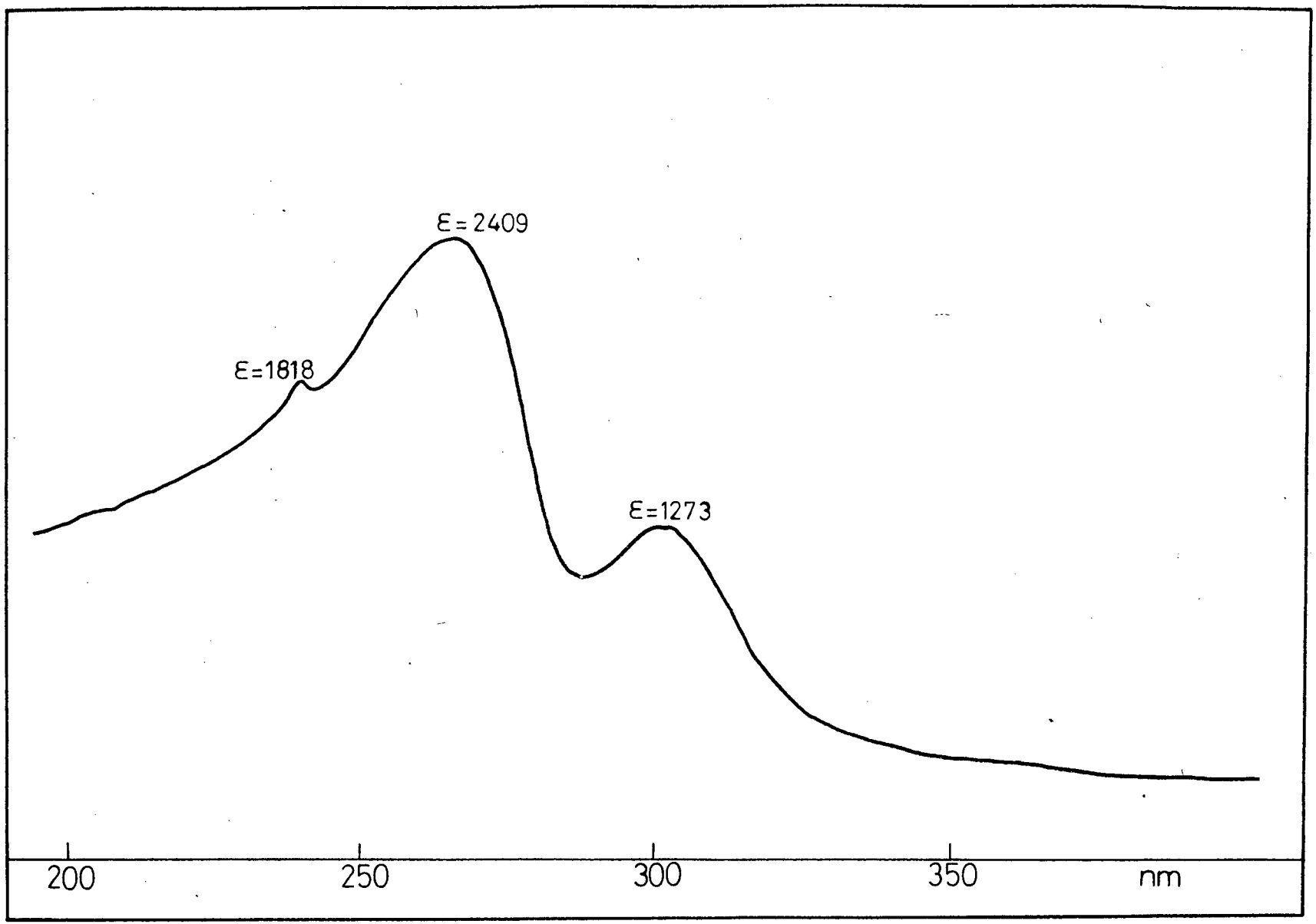

Figure 48. The uv spectrum of *trans*-$[PtCl_2(C_2H_4)(Him)]$

Table 35. Electronic spectra data for the complexes of types (I) and (II)

X	λ_{max} nm	ε	Assignment
Type (I) complexes			
Cl	240	4454	$Cl^- \rightarrow Pt^{2+}$
	271	6514	$\pi \rightarrow \pi^*(pz)$, $\pi \rightarrow \pi^*(C_2H_4)$
	316 broad	1781	$5d \rightarrow \pi^*(pz)$, $5d \rightarrow \pi^*(C_2H_4)$
Br	240	5571	$Br^- \rightarrow Pt^{2+}$
	268	4269	$\pi \rightarrow \pi^*(pz)$, $\pi \rightarrow \pi^*(C_2H_4)$
	326 broad	1085	$5d \rightarrow \pi^*(pz)$, $5d \rightarrow \pi^*(C_2H_4)$
I	241	12875	$I^- \rightarrow Pt^{2+}$
	292	5909	$\pi \rightarrow \pi^*(pz)$, $\pi \rightarrow \pi^*(C_2H_4)$
	336 shoulder	2197	$5d \rightarrow \pi^*(pz)$, $5d \rightarrow \pi^*(C_2H_4)$
Type (II) complexes			
Cl	240	4245	$Cl^- \rightarrow Pt^{2+}$
	269	3827	$\pi \rightarrow \pi^*(pz)$, $\pi \rightarrow \pi^*(C_2H_4)$
	320	1322	$5d \rightarrow \pi^*(C_2H_4)$
	356	696	$5d \rightarrow \pi^*(pz)$
Br	240	7431	$Br^- \rightarrow Pt^{2+}$
	258	5642	$\pi \rightarrow \pi^*(pz)$, $\pi \rightarrow \pi^*(C_2H_4)$
	335	1134	$5d \rightarrow \pi^*(C_2H_4)$
	378	630	$5d \rightarrow \pi^*(pz)$
I	240	1831	$I^- \rightarrow Pt^{2+}$
	268 shoulder	1212	$\pi \rightarrow \pi^*(pz)$, $\pi \rightarrow \pi^*(C_2H_4)$
	too broad		$5d \rightarrow \pi^*(C_2H_4)$
	too broad		$5d \rightarrow \pi^*(pz)$

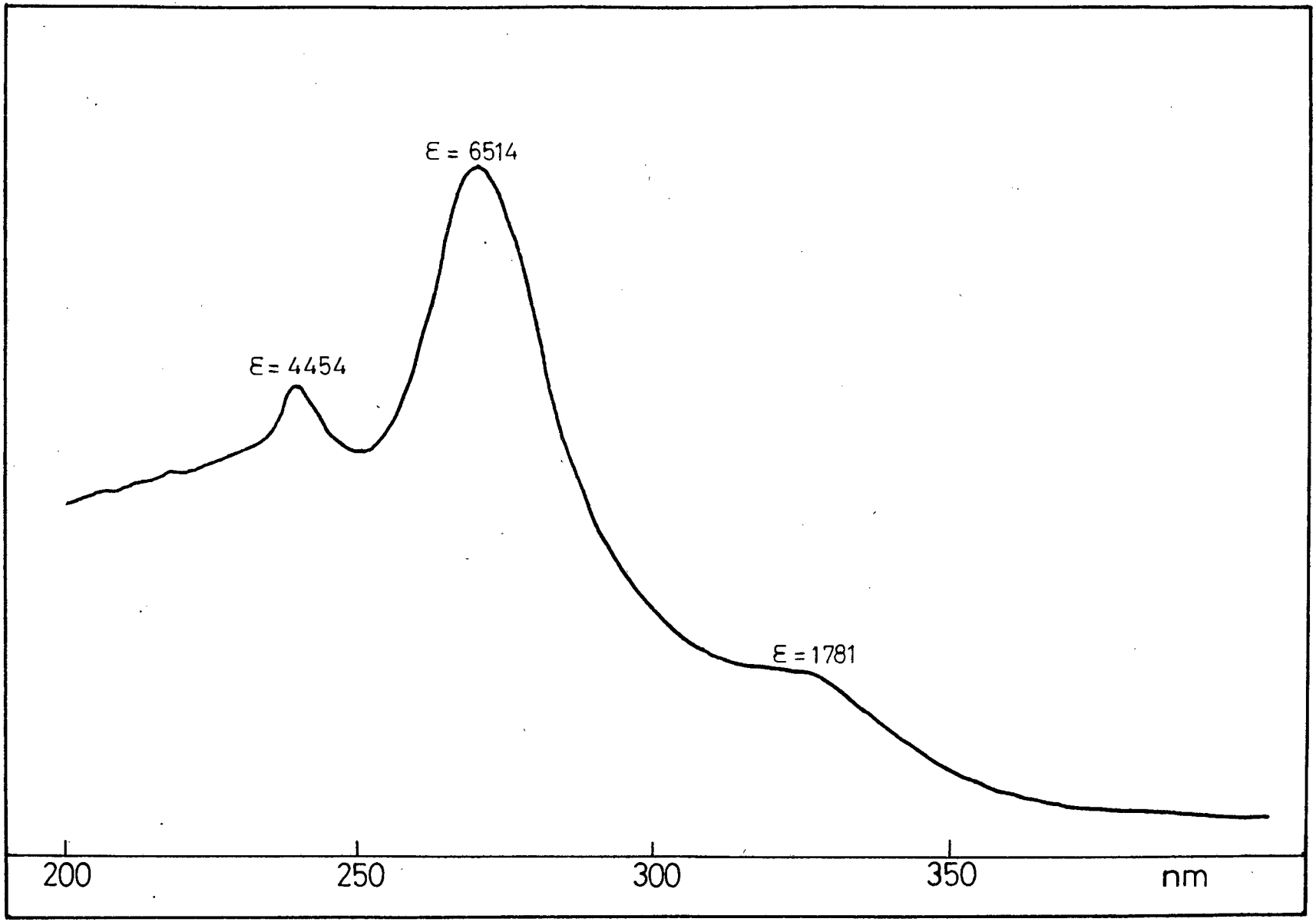

Figure 49. The uv spectrum of *trans*-$[PtCl_2(C_2H_4)(pz)]$

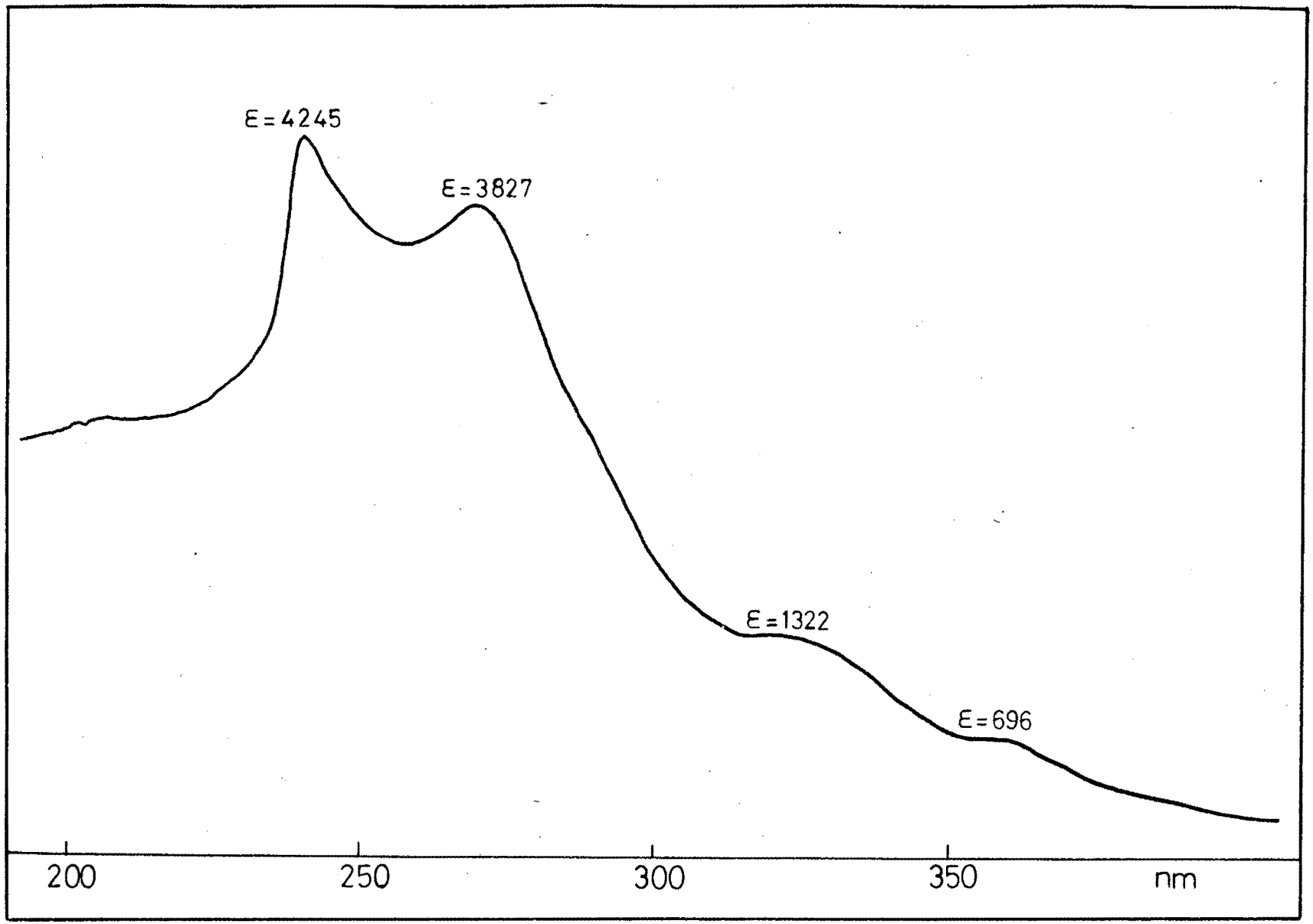

Figure 50. The uv spectrum of *trans*-$[Pt_2Cl_4(C_2H_4)_2(pz)]$

Table 36. Uv data for the complexes *trans*-$[PtCl_2(CH_2{=}CH_2)(R\text{-an})]$

R	σ	λ_{max} nm	ε	Assignment
p-NO_2	0.778	240	8507	$Cl^- \rightarrow Pt^{2+}$
		288	9318	$\pi\rightarrow\pi^*$(an) + $\pi\rightarrow\pi^*$ (C_2H_4)
		345	11546	5*d*(Pt)$\rightarrow\pi^*$ + $\pi\rightarrow\pi^*(NO_2)$ (or $n\rightarrow n^*(NO_2)$)
m-NO_2	0.710	250	10442	$Cl^- \rightarrow Pt^{2+}$, $\pi\rightarrow\pi^*$(an), $\pi\rightarrow\pi^*(C_2H_4)$
		292	2520	5*d*(Pt$\rightarrow\pi^*$), $\pi\rightarrow\pi^*(NO_2)$
m-Br	0.391	241	7626	$Cl^- \rightarrow Pt^{2+}$, $\pi\rightarrow\pi^*$(an), $\pi\rightarrow\pi^*(C_2H_4)$
		299	1679	5*d*(Pt)$\rightarrow\pi^*(C_2H_4)$
m-Cl	0.373	249	6324	$Cl^- \rightarrow Pt^{2+}$, $\pi\rightarrow\pi^*$(an), $\pi\rightarrow\pi^*(C_2H_4)$
		300	1713	5*d*(Pt)$\rightarrow\pi^*(C_2H_4)$
m-I	0.352	241	11274	$Cl^- \rightarrow Pt^{2+}$
		∿255	7333	$\pi\rightarrow\pi^*$(an), $\pi\rightarrow\pi^*(C_2H_4)$
		299	1832	5*d*(Pt$\rightarrow\pi^*(C_2H_4)$
m-F	0.337	248	5198	$Cl^- \rightarrow Pt^{2+}$
		∿264	4709	$\pi\rightarrow\pi^*$(an), $\pi\rightarrow\pi^*(C_2H_4)$
		296	1502	5*d*(Pt)$\rightarrow\pi^*(C_2H_4)$
p-I	0.276	247	5648	$Cl^- \rightarrow Pt^{2+}$
		261	6764	$\pi\rightarrow\pi^*$(an), $\pi\rightarrow\pi^*(C_2H_4)$
		302	1397	5*d*(Pt)$\rightarrow\pi^*(C_2H_4)$
p-Br	0.232	252	9746	$Cl^- \rightarrow Pt^{2+}$, $\pi\rightarrow\pi^*$(an) $\pi\rightarrow\pi^*(C_2H_4)$
		301	2119	5*d*(Pt)$\rightarrow\pi^*(C_2H_4)$
H	0	254	6301	$Cl^- \rightarrow Pt^{2+}$, $\pi\rightarrow\pi^*(C_2H_4)$, $\pi\rightarrow\pi^*$(an)
		304	1613	5*d*(Pt)$\rightarrow\pi^*(C_2H_4)$
p-PhO	-0.028	241	9758	$Cl^- \rightarrow Pt^{2+}$
		266	9310	$\pi\rightarrow\pi^*(C_2H_4)$, $\pi\rightarrow\pi^*$(an), $\pi\rightarrow\pi^*$(PhO)
		∿300	2898	5*d*(Pt)$\rightarrow\pi^*(C_2H_4)$
m-CH_3	-0.069	248	6588	$Cl^- \rightarrow Pt^{2+}$
		257	6875	$\pi\rightarrow\pi^*$(an), $\pi\rightarrow\pi^*(C_2H_4)$
		303	1948	5*d*(Pt)$\rightarrow\pi^*(C_2H_4)$
p-*t*-C_4H_9	-0.120	243	4768	$Cl^- \rightarrow Pt^{2+}$
		262	5585	$\pi\rightarrow\pi^*$(an), $\pi\rightarrow\pi^*(C_2H_4)$
		302	1568	5*d*(Pt)$\rightarrow\pi^*(C_2H_4)$
p-CH_3	-0.17	247	5334	$Cl^- \rightarrow Pt^{2+}$
		263	6818	$\pi\rightarrow\pi^*(C_2H_4)$, $\pi\rightarrow\pi^*$(an)
		304	1885	5*d*(Pt)$\rightarrow\pi^*(C_2H_4)$
3,4-di-CH_3	-0.24	244	7696	$Cl^- \rightarrow Pt^{2+}$
		264	9252	$\pi\rightarrow\pi^*(C_2H_4)$, $\pi\rightarrow\pi^*$(an)
		301	3026	5*d*(Pt)$\rightarrow\pi^*(C_2H_4)$
p-CH_3O	-0.268	241	4753	$Cl^- \rightarrow Pt^{2+}$
		273	8820	$\pi\rightarrow\pi^*(C_2H_4)$, $\pi\rightarrow\pi^*$(an)
		325	1901	5*d*(Pt)$\rightarrow\pi^*(C_2H_4)$

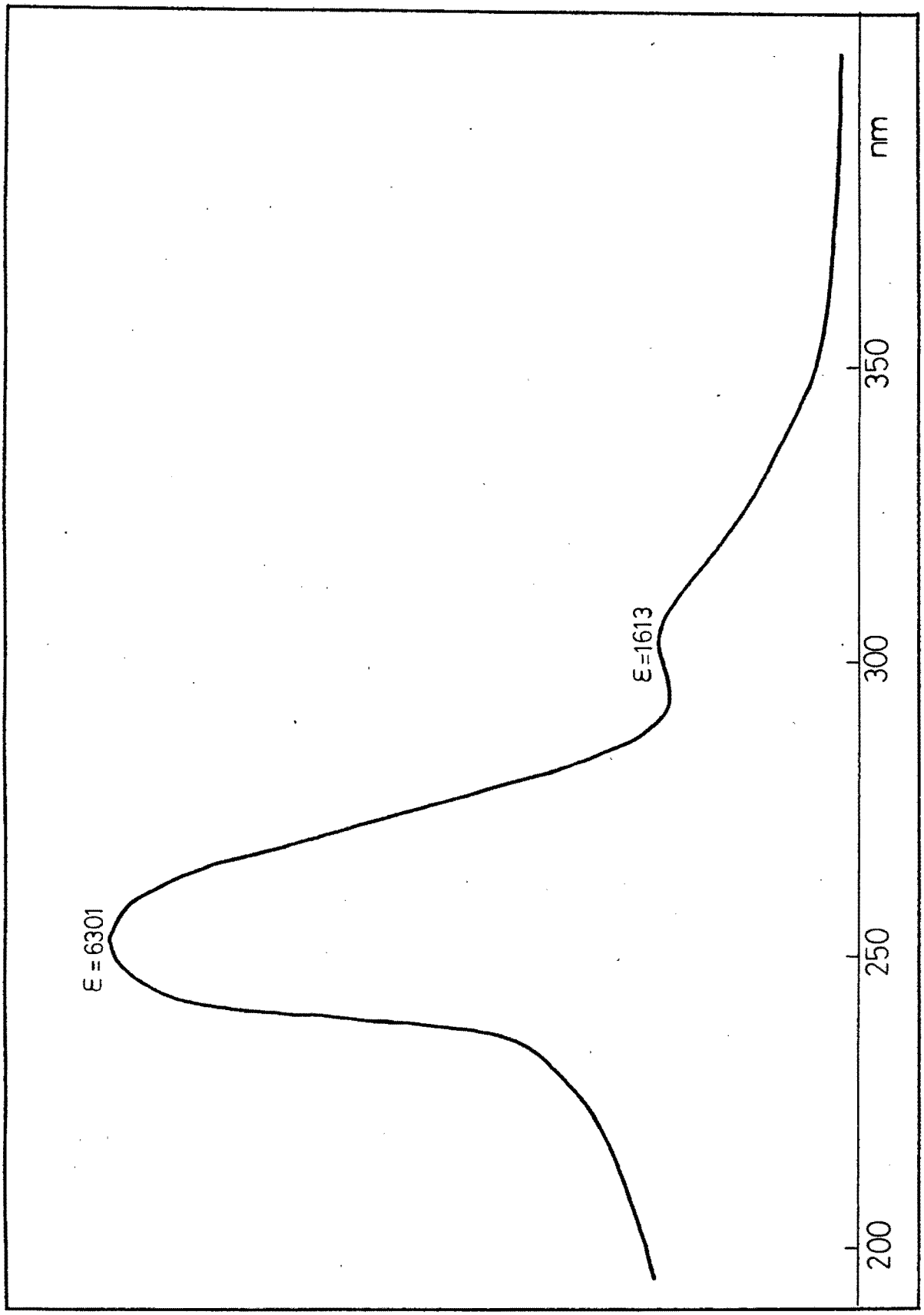

Figure 51. The uv spectrum of *trans*-$[PtCl_2(C_2H_4)(an)]$

4.7 DISCUSSION

4.7.1 The complexes *trans*-[$PtX_2(C_2H_4)(L)$], (X = Cl, Br; L = NH_3, pyridine, pyridine *N*-oxide, aniline and imidazole)

4.7.1.1 *^{1}H-nmr results*

The ^{1}H-nmr data for the above complexes are given in Tables 24 (L = pyO), 25 (L = py), 26 (L = an), 27 (L = Him) and 28 (L = NH_3). The coupling between Pt (I = ½) and the coordinated ethylene is consistent with *trans*-coordination, and varies little with variation in both X and L.

The chemical shift of the ethylene protons varies both with varying X and L. The variation of δ(ethylene protons) with X is in the region of 0.13 ppm with the protons being deshielded through the series X = Cl, Br. It appears that as one proceeds from X = Cl to X = Br, the Pt-X bond strength increases at the expense of the Pt-C_2 and Pt-L bonds. The variation of δ(ethylene protons) with L is more pronounced with the greatest difference occurring between the complexes where L = pyridine *N*-oxide and L = pyridine (0.52 ppm). This is to be expected since L is *trans* to ethylene and electronic effects are more effectively transmitted. However the individual effects of L cannot be effectively compared since some of the ligands bond only *via* σ bonds (*e.g.* NH_3), whereas others are capable of π-interactions (*e.g.* pyridine).

4.7.1.2 *Infrared and Raman spectra*

The vibrational spectra of Zeise's salt, $K[PtCl_3(C_2H_4)]$, and its derivatives *trans*-$[PtX_2(C_2H_4)(L)]$, where L represents various oxygen and nitrogen ligands, have elicited much interest[76,85-92] but isotopic (C_2D_4) labelling has been applied only to Zeise's salt itself. In the absence of the latter technique, certain of the assignments remain in doubt. In this study, the coordinated ethylene and ligands L, have been independently deuterated with the object of providing firm assignments for the νPt-C_2, νPt-L and νPt-X modes.

The spectrum of each compound was determined three times: firstly in the unlabelled form, then with the ethylene deuterated and finally with the ligand, L, deuterated. The frequencies of the internal ligand modes for the chloro complexes are recorded in Table 18 and depicted in Figure 52. while those for the bromo complexes are recorded in Table 19 and depicted in Figure 53.

Internal ligand modes

The internal modes of ethylene are assigned to those bands which are found to shift significantly on deuteration of ethylene. These bands are principally the stretching and bending vibrations of the CH_2 groups and the C-C stretching modes. The latter are very weak in the infrared spectra but, as expected, are intense in the Raman spectra. There has been some previous confusion in the assignment of this vibration. Originally thought[76,88] to be near 1500 cm^{-1}, it is now considered[89] to be in the 1250 cm^{-1} region, the former band being assigned to the CH_2 scissoring mode. Undoubtedly there is vibrational coupling

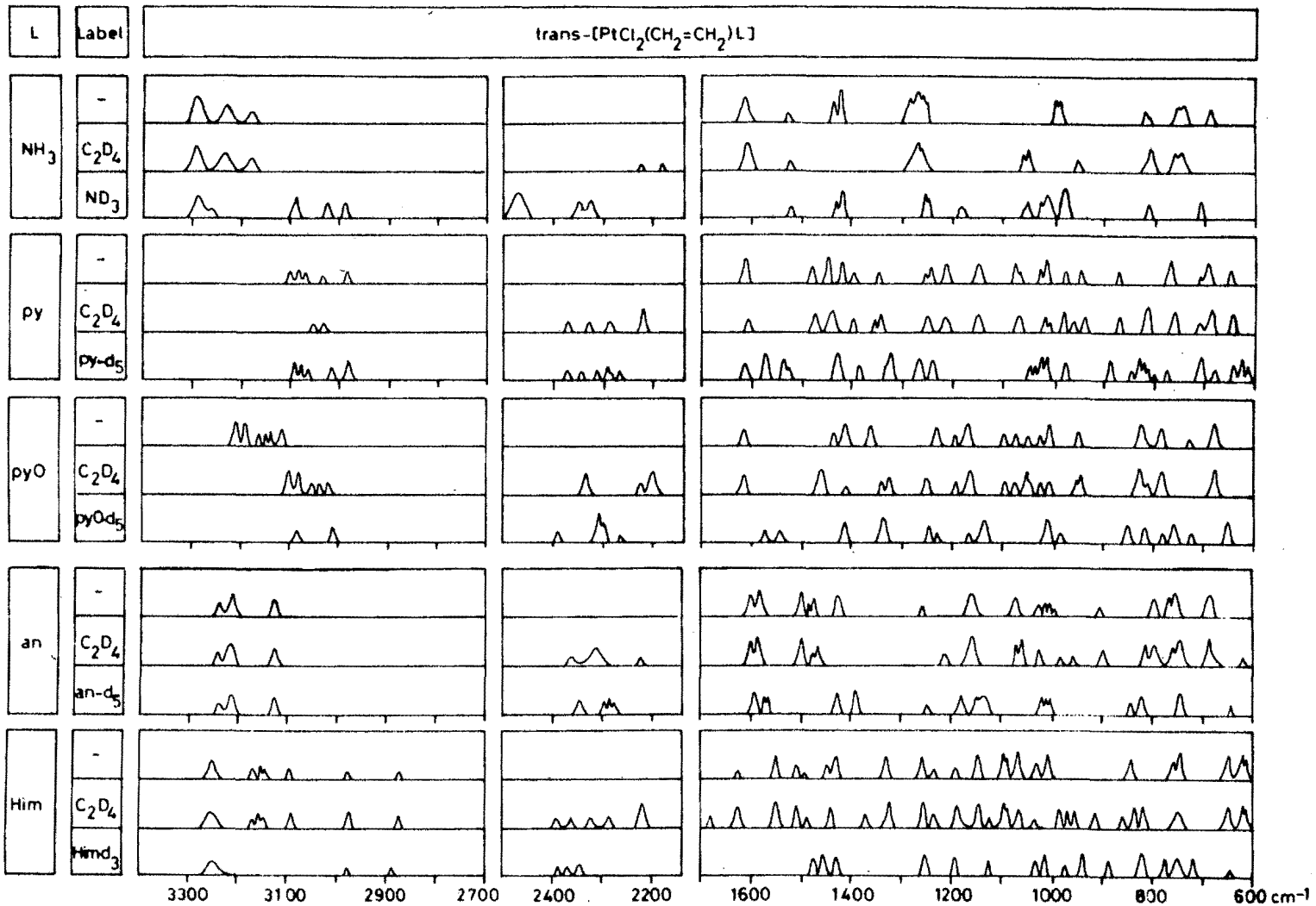

Figure 52. The infrared spectrum of *trans*-$[PtCl_2(CH_2{=}CH_2)(L)]$

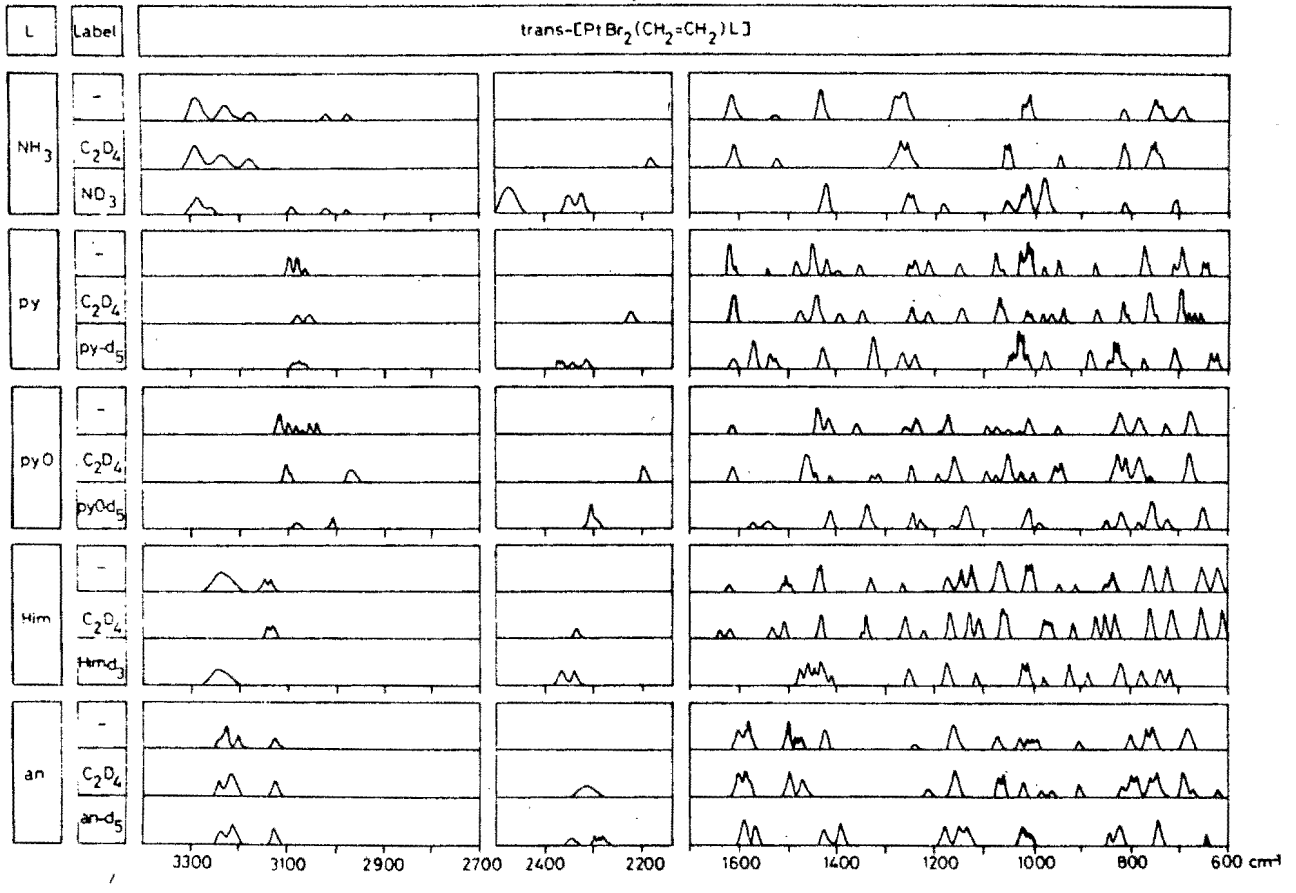

Figure 53. The infrared spectrum of *trans*-[$PtBr_2(CH_2{=}CH_2)(L)$]

between these modes, as proposed by Hiraishi,[89] but the 1250 cm^{-1} region seems much more appropriate to a C-C stretching mode in which the bond has lost much of its double bond character. We have therefore adopted the more recent assignments in the present work.

The internal vibrations of the ligands L are assigned to those bands which shift significantly on deuteration of L but not on ethylene deuteration. The more specific assignments are made from the ν^D/ν^H ratio.[20] The assignments are straightforwardly made in relation to earlier studies of the use of the ν^D/ν^H ratio in complexes of pyridine,[20] pyrazine,[93] aniline[20] and imidazole.[53] The assignments in the pyridine *N*-oxide complexes follow those reported from a normal coordinate analysis of the free ligand.[94]

Metal-ligand modes

The far-infrared spectra (600 - 80 cm^{-1}) are depicted in Figure 54 and the frequencies are reported in Table 20. The νPt-C_2 modes are assigned to the bands of highest frequency within the range 600 - 80 cm^{-1} which exhibit significant shifts on ethylene-d_4 labelling but which are substantially less sensitive to deuteration of L. Conversely, those bands which shift most on deuteration of L are assigned to νPt-L. Bands which are relatively insensitive to deuteration of both L and ethylene but which shift on substitution of the halides are assigned to the νPt-X. In this way, clear distinction between the three types of metal-ligand stretching frequency is possible.

Earlier empirical assignments[87] for νPt-N, νPt-C_2 and νPt-Cl in the

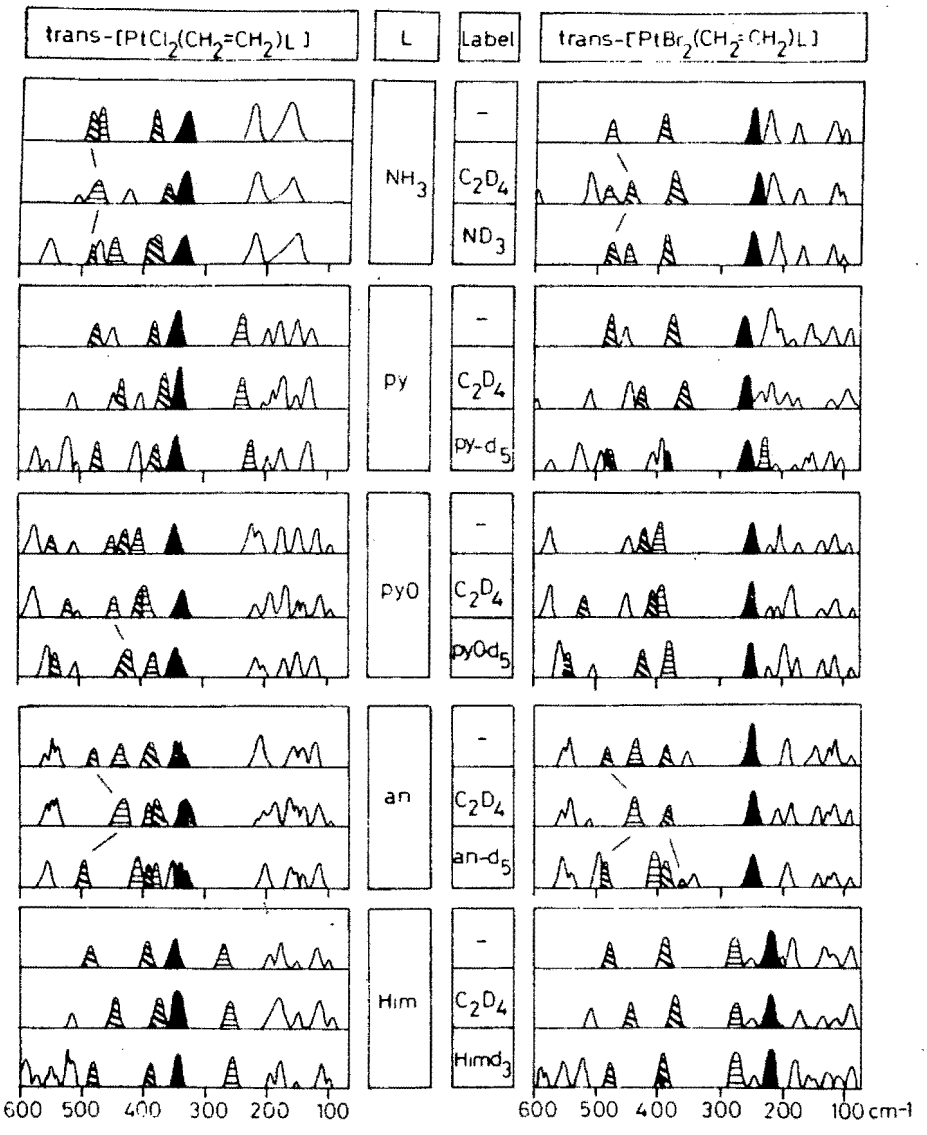

Figure 54. The infrared spectrum of *trans*-$[PtCl_2(CH_2{=}CH_2)(L)]$ and *trans*-$[PtBr_2(CH_2{=}CH_2)(L)]$

complex with L = NH_3, X = Cl are supported here, except that the assignments for the two components of the 478, 471 cm^{-1} doublet are now reversed. Three previous studies of the spectra of the complexes with L = py, X = Cl have been made.[87,90,91] All three sets of data are internally consistent and are supported by the present results. Only one study[92] has been reported for the complex with L = aniline, X = Cl; our labelling results suggest that the νPt-N and νPt-C_2 bands coincide at 384 cm^{-1}. The band at 346 cm^{-1}, previously assigned to νPt-N is now considered to be νPt-Cl. None of the bromo complexes has previously been studied by infrared spectroscopy.

In genral, with the exceptions noted above, the earlier empirical assignments are well supported by the present labelling study.

4.7.1.3 *Electronic spectra*

The electronic spectra frequencies of $K[PtX_3(C_2H_4)]$ and its derivatives *trans*-$[PtX_2(C_2H_4)(L)]$, (X = Cl, Br; L = py, pyO, NH_3, Him and aniline) are recorded in Table 38. The spectra vary according to the type of ligand, L, *trans* to the ethylene.

When L is a ligand that only forms a σ-bond with Pt (*e.g.* NH_3), the resultant uv spectrum is very similar to that of the $[PtX_3(C_2H_4)]^-$ anion. The major electronic transitions taking place are $\pi \rightarrow \pi^*$(ethylene), $X^- \rightarrow Pt^{2+}$ charge transfer, and the *5d*(Pt) → π*(ethylene) inverse charge transfer. These transitions will occur in all complexes of the type *trans*-$[PtX_2(C_2H_4)(L)]$.

When L is a ligand that has π-electrons present that may interact with Pt, the uv spectrum becomes more complicated. In addition to the electronic transitions mentioned previously, there is now the possibility of a $5d(Pt) \rightarrow \pi^*$(ligand) inverse charge transfer.

It should be noted that some of the assignments are tentative as there is a degree of overlap in some of the spectra manifested by fairly broad bands.

4.7.2 The complexes *trans*-$[PtX_2(C_2H_4)(pyrazine)]$ and *trans*-$[Pt_2X_4(C_2H_4)_2(pyrazine)]$

Depending on the preparative conditions, pyrazine (pz) reacts with Zeise's salt to form two complexes in one of which the pz is terminal (I) and in the other bridging (II). Complexes of type (I) have previously been reported with pz replaced by pyridine,[91] aniline, pyridine *N*-oxide and imidazole,[96] or a substituted aniline.[97] Complexes of type (II) have not previously been described.

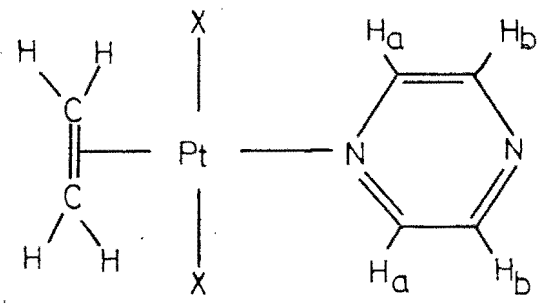

(I)

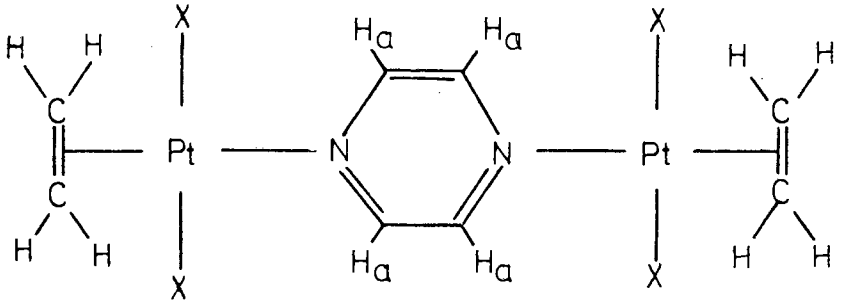

(II)

Figure 55. *Trans*-$[PtX_2(C_2H_4)(pz)]$, (I), and *trans*-$[Pt_2X_4(C_2H_4)_2(pz)]$ (II).

4.7.2.1 *^{1}H-nmr results*

^{1}H-nmr data for both types of complexes are given in Tables 29 and 30. The values of J_{Pt-H} are consistent with *trans*-coordination.[88,90,92,98,99] The aromatic protons of the pyrazine ring in (I) are rather insensitive to the nature of the halide whereas the olefin protons are progressively deshielded through the series X = Cl, Br, I. It appears that through this series the Pt-X bond strength increases at the expense of the Pt-C_2 and Pt-N bonds.

It is suggested that the pyrazine in fluxional as manifested by the appearance of a single resonance for the H_a and H_b protons of (I), indicating that they are equivalent.

The bridging role of pyrazine in (II) is suggested by the resonance of the aromatic protons which integrates for four protons which are

less shielded than those of (I). In structure (II) both the pyrazine and ethylene protons are halogen-sensitive, the increase in shielding of the pyrazine protons being at the expense of the ethylene proton shielding through the series X = Cl, Br, I.

As far as exchange of the pyrazine in (II) is concerned, one would expect it to be more difficult than in case (I), but as all protons are equivalent only a variable temperature study could elaborate (see chapter 5).

4.7.2.2 *Infrared spectra*

The spectrum of each compound was determined three times; firstly in the unlabelled form, then with the ethylene deuterated and finally, with the pyrazine deuterated. The mid-ir spectra are reported in Table 21 and depicted in Figures 56 and 57.

The internal ethylene modes are assigned to those bands which shift significantly on ethylene deuteration but not on pyrazine deuteration. These bands are principally the stretching and bending vibrations of the CH_2 groups and the C-C stretch. The latter, being ir-forbidden, are absent from the spectra of the complexes of type (I), and weak in or absent from the spectra of the complexes of structure (II). It is interesting to note that as νC-C decreases from (II; X = Cl) to (II; X = Br), the nmr data indicate a corresponding deshielding of the ethylene protons.

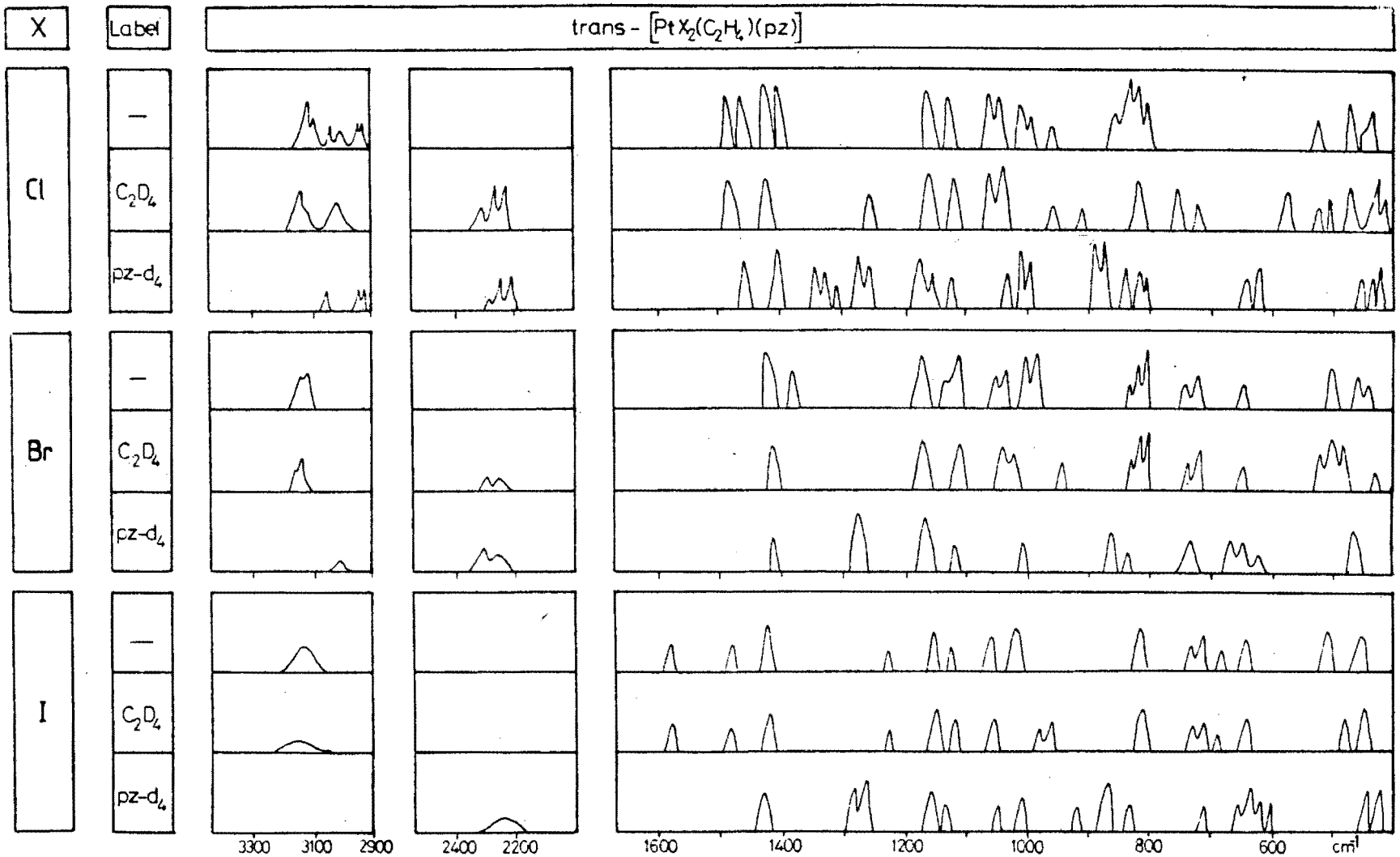

Figure 56. The infrared spectrum of *trans*-$[PtX_2(C_2H_4)(pz)]$

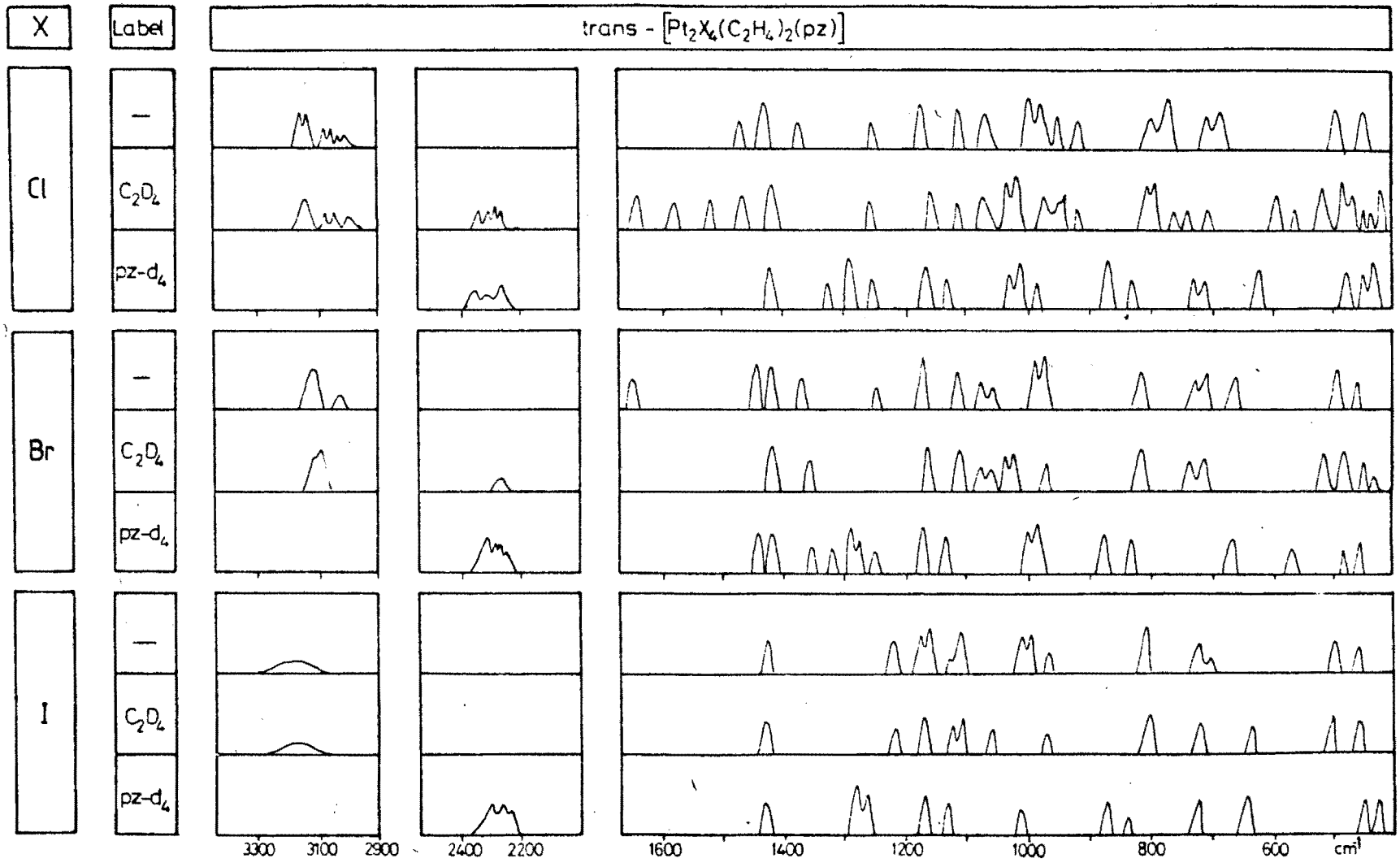

Figure 57. The infrared spectrum of *trans*-$[Pt_2X_4(C_2H_4)_2(pz)]$

The internal pyrazine modes are assigned to those bands which shift significantly on pyrazine deuteration but not on ethylene deuteration. Specific assignments are made from the ν^D/ν^H ratio as used previously.[20]

The far-ir data are reported in Table 22 and the spectra are depicted in Figure 58. The bands of highest frequency within the range 600 - 50 cm^{-1} which shift significantly on ethylene-d_4 labelling are assigned to νPt-C_2. Bands within this range which are specially sensitive to pyrazine deuteration are assigned to νPt-N, while those which shift on varying the halide are ascribed to νPt-X. The latter are relatively unaffected by deuteration of both ethylene and pyrazine.

In both series of complexes νPt-C_2 increases significantly the softer the halide ligand. This can be explained if one considers the Pt-X interaction getting stronger with the result that electron density is pulled from the ethylene "double" bond into the Pt-C_2 bond. As might be expected, νPt-N is significantly higher in the complexes (I) where pyrazine acts as a monodentate ligand than in (II) where it is bidentate.

It is of interest to compare the nmr and ir data. νPt-N in the complexes (I) is relatively unaffected by changing the halide; likewise the chemical shift of the aromatic protons is not greatly affected in the complexes (I). In the bridged compounds (II), both νPt-N and the chemical shift of the aromatic protons are halogen-sensitive.

The point group symmetry of both series of complexes is C_{2v} and three ir-active stretching modes are expected. These are all observed in

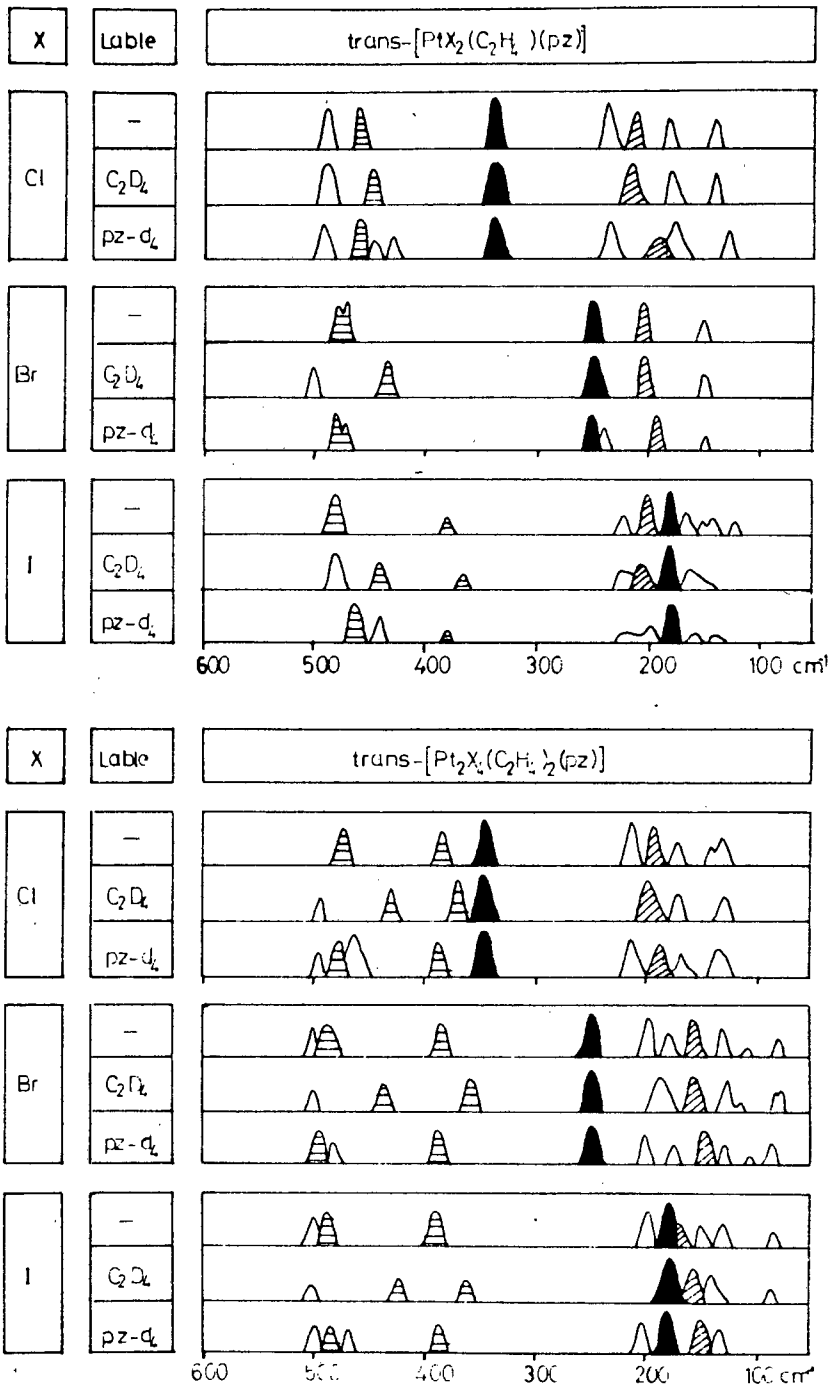

Figure 58. Far-infrared spectra of the complexes of type (I) and type (II). (Solid bands: νPt-X, horizontal bars: νPt-C_2, diagonal bars: νPt-pz)

the spectra of the type (I) complexes, while in the type (II) spectra the ir-forbidden symmetric $\nu Pt\text{-}C_2$ band is also observed.

4.7.2.3 *Electronic spectra*

The data for the electronic spectra of complexes (I) and (II) are listed in Table 35. Two bands of high intensity occur within the range 200 - 300 nm. The band of higher energy is assigned to a charge transfer $X^- \rightarrow Pt^{2+}$ transition while the band of the lower energy is attributed to a combination of the $\pi \rightarrow \pi^*$ transitions of both ethylene and pyrazine. Generally a $\pi \rightarrow \pi^*$ transition for ethylene would occur at higher energy, but the energy difference between the π and π^* levels is decreased on coordination with Pt^{2+} and some of the π-character is lost. This latter assignment; the $\pi \rightarrow \pi^*$(coordinated ethylene), is based on the spectrum of *trans*-$[PtCl_2(C_2H_4)(NH_3)]$, which exhibits a band at 262 nm assigned as $\pi \rightarrow \pi^*$(coordinated ethylene).

In the series (I) complexes, one broad low energy band occurs near 320 nm. The high extinction coefficient rules out the possibility of a $d \rightarrow d$(Pt) transition and in these compounds the band is assigned to a combination of $5d$(Pt) $\rightarrow \pi^*$(ethylene) and $5d$(Pt) $\rightarrow \pi^*$(pyrazine). That the two bands are superimposed is seen in the spectra of the type (II) complexes where resolution of the two bands is obtained. This is due to the fact that the pyrazine is now bridging and as a result the π^*(pyrazine) energy level has dropped.

4.7.3 The complexes *trans*-$[PtCl_2(C_2H_4)(R\text{-an})]$, where R-an is a *meta*-, *para*- or 3,4-disubstituted aniline

It has previously been shown in complexes *trans*-$[PtCl_2(C_2H_4)(4\text{-R-py})]$, (4-R-py = *para*-substituted pyridine), that variation in R affected νPt-N, but hardly influenced the ethylene vibrations.[91] Here we look at the complexes *trans*-$[PtCl_2(C_2H_4)(R\text{-an})]$ and show that νPt-N as well as the ethylene vibrations are affected by variations in R.

4.7.3.1 *^{1}H-nmr results*

The ^{1}H-nmr data referred to the following structures are recorded in Tables 31, 32 and 33.

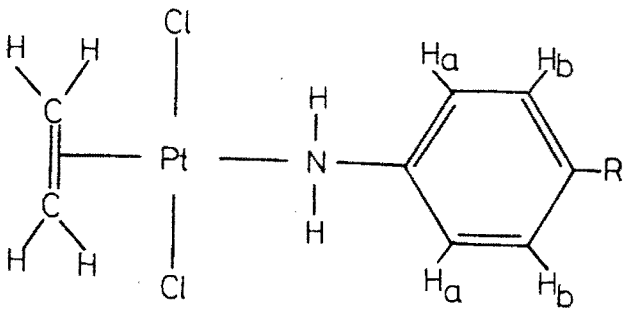

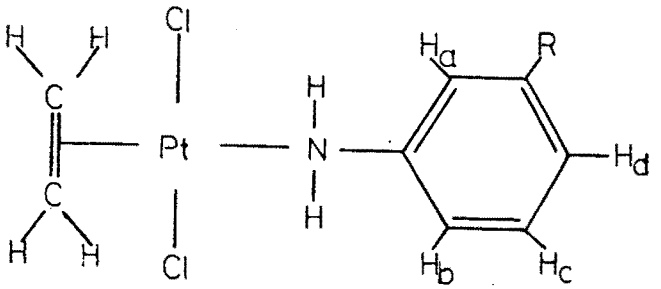

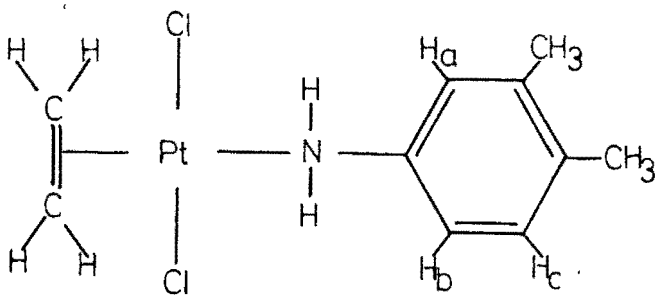

Figure 59. *Trans*-$[PtCl_2(C_2H_4)(R\text{-an})]$, where R-an is a substituted aniline

$J_{Pt\text{-}H}$ is relatively constant and its value is consistent with the nmr data for analogous complexes in which the aniline is replaced by pyridine, pyrazine, imidazole, ammonia and pyridine *N*-oxide.[88,90,92,98,100] There is also very little variation in the chemical shift of the olefin protons which are too far removed from the substituent for its shielding effect to be transmitted. A similar observation was made[91] for the complexes *trans*-$[PtCl_2(C_2H_4)(4\text{-R-py})]$.

The chemical shifts of the aromatic protons tend to be higher for electron withdrawing substituents. If one considers deshielding due to ring currents alone, then the opposite is expected. However, if one considers the electron density at the aromatic protons alone then the observed trend is correct. Since the variation with R is small it is suggested that both effects are in operation.

4.7.3.2 *Infrared spectra*

The bands of primary interest which are most likely to be influenced by the substituent effects are νPt-C_2 (antisymmetric and symmetric), νPt-N and νC-C (ethylene). Assignment of the bands are readily made in relation to our earlier isotopic labelling study.[96]

A plot of the frequencies of these four bands against σ is shown in Figures 60 and 61, and the frequency data are presented in Table 23. It is clear that all of these bands move to higher frequency with electron-releasing substituents, indicating that the electronic effects of the substituents are transmitted throughout the complex molecule. Electron-withdrawing substituents have the opposite effect. It is interesting to note that the mass effects of the substituents do not appear to influence the frequencies to any marked extent. This is most probably due to the fact that the substituents are fairly far removed from the vibrational modes being studied.

The complexes discussed here differ from their substituted pyridine analogues[91] in that the latter fail to yield any correlation between νPt-C_2 and σ. In fact these bands remain approximately constant as R is varied in the pyridine series. This is probably associated with the fact that metal-ligand π-bonding (in the form of a $5d(\mathrm{Pt}) \rightarrow \pi^*$ inverse charge transfer) is possible in the pyridine complexes but not in those of aniline where only σ bonding is present.

.7.3.3 *Electronic spectra*

The uv data are listed in Table 36. By analogy with similar complexes

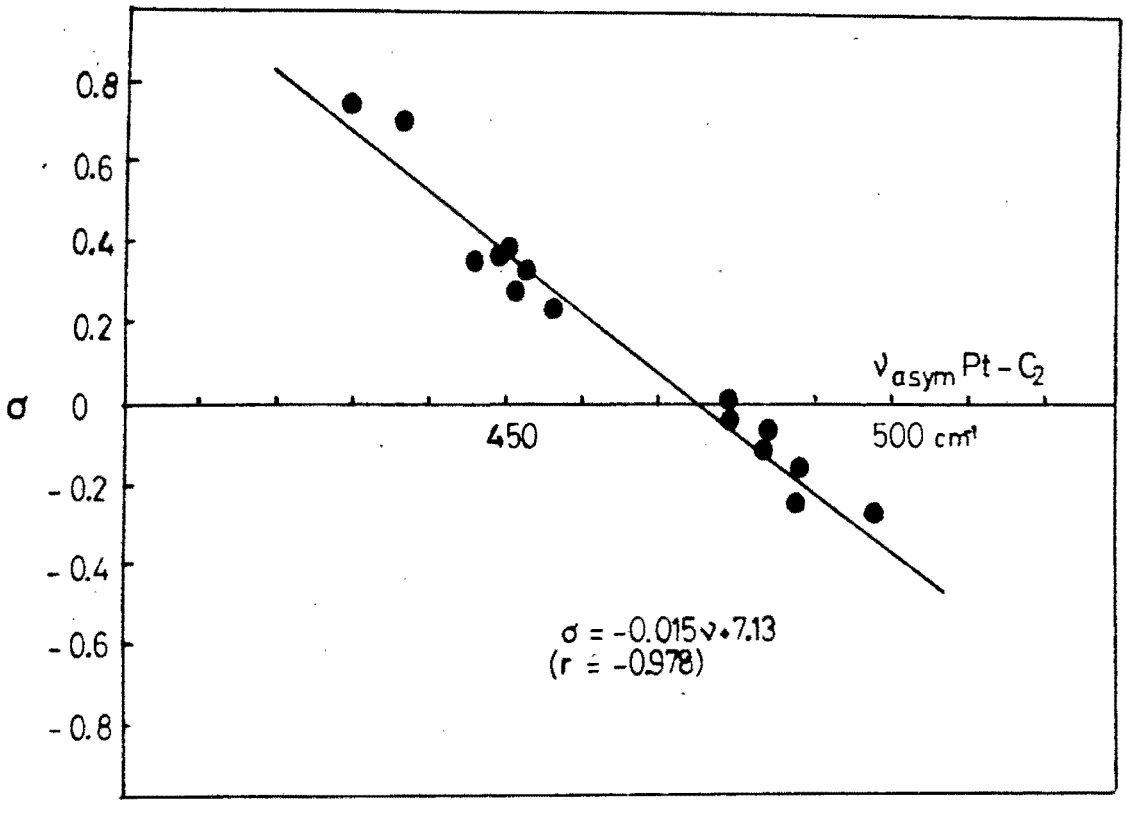

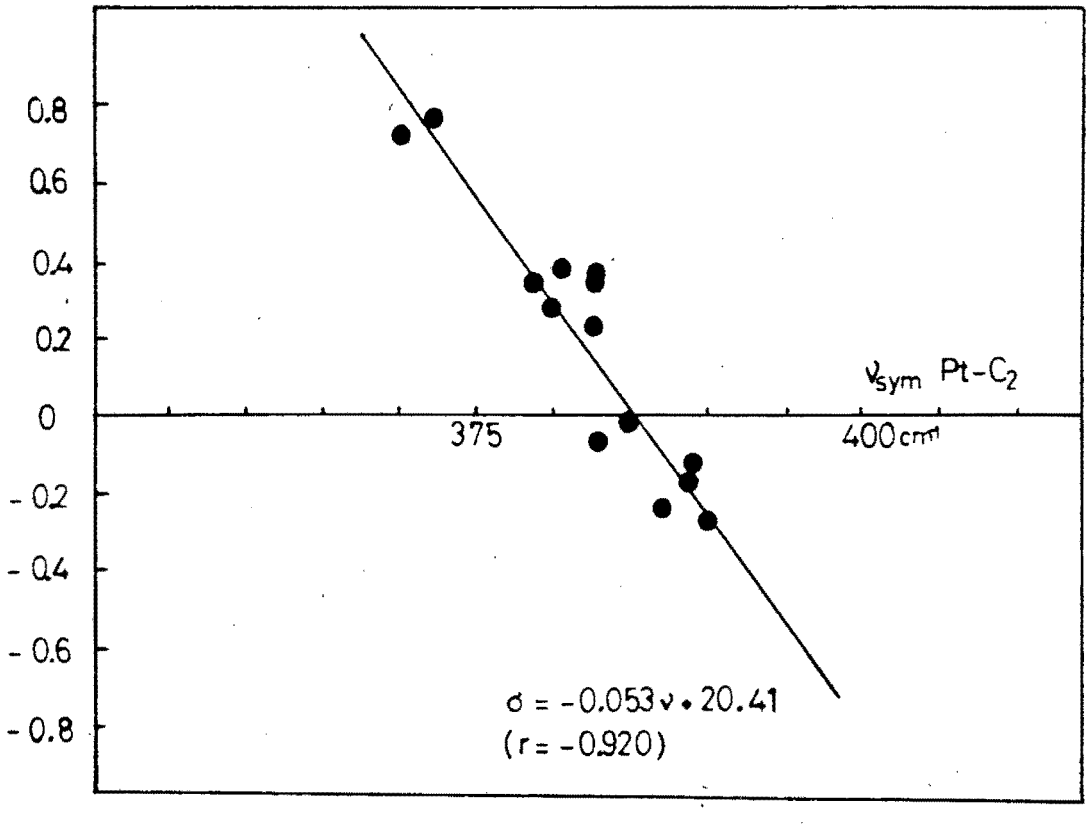

Figure 60. Relationship between Hammett σ-value of R and νPt-C_2

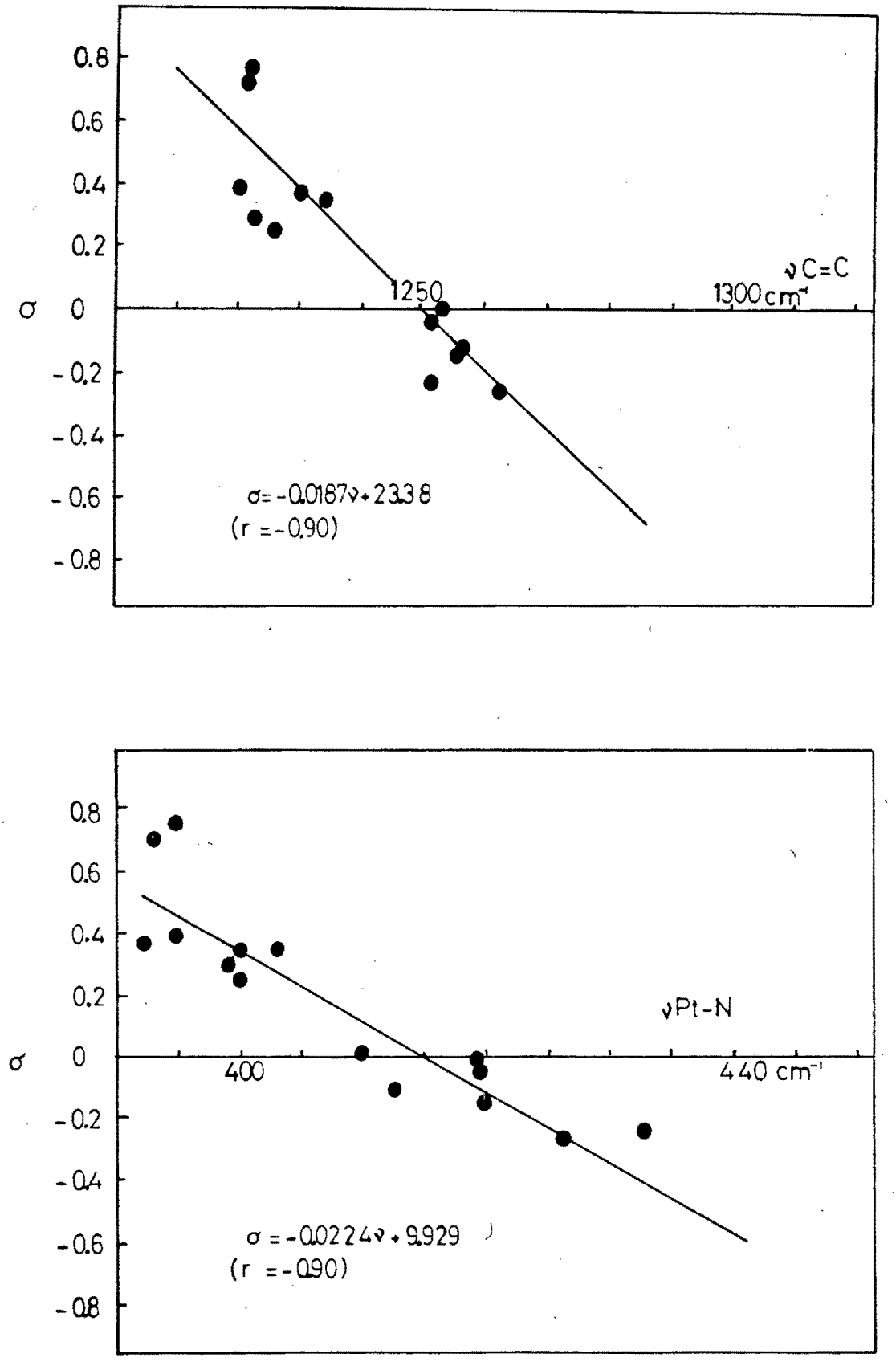

Figure 61. The relationsip between Hammett σ-value of R and νC=C (top) and νPt-N (bottom)

previously studied (Sections 4.7.1.3 and 4.7.1.2),[69,98] we expect to observe the $\pi \rightarrow \pi^*$ transmitions of both the coordinated aniline and ethylene as well as the $5d(Pt) \rightarrow \pi^*$(ethylene) inverse charge transfer and $Cl^- \rightarrow Pt^{2+}$ charge transfer bands. Although, because of the breadth of the electronic bands, no linear correlation can be found, the maximum effect of R is on the $\pi \rightarrow \pi^*$(aniline) transition as might be expected. This is observed from the range of wavelengths which is spanned by the various transitions:

$\pi \rightarrow \pi^*$(aniline)	:	96 nm
$\pi \rightarrow \pi^*$(ethylene)	:	39 nm
$5d(Pt) \rightarrow \pi^*$(ethylene)	:	33 nm
$Cl^- \rightarrow Pt^{2+}$	:	8 nm

CHAPTER 5

CHAPTER 5

5. THE SPIN DYNAMICS OF *trans*-$[PtX_2(C_2H_4)(L)]$, (X = Cl, Br; L = pyrazine (pz), imidazole (Him) and N-methyl imidazole (N-Me Him)

5.1 INTRODUCTION

Nuclear magnetic resonance studies, in conjunction with X-ray crystallography and infrared spectroscopy, has been used extensively in providing evidence for the structure of Pt^{2+}-olefin complexes.

Thus far the main area of interest has been the configuration of the olefin. This has been studied in terms of rotation, which gives valuable information about the bonding taking place, possible changes in hybridization of the C atoms of the double bond on complexation, and the equilibria that are set up when the complexes are dissolved in various solvents.

Solid state studies of polycrystalline $[PtCl_2(C_2H_4)]_2$ show that there are two movements taking place *viz.* a rocking motion of the olefin perpendicular to the Pt-C_2H_4 bond, and a wagging about the C = C axis.[101] In addition there is strong evidence in support of lengthening of the olefin bond on coordination.

Work done by Maricic and coworkers on the nmr spectra of single crystals, at a number of orientations to the magnetic field, of $K[PtCl_3(C_2H_4)].H_2O$

and its D_2O analogue, suggests that the coordinated ethylene is rotating about the Pt-C_2H_4 bond axis as well as the C = C axis.[102]

In solution it appears that there are three main movements of the olefin. These are rotation about the axis of the olefinic double bond, rotation of the olefin about the Pt-olefin bond and exchange of the olefin.

Rotation about the C = C axis is manifested by the Pt-olefin proton coupling constants in complexes containing asymmetrical olefins. A good example is given by Hartley[103] whose data are listed in Table 37.

Table 37. $J_{^{195}Pt-^{1}H}$ coupling constants for the olefinic protons of Bu_4N^+ $[Pt(CH_3CH{=}CH_2)Cl_2]^-$ in acetone-d_6

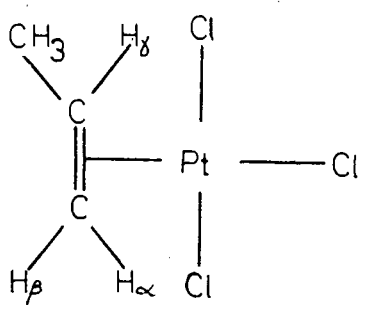

Table 37 continued/

Proton	δ(ppm)	$J_{^{195}Pt-^{1}H}$ (Hz)
H_α	4.265	67
H_β	4.097	60
H_γ	5.193	65

It is suggested that the lower coupling constant for H_β accounts for the fact that the olefin rotates about the C = C axis in such a way as to minimize the interaction between the methyl group and the central metal group. The small difference in the coupling constants of H_α and H_β suggests that the twisting effect is small.

Extensive research has been done on the rotation of the olefin about the Pt-olefin bond[104-106] and three methods of determining the free energy barrier to rotation of the olefin have been used.

The most common method is the use of an asymmetrical olefin in a complex of the form *trans*-$[PtCl_2(ol)(L)]$, (where ol = asymmetric olefin *e.g.* styrene, *t*-butylethylene *etc*; L = some bulky ligand *e.g.* 2,4,6-trimethylpyridine). From the coalescence temperature of the olefinic proton signals it is found that the free energy barrier to rotation lies between 40 and 60 kJ mol^{-1}.

A second method is the use of a complex such as *trans*-[PtXY(ol)(L)], (X = Cl, Y = Br and L = another ligand). This was done by Miya and

Saito,[6] who studied the ^{1}H-nmr spectra of $[PtClBr(C_2H_4)(4\text{-R-py})]$, (4-R-py = *para*-substituted pyridine) at various temperatures. From the coalescence temperature of the olefinic proton signals they found the free energy barrier to rotation of the olefin to lie between 60 and 67 kJ mol^{-1} for the range of substituted pyridine complexes.

A third method was used by Boucher and Bosnich[105] who studied the rotational properties of *cis*-$[PtCl_2(propene)(dmso)]$. This method involves the use of an asymmetric olefin as well as the *cis*-geometry, although the latter by itself should also be sufficient. From the coalescence temperature of the olefinic proton signals they found the free energy barrier to rotation of the propene to be 61 kJ mol^{-1}.

In the case of $[PtCl_3(CH_2CH_2)]^-$, apart from rotation of the olefin about the C = C axis and the Pt-olefin axis, there is the possibility of exchange. Nmr studies suggest that the rate of exchange of free and coordinated ethylene in Zeise's salt is greater than 70 s^{-1} at 75°, and occurs *via* an associative mechanism.[107]

When Zeise's salt reacts with another ligand, L, we have the possibility of looking at the exchange of L. This has been done for L = pyridine,[108] where the exchange was found to be so fast that there was no coupling between Pt and α-protons of the pyridine ring at ambient temperature. It is expected that the rate of exchange of pyridine in $[PtCl_2(C_2H_4)(py)]$ is much faster than in $[PtCl_2(py)_2]$ due to the high *trans*-labilising effect of C_2H_4.

In this chapter we look at the exchange processes of L (L = pyrazine

and imidazole) taking place in the complex *trans*-$[PtX_2(C_2H_4)(L)]$, (X = Cl, Br). Because both pyrazine and imidazole each have two coordination sites, there is the possibility of both intramolecular as well as intermolecular exchange.

By using computer simulation methods as described in Chapter 1.5 it is possible to calculate the activation parameters for the exchange of L and in doing so one can obtain information about the type of exchange taking place.

5.2 RESULTS

Table 38. The ^{1}H-nmr spectrum of *trans*-[$PtCl_2(C_2H_4)$(pyrazine)] run at 203 K in acetone-d_6 using TMS as reference

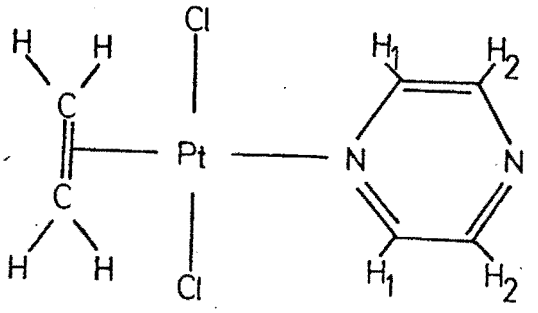

Chemical shift (ppm)	
Olefin protons	Pyrazine protons
H	H_1, H_2 [a]
4.87	8.98

Coupling constants (Hz)		
Olefin protons	Pyrazine protons	
^{J}Pt-H	^{J}Pt-H	^{J}Pt-H_2
60.3	b	b

[a] Only one resonance for H_1 and H_2 at δ = 8.98 integrating four protons

[b] No coupling observed

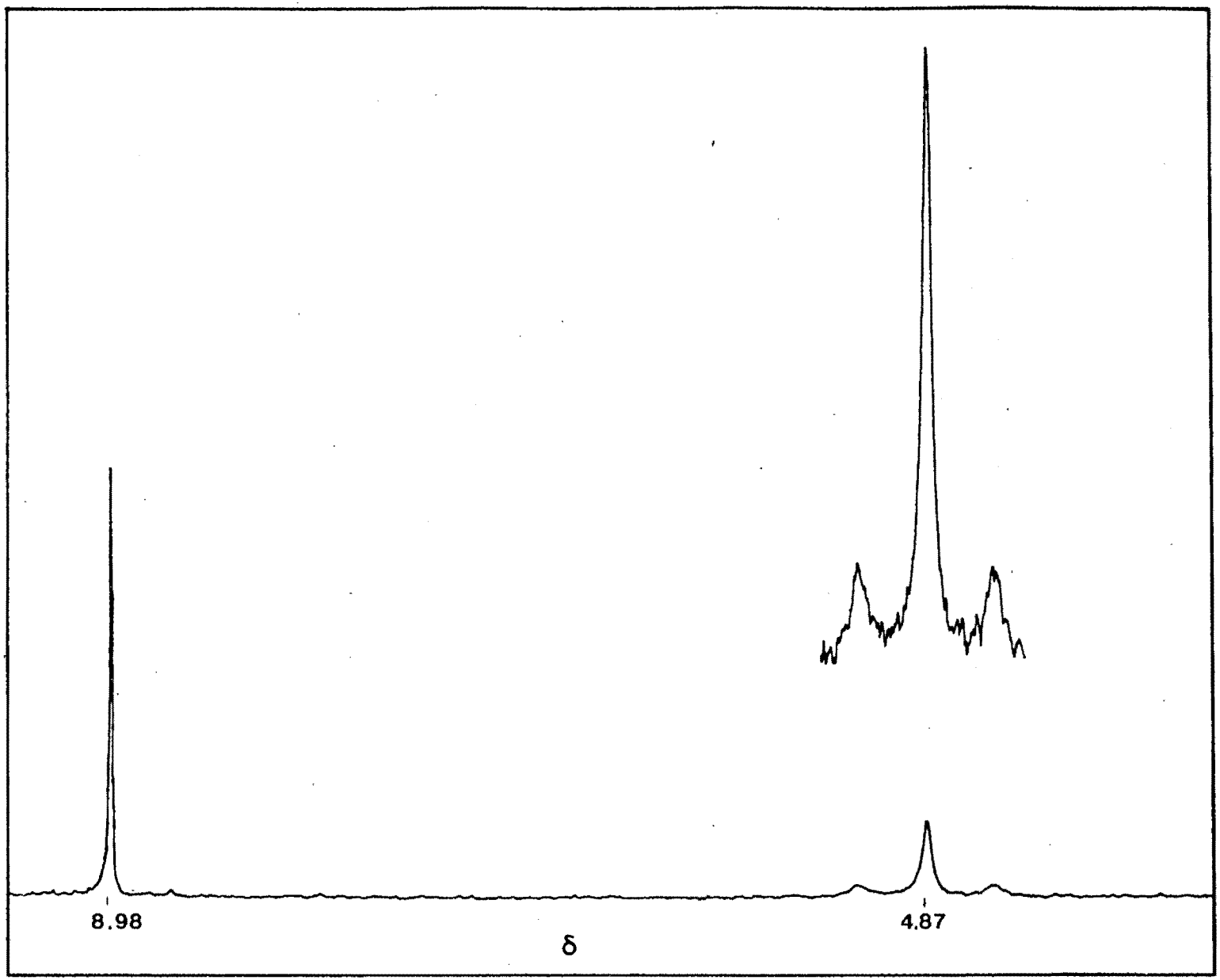

Figure 62. ^{1}H-nmr spectrum of *trans*-[$PtCl_2(C_2H_4)(pz)$] run in acetone-d_6 at 203 K (scale: 1 cm = 27 Hz)

Table 39. The ^{1}H-nmr spectrum of *trans*-$[PtCl_2(C_2H_4)(imidazole)]$ run at 223 K in acetone-d_6 using TMS as reference

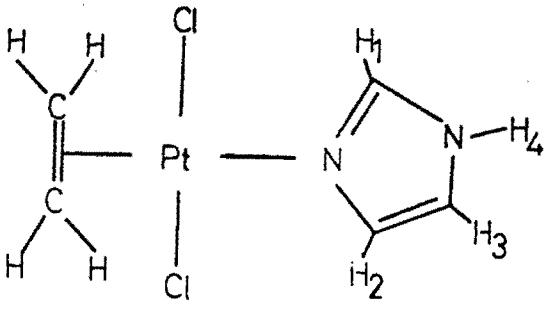

Chemical shift (ppm)					
Olefin protons		Imidazole protons			
H		H_1	H_2	H_3	H_4
4.56		8.55	7.66	7.38	3.12
Coupling constants (Hz)					
Olefin protons		Imidazole protons			
J_{Pt-H}		J_{Pt-H_1}	J_{Pt-H_2}	J_{Pt-H_3}	
60.0		19.0	20.0	a	

a Coupling constants not observed. (J_{Pt-H_3} was assumed to be 7 Hz in the computer simulation based on previous work)[9]

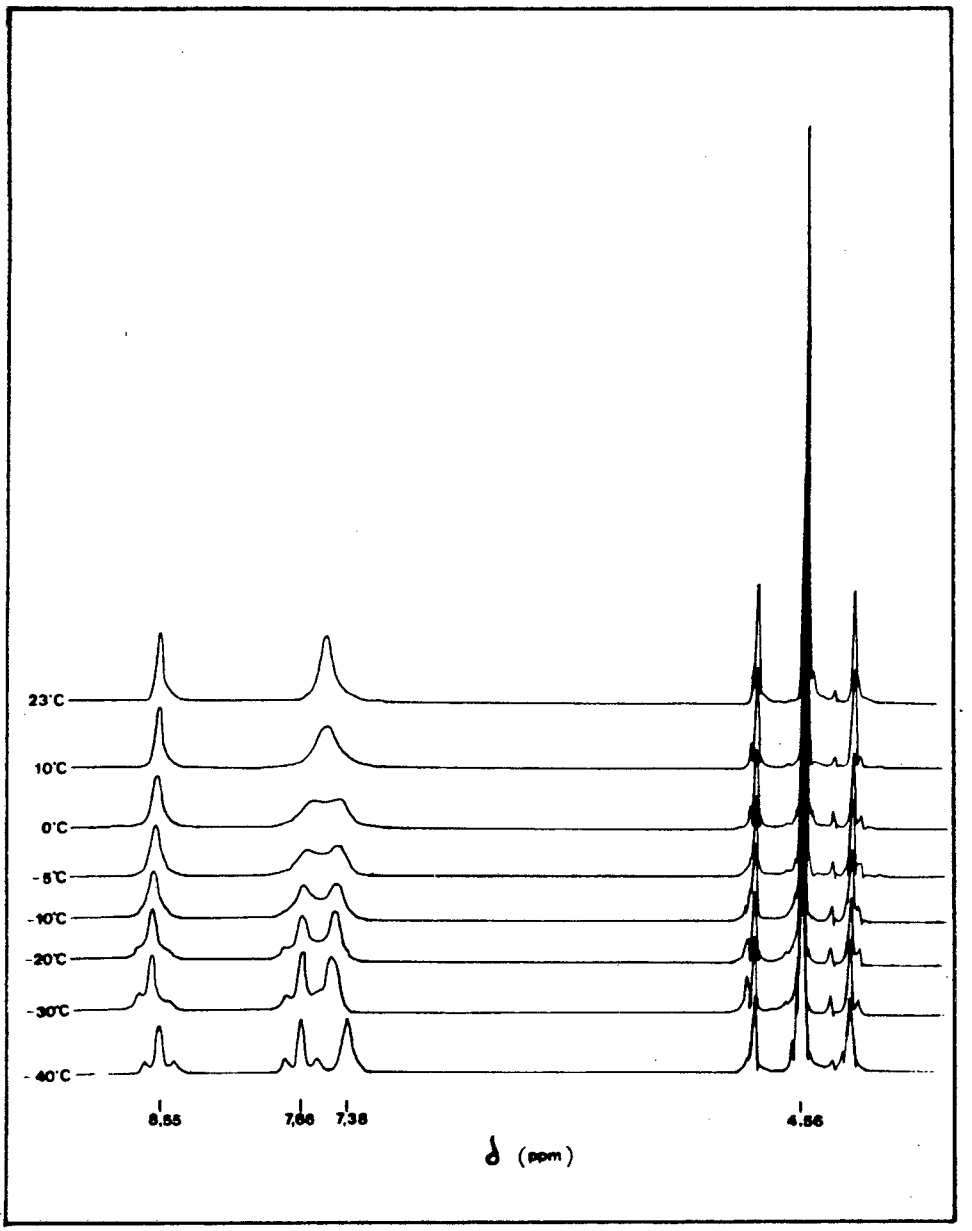

Figure 63. ^{1}H-nmr spectra of *trans*-[$PtCl_2(CH_2{=}CH_2)$imidazole)] run at variable temperature in acetone-d_6

5.3.2 The ^{1}H-nmr spectrum of *trans*-[$PtCl_2(C_2H_4)$(imidazole)]

The results for *trans*-[$PtCl_2(C_2H_4)$(Him)] are listed in Table 39 and shown in Figure 63. At ambient temperature the spectrum contains three signals. The ethylene protons resonate at δ = 4.57 ppm and exhibit a coupling constant of 60 Hz with Pt(I = $\frac{1}{2}$), characteristic of compounds of this type. The two other signals occur at δ = 8.56 and δ = 7.54, and integrate for 1 and 2 protons respectively. The resonance at δ = 8.56 is assigned to H_1 while the resonance at δ = 8.56 is assigned to H_2 and H_3, which are equivalent if exchange is taking place.

If exchange is taking place then the resonance for H_2 and H_3 should collapse into two resonances on cooling. This is manifested in the spectra run at different temperatures (see Figure 63). On cooling two changes take place:

(a) the single resonance for H_2 and H_3 at δ = 7.54 collapses into two resonances at δ = 7.66 and δ = 7.38 respectively,

(b) coupling is observed between Pt(I = $\frac{1}{2}$) and H_1 (19 Hz) and H_2 (20 Hz). The coupling between Pt(I = $\frac{1}{2}$) and H_3 is not observed, but indications are that it is in the region of 7 Hz.[32]

Thus it appears that there is exchange between imidazole and the parent complex.

On the basis of the fast nature of the exchange and the collapse of the H_1 platinum satellites it was assumed that the exchange process was one of an intramolecular nature using different N atoms *i.e.* during exchange the proton on the nitrogen atom has to migrate.

Table 40. Activation parameters for *trans*-[$PtCl_2(C_2H_4)$(imidazole)] derived by means of band shape analysis of the H_2 and H_3 resonances using DNMR5[10] as an iterative simulation program,[a] assuming intramolecular exchange

T (°K)	k (sec^{-1})	$\ln k$	Error analysis factor for $\ln k$	$\frac{1}{T} \times 10^3$
283	80 ± 5	4.38 ± 0.13	0.295	3.53
273	50 ± 5	3.91 ± 0.20	0.192	3.66
268	40 ± 5	3.69 ± 0.25	0.154	3.73
263	32 ± 3	3.47 ± 0.19	0.202	3.80
253	17 ± 5	2.83 ± 0.61	0.063	3.95
243	10 ± 2	2.30 ± 0.41	0.094	4.12

[a] Parameters used in the above simulation are listed below:

$J_{Pt\text{-}H_1}$ = 19 Hz δ = 8.55 ppm

$J_{Pt\text{-}H_2}$ = 20 Hz δ = 7.66 ppm

$J_{Pt\text{-}H_3}$ = 7 Hz[32] δ = 7.38 ppm

T_2 = 0.076 sec (obtained from width at half height of H_2 signal)

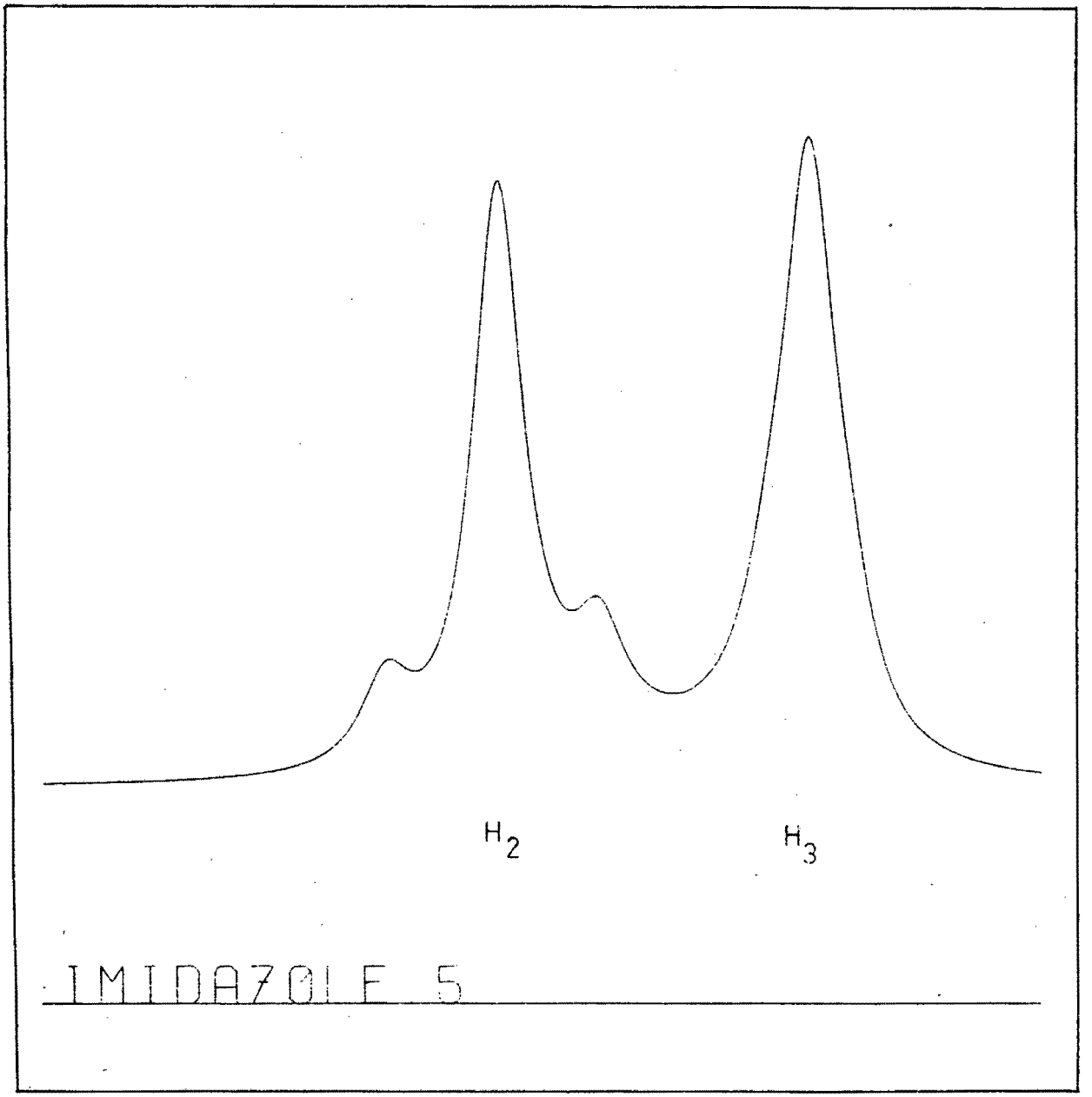

Figure 64. Computer simulation of the H_2 and H_3 resonance band shapes in *trans*-$[PtCl_2(C_2H_4)(imidazole)]$ where k = 5 sec^{-1}

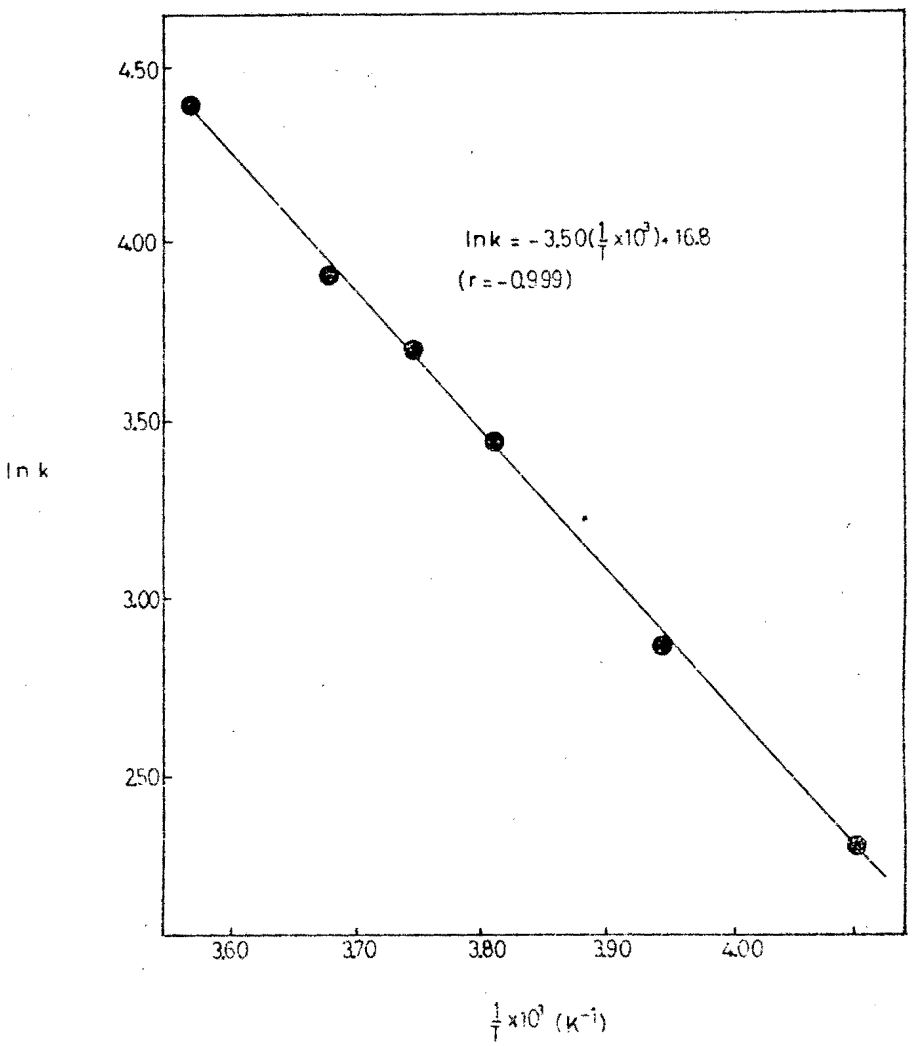

Figure 65. Plot of ln k vs. $1/T$ x 10^3 for *trans*-[$PtCl_2(CH_2{=}CH_2)$(imidazole)]

Table 41. The ^{1}H-nmr spectrum of *trans*-[$PtBr_2(C_2H_4)$(imidazole)] run at 193 K in acetone-d_6 using TMS as reference

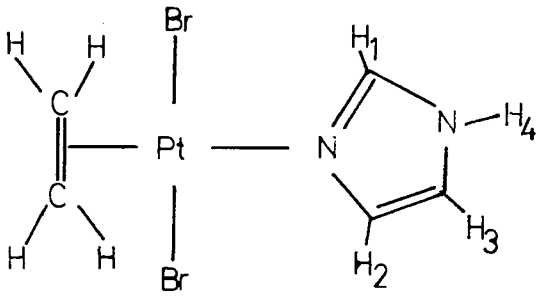

Chemical shift (ppm)						
Olefin protons		Imidazole protons			
H		H_1	H_2	H_3	H_4
4.76		8.62	7.63	7.51	3.84

Coupling constants (Hz)						
Olefin protons		Imidazole protons			
^{J}Pt-H		^{J}Pt-H_1	^{J}Pt-H_2	^{J}Pt-H_3	
60.0		18.0	20.0	a	

[a] Coupling constant not observed (J_{Pt-H_3} was assumed to be 7 Hz in the computer simulation based on previous work)[32]

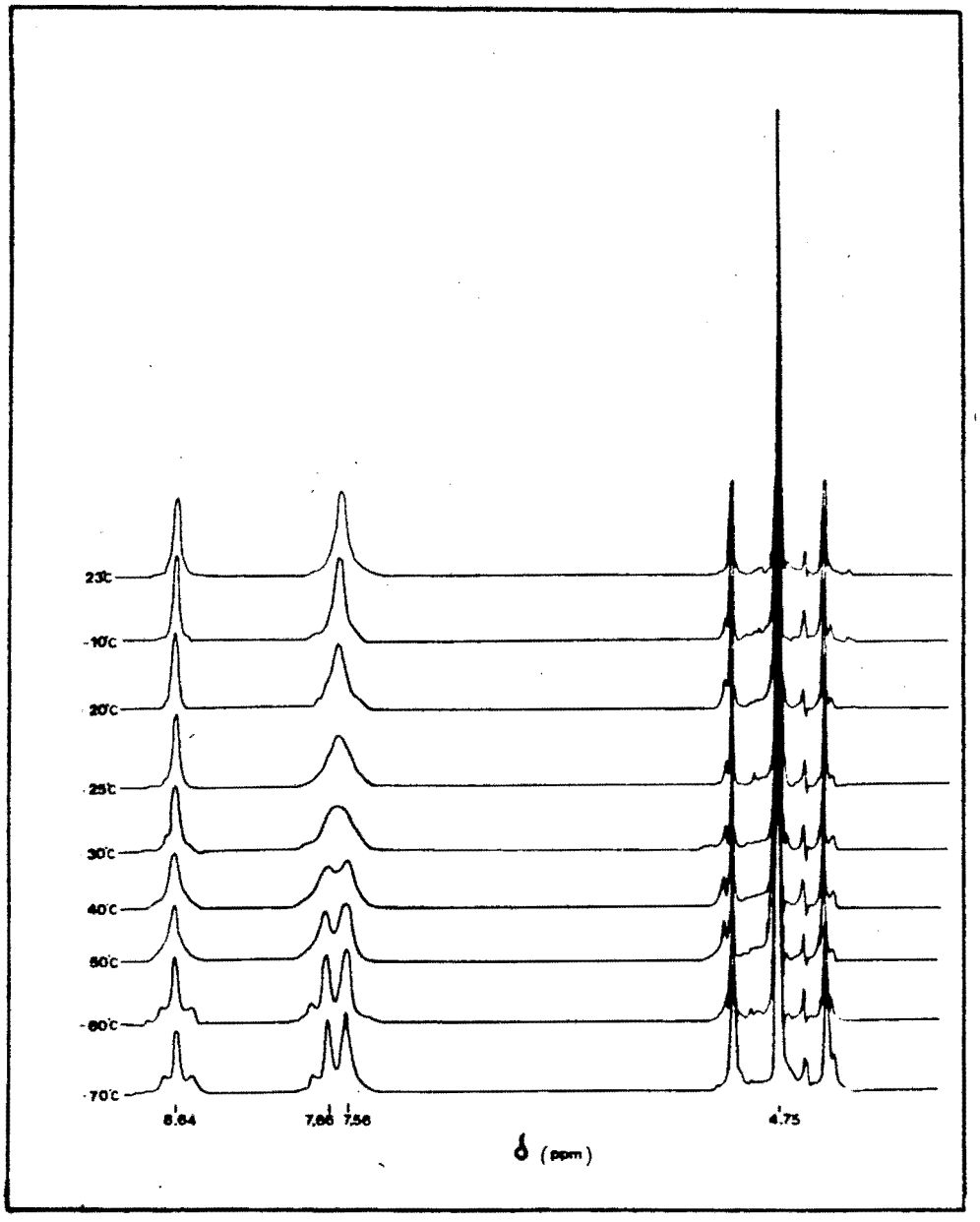

Figure 66. ^{1}H-nmr spectra of *trans*-[$PtBr_2(CH_2{=}CH_2)$(imidazole)] run at variable temperature in acetone-d_6

In summary, it is suggested that imidazole exchanges with the parent complex fairly easily, as manifested by $\Delta H^{\ddagger}$, and that the predominant mechanism of exchange at these temperatures is one of an intramolecular nature with use of both nitrogen atoms in the bonding.

5.3.3 The ^{1}H-nmr spectrum of *trans*-[$PtBr_2(C_2H_4)$(imidazole)]

The results for *trans*-[$PtBr_2(C_2H_4)$(imidazole)] are listed in Table 41 and shown in Figure 66. As in the case of the chloride analogue, the spectrum contains three signals at ambient temperature. The ethylene protons resonate at δ = 4.76 ppm and exhibit a coupling constant of 60 Hz with Pt (I = ½). The H_1 resonance occurs at δ = 8.62, while the resonance for the equivalent H_2 and H_3 protons occurs at δ = 7.56.

On cooling the expected changes occur, namely:

(a) the single resonance for H_2 and H_3 at δ = 7.56 collapses into two resonances at δ = 7.65 and δ = 7.52 respectively,

(b) coupling is observed between Pt (I = ½) and H_1 (18.0 Hz) and H_2 (20.0 Hz). Once again the coupling between Pt (I = ½) and H_3 is not observed.

Thus it appears that there is exchange between the imidazole ligand and the parent complex, and that this exchange is faster than in the chloride case, as manifested by the lower coalescence temperature (see Figure 66).

Table 42. Activation parameters for *trans*-[$PtBr_2(C_2H_4)$(imidazole)] derived by means of band shape analysis of the H_2 and H_3 resonances using DNMR5[10] as an iterative simulation program[a], assuming intramolecular exchange

T (°K)	k (sec^{-1})	ln k	Error analysis factor for ln k	$\frac{1}{T} \times 10^3$
233	12 ± 2	2.49 ± 0.34	0.161	4.29
223	5 ± 1	1.61 ± 0.41	0.133	4.48
213	3 ± 1	1.10 ± 0.69	0.079	4.70
203	1.1 ± 0.1	0.095 ± 0.087	0.627	4.93

a

Parameters used in the above simulation are listed below:

$^{J}Pt\text{-}H_1$ = 18.0 Hz $\quad$ δ_{H_1} = 8.62 ppm

$^{J}Pt\text{-}H_2$ = 20.0 Hz $\quad$ δ_{H_2} = 7.63 ppm

$^{J}Pt\text{-}H_3$ = 7.0 Hz[32] $\quad$ δ_{H_3} = 7.51 ppm

T_2 = 0.10 sec. (obtained from width at half height of H_2 signal)

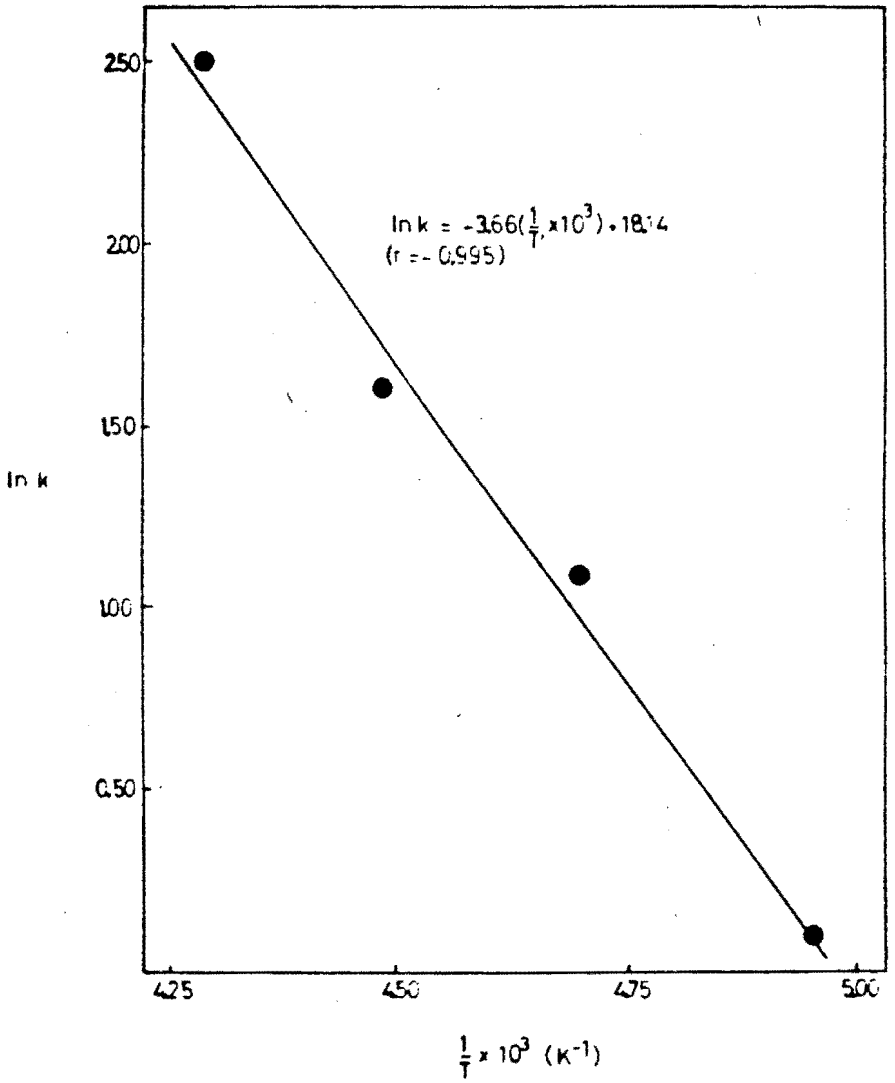

Figure 67. Plot of $\ln k$ vs. $1/T \times 10^3$ for *trans*-[$PtBr_2(CH_2{=}CH_2)$(imidazole)]

Table 43. The ^{1}H-nmr spectrum of *trans*-[$PtBr_2(C_2H_4)$(*N*-methylimidazole)] run at 193 K in acetone-d_6 using TMS as reference

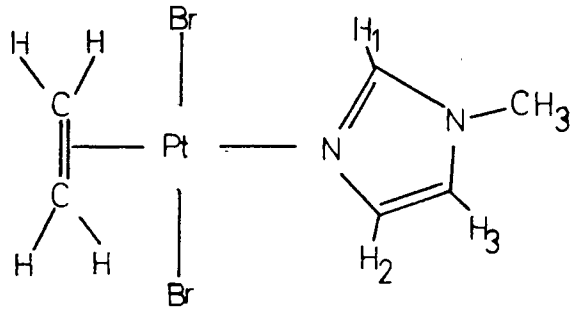

Chemical shift (ppm)					
Olefin protons		Imidazole protons			
H		H_1	H_2	H_3	CH_3
4.74		8.42	7.58	7.26	3.91
Coupling constants (Hz)					
Olefin protons		Imidazole protons			
$^JPt\text{-}H$		$^JPt\text{-}H_1$	$^JPt\text{-}H_2$	$^JPt\text{-}H_3$	
60.0		18.0	19.0	a	

a Coupling constant not observed. ($J_{Pt\text{-}H_3}$ was assumed to be 7 Hz in the computer simulation based on previous work)[33]

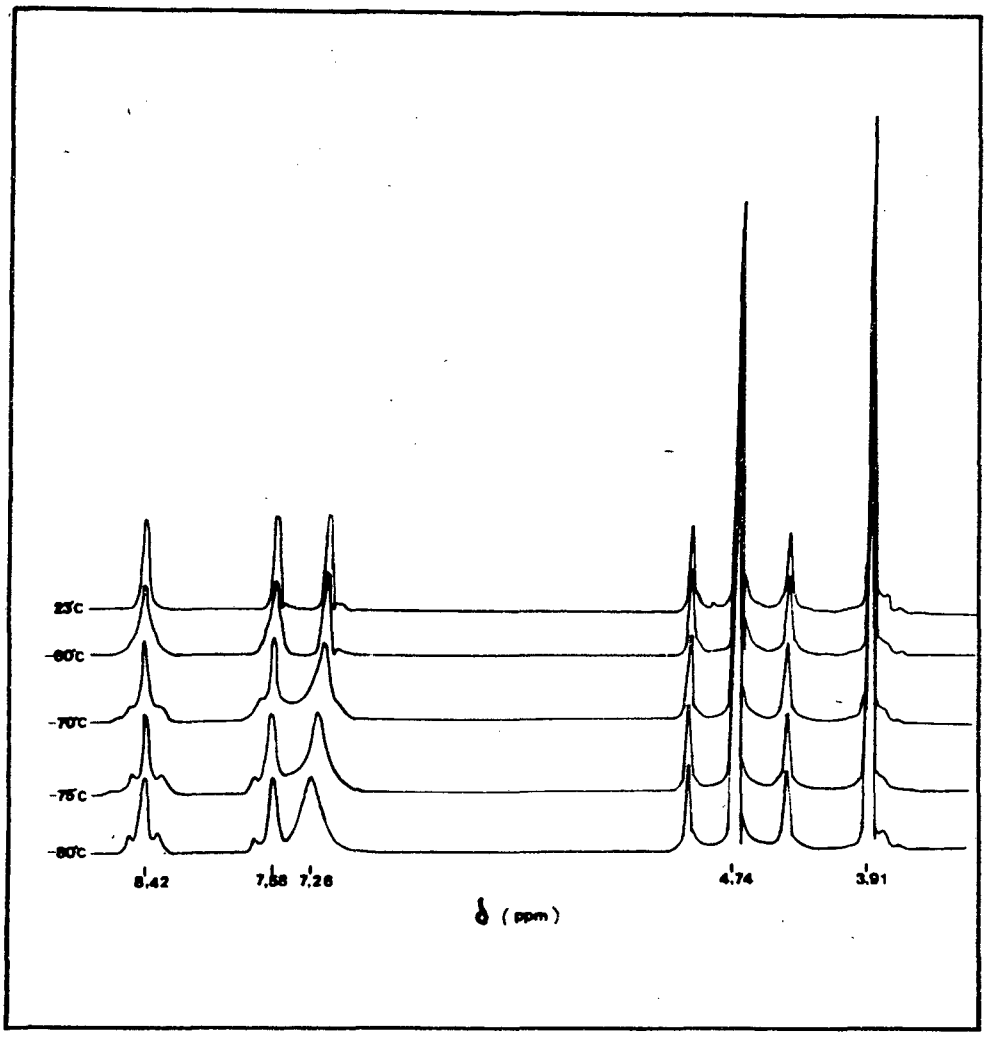

Figure 68. ^{1}H-nmr spectra of *trans*-[$PtBr_2(CH_2{=}CH_2)$(*N*-methylimidazole)] run at variable temperature in acetone-d_6

5.3 DISCUSSION

In the case of *trans*-$[PtX_2(C_2H_4)(L)]$, where L = pyrazine or imidazole there are four possible nuclear configurations; two with Pt(I = $\frac{1}{2}$) and two with Pt(I = 0). The nuclear configurations for L = pz are shown in Figure 69 while those for L = Him are shown in Figure 70.

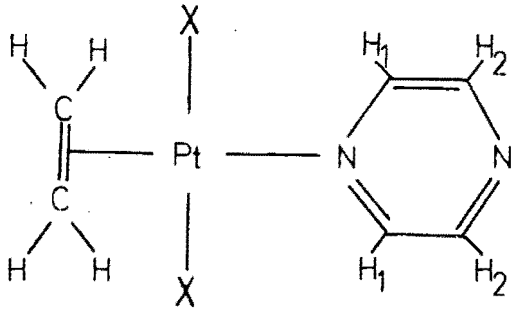

1,2*

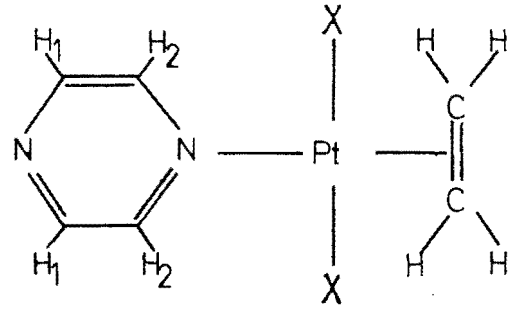

3,4*

Figure 69. The nuclear configurations for *trans*-$[PtX_2(C_2H_4)(pz)]$

* (The asterisk denotes the configuration with Pt(I = 0))

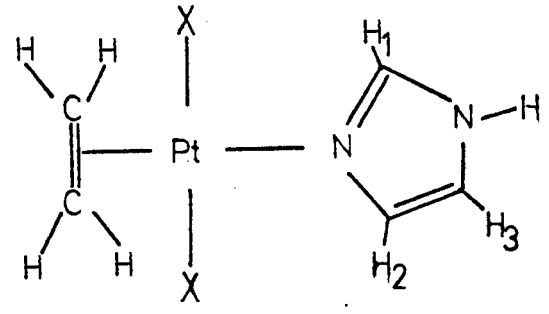

1,2*

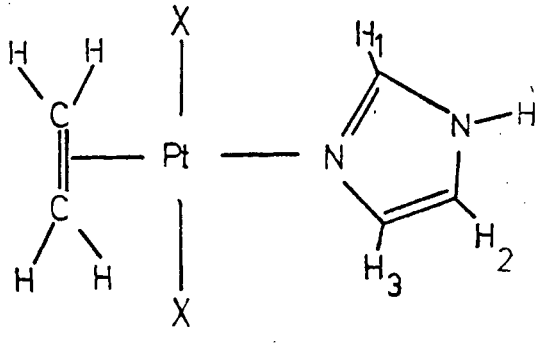

3,4*

Figure 70. The nuclear configurations for *trans*-$[PtX_2(C_2H_4)(Him)]$

* (The asterisk denotes the configuration with Pt(I = 0))

Considering the above, apart from intramolecular exchange it is possible to get six intermolecular exchanges between the four nuclear configurations (see Figure 71). The problem is however simplified by the fact that the rate of all the intermolecular exchanges are equivalent. Thus there are three possible movements of L that can occur: (a) Exchange with solvent. In this case L moves outside the coordination sphere, is replaced by a solvent molecule, before returning to bond *via* the same N atom.

(b) intramolecular exchange using different N atoms,

(c) intermolecular exchange.

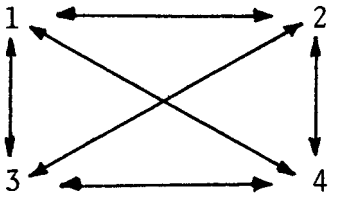

Figure 71. Possible intermolecular exchange between four nuclear configurations.

In the case of *trans*-$[PtX_2(C_2H_4)(N\text{-Me Him})]$ there are only two nuclear configurations (see Figure 72).

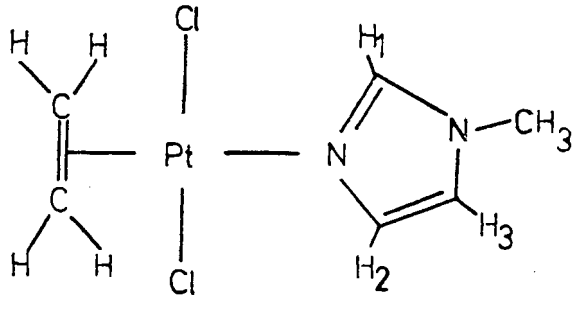

1,2*

Figure 72. The nuclear configurations for *trans*-$[PtX_2(C_2H_4)(N\text{-Me Him})]$
* (The asterisk denotes the configuration with Pt(I = 0))

Thus in the case where L = *N*-methylimidazole the following processes can occur:

(a) Intramolecular exchange using the same N atom for bonding.

(b) Intermolecular exchange.

The ^{1}H-nmr results for the complexes are considered seperately.

5.3.1 The ^{1}H-nmr spectrum of *trans*-[$PtCl_2(C_2H_4)$(pyrazine)]

The results for *trans*-[$PtCl_2(C_2H_4)$(pz)] are listed in Table 38 and shown in Figure 62. The ethylene protons resonate at δ = 4.87 and couple with Pt(I = ½) exhibiting a 60 Hz coupling constant, characteristic for compounds of this type.

What is more striking is the resonance at δ = 8.98 integrating four protons. This corresponds to the pyrazine protons which apparently are all equivalent indicating that pyrazine is exchanging with the parent complex. This resonance would be expected to collapse into a pair of multiplets, one for the α-protons and one for the β-protons, on cooling. However even at 203 K does the resonance remain a sharp singlet with no coupling indicating that there is very rapid exchange.

As a result no kinetic data for the exchange process could be obtained and it is debatable as to which exchange process or combination of exchange processes is taking place. What can be concluded however, is that the exchange process is very rapid and that $\Delta G^{\ddagger}$ is less than 42.2 kJ mol^{-1}.

The spin dynamic parameters were fed into DNMR5,[22] an iterative simulation program, assuming intramolecular exchange. By means of band shape analysis,[21] the rate constants, k, for the exchange process were determined, and are listed in Table 40.

A plot of $\ln k$ vs $1/T$ was made (see Figure 65) using error analysis which has been shown to be the only valid means of determining the slope and intercept accurately since measurements near the coalescence temperature are most accurate.[22]

The result of the above plot, is a straight line whose slope gives $\Delta H^{\ddagger}$, the enthalpy of activation, directly and an intercept from which $\Delta S^{\ddagger}$, the entropy of activation, may be determined, since we have:

$$\ln k = \ln A - \frac{\Delta H^{\ddagger}}{RT}$$

and

$$\ln A = \ln \frac{{}^{\circ}kI}{h} + \frac{\Delta S^{\ddagger}}{R}$$

where k = rate constant (sec^{-1})

T = temperature in degrees Kelvin

${}^{\circ}k$ = Boltzman constant

h = Planck constant.

The results were as follows:

$$\Delta H^{\ddagger} = 29.3 \pm 0.60 \text{ kJ mol}^{-1}$$

$$\Delta S^{\ddagger} = -105 \pm 2.0 \text{ kJ mol}^{-1}\text{K}^{-1}.$$

The enthalpy of the exchange process is low compared to that obtained for substitution reactions at the square planar platinum centre.

This is indicative of the strong *trans*-labelising effect of ethylene. $\Delta S^{\ddagger}$ is a fairly large negative valve, much more so than for most organic exchange processes where it is often assumed to be zero. However it is of the same order of magnitude as that for substitution reactions at the square planar platinum centre. This high $\Delta S^{\ddagger}$ value also seems to indicate that solvent has a noticeable effect in the exchange process. A suggested exchange mechanism is shown in Figure 73.

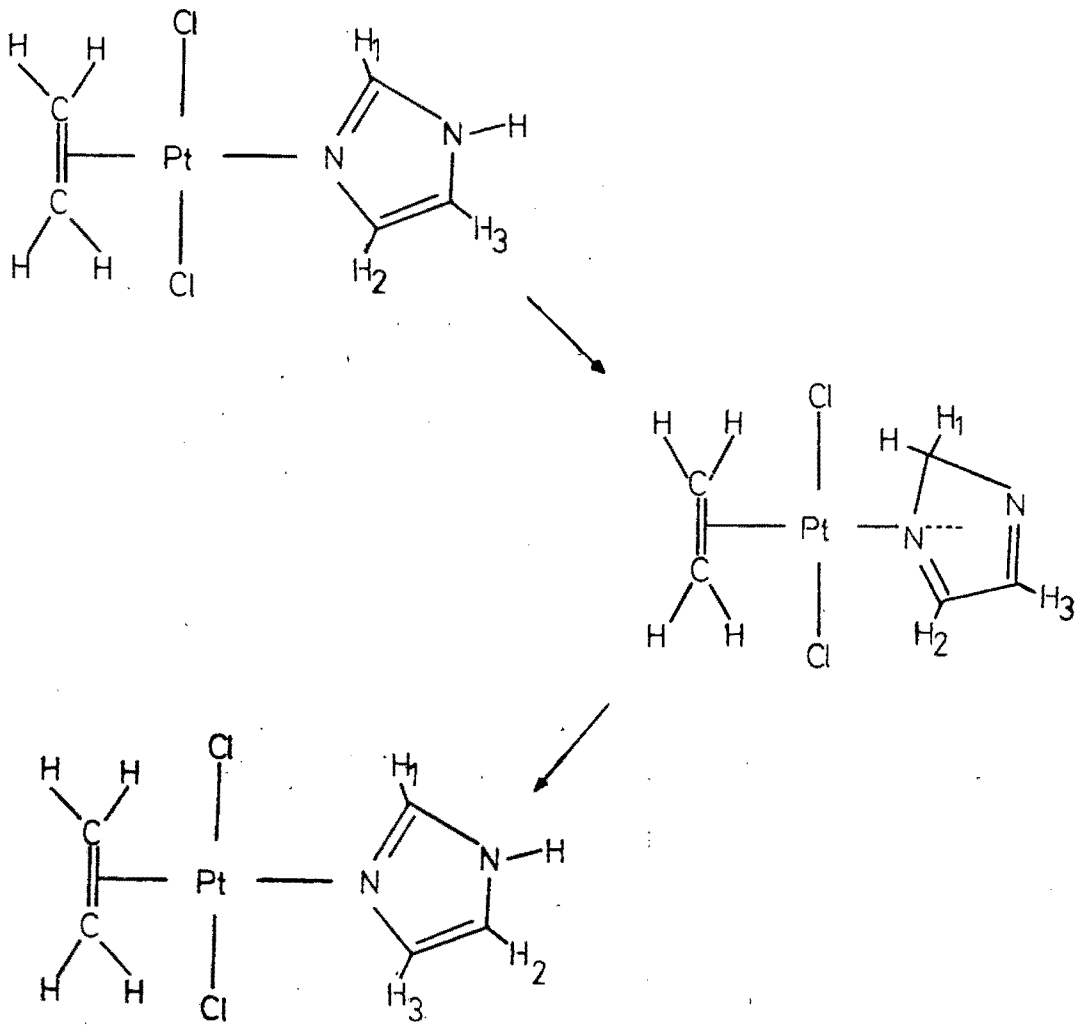

Figure 73. Suggested intramolecular exchange mechanism for *trans*-$[PtCl_2(C_2H_4)(Him)]$

On the basis of the fast nature of the exchange and the collapse of the H_1 platinum satellites it was again assumed that the exchange process was one of an intramolecular nature using different N atoms, with migration of the labile proton.

Once again DNMR5[22] was used to determine the rate constants, k, for the exchange process, and these are listed in Table 42. However it was found that at high temperatures there was some deviation in the simulated spectrum. This was attributed to intermolecular exchange, or intramolecular exchange using the same N atom for bonding, where the imidazole leaves the coordination sphere, is replaced by solvent, before returning to the coordination site.

The enthalpy and entropy changes for the intramolecular exchange process occurring in the lower temperature region near coalescence were calculated as before (see Figure 67).:

$$\Delta H^{\ddagger} = 30.4 \pm 0.60 \quad \text{kJ mol}^{-1}$$

$$\Delta S^{\ddagger} = -94.1 \pm 2.2 \quad \text{kJ mol}^{-1}$$

Considering the above it is suggested that in the case of *trans*-$[PtBr_2(C_2H_4)(Him)]$, the exchange process at lower temperatures is similar to that suggested for the *trans*-$[PtCl_2(C_2H_4)(Him)]$, but that at higher temperatures intermolecular exchange or intramolecular exchange where the imidazole leaves the coordination site becomes increasingly more important.

5.3.4 The ^{1}H-nmr spectrum of *trans*-[$PtBr_2(C_2H_4)$(*N*-methylimidazole)]

The results for *trans*-[$PtBr_2(C_2H_4)$(*N*-Me Him)] are listed in Table 43, and shown in Figure 68. At ambient temperature the spectrum contains five signals. The ethylene protons resonate at δ = 4.74 ppm and exhibit a coupling constant of 60 Hz with Pt (I = $\frac{1}{2}$). The H_1 proton resonates at δ = 8.42 while H_2 (δ = 7.58) and H_3 (δ = 7.26) are now separated since they are no longer equivalent. It is interesting to note however, that neither H_1, H_2 nor H_3 exhibit coupling with Pt (I = $\frac{1}{2}$) at ambient temperature. The methyl protons resonate at δ = 3.91.

When the temperature is lowered, it is found that platinum satellites occur for H_1 ($J_{Pt\text{-}H_1}$ = 18 Hz) and H_2 ($J_{Pt\text{-}H_2}$ = 19 Hz), whereas the coupling between H_3 and Pt (I = $\frac{1}{2}$) is once again not observed (see Figure 68).

Since there is only one N atom available for coordination, the exchange may be intermolecular or intramolecular where the ligand leaves the coordination sphere, is replaced by solvent, and then returns to the coordination site. Problems with the computer simulation are now encountered since if the exchange occurs *via* the second process, we need to know the concentration of free ligand. This will be done in future work where the temperature will be held constant while the concentration of free ligand will be varied.

5.3.5 Conclusion

Considering the preceeding discussion we can conclude that in compounds of the type *trans*-$[PtX_2(C_2H_4)(L)]$, (X = Cl, Br; L = pyrazine, imidazole and *N*-methylimidazole) there is rapid exchange between L and the parent complex.

In the case where L = pyrazine, this exchange is too fast to monitor and no conclusions can be drawn as to the type of exchange taking place.

Where L = imidazole it is suggested that for X = Cl, intramolecular exchange involving both N atoms is the predominant exchange process in the temperature range considered, but for X = Br intramolecular exchange involving both N atoms is only dominant in the lower temperature region near coalescence, and that exchange with solvent becomes more important at higher temperatures. The fact that solvent is a decisive factor in the exchange process is manifested by the very similar $\Delta H^{\ddagger}$ values, but vastly different $\Delta S^{\ddagger}$ values.

Finally, further work will be done in order to establish an estimate of free ligand concentrations, and once these have been obtained, the exchange process involving the complex and solvent will be accounted for in the computer simulation. This hopefully will give a better simulation for the exchange process in *trans*-$[PtBr_2(C_2H_4)(N\text{-Me Him})]$ and for the exchange process at higher temperatures in *trans*-$[PtBr_2(C_2H_4)(Him)]$.

REFERENCES

REFERENCES

1. F.A. Cotton and G. Wilkinson, *Advanced Inorganic Chemistry*, John Wiley & Sons, Inc., (1980) 901.

2. F.R. Hartley, *The Chemistry of Platinum and Palladium*, Applied Science Publishers Ltd., London (1973) Chapter 1.

3. Reference 2, Chapter 2.

4. St. Ahrland, J. Chatt and N.R. Davies, *Quart. Rev.*, 12 (1958) 265.

5. R.G. Pearson, *J. Amer. Chem. Soc.*, 85 (1963) 3533.

6. K. Nakamoto, *Infrared Spectra of Inorganic and Coordination Compounds*, Wiley, New York (1963).

7. G.A. Foulds and D.A. Thornton, *J. Mol. Struct.*, (in press).

8. G.T. Belinke and K. Nakámoto, *Inorg. Chem.*, 6 (1967) 433.

9. S. Pinchas and I. Laulicht, *Infrared Spectra of Labelled Compounds*, Academic Press, New York (1971).

10. K. Nakamoto, *Angew. Chem. Internat. Ed.*, 11 (1972) 666.

11. G.C. Percy and H.S. Stenton, *J. Chem. Soc. Dalton*, (1976) 1466.

12. G.C. Percy and H.S. Stenton, *J. Chem. Soc. Dalton*, (1976) 2429.

13. E.B. Wilson Jr., J.C. Decius and P.C. Cross, *Molecular Vibrations*, McGraw-Hill, New York (1955).

14. F.A. Cotton, *Chemical Applications of Group Theory, Second Edition*, Wiley-Interscience, New York (1971).

15. J.R. Ferraro and J.S. Ziomek, *Introductory Group Theory and its Applications to Molecular Structure*, Plenum, New York (1969).

16. R.S. Halford, *J. Chem. Phys.*, 14 (1946) 8.

17. D.M. Adams, *Coord. Chem. Rev.*, 10 (1974) 183.

18. D.M. Adams and D.C. Newton, *Tables for Factor Group and Point Group Analysis*, Beckman-RIIC Ltd., Croydon (1970).

19. L.P. Bicelli, *Ann. Chim. Rome*, 48 (1958) 749.

20. G.A. Foulds, J.B. Hodgson, A.T. Hutton, M.L. Niven, (the late) G.C. Percy, P.E. Rutherford and D.A. Thornton, *Spectroscopy Letters*, 12 (1) (1979) 25.

21. L.M. Jackman and F.A. Cotton, *Dynamic Nuclear Magnetic Resonance Spectroscopy*, Academic Press, New York (1975).

22. D.S. Stephenson and G. Binsch, *QCPE Program No. 365*, Chemistry Department, Indiana University.

23. R.R. Shaup, E.D. Becker and M.L. McNeel, *J. Phys. Chem.*, 76 (1972) 71.

24. A. Allerhand and E. Thiele, *J. Chem. Phys.*, 45 (1966) 902.

25. R.J. Goodfellow *et al.*, *J. Chem. Soc. (A)*, (1968) 1604.

26. R.J. Cross, T.H. Green and R. Keat, *J.C.S. Dalton*, (1976) 382.

27. J.M. Jenkins and B.L. Shaw, *J. Chem. Soc. (A)*, (1966) 770.

28. D.A. Redfield and J.H. Nelson, *Inorg. Chem.*, 12 (1973) 15.

29. F. Basalo and R.G. Pearson, *Mechanisms of Inorganic Reactions, Second Edition*, Wiley, New York (1967).

30. W.J. Louw, *Inorg. Chem.*, 16 (1977) 2147.

31. Reference 2, page 315.

32. C.G. Van Kralingen, J.K. De Ridder and J. Reedijk, *Inorganica Chimica Acta*, 36 (1979) 69.

33. C.G. Van Kralingen and J. Reedijk, *Inorganica Chimica Acta*, 30 (1978) 171.

34. D.R. Williams, *Inorg. Chim. Acta Rev.*, 6 (1972) 123.

35. M.J. Cleare, *Coord. Chem. Rev.*, 12 (1972) 349.

36. L.L. Munchausen, *Proc. Nat. Acad. U.S.A.*, 71 (1974) 4519.

37. J.P. Macquet and T. Theophanides, *Bioinorg. Chem.*, 5 (1975) 59.

38. G.H.W. Milburn and M.R. Truter, *J. Chem. Soc. (A)*, (1966) 1609.

39. J.R. Ferraro, *Low-Frequency Vibrations of Inorganic and Coordination Compounds*, Plenum Press, New York (1971) 155.

40. J.R. Ferraro, W. Wozniak and G. Roch, *Ric. Sci.*, 38 (1968) 433.

41. J.R. Ferraro, J. Zipper and W. Wozniak, *Applied Spectrosc.*, 23 (1969) 160.

42. R. Bayer and J.R. Ferraro, *Inorg. Chem.*, 8 (1969) 1654.

43. M. Goldstein and W.D. Unsworth, *Inorg. Chim. Acta* 4 (1970) 342.

44. M. Goldstein and W.D. Unsworth, *Spectrochim. Acta*, 27A (1971) 1055.

70. C.H. Langford and H.B. Gray, *Ligand Substitution Processes*, W.A. Benjamin, New York (1965) chapter 2.

71. G.B. Bokii and G.A. Kukina, *Zh. Strukt. Khim.*, 6 (5) September-October (1965) 706-715.

72. J.A. Jarvis, B.T. Kilbourn and P.G. Owston, *Acta Cryst.*, B27 (1971) 366.

73. R.A. Love *et al.*, *Inorg. Chem.*, 14 (11) (1975) 2653.

74. W.C. Hamilton, K.A. Klauderman and R. Spratley, *Organometallic and Coordination Compounds*, XIV, S172.

75. P.G. Eller, R.R. Ryan and R.O. Schaeffer, *Cryst. Struct. Comm.*, 6 (1977) 163.

76. M. Orchin and P.J. Schmidt, *Coord. Chem. Rev.*, 3 (1968) 345.

77. Reference 2, p. 368.

78. D. Sutton, *Electronic Spectra of Transition Metal Complexes*, McGraw-Hill Ltd., Great Britain, 189.

79. R.G. Denning and L.M. Venanzi, *J. Chem. Soc.*, (1963) 3241.

80. S.J. Lokken and D.S. Martin, *Inorg. Chem.*, 2 (1963) 562.

81. S.I. Shupack and M. Orchin, *J. Amer. Chem. Soc.*, 86 (1964) 586.

82. R.G. Denning, F.R. Hartley and L.M. Venanzi, *J. Chem. Soc. (A)*, (1967) 1322.

83. M.A.M. Meester and K. Olie, *Cryst. Struct. Comm.*, 4 (1975) 725.

84. F. Caruso, R. Spagna and L. Zambonelli, *Journal of Crystal and Molecular Structure*, 8 (2) (1978) 47.

85. S.I. Shupack and M. Orchin, *J. Amer. Chem. Soc.*, 85 (1963) 902.

86. S.I. Shupack and M. Orchin, *Inorg. Chem.*, 3 (1964) 374.

87. H.P. Fritz and D. Sellman, *J. Organomet. Chem.*, 6 (1966) 558.

88. M. Orchin and P.J. Schmidt, *Inorg. Chim. Acta Rev.*, 1 (1968) 123.

89. J. Hiraishi, *Spectrochim. Acta*, 25A (1969) 749.

90. T. Iwayanagi and Y. Saito, *Inorg. Nucl. Chem. Lett.*, 11 (1975) 459.

91. M.A.M. Meester, D.J. Stufkens and K. Vrieze, *Inorg. Chim. Acta*, 14 (1975) 25.

92. M.A.M. Meester, D.J. Stufkens and K. Vrieze, *Inorg. Chim. Acta*, 16 (1976) 191.

93. G.A. Foulds and D.A. Thornton, *Spectrochim. Acta*, 37A (1981) 917.

94. A. Gambi and S. Ghersetti, *Spectrosc. Lett.*, 8 (1977) 627.

95. C.H. Kline and J. Turkevich, *J. Chem. Phys.*, 12 (1944) 300.

96. T.P.E. Auf der Heyde, G.A. Foulds, D.A. Thornton, H.O. Desseyn and B.J. van der Veken, *J. Mol. Struct.*, (in press).

97. G.A. Foulds and D.A. Thornton, *J. Mol. Struct.*, (in press).

98. T.A. Weil, P.J. Schmidt and M. Orchin, *Inorg. Chem.*, 8 (1969) 2138.

99. K.J. Coshran, R.D. Bertrand and J.G. Verkade, *J. Amer. Chem. Soc.*, 89 (1967)

100. P.D. Kaplan, P.J. Schmidt and M. Orchin, *J. Amer. Chem. Soc.*, 89 (1967) 4537.

101. L.W. Reeves, *Canadian J. Chem.*, 38 (1960) 736.

102. S. Maricic, C.R. Redpath and J.A.S. Smith, *J. Chem. Soc.*, (1963) 4905.

103. Reference 2, page 157.

104. A.R. Brause, F. Kaplan and M. Orchin, *J. Amer. Chem. Soc.*, 89 (1967) 2661.

105. H. Boucher and B. Bosnick, *Inorg. Chem.*, 16 (3) (1977) 717.

106. S. Miya and K. Saito, *Inorg. Chem.*, 20 (1981) 287.

107. R. Cramer, *Inorg. Chem.*, 4 (1965) 445.

108. P.D. Kaplan, P. Schmidt and M. Orchin, *J. Amer. Chem. Soc.*, 91 (1969) 85.

109. W.L. Jorgensen and L. Salem, *The Organic Chemists Book of Orbitals*, p. 263.